UNIVERSITY OF SOUTHAMPTON

Fast transient sources observed with INTEGRAL

Vito Sguera
Submitted for the degree of Doctor of Philosophy
SCHOOL OF PHYSICS AND ASTRONOMY
FACULTY OF SCIENCE

May 9, 2007

Ai miei genitori, Raffaella e Giuseppe

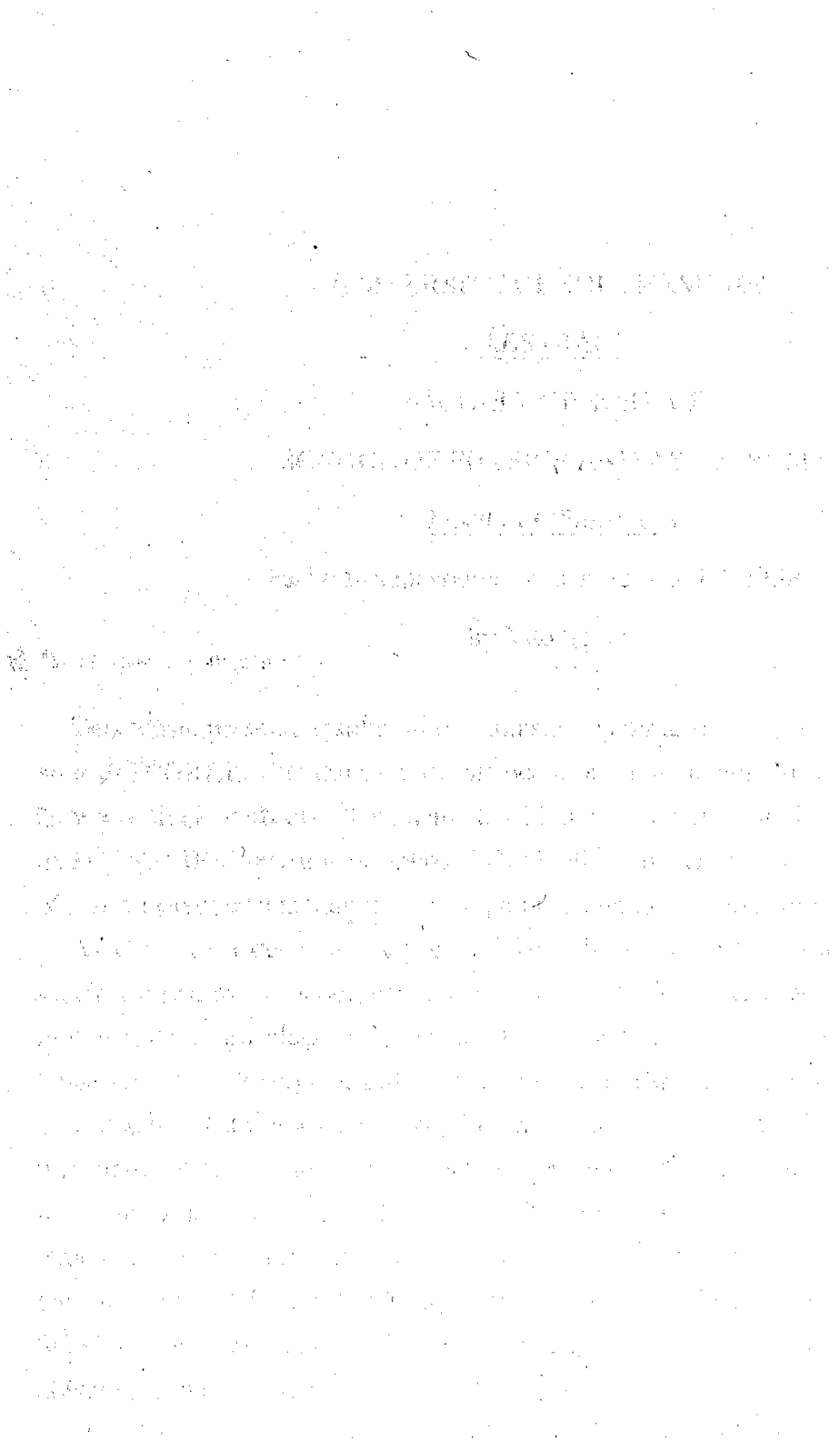

UNIVERSITY OF SOUTHAMPTON

ABSTRACT

FACULTY OF SCIENCE

SCHOOL OF PHYSICS AND ASTRONOMY

Doctor of Philosophy

Fast transient sources observed with INTEGRAL

by Vito Sguera

This thesis presents results on fast transient gamma-ray sources detected and studied with INTEGRAL. Fast transient events occur at unpredictable locations and times and it is very difficult to observe them using traditional narrow field of view (FOV) X-ray instruments. The IBIS instrument onboard INTEGRAL is particularly suited to the detection of fast transient events thanks to its large FOV and good sensitivity.

As result of a detailed study of a 3 year dataset of IBIS observations, designed to search for fast transient sources, this thesis shows that INTEGRAL is playing a key role in unveiling a new class of Supergiant High Mass X-ray Binaries (SGXBs) which have been named as Supergiant Fast X-ray Transients (SFXTs). Most of the time they are undetectable, with quiescent X-ray luminosities $\leq 10^{32}$–10^{33} erg s^{-1}. Then occasionally they undergo fast X-ray transient activity lasting less than a day, typically a few hours, reaching peak luminosities of $\sim 10^{36}$–10^{37} erg s^{-1}. Their outbursts show complex time structures, being characterized by several fast flares with a duration of typically a few tens of minutes. This kind of X-ray behaviour is very different from that seen in classical SGXBs, which are known to be persistent bright X-ray sources with X-ray luminosities always detectable in the range 10^{36}–10^{38} erg s^{-1}.

INTEGRAL results on 8 firm SFXTs as well as 6 candidates are presented in chapter 4 and chapter 5, respectively. The number of SFXTs discovered in only a few years is already comparable to that of persistent classical SGXBs discovered in $\sim$ 40 years of X-ray astronomy. The class of SFXTs could be much larger than the 14 objects reported in this thesis. An entire population of still undetected SFXTs could be hidden in the Galaxy.

Publications

The following list reports the papers directly related to this thesis and written from the work made during the three years of my Ph.D. course. They correspond to part of chapter 4 and chapter 5 of this thesis and they have been accepted for publication on the refereed journals Astronomy & Astrophysics and Astrophysical Journal.

1. **Sguera V.**, Hill, A.B., Bird, A.J., et al. 2007, accepted for publication on A&A, in press, astroph/0702477.
   IGRJ18483–0311: an accreting X-ray pulsar observed by INTEGRAL.

2. **Sguera V.**, Bird, A.J.; Dean, A.J., et al. 2007, A&A, 462, 695.
   INTEGRAL and Swift observations of the supergiant fast X-ray transient AX J1845.0–0433 = IGR J18450–0435.

3. **Sguera V.**,;Bazzano,A.;Bird, A.J., et al. 2006, ApJ, 646, 452.
   Unveiling Supergiant Fast X-Ray Transient sources with INTEGRAL.

4. **Sguera V.**,;Barlow,E.J.;Bird, A.J., et al. 2005, A&A, 444, 221.
   INTEGRAL observations of recurrent fast X-ray transient sources.

5. **Sguera V.**, Bazzano,A.;Bird A.J., et al. 2007, submitted to A&A.
   INTEGRAL high energy detection of the transient IGR 11321–5311.

The following list reports the papers not directly related to this thesis, for which I gave a contribution as a member of the IBIS survey team, during the three years of my Ph.D. course.

1. A.J.Bird, A.Malizia, A.Bazzano, et al. 2007, accepted for publication on APJ, in press, astroph/0611493
   The 3rd IBIS/ISGRI soft gamma-ray survey catalog

2. A.J.Bird,E.J.Barlow,L.Bassani, et al. 2006, ApJ, 636, 765
   The 2rd IBIS/ISGRI soft gamma-ray survey catalog

3. E.J.Barlow,C.Knigge,A.J.Bird, et al. 2006, MNRAS, 372, 224
The 20–100 keV properties of cataclysmic variables detected in the INTEGRAL/IBIS survey

4. M.Molina,A.Malizia,L.Bassani, et al. 2006, MNRAS, 371, 821
INTEGRAL observations of active galactic nuclei obscured by the Galactic plane

5. A.J.Dean,A.Bazzano,A.B.Hill, et al. 2005, A&A, 443, 485
Global characteristics of the first IBIS/ISGRI catalogue sources: unveiling a murky episode of binary star evolution

6. A.Malizia,L.Bassani,J.B.Stephen, et al. 2005, ApJ, 630, 157
The INTEGRAL/IBIS Source AX J1838.0–0655: A Soft X-Ray-to-TeV-Ray Broad-band Emitter

7. E.J.Barlow,A.J.Bird,D.J.Clark, et al. 2005, A&A, 437, 27L
Detection and analysis of a new INTEGRAL hard X-ray Transient, IGR J17285–2922

Declaration

The Author, Vito Sguera, is a member of the IBIS survey team with the principal role of studying fast transient sources detected by IBIS. The work presented in this thesis represents the result of three years of research performed by the Author. However, this work was not completed in isolation, being carried out within the IBIS survey project which is a multi-national collaboration. The contribution of other people is dictated below:

- The Author worked jointly with Dr. A. B. Hill on the period analysis of the sources IGR J18483–0311 and IGR J11321–5311 (in chapter 5). Dr. A. B. Hill was responsible for the Monte-Carlo simulations.
- Dr. N. Masetti was responsible for the reported optical characteristics of the source IGR J18483–0311 (in chapter 5).
- Dr. R. Landi provided all the *Swift* XRT data presented in this thesis. The Author was responsible for their spectral and temporal analysis (in chapter 4 and 5).

Acknowledgements

I would like to start by thanking my supervisor Prof. Tony Dean. I am greatly indebted to him for giving me the fantastic opportunity to work on INTEGRAL. Thanks so much for believing in my capabilities in spite of "my very poor spoken english", for the unremitting and enthusiastic guidance, for countless suggestions and stimulating scientific discussions, for giving me "a space to discuss" which was very important for my professional growth.

My sincere gratitude goes to Dr. Tony (aka Ralph) Bird for his unremitting help and guidance. Thanks so much for countless stimulating scientific discussions, for always having a "script" and an answer to my boring questions, for assistance whenever my computer "crashed". Most of all, I would like to thank him for the most important thing: countless enjoyable discussions on english and italian football as well as countless entertaining football matches watched in pub. I really appreciated his huge passion for football, although he is never going to celebrate a world cup victory (born in the wrong country, mate!).

I wish to thank my office-mates and the rest of the INTEGRAL group in Southampton, past and present, for keeping the atmosphere light and the office full of "ideas". Thanks to Manuela (my fellow italian expatriate and good friend), Adam, Liz, Fiamma (my fellow italian year mate and good friend), Vanessa, Dave W., Simon, Dave C.,Simone, Lynn.

Big thanks to everybody in the astronomy group at Southampton, past and present, for providing a very friendly, helpful and sociable atmosphere. They are really too many to be mentioned, but hey you know who you are, so thank you so much! Special thanks to Colin and Matt for the "longest Saturdays" watching rugby RBS6 while drinking liters/gallons of beer, to Ed Pope for many played and watched football matches, to Omar for the laughs and many "entertaining discussions".

I am very thankful to Loredana, Angela B., Angela M. and Pietro for their collaboration full of enthusiasm from the beginning of my PhD project and for supporting me. They are for me source of enthusiasm on the astronomy research, a reference of scientific passion and professionality.

Special and big thanks to Winston for being the "perfect flatmate" and most of all a very good friend. I wish to thank him for his unremitting help, for the laughs, for.....ehm the list could be very very long, so thanks for everything my friend!

Thanks to my flatmates of the "legendary" flat 28 in St. Margaret's house and to everybody who I met and knew during countless unforgettable parties and dinners. In particular, big thanks to Sarah and Annagrazia for being good friends and for the amusing late nights out downtown.

It is impossible not to thank my italian best friends: Mirco, Barbara, Mauro, Fenia, Gracco, Alessandra, Alessandro, Matteo Depa, Matteo V., Federico, Luana. They are like a family for me, they were far away but close in my mind and heart. Thanks for supporting me, for preventing me from sleeping under the "portici" in Bologna!

Finally, thanks from the deepest of my heart to my whole family for the unremitting support. My parents Raffaella and Giuseppe, my brother Raffaele, my uncle Salvatore and aunt Chiara, my "sisters" Marisa, Silvia and Elisabetta. My parents may have absolutely no idea what X/γ-ray astronomy is about, but they always supported me, regardless. They don't know how much I am proud of them.

Contents

1 Introduction: gamma-ray astronomy **1**
1.1 Introduction 1
1.2 Gamma-ray production mechanisms 2
1.2.1 Energy yield in accretion 3
1.3 Instrumentation and techniques of γ-ray astronomy 5
1.3.1 Gamma-ray interaction methods 6
1.3.1.1 The photoelectric effect 6
1.3.1.2 Compton scattering 7
1.3.1.3 Pair production 8
1.3.2 Gamma-ray telescopes 8
1.3.2.1 Detector types 9
1.3.2.2 Coded aperture mask 9
1.3.2.3 Compton telescope 11
1.3.2.4 The pair telescope 12
1.3.3 Gamma-ray astronomy missions 13

2 Transient characteristics of the gamma-ray sky **19**
2.1 Introduction 19
2.2 Accreting X-ray binaries 19
2.2.1 High Mass X-ray Binaries HMXBs 20
2.2.1.1 Be HMXBs 22
2.2.1.2 Supergiant HMXBs 24
2.2.1.3 Supergiant HMXBs in the INTEGRAL era 28
2.2.2 Low Mass X-ray Binaries LMXBs 29
2.2.2.1 Type I and II X-ray bursts from LMXBs 30
2.2.2.2 Soft X-ray transients 34
2.3 Fast X-ray transients 34
2.3.1 The first detections of FXTs 35

2.3.2 FXTs in the BeppoSAX era 37
2.4 Gamma-ray bursts 40
2.5 Active Galactic Nuclei 42
2.6 Summary 45

3 The INTEGRAL gamma-ray satellite 46
3.1 The INTEGRAL mission 46
3.1.1 INTEGRAL observing program 47
3.1.2 INTEGRAL observing modes 48
3.2 The INTEGRAL payload 49
3.2.1 IBIS, the gamma-ray imager 51
3.2.2 The spectrometer SPI and the monitors JEM–X and OMC 53
3.3 Techniques to detect fast transient events with IBIS 54
3.4 Summary 56

4 Unveiling supergiant fast X-ray transient sources with INTEGRAL 58
4.1 Introduction 58
4.2 Firm supergiant fast X-ray transients detected by INTEGRAL 59
4.2.1 XTE J1739–302=IGR J17391–3021 59
4.2.1.1 Archival X-ray observations of the source 59
4.2.1.2 Archival INTEGRAL observations of the source 60
4.2.1.3 Analysis of newly discovered outbursts by INTEGRAL 61
4.2.2 IGR J17544–2619 67
4.2.2.1 Archival X-ray observations of the source 67
4.2.2.2 Analysis of newly discovered outbursts by INTEGRAL 67
4.2.3 AX J1841.0–0536=IGR J18410–0535 72
4.2.3.1 Archival X-ray observations of the source 72
4.2.3.2 Analysis of newly discovered outbursts by INTEGRAL 72
4.2.4 AX J1845.0–0433=IGR J18450–0435 75
4.2.4.1 Archival X-ray observations of the source 75
4.2.4.2 Analysis of newly discovered outbursts by INTEGRAL and *Swift* 76
4.2.5 SAX J1818.6–1703 83
4.2.5.1 Archival X-ray observations of the source 83
4.2.5.2 Analysis of newly discovered outbursts by INTEGRAL 84
4.2.5.3 Search for counterparts at other wavebands 90
4.2.6 IGR J11215–5952 91

4.2.6.1 Archival X-ray observations of the source 91
4.2.6.2 Analysis of outbursts detected by INTEGRAL 93
4.2.7 IGR J16465–4507 96
4.2.7.1 Archival X-ray observations of the source 96
4.2.7.2 Analysis of the outbursts detected by INTEGRAL . . . 96
4.2.8 IGR J08408–4503 99
4.2.8.1 Archival X-ray observations of the source 99
4.2.8.2 Analysis of the outburst detected by INTEGRAL 101

5 Candidate Supergiant Fast X-ray transients 102
5.1 Introduction 102
5.2 Candidate SFXTs observed with INTEGRAL 103
5.2.1 IGR J16479–4514 103
5.2.1.1 Archival X-ray observations of the source 103
5.2.1.2 Analysis of newly discovered outbursts by INTEGRAL 104
5.2.2 IGR J17407–2808 112
5.2.2.1 Archival X-ray observations of the source 112
5.2.2.2 Analysis of newly discovered outbursts by INTEGRAL 113
5.2.3 AX J1749.1–2733 116
5.2.3.1 Archival X-ray observations of the source 116
5.2.3.2 Analysis of a newly discovered outburst by INTEGRAL 116
5.2.4 IGR J11321–5311 120
5.2.4.1 Archival X-ray observations of the source 120
5.2.4.2 Analysis of the outburst detected by INTEGRAL 120
5.2.4.3 Discussion 126
5.2.5 IGR J18483–0311 128
5.2.5.1 Archival X-ray observations of the source 128
5.2.5.2 Analysis of newly discovered outbursts by INTEGRAL 128
5.2.5.3 Recurrence timescale 137
5.2.5.4 Looking for missed outbursts 139
5.2.5.5 Searching for a pulse period 140
5.2.5.6 *Swift* observations and results 140
5.2.5.7 An highly reddened star as optical counterpart of IGR J18483–0311 143
5.2.5.8 Summary on IGR18483–0311 145
5.2.6 IGR J16195–4945=AX J161929–4945 145

5.2.6.1 Archival X-ray observations of the source 145
5.2.6.2 Analysis of newly discovered outbursts by INTEGRAL 147
5.3 Summary and conclusions 150

6 Discussion and Conclusions **152**

List of Figures

1.1 γ-ray interaction processes as a function of energy and atomic number of absorbing material. 7
1.2 Diagram of Compton scattering 8
1.3 Simplified model of a coded mask system. 10
1.4 Example of Compton telescope. If a photon undergoes one or more Compton scatters in the instrument and then is photoelectrically absorbed, then by using the positions $(\vec{r}_1, \ldots, \vec{r}_N)$ and energy deposits $(E_1, \ldots, E_N)$ of the interactions, the initial direction of the photon can be determined by the Compton scatter formula to within an annulus on the sky, ϕ_1. The width of this annulus is determined by the uncertainties in both the interaction locations and energy deposits 11
1.5 Principle of photon detection in a pair telescope. The instrument is basically made of an anti-coincidence detector, a tracker/converter module and a calorimeter for the measure of the energy. 12
1.6 Second COS-B catalog of point like γ-ray sources. Open circles denote faint sources, filled circles brighter ones. The dividing line is at 1.3 10^{-6} ph/cm^{2}sec. The shaded area was not searched for sources since the coverage by COS-B was not adequate. Picture taken from Swanenburg et al. 1981. 13
1.7 Gamma-ray sky as seen by EGRET at energies greater than 100 MeV. . . 15
1.8 Distribution in the sky, in galactic coordinates, of all 271 gamma-ray point-sources reported in the 3EG catalog. 16
2.1 Schematic view of accretion onto a neutron star. 21
2.2 Classical view of a Be/X-ray transient system. 23
2.3 The geometry of accretion onto a compact object in a SGXB. The wind is assumed to be spherically symmetric and smooth. The red line represents the equipotential surface of the Roche lobe. 25

2.4 The Corbet diagram illustrating the relationship between orbital and spin periods in HMXBs systems. Picture taken from Bildsten et al. (1997). . . 26
2.5 ISGRI light curve (20–30 keV) of a fast flare detected by INTEGRAL from Vela X-1 on November 2003. The bin time is 280 seconds. 27
2.6 ASM light curve (2–12 keV) of Cygnus X-1 from approximately October 1995 to March 2006. 27
2.7 The geometry of accretion onto a compact object in a LMXB. The red line represents the equipotential surface of the Roche lobe and the companion donor star has filled its Roche lobe. 30
2.8 A schematic view of a type I X-ray burst. Credit picture: Hill 2006. . . . 31
2.9 Type I X-ray burst from 4U1702–429 as observed with EXOSAT in two different energies bands: 1.2–5.3 keV (left) and 5.3–19 keV (right). The softening of the X-ray spectrum during the decay is apparent as a relatively long tail in the low energy burst profile (taken from Lewin et al. 1993). 31
2.10 An artist conception (not to scale) of a soft X-ray transient. 33
2.11 Ginga X-ray light curve of a X-ray outburst from the black hole candidate soft X-ray transient GS 2000+25. 33
2.12 Collage of X-ray light curves of FXTs detected by Ariel–V (2–18 keV). Each data point represents an interval of ~ 100 minutes (one satellite orbit). Picture taken from Pye & Mchardy (1983). 36
2.13 Distribution in the sky in galactic coordinates of FXTs detected by Ariel–V. Picture taken from Pye & McHardy (1983). 37
2.14 Histogram of durations of FXTs detected by WFCs. The distribution appears to be bimodal. The long duration events are galactic coronal sources, the short duration events are X-ray flashes. Picture taken from Heise & in't Zand (2004). 38
2.15 WFCs (top, 2–28 keV) and GRBM (bottom, 40–700 keV) light curves of a XRF detected on 23 August 1997. Picture taken from Heise & in't Zand (2004). 38
2.16 A sample variety of light curves of GRBs observed by BATSE. 41
2.17 Schematic view of the relativistic fireball shock model for GRBs. 42
2.18 Schematic view describing the classification scheme for AGNs. 43
2.19 Unification model of AGN (picture credit ESA/ISDC). 45

3.1 Schematic view of two consecutive Galactic Plane Survey (GPS) scans. The scans are performed by executing a "slew and stare" manoeuvre of the spacecraft, resulting in 20 to 55 different pointings (staring) separated by 6°. The extremes in latitude of the pointings are at |b| = 6°.45 and follow a saw-tooth pattern inclined at 21° to the galactic equator. Each subsequent scan will be shifted by 27°.5 in galactic longitude. Each pointing lasts about 2200 sec, while the slew lasts about 200 sec. 47

3.2 Dither patterns adopted for INTEGRAL observations: rectangular dithering and hexagonal dithering. 49

3.3 The INTEGRAL satellite. 50

3.4 Scheme of the IBIS instrument showing the PICsIT and ISGRI detector planes and shielding systems. Above the detector planes is the lower part of the collimating system (hopper). 52

3.5 The IBIS coded mask. 52

3.6 Overall design of JEM–X, showing the two units, with only one of the two coded masks. 53

3.7 The exposure map for the dataset. Contour levels are at 10 ksec, 500 ksec, 1 Ms and 3 Ms. 57

3.8 The number of ScWs belonging to the dataset versus galactic latitude of their pointing. 57

4.1 The ISGRI light curve (20–60 keV) of a newly discovered outburst (No. 1 in table 4.1) of XTE J1739−302. 62

4.2 ISGRI Science Window (ScW) image sequence (20–30 keV) of a newly discovered outburst (No. 1 in Table 4.1) of XTE J1739−302 (encircled). The duration of each ScW is ~ 2000 s. The source was not detected in the first ScW (significance less than 2σ), then it was detected during the next 3 ScWs with a significance, from left to right, equal to 14σ, 16σ and 23σ, respectively. Finally in the last ScW the source was not detected (significance less than 2σ). A weak persistent source (1E 1740.7–2942) is also visible in the field of view 62

4.3 JEM–X mosaic significance image of outburst No. 1 in table 4.1. From left to right, XTE J1739−302 is detected at a level of ~ 78σ (4–10 keV), ~ 65σ (10–20 keV) and ~ 40σ (15–35 keV). 63

4.4 Unfolded cutoff power law spectrum (3–80 keV) of XTE J1739−302 during the outburst No.1 in table 4.1. 63

4.5 The ISGRI light curve (20–30 keV) of a newly discovered outburst (No. 4 in table 4.1) of XTE J1739–302. 63
4.6 The ISGRI light curve (20–30 keV) of a newly discovered outburst (No. 5 in table 4.1) of XTE J1739–302 63
4.7 The ISGRI light curve (20–60 keV) of a newly discovered outburst (No. 6 in table 4.1) of XTE J1739–302. 65
4.8 The ISGRI light curve (20–60 keV) of a newly discovered outburst (No. 7 in table 4.1) of XTE J1739–302. 66
4.9 Unfolded power law spectrum (3–60 keV) of a newly discovered outburst (No. 7 in table 4.1) of XTE J1739–302. 66
4.10 ISGRI light curve (20–40 keV) of the IBIS detection of IGR J17544–2619 on Sep 2003 01h10 UTC (outburst No. 1 in table 4.2). 69
4.11 Unfolded bremsstrahlung spectrum (20–60 keV) of IGR J17544–2619 during the outburst No.1 in table 4.2. 69
4.12 ISGRI light curve (20–60 keV) of the IBIS detection of IGR J17544–2619 on 2004 March 8 (outburst No. 3 in table 4.2). 70
4.13 ISGRI light curve (20–30 keV) of the IBIS detection of IGR J17544–2619 on 12 March 2005 (outburst No. 4 in table 4.2). 70
4.14 Unfolded black body spectrum (20–40 keV) of IGR J17544–2619 during the outburst that occurred on 12 March 2005 (No.4 in table 4.2). 71
4.15 ISGRI light curve (20–40 keV) of the IBIS detection of IGR J17544–2619 on 12 March 2006 (outburst No. 5 in table 4.2). 71
4.16 ISGRI light curve (20–80 keV) of AX J1841.0-0536 during outburst No. 1 in table 4.3. 73
4.17 ISGRI light curve (20–80 keV) of AX J1841.0-0536 during outburst No. 2 in table 4.3. 73
4.18 ISGRI light curve (20–60 keV) of AX J1841.0-0536 during outburst No. 3 in table 4.3. 74
4.19 ISGRI light curve (20–40 keV) of outburst No. 4 in table 4.3. 74
4.20 ASCA light curve (2–10 keV) of AX J1845.0-0433 when the source was discovered in 1993. 76
4.21 ISGRI light curve (20–40 keV) of a newly discovered outburst of AX J1845.0–0433 on 28 April 2005. Time axis is in MJD. Each data point represents the average flux during one ScW (~2000 seconds). 78
4.22 Expanded view of the light curve of the outburst activity from AX J1845.0–0433 highlighted in the box in figure 4.21. The bin time is 900 s 78

4.23 Unfolded Bulk Motion Comptonization (BMC) spectrum (3–100 keV) of AX J1845.0–0433 during the flare that occurred on 28 April 2005. . . . 80
4.24 ISGRI light curve (20–40 keV) of a newly discovered outburst of AX J1845.0–0433 occurred on 20 April 2006. 80
4.25 *Swift* XRT image (0.2–10 keV) of the observation of AX J1845.0–0433 performed on 11 November 2005. The source is clearly detected at $\sim 68\sigma$ at the center of the field of view. 81
4.26 *Swift* XRT light curve (0.2–10 keV) during the observation on 11 November 2005. 82
4.27 *Swift* XRT light curve (0.2–10 keV) during the observation on 5 March 2006. 82
4.28 RXTE ASM dwell by dwell light curve (2–12 keV) of SAX J1818.6–1703 from 1996 to 2006. In the light curve 30 c s^{-1} is equivalent to a flux of $\sim$ 400 mCrab. Time axis is in MJD. The six outbursts detected by RXTE, with a flux greater than 400 mCrab, are indicated by the numbers from 1 to 6. 84
4.29 ISGRI light curve (20–100 keV) of a newly discovered outburst (No.1 in table 4.5) of SAX J1818.6–1703. 86
4.30 Expanded view of the light curve (20–100 keV) of the outburst from SAX J1818.6–1703 showed in figure 4.29 86
4.31 ISGRI light curve (20–60 keV) of a newly discovered outburst (No. 2 in table 4.5) of SAX J1818.6–1703. 88
4.32 Unfolded black body spectrum of a newly discovered outburst (No. 2 in table 4.5) of SAX J1818.6–1703. 88
4.33 ISGRI light curve (20–30 keV) of a newly discovered outburst (No. 3 in table 4.5) of SAX J1818.6–1703. 88
4.34 ISGRI Science Window (ScW) image sequence (20–30 keV) of a newly discovered outburst (No.3 in table 4.5) of SAX J1818.6–1703 (encircled). The duration of each ScW is $\sim$ 2000 s. The source was not detected in the first ScW on the left (significance less than 1σ), then it was detected during the next 6 ScWs with a significance, from left to right, equal to 5σ, 10.5σ, 7.5σ, 7σ, 5σ and 4.5σ, respectively. Finally in the last ScW the source was not detected (significance less than 2σ). 89
4.35 ISGRI light curve (20–40 keV) of a newly discovered outburst (No. 4 in table 4.5) of SAX J1818.6–1703. 89

4.36 USNO R1 optical image superimposed on the ISGRI error circle of SAX J1818.6–1703 (the bigger one, radius of 42″) and on the Chandra error circle (the smaller one, in white, radius of 0″.62). 90
4.37 RXTE light curve (2–10 keV) of IGR J11215–5952 in outburst on March 2006 (Credit:Smith at al. 2006b). 92
4.38 *Swift* XRT light curve (1–10 keV) of IGR J11215–5952 in outburst on February 2007 (Credit:Mangano at al. 2007). 92
4.39 ISGRI light curve (20–40 keV) of outburst No. 1 in table 4.6. Time axis is in MJD. Each data point represents the average flux during one ScW (~2000 seconds). 93
4.40 ISGRI light curve (20–40 keV) of outburst No. 2 in table 4.6. Time axis is in MJD. Each data point represents the average flux during one ScW (~2000 seconds). 94
4.41 ISGRI light curve (20–60 keV) of outburst No. 3 in table 4.6. 95
4.42 Unfolded power law spectrum of outburst No.3 in table 4.6. 95
4.43 ISGRI light curve (20–30 keV) of outburst No.2 in table 4.7. 97
4.44 Unfolded bremsstrahlung spectrum (20–80 keV) of IGR J16465–4507 during outburst No. 2 in table 4.7. 97
4.45 ISGRI light curve (20–40 keV) of outburst No.1 in table 4.7. 97
4.46 ISGRI mosaic significance map (17–40 keV) of ScWs during which outburst No. 1 was detected. IGR J16465–4507 is encircled in the picture, it was detected at a level of ~ 13σ. 98
4.47 *Swift* XRT error circle of IGR J08408–4503 superimposed on the 2MASS infrared image band (J band). 100
4.48 ISGRI light curve (20–40 keV) of outburst No. 1 in table 4.8. 100
4.49 Unfolded power law spectrum (20–80 keV) of IGR J08408–4503 during outburst No. 1 in table 4.8. 101
5.1 The ISGRI light curve (20–30 keV) of a newly discovered outburst (No. 1 in table 5.1) of IGR J16479–4514. 105
5.2 Expanded view of the light curve (20–30 keV) of the outburst from IGR J16479–4514 showed in figure 5.1 105
5.3 Unfolded black body spectrum (20–60 keV) of IGR J16479–4514 during the decay of outburst No.1 in table 5.1 107
5.4 The ISGRI light curve (20–30 keV) of the detection of IGR J16479–4514 on 10 August 2003 (No.4 in table 5.1). 107

5.5 The ISGRI light curve (20–30 keV) of the detection of IGR J16479–4514 on 11 August 2004 (No.6 in table 5.1). 109
5.6 The ISGRI light curve (20–40 keV) of the detection of IGR J16479–4514 on 7 September 2004 (No.7 in table 5.1). 109
5.7 The ISGRI light curve (20–60 keV) of outburst No. 8 (in table 5.1) of IGR J16479–4514. 110
5.8 The ISGRI light curve (20–60 keV) of outburst No. 9 (in table 5.1) of IGR J16479–4514. 110
5.9 The ISGRI light curve (20–60 keV) of the detection of IGR J16479–4514 on 12 August 2005 (No.10 in table 5.1). 110
5.10 The ISGRI light curve (20–60 keV) of the detection of IGR J16479–4514 on 30 August 2005 (No.11 in table 5.1). 111
5.11 Unfolded black body spectrum (20–60 keV) of IGR J16479–4514 during the outburst No. 11 in table 5.1. 111
5.12 RXTE ASM dwell by dwell light curve (2–12 keV) of IGR J17407–2808 from 1996 to 2006. In the light curve 20 c s^{-1} is equivalent to a flux of 250 mCrab. Time axis is in MJD. The seven outbursts detected by RXTE, with a flux greater than 250 mCrab, are indicated in the light curve by means of numbers from 1 to 7. 113
5.13 The ISGRI light curve (20–30 keV) of the detection of IGR J17407–2808 on 20 march 2003 (No.1 in table 5.3). 114
5.14 Unfolded black body spectrum of outburst No. 1 of IGR J17407–2808 . 114
5.15 The ISGRI light curve (20–60 keV) of the detection of IGR J17407–2808 on 9 October 2004 (outburst No.2 in table 5.3). 115
5.16 ISGRI 20–60 keV significance image extracted during the strongest flare in figure 5.15 (69 seconds exposure time). IGR J17407–2808 is clearly detected at a level of $\sim 15\,\sigma$. 115
5.17 Unfolded bremsstrahlung spectrum of the strongest flare in figure 5.15. . 115
5.18 ISGRI light curve (20–60 keV) of AX J1749.1–2733 during the newly discovered outburst occurred on 9 September 2003. Time axis is on MJD. Each data point represents the average flux during one ScW (~2000 seconds). 117
5.19 Zoomed view of the flaring activity of AX J1749.1–2733 shown in figure 5.18. Note that the bin time is smaller than that in figure 5.18. 117
5.20 JEM–X significance mosaic map in the energy band 10–20 keV. AX J1749.1–2733 is circled in the map, detected at $\sim 40\sigma$ level. 118

5.21 Unfolded absorbed power law spectrum of AX J1749.1−2733 (3–80 keV) during the outburst occurred on 9 September 2003. 118
5.22 Unfolded black body spectrum (20–80 keV) of AX J1749.1−2733 during the outburst that occurred on 9 September 2003. 118
5.23 MSX infrared image (8.28 μm) overlapped on the ISGRI error circle of AX J1749.1−2733 119
5.24 ISGRI ScW significance image sequence (20–300 keV) of the outburst from IGR J11321−5311 (encircled). The source was not detected in the first ScW, then it was detected during the next 4 ScWs with a significance, from left to right, equal to 12σ, 8σ, 5σ and 4σ, respectively. Finally in the last ScW there is no detection. 121
5.25 ISGRI light curve (20–300 keV) of IGR J11321−5311. 121
5.26 ISGRI light curves of IGR J11321−5311 in the energy bands 20–100 keV (middle panel) and 100–300 keV (top panel). In the lower panel, the ratio of the two light curves is shown. 122
5.27 Unfolded power law plus black body spectrum (17–300 keV) of IGR J11321−5311 extracted during its total outburst activity. 122
5.28 Unfolded power law plus black body spectra (17–300 keV) of IGR J11321−5311 extracted from the sum of ScW A and B (top), C and D (bottom). 124
5.29 Confidence countour levels for the photon index and the normalization costant of the power law model pertaining the spectra extracted from the sum of ScW A+B and C+D. 124
5.30 *Swift* XRT observation of IGR J11321−5311 (circled) on December 2006 (0.2–10 keV). 125
5.31 *Swift* XRT observation of IGR J11321−5311 (circled) on January 2007 (0.2–10 keV). 125
5.32 ISGRI light curve (20–100 keV) of a newly discovered outburst of IGR J18483−0311 that occurred in April 2006 (No.1 in table 5.4). 129
5.33 Unfolded JEM−X and ISGRI spectrum (3–50 keV) of IGR J18483−0311 during outburst No.1 in table 5.4. 130
5.34 Confidence contours level for the photon index and the cutoff energy from the spectral analysis of the outburst No.1 in table 5.4. 130
5.35 ISGRI light curve (20–60 keV) of a newly discovered outburst of IGR J18483−0311 that occurred in September 2004 (No.2 in table 5.4). . . . 131
5.36 Unfolded bremsstrahlung spectrum (20–60 keV) of IGR J18483−0311 during outburst No.2 in table 5.4. 131

5.37 ISGRI light curve (20–60 keV) of a newly discovered outburst of IGR J18483–0311 that occurred in April 2004 (No.3 in table 5.4). 132
5.38 Unfolded bremsstrahlung spectrum of outburst No.3 in table 5.4. 132
5.39 ISGRI light curve (20–40 keV) of a newly discovered outburst of IGR J18483–0311 that occurred in March 2004 (No. 4 in table 5.4). 134
5.40 Unfolded bremsstrahlung spectrum of outburst No.4 in table 5.4. 134
5.41 ISGRI light curve (20–60 keV) of a newly discovered outburst of IGR J18483–0311 that occurred in May 2003 (No. 5 in table 5.4). 135
5.42 Unfolded bremsstrahlung spectrum (20–60 keV) of outburst No.5 in in table 5.4. 135
5.43 Lomb-Scargle periodogram generated from the 20–40 keV light long term curve of IGR J18483–0311 138
5.44 The phase-folded 20–40 keV light curve of IGR J18483–0311. The data are folded on a period of 18.52 days. 138
5.45 Lomb-Scargle periodogram generated from the JEM–X 4–20 keV light curve of IGR J18483–0311 during the outburst No.1 in table 5.4. The periodicity at 0.04750 Hz is clearly apparent, as are the 1^{st}, 2^{nd} and 3^{rd} harmonics. 141
5.46 The phase-folded 4–20 keV light curve of IGR J18483–0311. The data are folded on a period of 21.0526 seconds. 141
5.47 *Swift* XRT light curve (0.2–10 keV) light curve of the two *Swift* XRT observations. The bin time is 200 seconds. Time axis is in seconds, counted from the beginning of the first *Swift* XRT observation. Flux axis is in count/sec. 142
5.48 USNO B1.0 optical field image (R2 magnitude). The circles represent, from larger to smaller, the ISGRI error circle of IGR J18483–0311 (Bird et al. 2006), ROSAT (Stephen et al. 2006) and *Swift* (this PhD thesis). As we can note, the accurate *Swift* position allow us to identify the likely optical counterpart for IGR J18483–0311. 144
5.49 ASCA light curve (1–10 keV) of AX J161929–4945 during the observation on September 1997. Credit: Sidoli et al. (2005) 146
5.50 ISGRI light curve (20–40 keV) of AX J161929–4945 during the outburst occurred on 26 September 2003 (No. 3 in table 5.8). Time axis is in MJD. Each data point represents the average flux during one ScW (~2000 seconds). 148

5.51 Zoomed view of the flare showed in figure 5.50. Note that the bin time is smaller than that in figure 5.50. 148
5.52 Unfolded black body spectrum (20–60 keV) of the outburst No. 3 in table 5.8. 149
5.53 ISGRI mosaic significance map of AX J161929–4945 (circled) during outburst No. 4 in table 5.8. The source is detected at ~ 6σ level (20–30 keV). 149
5.54 ISGRI light curve (20–30 keV) of AX J161929–4945 during the outburst No. 4 in table 5.8. 149
6.1 Angular distribution off the galactic plane of the 8 SFXTs reported in table 6.1 (horizontal hatched bars), of the 6 candidate SFXTs in table 6.2 (filled black bars) and of all galactic HMXBs (empty white bars) as taken from the third IBIS/ISGRI gamma-ray catalog (Bird et al. 2007). . 154
6.2 Duration of all outbursts detected by IBIS from the 8 SFXTs (filled black bars) and from the 6 candidate SFXTs (diagonal hatched bars). 154
6.3 Distribution of the temperature kT of the bremsstrahlung spectra of the firm SFXTs (horizontal hatched bars) and of the candidate SFXTs (filled black bars). 155
6.4 Distribution of the temperature kT of the black body spectra of the firm SFXTs (filled black bars) and of the candidate SFXTs (horizontal hatched bars). 155
6.5 Distribution of the radius of the emitting black body regions (Km) of firm SFXTs with known distances (horizontal hatched bars) and unknown distances (filled black bars). For the latter, a rough estimation of the distance was obtained from their location in the direction of the galactic spiral arms Norma and Scutum (see table 6.1). 156
6.6 Schematic representation of a pulsar magnetosphere. The field lines from the magnetic dipole moment μ are inclined at angle α with the rotation axis. They will corotate with the pulsar at angular velocity Ω out to a radial distance R_L=c/ Ω where the field lines will be swept along at the speed of light c. Field lines which cross the light cylinder defined by R_L do not return to the surface of the neutron star, and are referred to as open field lines. Radiation escapes along these open field lines outside the shaded regions. The last closed magnetic field lines, which just touch the light cylinder, define the edge of the two polar cap regions on the neutron star surface. 157

6.7 Distribution of the photon index of the power law spectra of the 8 SFXTs (horizontal hatched bars) and the 6 candidate SFXTs (filled black bars). . 158

List of Tables

3.1 An overview of the IBIS scientific capabilities. 50

4.1 Summary of ISGRI observations of outbursts of XTE J1739–302. 61

4.2 Summary of ISGRI observations of outbursts of IGR J17544–2619 68

4.3 Summary of IBIS observations of outbursts of AX J1841.0-0536 72

4.4 Summary of INTEGRAL, *Swift* and ASCA observations of outbursts of AX J1845.0–0433 77

4.5 Summary of newly discovered outbursts of SAX J1818.6–1703 by INTEGRAL 85

4.6 Summary of ISGRI observations of outbursts of IGR J11215–5952 93

4.7 Summary of INTEGRAL observations of outbursts of IGR J16465–4507 96

4.8 Summary of INTEGRAL observations of outbursts of IGR J08408–4503 101

5.1 Summary of INTEGRAL observations of outbursts of IGR J16479–4514. 103

5.2 USNO–B1.0 optical sources located inside the ROSAT error circle of IGR J17407–2808. 112

5.3 Summary of ISGRI observations of outbursts of IGR J17407–2808. . . . 113

5.4 Summary of IBIS detections of newly discovered outbursts from IGR J18483–0311. 129

5.5 Summary of spectral analysis of the 5 newly discovered outbursts from IGR J18483–0311. The name of the spectral models are written in XSPEC terminology. 136

5.6 Analysis of the 20–40 keV long term light curve of IGR J18483–0311 around the expected start time of outbursts based upon the 18.52 days periodicity. For the outburst numbers not listed there was no significant coverage of the source by INTEGRAL around those times. 139

5.7 Summary of *Swift* XRT observations of IGR J18483–0311. 143

5.8 Summary of INTEGRAL observations of outbursts of AX J161929–4945. 147

6.1 Summary of characteristics of the 8 SFXTs , •=assuming a distance of 10 kpc, ⊙ = assuming a distance of 6 kpc 161
6.2 Summary of characteristics of the 6 candidate SFXTs 162

Chapter 1

Introduction: gamma-ray astronomy

I do not know what I may appear to the world, but to myself
I seem to have been only a boy playing on the sea-shore,
and diverting myself in now and then finding a smoother
pebble or a prettier shell than ordinary, whilst the
great ocean of truth lay all undiscovered before me.
– Isaac Newton

1.1 Introduction

Up to ~ 60 years ago, astronomy essentially meant optical astronomy since the universe could only be studied in the optical waveband. Since then, there has been a huge development of other wavebands for astronomical studies which has led to the birth and growth of new disciplines such as radio, millimetre, infrared, ultraviolet, X-ray and γ-ray astronomy. In particular, none of these developments has been more dramatic than the rise of γ-ray astronomy which is only now becoming part of the mainstream astrophysics. The techniques needed to detect γ-ray photons have only become available since the late 1960's, moreover the most important results in this relatively new and young field have been obtained in little more than twenty years, during which we learned that the γ-ray sky is very rich in high energy phenomena. It is in the γ-ray band that non-thermal emission processes dominate and in which we can study the behaviour of some of the most energetic and extreme objects in the universe.

The classification of high energy photons is arbitrary and considerable overlaps are noted in the literature. Therefore to avoid confusion, in this thesis the term γ-ray is used to denote electromagnetic photons with energies greater than ~ 100 keV; the term soft γ-ray refers to photons with energies in the range 15–100 keV.

1.2 Gamma-ray production mechanisms

There are several important mechanisms which can produce γ-rays in astrophysical objects:

- **Blackbody emission** – if the temperature is in excess of $\sim 6{\times}10^7$ Kelvin, the maximum intensity of a black body will emit at energies greater than 20 keV, producing soft γ-ray photons. Temperatures of this order can be obtained only in extreme astrophysical environments, i.e. the accretion disks of stellar mass black holes.

- **Bremsstrahlung radiation** – the name is German for braking radiation. It is emitted by a charged particle moving in an electric field, such as the Couloumb field of an ion. The charged particle emits energy in the form of electromagnetic radiation, at the expense of its kinetic energy, hence the name braking radiation. The energy emitted is proportional to 1/m, with m the rest mass of the particle; bremsstrahlung therefore plays a particularly important role for light particles, i.e. electrons. Considering a population of electrons with a uniform temperature in the presence of an electric field, the total emission by all electrons in this population is called thermal bremsstrahlung. The higher the temperature, the faster the motion of the electrons and consequently the higher the energy of the emitted photons. Temperatures of the order of $\sim 10^8$ K are necessary to produce γ-rays.

- **Synchroton radiation** – is emitted when a fast electron interacts with a magnetic field. The latter will cause the electron to change direction by exerting a force on it perpendicular to the direction of the electron. As a result, the electron will be accelerated, causing it to radiate electromagnetic energy. This is called synchroton radiation after radiation observed from particle accelerators by that name. The resulting emission is concentrated in a narrow beam in the direction of the path of the electron. In an ensemble of electrons moving in an isotropic fashion, the frequency of the emitted radiation depends on the magnetic field strength and on the energy of the electron. If the initial energy distribution of the electrons is a power-law, then the resulting synchroton emission will also have a power-law distribution (i.e. non thermal). If the electrons and the magnetic field are energetic enough, the emitted radiation can be in the form of γ-rays.

- **Inverse Compton scattering** – takes place when a high energy relativistic electron scatters a low energy photon to high energy so that the photon gains and the electron loses energy. This process requires high photon densities. In the case of

an ensemble of electrons where there are multiple scatterings, the frequency of the up-scattered photons is proportional to $\gamma_e^2\nu$, where γ_e is the Lorentz factor of the electron and ν is the initial photon frequency. This has important implications in high energy astrophysics. There are electrons with Lorentz factor of $\gamma_e \sim$ 100–1000 in many astronomical sources, consequently they scatter any low energy photons to very much high energies whenever they pass through a region in which there is a large energy density of photons. For example, optical photons with $\nu=4\times10^{14}$ Hz become γ-rays with frequency $\nu=4\times10^{20}$ Hz ($\sim$ 1.6 MeV) when scattered by electrons with $\gamma_e=1000$.

- **Electron – Positron Annihilation** – when a positron meets an electron, they annihilate, producing two γ-ray photons with energies equivalent to the rest mass of an electron (511 keV). Sometimes however, depending on the temperature and density of the ambient medium, the annihilation is preceded by the formation of positronium, which is like a hydrogen atom with the proton replaced by a positron. Positronium is unstable and comes in two states. The singlet state decays into two 511 keV γ-ray photons, whereas the triplet state decays in three γ-ray photons continuum with a long tail below the 511 keV line. Positrons can be produced from the decay of pions, from the decay of radioactive nuclei, and from the de-excitation of excited nuclei.

- **De-excitation of nuclei** – results in characteristic γ-rays being emitted. The classic example of this is through the radioactive decay of unstable isotopes. However, nuclei may also be placed in an excited state through collisions with energetic particles, e.g. cosmic rays. As the γ-rays emitted are dependent upon the type of nucleus and the level of excitation, this leads to line emission which can be used to identify isotopic abundances.

- **Nuclear interactions** – when cosmic rays (relativistic protons and nuclei) collide with atomic nuclei of the intestellar gas, then neutral pions are produced, the decay of which produces emission at energy greater than 100 MeV. This is an important process in the production of diffuse γ-ray photons.

1.2.1 Energy yield in accretion

The engine that drives the powerful high energy output characteristic in galactic (i.e. X-ray binaries) and extragalactic (i.e. Active Galactic Nuclei AGN) systems is the accretion of matter onto a compact object. The energy available through accretion is the release of

gravitational potential energy as material falls onto the compact object. The gravitational potential energy E released by the accretion of mass m onto the surface of a compact object having mass M_c and radius R_c is given by:

$$E_{acc} = \frac{GM_c m}{R_c} \tag{1.1}$$

If matter is continuously supplied over time, then the luminosity attributable to accretion is given by:

$$L_{acc} = \frac{GM_c}{R_c}\frac{dm}{dt} \tag{1.2}$$

As the matter is accreted, the gravitational potential energy is released by heating the material within the accretion disk. The equation 1.2 can be rewritten in the form:

$$L_{acc} = \eta c^2 \frac{dm}{dt} \tag{1.3}$$

where η

$$\eta = \frac{GM_c}{R_c c^2} \tag{1.4}$$

is the efficiency of the accretion process. It simply depends on how compact the object is. For a neutron star with mass M_c=1 $M_\odot$ and R_c=15 km, the efficiency is $\eta \sim 0.1$. Thus, accretion onto neutron stars is a remarkably powerful source of energy, far more efficient than accretion onto a white dwarf ($\eta \sim 0.001$) or nuclear energy generation by fusion ($\eta \sim 0.001$). A simple interpretation of equation 1.4 suggests that it could be even better if the material were accreted onto a black hole. However in this case the situation is complicated by the fact that there is no solid surface onto which the material can be accreted as there is in the case of a neutron star, moreover a lot of the accretion energy may be dissipated. Assuming that the Schwarzchild radius plays the role of the surface of the black hole, the efficiency factor η is ~ 0.06 for a non rotating Schwarzchild black hole while it is equal to ~ 0.43 for a maximally rotating Kerr black hole. Thus, black holes are the most powerful energy sources known in the universe.

It might seem that it could be possible to generate arbitrarily large luminosities by accreting material at a sufficiently great rate onto a black hole. There is, however, a limit to the luminosity determined by the fact that, if the luminosity is too high, radiation pressure blows away the infalling material. This limiting luminosity is known as the Eddington luminosity and is obtained by balancing the inward force of gravity against the outward pressure of the radiation

$$L_{Edd} = \frac{GM_c mc4\pi}{\sigma_T} = 1.3 \times 10^{38}(M/M_\odot)ergs^{-1} \quad (1.5)$$

where M_c is the mass of the compact object, m is the mass of an accreting particle (~ proton mass) and σ_T is the Thomson cross section for scattering electrons.

1.3 Instrumentation and techniques of γ-ray astronomy

Several very important factors govern the techniques that are used in γ-ray astronomy. They are the main reason why γ-ray astronomy is such a difficult research field, and why it took so long to really explore this field.

1. γ-rays coming from space are mostly absorbed by the Earth's atmosphere. Thus γ-ray astronomy is as old as the space age, it could not develop until it was possible to get γ-ray detectors above all or most of the atmosphere, using balloons or spacecrafts.

2. The flux of high-energy charged cosmic rays is much larger than the γ-ray flux from astrophysical sources. These charged particles are bent in the interstellar magnetic fields so that they form an essentially isotropic background. In space, a γ-ray telescope is bombarded from all directions by this enormous background, so its rejection is extremely important. Shielding systems are required to limit the detector response to background γ-rays and hence to improve the instrument sensitivity. There are two main type of shielding: passive and active. Passive shielding uses high atomic number material (i.e. lead or tungsten) to block and fully absorb charged background γ-rays. This system is particularly efficient at energies less than few hundreds keV. However, with increasing background photon energy, passive shielding becomes impratical due to the increasing heaviness of the required amount of absorbing material. In this case active shielding is a better solution. It does not block and fully absorb the background γ-rays. On the contrary it uses a scattering event in a surrounding detector to act as a veto so that any simultaneous event in the primary detector can be rejected. Therefore, if there is a coincident event in the veto and detector, it is assumed to have come from outside the telescope FOV and so it is rejected.

3. γ-ray fluxes from astrophysical sources are extremely low, so sophisticated and large area instruments are an absolute must for γ-ray observations. However, since it is necessary to fly them on spacecraft, there are weight restrictions upon their

size. Moreover, γ-ray fluxes decrease rapidly as the photon energy increases, this means that above some energy (i.e. TeV) a detector onboard a satellite (i.e. $\sim$ 1000 cm^2) will be too small to detect enough photons to be useful. The pursuit of γ-ray astronomy at very high-energies (i.e. TeV) must be done using instruments much larger than that typically launched onboard satellites. This can be obtained using earth-based detectors (having a detector area very large, typically $> 10^4$ m^2) in the form of imaging atmospheric Cherenkov telescopes.

4. γ-ray photons, due to their high-energy nature, cannot be focused. Alternative imaging and detection techniques have to be used (i.e. coded masks, Compton telescopes, pair telescopes). This is probably the most important as it means that the standard solutions to (2) and (3) that have been employed in other wavebands do not work.

1.3.1 Gamma-ray interaction methods

A knowledge of γ-ray interactions is very important since a γ-ray must interact with a detector in order to be "seen". The γ-ray photons lose their energy interacting with matter (atoms, nuclei or electrons) mainly by these three major processes: photoelectric effect, Compton effect, and pair production. Which process is dominant is dependent upon the energy of the incoming γ-ray photon and the atomic number (Z) of the absorbing material. Figure 1.1 shows the three γ-ray interaction processes as a function of energy and atomic number of absorbing material. It is worth pointing out that in the energy range 500 keV–5 MeV all three processes make a significant contribution, this means that this is a particularly difficult energy range for the design and construction of γ-ray telescopes.

1.3.1.1 The photoelectric effect

This process dominates at low energies (<1 MeV) and in high Z materials. It rapidly diminishes in efficiency as the energy increases. The process arises by the interaction of the γ-ray photon with a tightly bound atomic electron. The energy of the γ-ray is transferred to the electron which is ejected from the atom with an energy E_e given by

$$E_e = h\nu - E_b \tag{1.6}$$

where $h\nu$ is the absorbed γ-ray photon energy and E_b is the binding energy of the photoelectron in its original shell. As the photoelectron is ejected, a vacancy is produced in the atomic orbital which is then filled with an electron from a higher atomic orbit. This

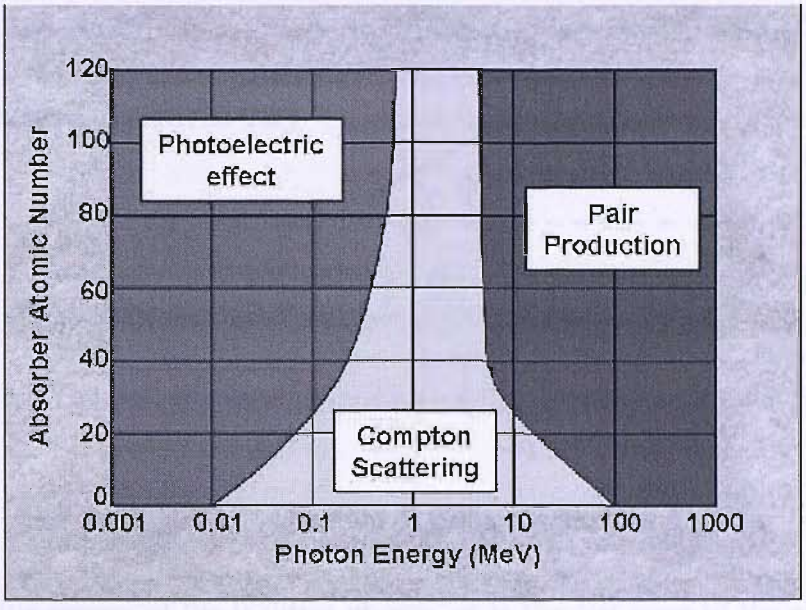

Figure 1.1: γ-ray interaction processes as a function of energy and atomic number of absorbing material.

process results in the emission of an X ray, which is itself absorbed in the material, resulting in all of the initial photon energy being absorbed in the material. The probability of photoelectric absorption (τ) is found to vary approximately with the atomic number (Z) of the detector material, according to

$$\tau \propto Z^5 \tag{1.7}$$

Therefore, high Z materials are used as γ-ray detectors and for shielding against X-rays and low energy γ-rays.

1.3.1.2 Compton scattering

Compton scattering is the dominant γ-ray attenuation process at energies of ~ 1 MeV, for which the binding energy of an electron in an atom becomes less important and the electrons can be considered free. It occurs when the incoming γ-ray photons collide with stationary electrons and transfer some of their energy and momentum to the electrons (see figure 1.2). Consequently, the photons come out of the collisions with less energy and momentum than they went in. The energy of the scattered photon can be expressed as:

$$E_\gamma^{'} = \frac{E_\gamma}{1 + \frac{E_\gamma}{mc^2}(1 - \cos\theta)} \tag{1.8}$$

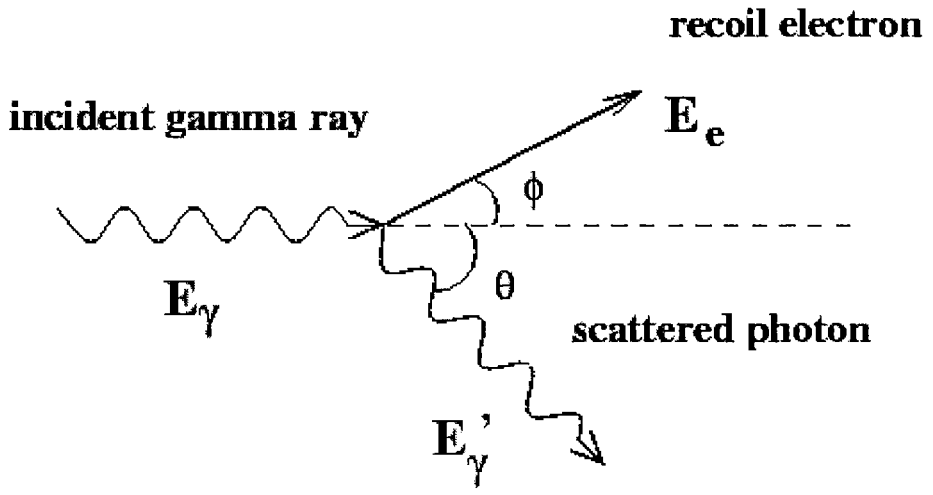

Figure 1.2: Diagram of Compton scattering

where E_γ is the energy of the incident photon, m is the rest mass of the electron and θ is the scattering angle of the photon. For θ=0° (i.e. no scattering) the recoil electron has very little energy, while for θ=180° (back scattering) maximum energy transfer occurs and the electron continues along the initial photon direction.

1.3.1.3 Pair production

Pair production refers to the creation of a particle and its antiparticle from a high energy photon interacting with an atomic nucleus, so that momentum can be conserved. The most common particle-antiparticle produced is an electron and positron requiring a γ-ray photon of energy greater than 1.022 MeV (i.e. twice the rest mass of an electron). Any excess energy is transferred in the form of kinetic energy of the electron-positron pair. The positron that is formed quickly disappears by reconversion into two γ-ray photons of energy 511 keV in the process of annihilation with another electron in matter. Pair production dominates over photoelectric and Compton effects at energies > 5 MeV.

1.3.2 Gamma-ray telescopes

When γ-rays interact with matter, they transfer some or all of their energy to the material. γ-ray detectors use materials in which the energy deposited produces a measurable change via production of electronic charge, a chemical change, an increase in temperature or emission of ultraviolet (UV) or optical photons. The aim of a γ-ray telescope is not only to register a γ-ray detection, but also provide additional information such as the amount of energy carried by the incident photon and its direction. The latter is indispensable to pinpoint the location of the source. However γ-ray photons, due to their high-energy

nature, can not be focused. Focusing is so far technically feasible only for photon energies up to $\sim$ 10 keV through grazing incidence reflection. Alternative imaging and detection techniques are required in the γ-ray domain. The following sections briefly outline the type of detectors and the different detection techniques used in γ-ray telescopes.

1.3.2.1 Detector types

Scintillation counters work by the interaction of a γ-ray with the scintillator material. Charged particles are produced, which will cause the material to scintillate generating low energy (usually optical/UV) photons. They are then collected by a photomultiplier tube or a solid state photo-diode. Scintillators can be of organic or inorganic material. Organic can exist in liquid or crystal form, they are of lower density (i.e. less stopping power). Therefore, the most common scintillators used in γ-ray astronomy are made of higher density inorganic materials such as sodium iodide (NaI) or caesium iodide (CsI).

A gas-filled detector consists of a chamber of gas across which an electric field is applied. These detectors are limited to an energy range up to $\sim$ 150 keV. An incident γ-ray photon is able to ionise the gas via the photoelectric effect and produce an electron-ion pair which will move under the influence of the applied voltage. If the voltage is high, the ions will gain sufficient kinetic energy to further ionise neutral atoms in the gas producing even more electrons, the resulting signal being proportional to the inital photon energy. The gas-filled detector working in the proportional regime are called proportional counters. The Geiger counters work at regimes of higher voltages, while the ionising chamber detectors work at very low voltage regimes.

Solid state detectors work on a similar principle to a gas counter but operate at higher energies, typically from few keV to MeV. An incoming γ-ray causes photoelectric ionisation of the material, so an electric charge will be collected if a voltage is applied to the material. Solid state detectors are usually made from Germanium or Cadmium-Zinc-Telluride semiconducting material.

1.3.2.2 Coded aperture mask

This technique enables the creation of images with arcminute resolution in the energy band 10 keV–20 MeV. A coded mask (see for a review in't Zand et al. 1992 and Skinner & Ponman 1994) consists of an optimal distribution of opaque and transparent elements through which a source will project a shadow onto the detector plane (shadowgram) allowing simultaneous measurement of source and background fluxes. The phase of the pattern in the detector plane will change depending on the position of the source in the

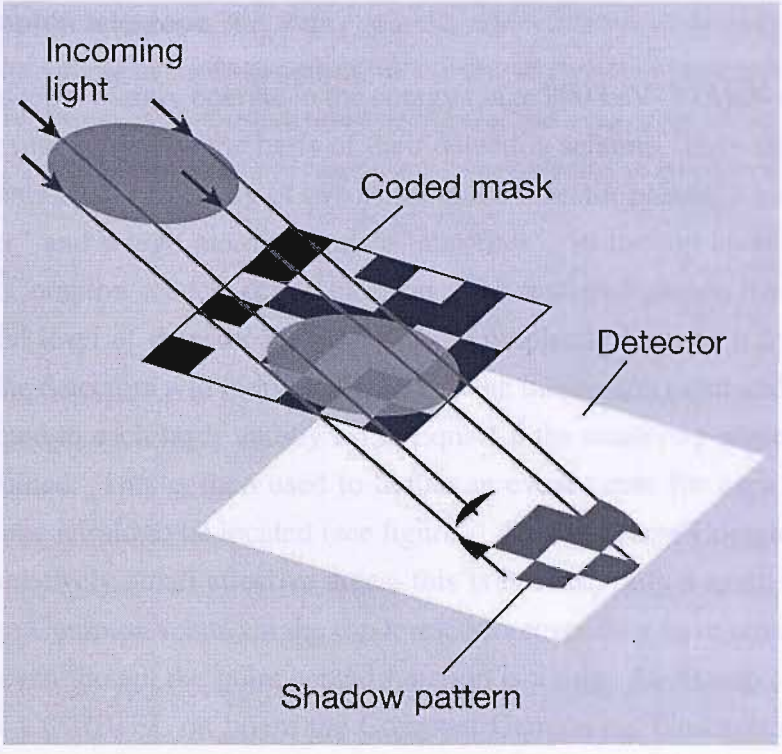

Figure 1.3: Simplified model of a coded mask system.

sky. By knowing the pointing direction of the telescope, an image of the area of the sky can be reconstructed by correlating the recorded image with a decoding array derived from the mask pattern. Figure 1.3 shows a simplified model of a coded mask system.

The angular resolution dθ of a coded mask is defined as:

$$d\theta = arctan\frac{S}{D} \tag{1.9}$$

where S is the mask element size and D is the distance between the mask and the detector. The point source location accuracy of a source with significance σ is:

$$d\phi = \frac{arctan\frac{P}{D}}{\sigma} \tag{1.10}$$

where P is the detector pixel size $\leq$ S.

A large field of view (FOV) can be obtained in coded aperture masks. Two kinds of FOV are defined: the fully coded (FC) for which the entire basic pattern shadow falls onto the detector, and the Partially Coded (PC) for which only a fraction of the pattern appears on the detector plane while the rest, if detected, cannot be distinguished from the background. If mask elements are uniformly distributed, the sensitivity is constant in the FC FOV and decreasing in the PC FOV.

1.3.2.3 Compton telescope

Compton telescopes mainly operate in the energy range 300 keV–30 MeV and use Compton scattering interactions as the basis of their detection scheme. They are typically two level instruments often consisting of two scintillation detector planes: a low atomic number "converter" and a high atomic number "absorber". In the top level scintillator the cosmic γ-ray Compton scatters off an electron. The scattered photon then travels down into the second level of detector material which completely absorbs it by photoelectric absorption. The detectors will individually record the interaction point and the amount of energy deposited in each layer and by using Eqn. 1.8 the scattering angle of the photon can be determined. This is then used to define an event circle for each photon within which the source is said to be located (see figure 1.4). Even large Compton-scatter telescopes have relatively small effective areas, this is because only a small number of the incident γ-rays Compton scatter in the top level. Moreover they have wide FOV and can form images even though the point spread function is a ring. An example of a Compton telescope was COMPTEL on board the Compton Gamma-ray Observatory (CGRO). It operated between 1 MeV–30 MeV with an angular resolution of ~ 1° (Schoenfelder et al. 1993).

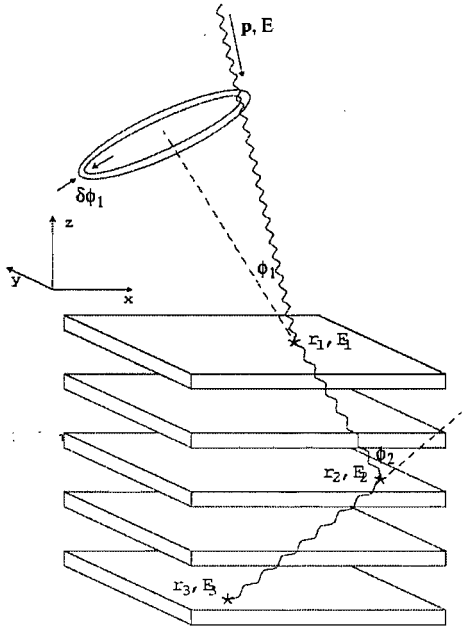

Figure 1.4: Example of Compton telescope. If a photon undergoes one or more Compton scatters in the instrument and then is photoelectrically absorbed, then by using the positions $(\vec{r}_1, \ldots, \vec{r}_N)$ and energy deposits $(E_1, \ldots, E_N)$ of the interactions, the initial direction of the photon can be determined by the Compton scatter formula to within an annulus on the sky, ϕ_1. The width of this annulus is determined by the uncertainties in both the interaction locations and energy deposits

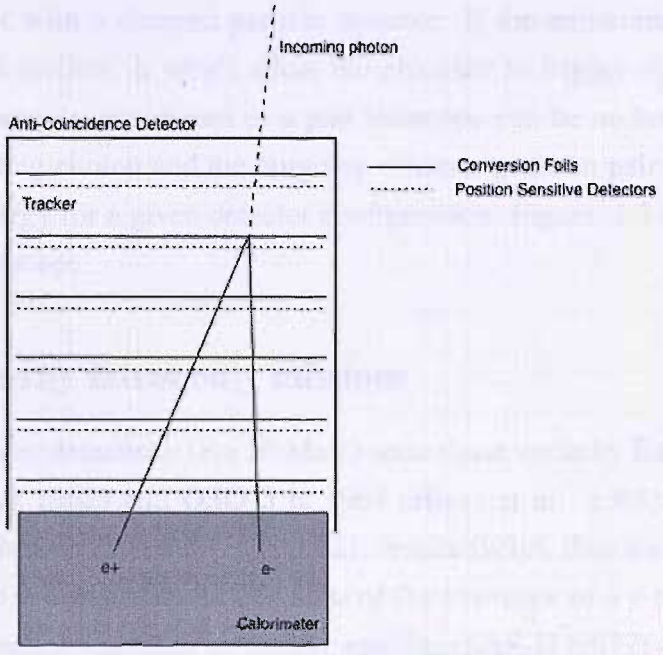

Figure 1.5: Principle of photon detection in a pair telescope. The instrument is basically made of an anti-coincidence detector, a tracker/converter module and a calorimeter for the measure of the energy.

1.3.2.4 The pair telescope

The pair telescope (often in the form of a spark chamber) detects high energy γ-ray photons (E > 30 MeV) using techniques which were developed in experiments at accelerators. At energies above 30 MeV, pair production is the dominant photon interaction in most materials. Pair telescopes are usually made of converter layers interleaved with tracking material. The converter layer is typically a high Z material (heavy metal) which provides the target for creating the initial pair. The tracking material is usually a gas filled region criss-crossed with wires which is aimed to detect the pair. As a γ-ray photon travels through the pair telescope, its interaction with one of the converter layers will produce an electron-positron pair. Then they traverse the tracking material ionizing the gas. Triggering the detector causes the wires to be electrified, attracting the free electrons which provides the detected signal. The trail of sparks essentially provides a three dimensional picture of the pair path. By reconstructing the tracks of the charged pair as it passes through the vertical series of trackers, the γ-ray direction and therefore its origin on the sky are calculated. In addition, through the absorption of the pair by a scintillator detector or a calorimeter after they exit the spark chamber, the total energy of the initial γ-ray can be determined. It is very important to keep the telescope from triggering on the overwhelming flux of cosmic rays. To this aim, anti–coincidence shields will cover

the entire telescope with a charged particle detector. If the anti-coincidence shield has detected a charged particle, it won't allow the chamber to trigger to prevent detecting cosmic rays. The angular resolution of a pair telescope can be no better than the angle between the incoming photon and the outgoing electron-positron pair and it is improved with increasing energy for a given detector configuration. Figure 1.5 shows a simplified model of a pair telescope.

1.3.3 Gamma-ray astronomy missions

The first cosmic γ-ray detections (E> 50 MeV) were those made by **Explorer-11** in 1961 (Kraushaar & Clark 1962) and **OSO-3** in 1968 (Hicks et al. 1965). Despite the low number of γ-ray photons detected (61 and 621, respectively), they served to confirm the presence of cosmic γ-rays and to furnish hints of the existence of a γ-ray background.

A major step forward was taken by the two satellites **SAS-II** (1972) and **COS-B** (1975) having energies range of 30 MeV–5 GeV and 100 MeV–5 GeV, respectively. An electronic failure terminated the SAS-II mission (Derdeyn et al. 1972) after only seven months of operation. Nevertheless, SAS-II provided evidence of emission above 100 MeV from the galactic plane as well as the detection of 4 γ-ray point sources (Crab, Vela, Cygnus X-3 and Geminga, the latter not identified at that time). The COS-B satellite (Scarsi et al. 1977) operated for 6.5 years producing the first detailed map of the γ-ray sky. The most important result was a catalog of 25 sources (E>300 MeV) of which only one (3C273) was extragalactic (Swanenburg et al. 1981). However, most of the sources were detected by COS-B but not identified at other wavelength due to lack of sufficient angular resolution imaging technology. Figure 1.6 shows the second COS-B catalog of point like γ-ray sources.

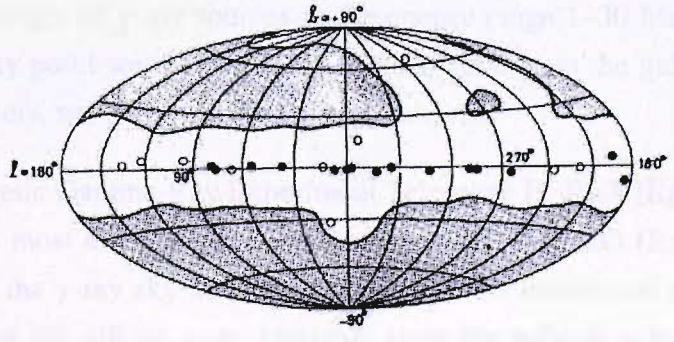

Figure 1.6: Second COS-B catalog of point like γ-ray sources. Open circles denote faint sources, filled circles brighter ones. The dividing line is at 1.3 10^{-6} ph/cm^{2}sec. The shaded area was not searched for sources since the coverage by COS-B was not adequate. Picture taken from Swanenburg et al. 1981.

During the 1980s there were no satellite γ-ray missions, the results in high energy γ-ray were still somewhat sparse. Then, in the 1990s γ-ray astronomy matured. This golden age started in December 1989 with the launch of the French telescope **SIGMA** onboard the Russian GRANAT mission. SIGMA (Paul et al. 1991) was the first γ-ray detector to employ a coded mask, allowing imaging in the transition region between X-ray and γ-ray astronomy (mainly around 100 keV) with an unprecedented angular resolution of $\sim$ 10 arcminutes. It mainly observed the galactic center region, detecting $\sim$ 30 sources, principally compact objects with stellar black hole candidates. The real breakthrough was achieved by the Compton Gamma-Ray Observatory **CGRO** (1991-1999) which established the role of γ-ray astronomy as an important branch of astrophysics. The CGRO (Gehrels et al. 1994) had four instruments on board that covered an unprecedented six decades of the electromagnetic spectrum, from 30 keV to 30 GeV. In order of increasing spectral energy coverage, these instruments were:

- The Burst And Transient Source Experiment, BATSE (Fishman et al. 1989). It served as the all-sky monitor for the CGRO detecting and locating strong transient sources, as gamma-ray bursts or outbursts from other sources, over the entire sky. There were eight detectors, one facing outward from each corner of the satellite, which were sensitive to γ-ray energies from 20 keV to over 1 MeV.

- The Oriented Scintillation Spectrometer Experiment OSSE (Gehrels et al. 1994). This instrument (50 keV–10 MeV) has produced observations of the energy spectrum of nuclear lines in solar flares, point sources, the radioactive decay of nuclei in supernova remnants, and the signature of matter-antimatter (electron-positron) annihilation in the galactic center region.

- The Imaging Compton Telescope COMPTEL (Schoenfelder et al. 1993). It reconstructed images of γ-ray sources in the energy range 1–30 MeV. Supernova remnants, γ-ray point sources and 1.8 MeV Al^{26} line from the galactic center region, among others, were studied with this instrument.

- The Energetic Gamma-Ray Experiment Telescope EGRET (Kanbach et al. 1988). It was the most energetic experiment onboard the CGRO (E>100 MeV). Figure 1.7 shows the γ-ray sky as seen by EGRET. This instrument made the first accurate map of the diffuse γ-ray emission from the galactic plane and detected 271 point-like sources (100 MeV–10 GeV) listed in the Third EGRET Catalogue 3EG (Hartman et al 1999). Ninety-three sources are AGNs classified as belonging to the blazar class, with the only exception being the nearby radio galaxy Cen A. Most of

them are located at latitude |b|>10°. Gamma-ray blazars represent a new class of objects discovered by EGRET, showing high and variable γ-ray luminosities. Most of the EGRET blazars are very strong radio sources with flat radio spectra, they also show high variability in various wavebands and superluminal motions have been observed in some cases. The combination of these characteristics support the argument of relativistic beaming in jets which are pointing close to the line of sight. Apart from blazars, EGRET detected pulsed and non variable high-energy emission from 7 pulsars (e.g. Crab, Vela, Geminga). The remaining 171 sources listed in the 3EG catalog are still unidentified, with no firmly established counterparts at other wavebands. Seventy-five unidentified EGRET sources are located at latitudes |b|<10° while the remaining 96 are located at |b|>10°. Figure 1.8 shows the distribution in the sky in galactic coordinates of all 271 point-sources reported in the 3EG catalog. The huge number of unidentified sources is mainly due to the quite large positional uncertainty of the EGRET error boxes. Low counting rates combined with a broad energy-dependent point spread function (PSF) produce error boxes having typically a radius from 0.5 to 1 degree. Additional problems are encountered in the galactic plane where the diffuse background is strong and EGRET error boxes are often confused and hugely crowded of sources at other multiwavelengths (radio, optical, infrared, X-rays). All this makes identifications on the basis of positional correlations alone very difficult.

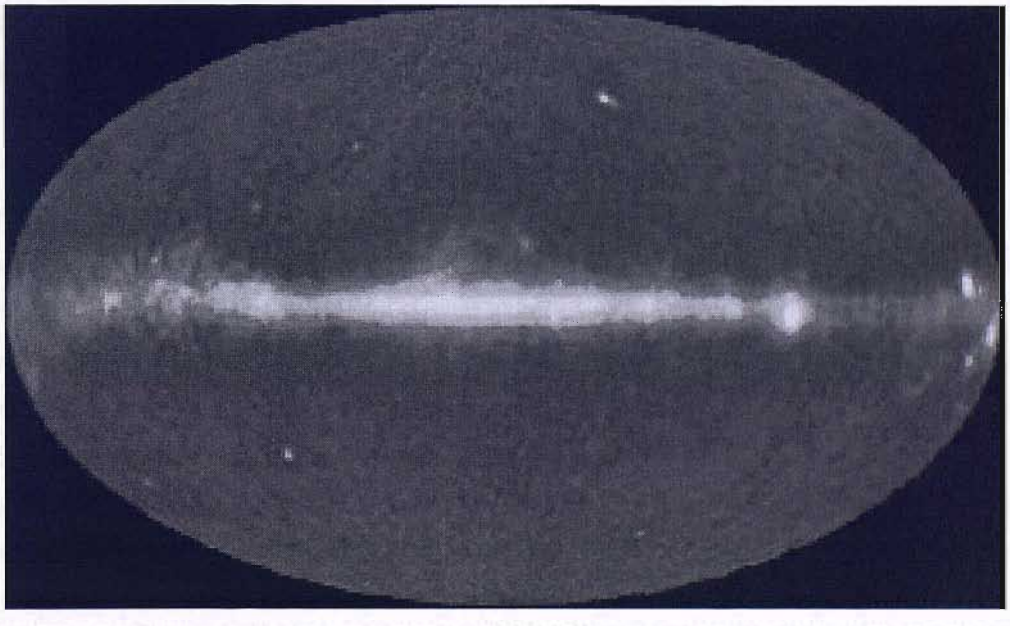

Figure 1.7: Gamma-ray sky as seen by EGRET at energies greater than 100 MeV.

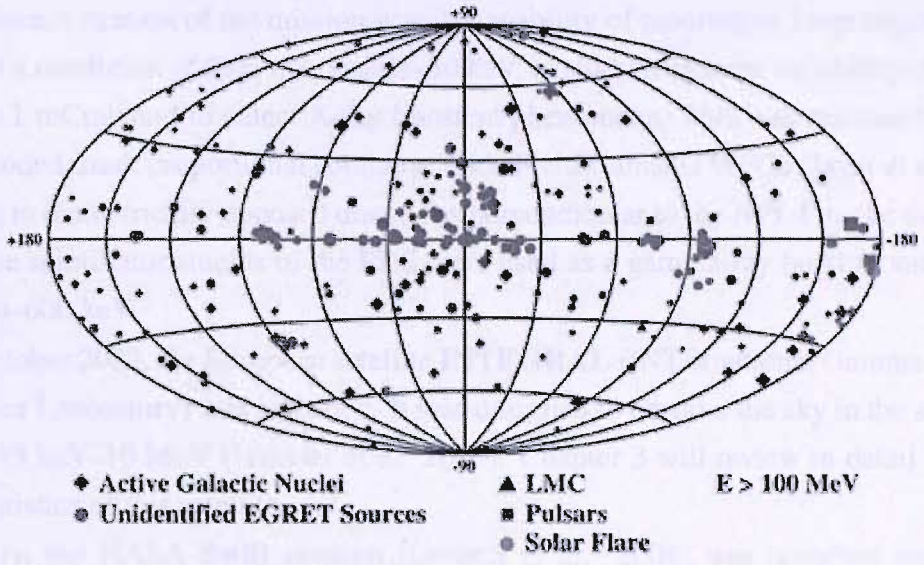

Figure 1.8: Distribution in the sky, in galactic coordinates, of all 271 gamma-ray point-sources reported in the 3EG catalog.

The Rossi X-ray Timing Explorer **RXTE** (Bradt et al. 1993) was launched in December 1995 and is still operational. It is designed to facilitate the study of time variability in the emission of X-ray sources, with moderate spectral resolution. Time scales from microseconds to months are covered in an instantaneous spectral range from 2 to 250 keV. The mission carries two pointed instruments: the Proportional Counter Array (PCA) developed to cover the lower part of the energy range (2–60 keV), and the High Energy X-ray Timing Experiment (HEXTE) covering the upper energy range 60–200 keV. These instruments are equipped with collimators yielding a FWHM of one degree. The other instrument onboard the RXTE satellite is an All-Sky Monitor (ASM) that scans about 80% of the sky every orbit (2–10 keV), allowing monitoring at time scales of 90 minutes or longer. The ASM observes the brightest known X-ray sources for variability and also alerts the community when new sources appear.

In April 1996, the **BeppoSAX** satellite (Boella et al. 1997) was launched. This mission was a major program of the Italian Space Agency with participation of the Netherlands Agency for Aereospace Programs. For six years BeppoSAX provided observations of the X/soft γ-ray sky, covering more than three decades of energy (0.1–300 keV) with a relatively large area and a good energy resolution, associated with imaging capabilities (resolution of $\sim 1'$) in the range of 0.1–10 keV. The payload included: a medium energy (1–10 keV) concentrator optics/spectrometer MECS, a low energy (0.1–10 keV) concentrator optics/spectrometer LECS, a high pressure gas scintillation proportional counter HPGSPC (3–120 keV), and a phoswich detector system PDS (15–300 keV). All of them had narrow FOV and pointed in the same direction (Narrow Field Instruments, NFI). The

other characterization of the mission was its capability of monitoring large regions of the sky with a resolution of 5' in the range 2–30 keV, to study long term variability of sources down to 1 mCrab and to detect X-ray transient phenomena. This was realized by means of two coded mask proportional counters, Wide Field Cameras WFCs (Jager et al. 1997), pointing in diametrically opposed directions perpendicular to the NFI. Finally, the anticoincidence scintillator shields of the PDS were used as a gamma-ray burst monitor in the range 60–600 keV.

In October 2002, the European satellite **INTEGRAL** (INTErnational Gamma-Ray Astrophysics Laboratory) was launched. It was designed to observe the sky in the soft γ-ray regime 15 keV–10 MeV (Winkler et al. 2003). Chapter 3 will review in detail the main characteristics of this satellite.

Finally, the NASA **Swift** mission (Gehrels et al. 2004) was launched recently in November 2004. It is a multiwavelength observatory dedicated to the study of γ-ray bursts (GRBs). The Swift telescope payload consists of three instruments which work in tandem to provide rapid identification and multiwavelength follow-up of GRBs and their afterglows. Within 20 to 75 seconds of a detected GRB with the wide FOV BAT instrument, the spacecraft slews autonomously so that the FOVs of the other pointed instruments overlap the location of the burst and the afterglows can be monitored over their durations. The three instruments are:

- BAT (The Burst Alert Telescope), energy range 15–150 keV (Gehrels et al. 2004). It is a coded aperture device, with a high sensitivity and a large FOV (1.4 steradians, partially coded). The BAT detects the γ-ray bursts, providing an initial position with an accuracy of $\sim$ 4 arcminutes, within seconds of detecting the burst. While searching for γ-ray bursts, the BAT performs an all-sky hard X-ray survey and a monitor for hard X-ray transients. The BAT accumulates detector plane maps every 5 minutes. The sensitivity of the survey is $\sim$ 1 mCrab (15–150 keV) for two years at high galactic latitudes (>45°) and $\sim$ 3 mCrab in regions where there are numerous strong sources in the BAT FOV (i.e. the galactic plane).

- XRT (X-ray Telescope), energy range 0.3 – 10 keV (Gehrels et al. 2004).
  Most GRBs show X-ray afterglow emission following the initial burst of γ-rays. Both the XRT and the UVOT (see below) are narrow field instruments, aligned with the BAT. After the BAT has detected the GRB, Swift will slew within $\sim$ 10 seconds to the localised position, allowing the XRT to improve on this position to $\sim$5 arcseconds. The FOV of the XRT is 23.6 arcminutes. The XRT has 4 operating modes, depending on the flux of the afterglow. As the emission fades, the

XRT will automatically change from one mode to the next; if the afterglow should become brighter again, the mode changes will reverse direction. This automatic mode changing allows the XRT to observe over a range of more than 7 orders of magnitude in flux.

- UVOT (UV/Optical Telescope), energy range 170–650 nm (Gehrels et al. 2004). Previous observations of GRBs indicate that the intensities of the optical afterglows decay quickly over time. Swift's autonomous slewing capability minimises the reaction time, so allowing the rapid observation of the optical counterparts and the determination of the redshift of the object. However ultraviolet measurements cannot be made from the ground and ground based optical observatories. The UVOT on board Swift can provide this additional information.

Chapter 2

Transient characteristics of the gamma-ray sky

A theory is something nobody believes,
except the person who made it.
An experiment is something everybody believes,
except the person who made it.
– Albert Einstein

2.1 Introduction

One of the most striking aspects of the high energy sky is its variability. Many sources suddenly appear and then disappear again, on a wide range of timescales, from bright accreting X-ray transients which last ~ months, to fast X-ray transients with timescales of the order of hours, and gamma–ray bursts with durations of the order of seconds. The aim of this chapter is to provide a general overview of these different types of transient X-ray sources.

2.2 Accreting X-ray binaries

Binary star systems contain two stars that orbit around their common center of mass. The majority of the stars in our galaxy have binary companions, isolated stars like the Sun are the exception rather than the norm. A small proportion of binary star systems will evolve into X-ray binaries, where one of the two stars is a collapsed compact object (neutron star or black hole) and the other normal star is called the companion. The separation between

them is small enough so that the strong gravity of the compact object drags material from the companion. The X-ray emission in these systems (White et al. 1995) is due to accretion of matter from the companion onto the compact object and it comes from the area around the compact object, where the material that is falling toward it is heated to very high temperatures, over millions of degrees. The geometry of the accretion flow (i.e. spherical accretion or disk) determines if the X-ray emission region is the magnetic polar cap of the neutron star, the hot accretion disk surrounding the black hole, a shock heated region in the spherical inflow, or the boundary layer between an accretion disk an a neutron star. The X-ray binaries were among the very first X-ray sources to be detected in the history of X-ray astronomy. Since the discovery of the first X-ray binary in 1962 (Giacconi et al. 1962), they have offered a unique insight into the physics of matter at extreme conditions.

Accreting X-ray binaries are rare among stellar systems (White et al. 1995). There are believed to be only a few hundred of them in our galaxy, according to the large number of improbable evolutionary steps a primordial binary needs to follow in order to become an X-ray source with an accreting compact object. Indeed, the progenitors of the compact objects are believed to be too large to fit in the tight orbits of most X-ray binaries. Moreover, the supernova explosions that precede the formation of the compact objects could disrupt most systems at the phase prior to the formation of the X-ray binary.

X-ray binaries can be divided into persistent and transient sources, being in both cases among the brightest sources in our galaxy (White et al. 1995). The transient X-ray binaries exhibit many orders of magnitude variations (typically 10^4–10^5) in their X-ray luminosities, with typical durations from several weeks to months. The transient activity could be due to instability in the accretion disk, or large fluctuations in the mass accretion rate onto the compact object (White et al. 1995). Many transients recur on a timescale ranging from days to tens of years. The recurrence behaviour is periodic for some sources and random for others. In general, X-ray binaries are classified into two different groups according to the mass of the companion donor star: High Mass X-ray Binaries (HMXBs) and Low Mass X-ray Binaries (LMXBs). The following sections will report on their characteristics.

2.2.1 High Mass X-ray Binaries HMXBs

The companion donor star in HMXBs (Liu et al. 2000) is a massive OB–type star (≥ 10 $M_\odot$). These systems are the descendants of massive binaries in which the initially most massive star exploded as a supernova, leaving behind a neutron star or a black hole as the

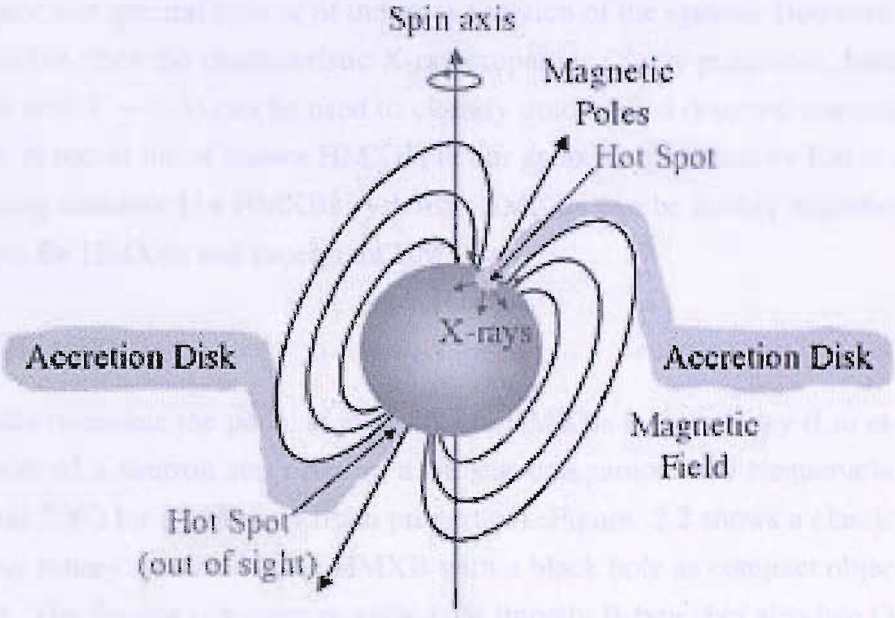

Figure 2.1: Schematic view of accretion onto a neutron star.

compact object. Due to a phase of mass transfer, the secondary star becomes the most massive one in the system before the primary supernova, so that the system remained bound (Van den Heuvel & Heise 1972). As long as the secondary is a massive main sequence star (and not a Be star), accretion of its relatively tenuous stellar wind onto the compact object does not result in an observable X-ray flux. Only when the secondary become a supergiant star with a strong stellar wind, or subsequently when it overflows its Roche lobe, the accretion flow is dense enough to power a strong X-ray source: the system has become a HMXB.

HMXBs are relatively young with short lifetimes ($\sim 10^5$–10^7 years). In fact the HMXB phase occurs relatively soon after the supernova explosion in the system, and cannot last longer than the nuclear burning time of the massive companion star. They are distributed along the galactic plane, as young stellar populations are (Grimm et al. 2002). However, HMXBs are sometimes runaways due to the kick velocity exerted by the supernova explosion. Moreover, with HMXBs being young systems, the neutron stars in them are expected to have magnetic fields that are strong ($\sim 10^{12}$ G) and dynamically important in the accretion processes. Such strong magnetic fields will disrupt the accretion flow at several hundred neutron star radii and funnel matter onto the magnetic poles. If the magnetic and rotation axes are misaligned, and if the beamed emission from the magnetic poles intercepts the line of sight, X-ray pulsations will be observed and these neutron stars will appear as accretion powered X-ray pulsars (figure 2.1).

The classification of a X-ray source as a HMXB is based upon the optical identification

of the donor star spectral type or of the mass function of the system. However, when this is not possible, then the characteristic X-ray properties (X-ray pulsations, hard spectrum 1–10 keV with $\Gamma \sim 0$–1) can be used to classify unidentified detected sources (White et al. 1995). A recent list of known HMXBs in our galaxy is provided by Liu et al. (2006), their catalog contains 114 HMXBs systems. HMXBs can be further classified into two subgroups: Be HMXBs and supergiant HMXBs.

2.2.1.1 Be HMXBs

Be HMXBs dominate the population of known HMXBs in our galaxy (Liu et al. 2006), they consist of a neutron star orbiting a Be star companion (see Negueruela 2004 and Ziolkowski 2002 for a review of basic properties). Figure 2.2 shows a classical view of a Be/X-ray binary system. No Be HMXB with a black hole as compact object has been found yet. The Be star is a massive early-type (mostly B-type, but also late O-type) star typically close to the main sequence, with a luminosity class in the range III-V, which at some time has shown one or more Balmer lines in emission. They are not evolved stars and are substantially smaller than their Roche lobes. The Balmer emission lines as well as the characteristic strong infrared excess are attributed to the presence of circumstellar material forming a disk around the equator of the Be star. The origins of this disk are not yet well understood, different mechanisms (fast rotation, non radial pulsation, magnetic loops) have been proposed (Negueruela et al. 1998). Accretion onto the neutron star is responsible for the X-ray emission in the system while the optical/infrared emission is completely dominated by the Be star. The orbits of Be HMXBs are elliptical and particularly eccentric ($e \geq 0.3$), the orbital periods are rather long being in the range 17–263 days. To date, in all but one Be HMXB, X-ray pulsations have been found (Negueruela 2004). The X-ray spectrum of Be HMXBs is very similar to that of other accreting X-ray pulsars, being mainly a high energy cutoff power law with absorption at low energies due to interstellar material (White et al. 1995).

A few Be HMXBs are persistent X-ray sources displaying a relatively constant low luminosity of $\sim 10^{34}$ erg s^{-1} (Reig & Roche 1999). They contain very slow pulsars with pulsations in the range 202–1404 seconds. Many Be HMXBs show only transient activity and so are named Be/X-ray transients, their spin period is in the range from 0.03 to a few hundred seconds. The transient nature is due to the fact that the neutron star is characterized by a very eccentric orbit, spending most of its time far away from the disk surrounding the Be star. Only during the time of its periastron passage does it accrete material from the dense equatorial Be star disk, producing outbursts (see figure 2.2). Two kinds of outbursts are observed:

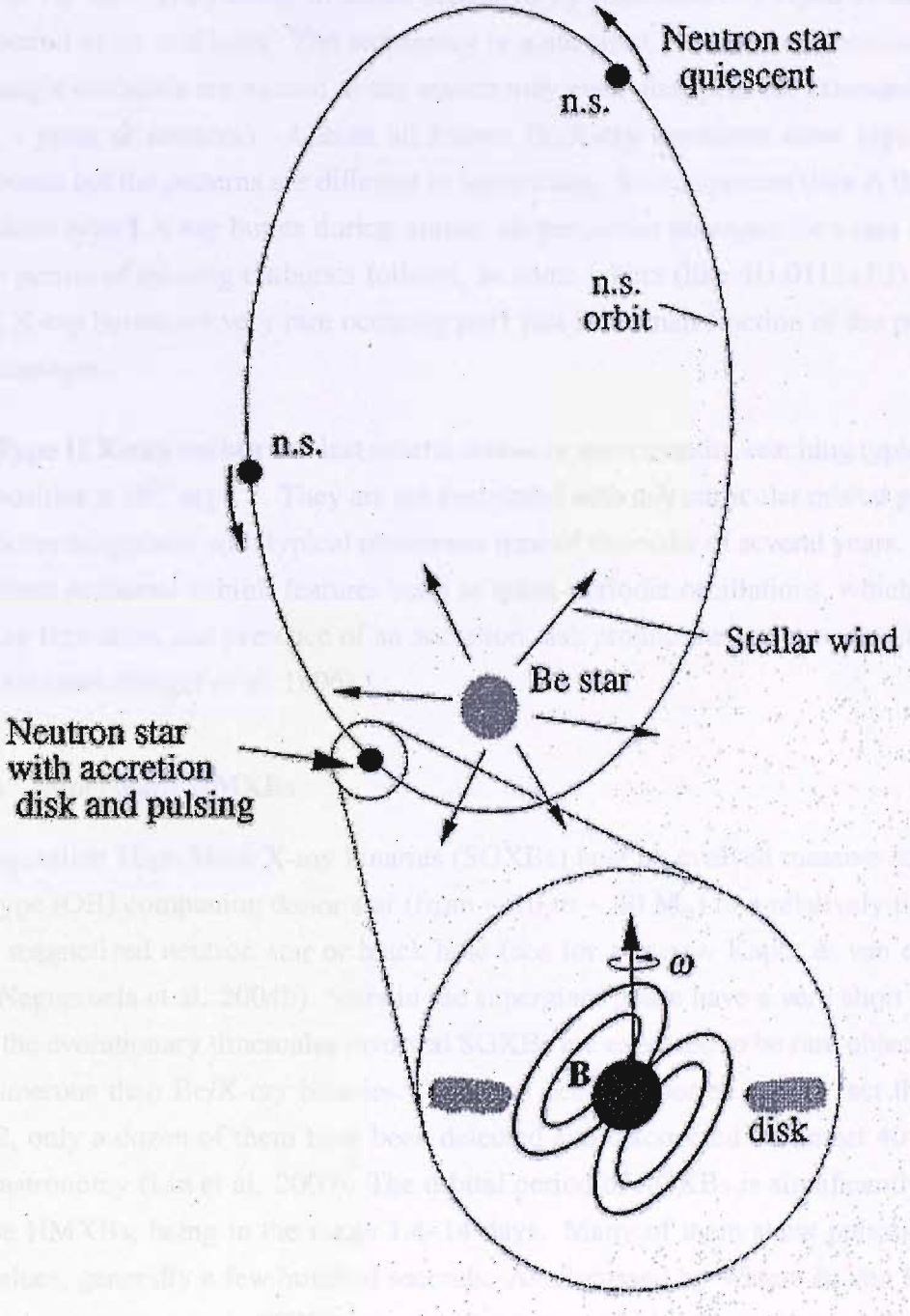

Figure 2.2: Classical view of a Be/X-ray transient system.

- **Type I X-ray outbursts**: last a few days, reaching typical luminosities of $\sim 10^{36}$ erg s^{-1}, and are connected to the periastron passage of the neutron star orbiting the Be star. They occur in series separated by time intervals equal to the orbital period or its multiples. The recurrency is quite strict, however on some occasions single outbursts are missed or the source may even disappear for extended periods ($\sim$ years or decades). Almost all known Be/X-ray transients show type I X-ray bursts but the patterns are different in some cases. Some systems (like A 0535+26) show type I X-ray bursts during almost all periastron passages for years and then a period of missing outbursts follows. In some others (like 4U 0115+63) the type I X-ray bursts are very rare occuring only just in a small fraction of the periastron passages.

- **Type II X-ray outbursts**: last several weeks or even months, reaching typical luminosities $\geq 10^{37}$ erg s^{-1}. They are not correlated with any particular orbital phase and occur irregularly with typical recurrence time of the order of several years. Some of these outbursts exhibit features such as quasi-periodic oscillations, which suggest the formation and presence of an accretion disk around the neutron star during the outbursts (Finger et al. 1996).

2.2.1.2 Supergiant HMXBs

The Supergiant High Mass X-ray binaries (SGXBs) host an evolved massive supergiant early-type (OB) companion donor star (from $\sim$ 10 to $\sim$ 60 $M_\odot$) in a relatively tight orbit with a magnetized neutron star or black hole (see for a review Kaper & van der Meer 2005, Negueruela et al. 2004b). Stars in the supergiant phase have a very short lifetime; due to the evolutionary timescales involved SGXBs are expected to be rare objects, much less numerous than Be/X-ray binaries. This has been supported by the fact that up to $\sim$ 2002, only a dozen of them have been detected and discovered in almost 40 years of X-ray astronomy (Liu et al. 2000). The orbital period of SGXBs is significantly shorter than Be HMXBs, being in the range 1.4–14 days. Many of them show pulsations with long values, generally a few hundred seconds. As discussed by Waters & Van Kerkwijk (1989), the neutron stars in SGXB systems were born with shorter spin period. During the main sequence lifetime of the present donor no accretion took place and the neutron stars were spun down to the present long values of spin periods because of the propeller effect. When the companion donor became a supergiant, the mass loss rate was high enough to fuel accretion, but since the latter was not accompanied by transfer of angular momentum, the neutron stars were not spun up back to their initial low values of spin periods. Since

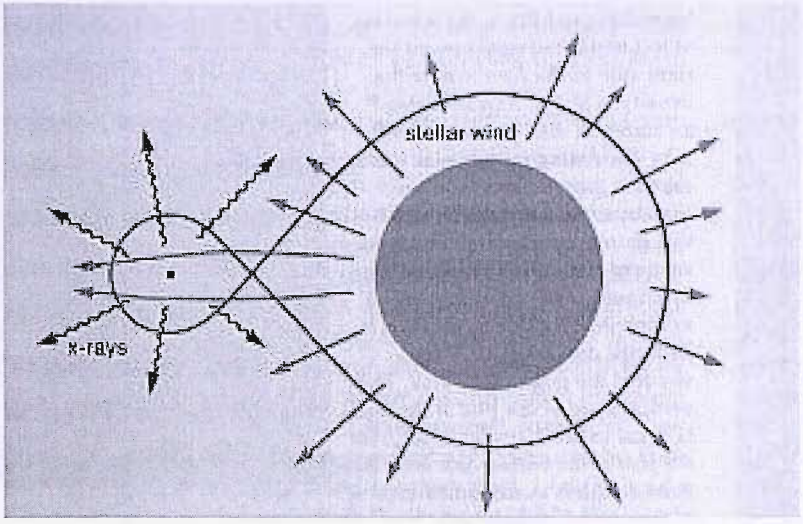

Figure 2.3: The geometry of accretion onto a compact object in a SGXB. The wind is assumed to be spherically symmetric and smooth. The red line represents the equipotential surface of the Roche lobe.

the X-ray emission must propagate through the stellar wind to the observer, the signature of intrinsic photoelectric absorption is clear in the X-ray spectrum of SGXBs.

The X-ray emission in SGXBs is powered by accretion of material originating from the donor supergiant through two different mechanisms (figure 2.3):

1. usually by **stellar wind**: early-type supergiant stars possess strong, dense, fast stellar winds and the neutron star orbits deep inside the stellar wind. The mass-loss rates are typically 10^{-6}–10^{-8} $M_\odot$ per year. The accretion via stellar wind is much less efficient than that via the inner Lagrangian point (see next) because the wind is practically emitted in a isotropic way, and then only a small part (0.1%–1%) of the expelled mass is captured by the compact object. These wind-fed systems are bright persistent X-ray sources with X-ray luminosities of $\sim 10^{36}$ erg s^{-1}. Moreover, they can show erratic flaring activity with, in some cases, luminosity variations up to a factor of 100 on a timescale of tens of minutes. These flares reflect inhomogeneities in the stellar wind.

2. occasionally by **Roche lobe overflow**: the Roche lobe is a volume around a star in a binary system, inside which material is gravitationally bound to that star. The point between the two Roche lobes in a binary system (inner Lagrangian point) is where the gravity from the companion is equal to the gravity from the compact object. When the supergiant donor star grows and fills its Roche lobe, some of the material in the star's outer edges is no longer bound to the star, flowing into the other lobe through the inner Lagrangian point (See figure 2.3). The flowing material

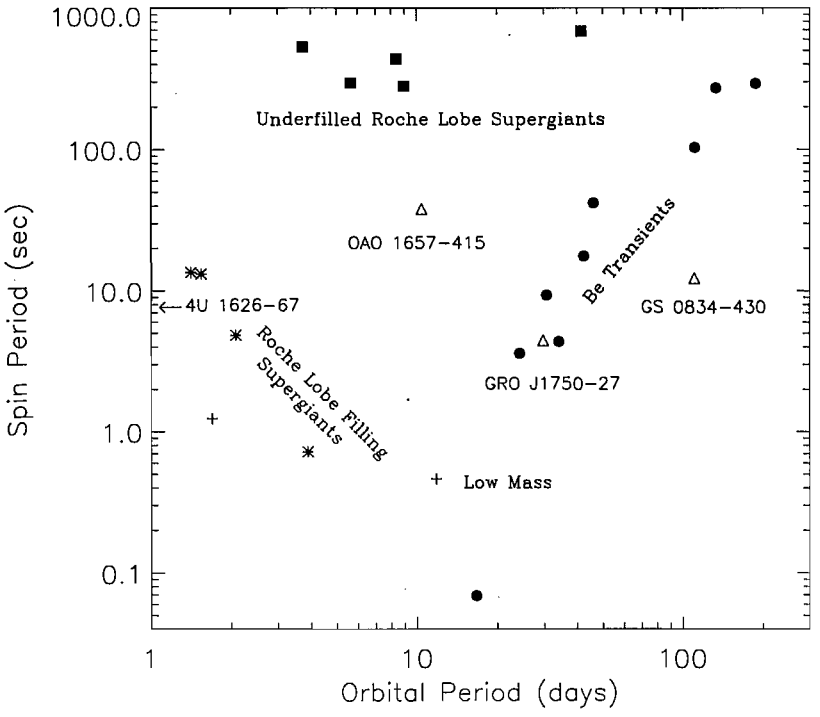

Figure 2.4: The Corbet diagram illustrating the relationship between orbital and spin periods in HMXBs systems. Picture taken from Bildsten et al. (1997).

has angular momentum from orbiting the companion star and will be almost entirely captured by the compact object, forming a geometrically thin accretion disk around it. Since more material is transfered to the compact object in Roche lobe overflow SGXBs than wind-fed SGXBs, this will result in a much higher accretion rate. Roche lobe overflow SGXBs are brighter persistent sources with a X-ray luminosity of $\sim 10^{38}$ erg s^{-1}, close to the Eddington luminosity. Moreover, angular momentum is transfered from the accreted material to the compact object. When accretion occurrs directly from the wind, the material does not have enough angular momentum. As a consequence, the Roche lobe overflow SGXBs host faster pulsars; they have shorter orbital periods (a few days) with lower eccentricity than wind-fed SGXBs, often because their orbits have circularised.

The modality of mass transfer onto the neutron stars determines their spin evolution. The Roche lobe filling SGXBs have shorter spin periods that are anticorrelated with their orbital periods. The wind-fed SGXBs have longer spin periods that do not show any correlation with the orbital period. Finally the Be HMXBs have long spin periods which are correlated with the orbital period. This is clearly summarised in the Corbet diagram shown in figure 2.4.

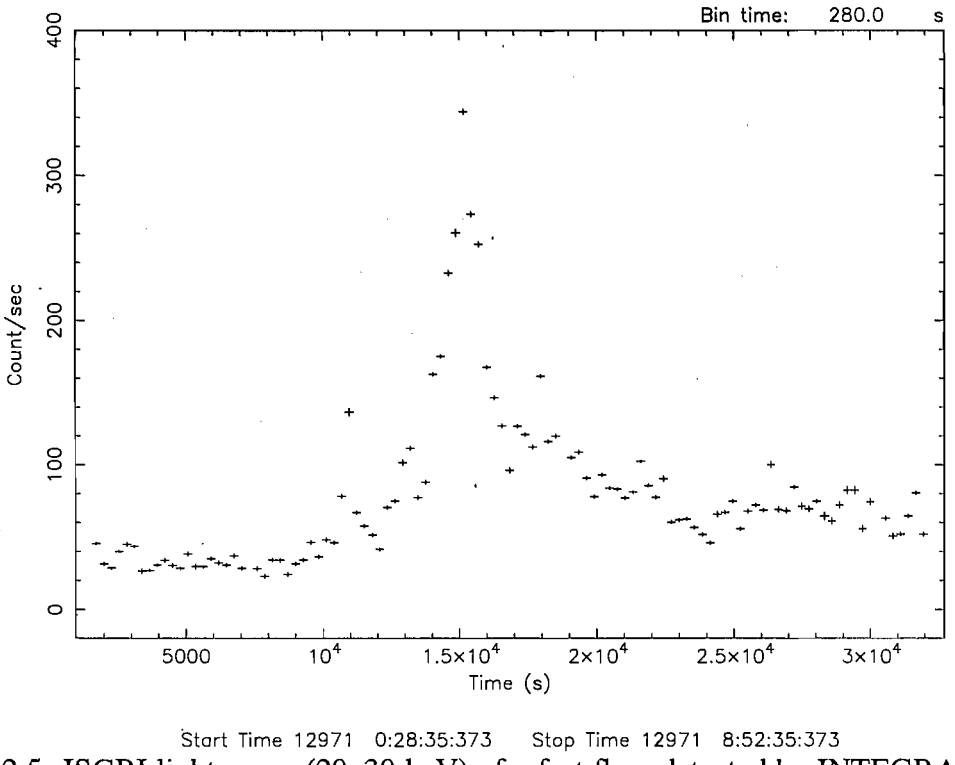

Figure 2.5: ISGRI light curve (20–30 keV) of a fast flare detected by INTEGRAL from Vela X-1 on November 2003. The bin time is 280 seconds.

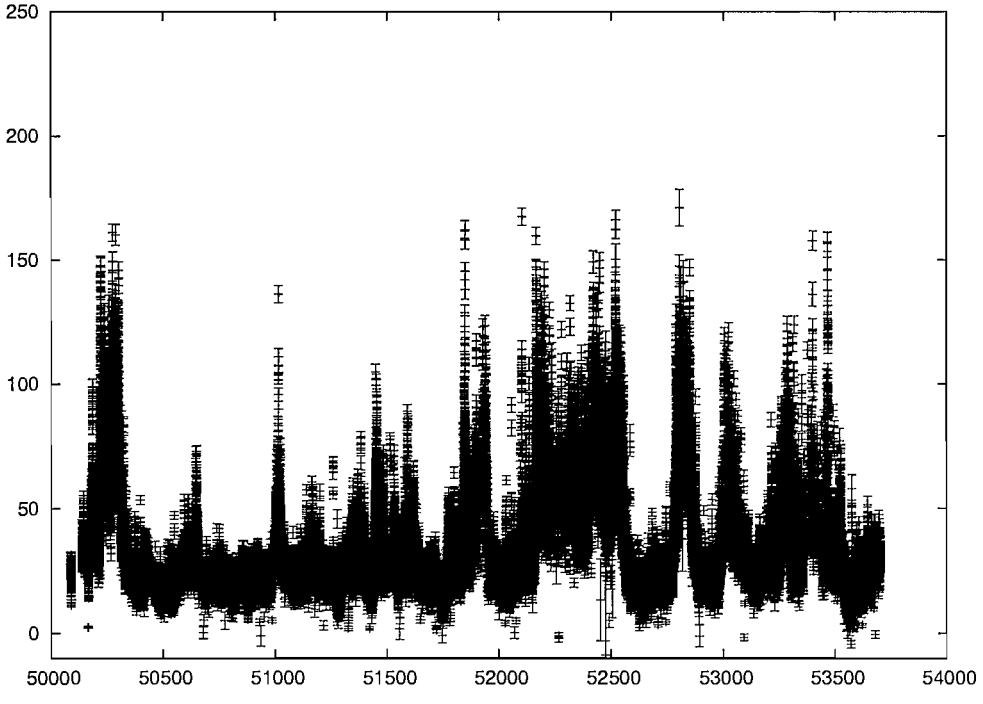

Figure 2.6: ASM light curve (2–12 keV) of Cygnus X-1 from approximately October 1995 to March 2006.

As stated before, SGXBs are bright persistent X-ray sources rather stable in the long term. However, at least three of them (Vela X-1, Cygnus X-1 and 1E 1145.1−6141) have been observed several times to undergo bright very short flares, having timescale of a few hours.

Vela X-1 is a wind-fed SGXB hosting a ~ 283 seconds neutron star. The donor is a supergiant of spectral type B0.5Ib and mass ~ 23 $M_{\odot}$, the orbital period is 8.96 days. Vela X-1 is a bright persistent source with a typical X-ray luminosity of ~ 4×10^{36} erg s^{-1}, however occasionally it undergoes fast X-ray flares lasting a few hours and reaching maximum peak luminosities of ~ 4×10^{37} erg s^{-1} (Staubert et al. 2004, Laurent et al. 1995). Even during the flares the source remains in the sub-Eddington regime of accretion. Moreover, it is interesting to point out that the spectrum of Vela X-1 during these fast strong flares appears to remain very similar to that observed during more usual normal states of luminosities (Kretschmar et al. 2004). Figure 2.5 shows a typical fast strong flare from Vela X-1 detected by INTEGRAL on 28 November 2003. The trigger for these flares could be episodes of dramatically increased mass accretion onto the compact object, which is deep inside the highly structured stellar wind environment of the supergiant donor star. The latter is known to be highly inhomogeneous and probably characterized by clumps and clouds of material with higher density.

Cygnus X-1 is another bright persistent SGXB which occasionally undergoes fast strong X-ray flares (Golenetskii et al. 2003). It hosts a black hole candidate and the donor star is a supergiant of spectral type O9.7Iab and mass ~ 25 $M_{\odot}$, the orbital period is 5.6 days. Figure 2.6 shows the RXTE All Sky Monitor (ASM) light curve of Cygnus X-1 (2–12 keV) from approximately October 1995 to March 2006. It is clearly evident that the source is persistent and undergoes flares.

2.2.1.3 Supergiant HMXBs in the INTEGRAL era

As stated before, until recently it was widely believed that the total galactic population of SGXBs could not be very large because of the evolutionary timescale involved. Only a dozen have been discovered in almost 40 years of X-ray astronomy, many of them during its early days. As SGXBs are bright persistent X-ray sources, they can be detected to large distances, many of them are located at distances of ~ 6 kpc. Up to recently, it was largely believed that the dozen known SGXBs represented a substantial fraction of all SGXBs in our galaxy.

Currently, the INTEGRAL satellite is changing this classical picture of SGXBs. Since its launch in 2002, INTEGRAL has discovered ~ 170 new hard X-ray sources (Bird et al. 2007), most of these are located towards the inner regions of the galaxy, which have been

extensively monitored. Many of the new sources are characterized by hard spectra, with little or no detectable emission in the soft X-rays since they are heavily absorbed by a huge intrinsic and local extinction. This explains why they have not been detected by any previous X-ray mission. As discussed by Dean et al. (2005) and Lutovinov et al. (2005), most of the newly discovered INTEGRAL sources should be HMXBs. This picture has been supported by various identifications with bright persistent highly absorbed SGXBs, either based on their secure identification at optical/infrared wavebands or on their X-ray characteristics and discovery of pulsations (Walter et al. 2006, Chaty & Rahoui 2006, Hill et al. 2005). In principle, their properties do not appear to be extremely different from those of classical SGXBs, except for the huge absorption which was the reason why they have not been detected earlier at lower photon energies. As well as the highly absorbed persistent SGXBs, INTEGRAL is also discovering members of a new kind of SGXBs which escaped detection by previous X-ray missions because of their fast X-ray transient behaviour, a characteristic never seen before from such systems. They have been labeled as Supergiant Fast X-ray Transients SFXTs (Negueruela et al. 2006a, Sguera et al. 2005, Sguera et al. 2006, Sguera et al. 2007). Chapter 4 and 5 in this thesis will extensively report on INTEGRAL results of this very interesting newly discovered class of sources. The recent discoveries by INTEGRAL of highly absorbed persistent SGXBs as well as fast X-ray transient SGXBs strongly suggest that the size of the population of SGXBs in our galaxy could have been severely underestimated.

2.2.2 Low Mass X-ray Binaries LMXBs

LMXBs are systems containing a neutron star or black hole as compact object and a low mass ($\leq$ 1 $M_{\odot}$) star as donor companion, typically a late type main sequence star or a white dwarf (Liu et al. 2001). The X-ray emission is powered by accretion of material originating from the donor star through Robe lobe overflow (see figure 2.7), as already previously described in section 2.2.1.2 for SGXBs. A bulge or hot-spot occurs where the accretion stream impact the accretion disk (see White et al. 1995 for a review on basic properties).

LMXBs can be transient or very bright persistent X-ray sources, for the latter the X-ray luminosities are typically in the range 10^{36}–10^{38} erg s^{-1}. It is not a surprise that the first X-ray source to be discovered and detected in the early days of the X-ray astronomy was the very bright Sco X-1, later identified as a LMXB. Currently $\sim$ 200 LMXBs are known in our galaxy, 150 are catalogued by Liu et al. (2001) and several tens have been discovered since then. Quite remarkably, all the known black hole LMXBs are transient

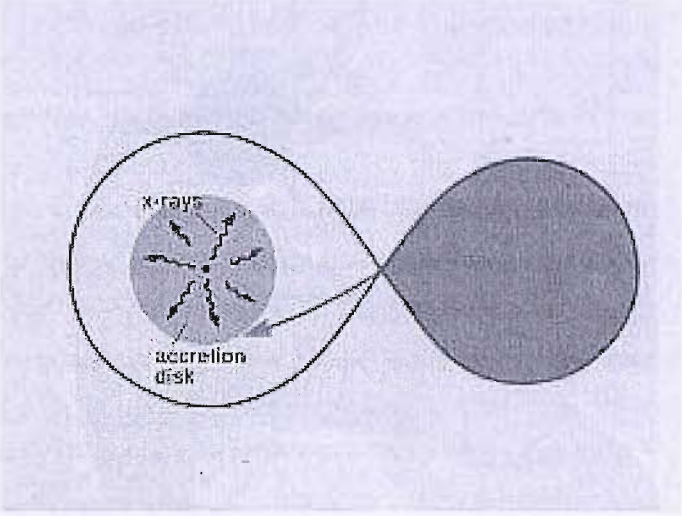

Figure 2.7: The geometry of accretion onto a compact object in a LMXB. The red line represents the equipotential surface of the Roche lobe and the companion donor star has filled its Roche lobe.

sources, whereas the three known persistent black hole X-ray binaries are all HMXBs: two are in the large Magellanic cloud (LMC X-1 and LMC X-3) leaving only one (Cyg X-1) in our own galaxy. In contrast, among the LMXBs for which the compact object is a neutron star, only $\sim$ 1/7 are transients.

LMXBs are found mostly around the galactic center (Grimm et al. 2002), moreover several of them ($\sim$ 17) are located in globular clusters. This implies that they are old stellar systems. Their old age, and consequent prolonged phase of accretion onto the neutron star, is believed to be responsible for the weakening of their magnetic field ($\leq 10^8$ G). The accretion flow is not disrupted and channelled onto the magnetic poles, as a consequence periodic X-ray pulsations are absent in all but a handful of LMXBs (e.g. Her X-1). LMXBs are observed to have orbital periods in the range 0.19–298 hours.

2.2.2.1 Type I and II X-ray bursts from LMXBs

About 40% of the LMXBs in our galaxy display bright Eddington-limited transient events called type I X-ray bursts (see Lewin et al. 1993 for a review). As a consequence, a type I X-ray burst is considered to identify the source emitting it unambiguously as a LMXB containing a neutron star. They are explained as energy release by rapid nuclear fusion of material on the surface of a neutron star. As neutron star accretes hydrogen from the accretion disk, a layer of hydrogen accumulates on its surface. This layer begins to burn under the action of fusion in a steady fashion, building up a layer of helium beneath the hydrogen layer. The helium layer eventually begins to burn to carbon, however, this

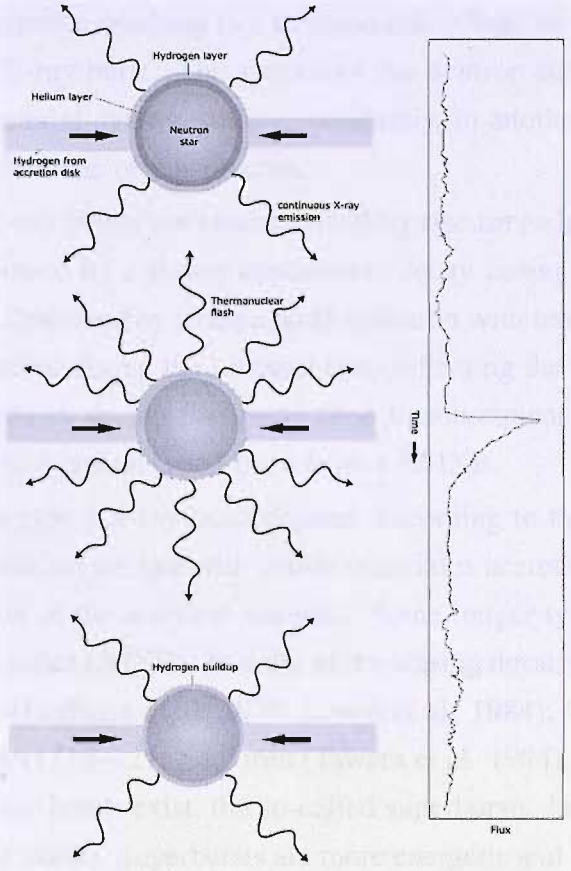

Figure 2.8: A schematic view of a type I X-ray burst. Credit picture: Hill 2006.

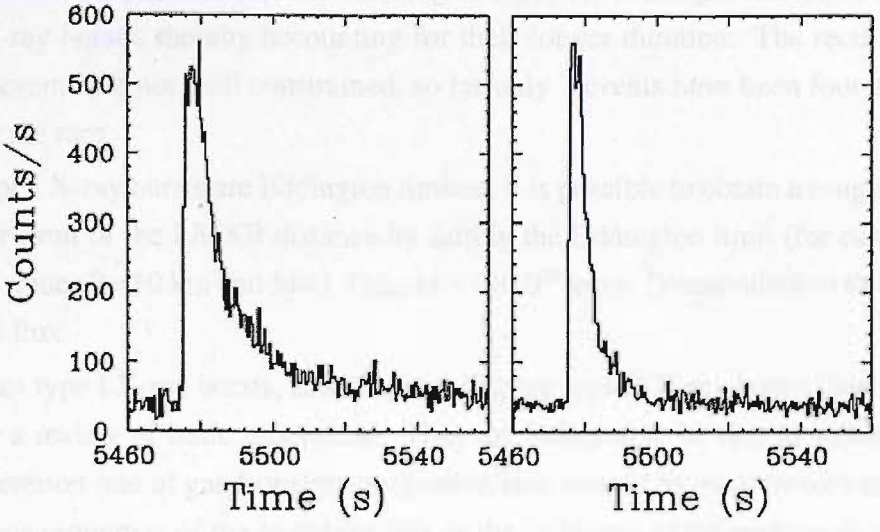

Figure 2.9: Type I X-ray burst from 4U1702−429 as observed with EXOSAT in two different energies bands: 1.2–5.3 keV (left) and 5.3–19 keV (right). The softening of the X-ray spectrum during the decay is apparent as a relatively long tail in the low energy burst profile (taken from Lewin et al. 1993).

process is rapid and unstable resulting in a thermonuclear flash on the neutron star which is observed as type I X-ray burst. The surface of the neutron star then cools, after this it begins to accrete material again resulting, eventually, in another thermonuclear flash. Figure 2.8 shows a schematic of this process.

Normally, type I X-ray bursts are characterized by rise times lasting from less than a second to ~ 10 s, followed by a slower exponential decay lasting from 10 s to minutes. Their spectra are well described by a black body emission with temperature of ~2–3 keV. The temperature increases during the outburst rise (reflecting the heating of the neutron star surface) and decreases during the decay (due to subsequent cooling). Figure 2.9 shows the light curve of a typical type I burst from a LMXB.

The properties of a type I X-ray burst depend, according to theory, on the mass and radius of the neutron star, on the rate with which material is accreted onto the neutron star and on the composition of the accreted material. Some longer type I X-ray bursts have been detected in many other LMXBs. In order of decreasing duration, some examples are: 4U1708–23, ≃25 min (Hoffman et al. 1978, Lewin et al. 1984); 4U1724–307, ≥10 min (Swank et al. 1977); 3A1715–321, ≥4.5 min (Tawara et al. 1984). It is worth noting that even longer type I X-ray bursts exist, the so-called superbursts, lasting for several hours (Cornelisse et al. 2000, 2002). Superbursts are more energetic and longer in duration than typical type I X-ray bursts, but with similar spectral evolution. This suggests that they result from thermonuclear flashes occuring in layers at much greater depth than typical type I X-ray bursts, thereby accounting for their longer duration. The recurrence times of these events are not well constrained, so far only 7 events have been found, indicating that they are rare.

As type I X-ray bursts are Eddington limited, it is possible to obtain a rough estimate to the upper limit of the LMXB distance by setting the Eddington limit (for canonical neutron star values R=10 km and M=1.4$M_\odot$, is ~ 2×10^{38} erg s^{-1}) equivalent to the bolometric observed flux.

Besides type I X-ray bursts, LMXBs also display type II X-ray bursts (see Lewin et al. 1993 for a review of basic properties). They are believed to be due to sudden increases in the accretion rate of gas from the companion star, caused by such factors as changes in the viscous properties of the accretion disk or the influence of the neutron star's magnetic field. The profiles of type II X-ray bursts also vary greatly, but are generally characterized by rapid successions of bursts a few minutes apart, sudden drops in flux without a gradual decay from peak values, no spectral softening in decay. Notably, type II bursts have been observed in only two sources: MXB 1730–335 (the Rapid Burster) and GRO J1744–28 (the Bursting Pulsar).

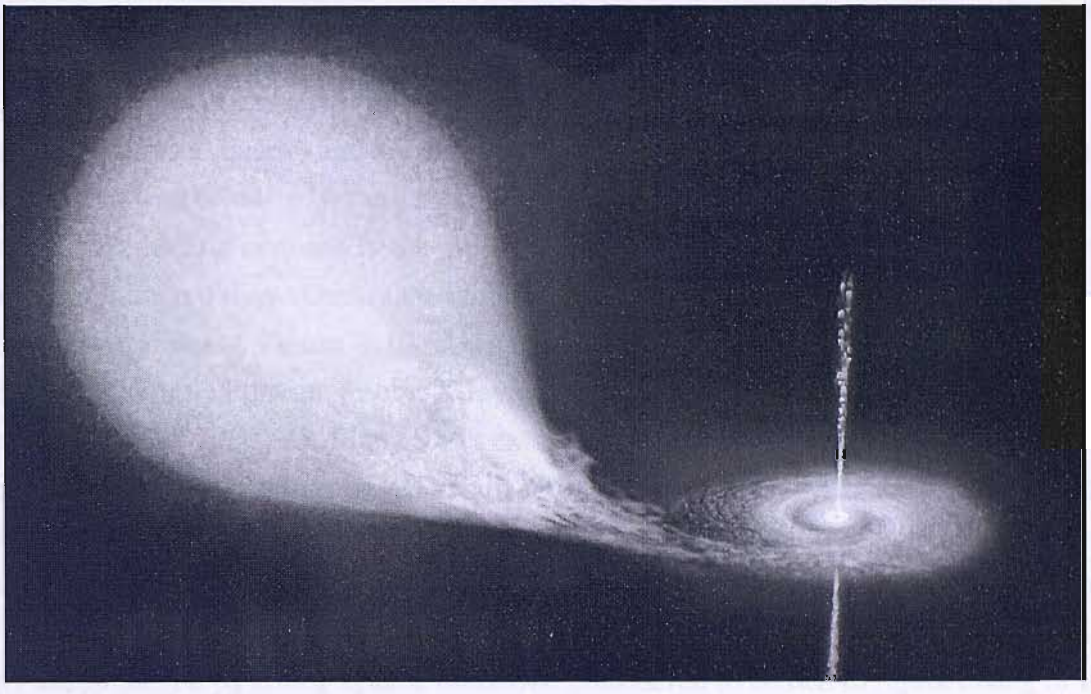

Figure 2.10: An artist conception (not to scale) of a soft X-ray transient.

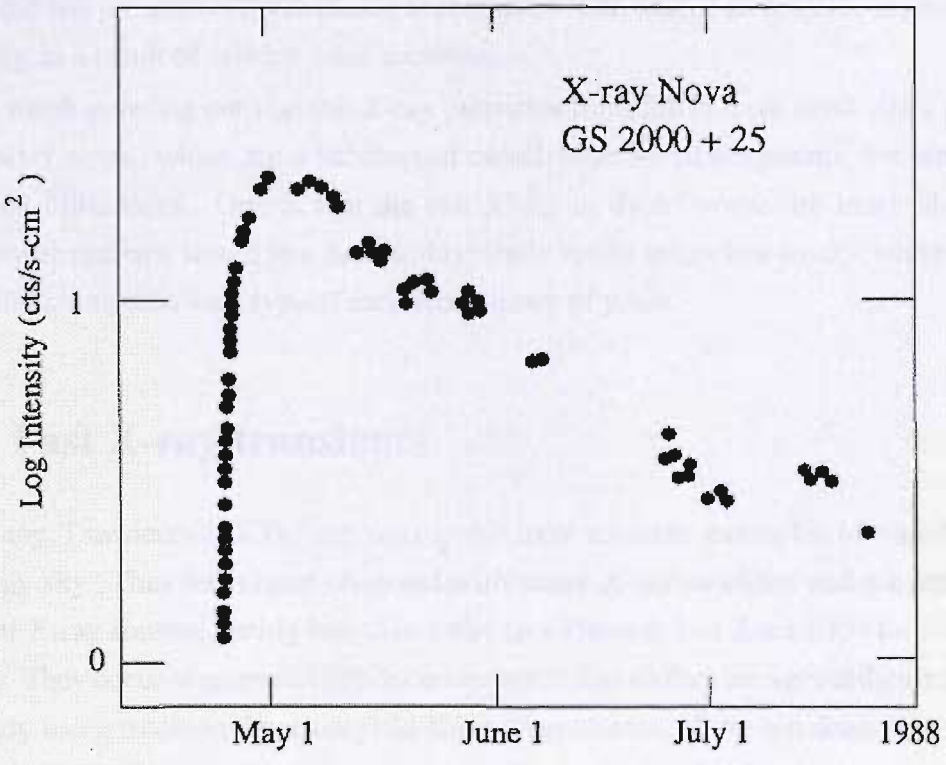

Figure 2.11: Ginga X-ray light curve of a X-ray outburst from the black hole candidate soft X-ray transient GS 2000+25.

2.2.2.2 Soft X-ray transients

X-ray novae, or soft X-ray transients (SXTs), form a subclass of LMXBs (see Tanaka & Lewin 1995 for a review) and are characterized by a sudden increase of the X-ray luminosity from well below $\sim 10^{33}$ erg s^{-1} to well above 10^{37} erg s^{-1} (1–10 keV) within several days. Then the flux declines to the pre-burst level on time scales of several tens of days to several hundred days. During the outburst, the X-ray spectrum is soft, hence the name soft X-ray transients. Figure 2.10 shows an artist conception of a SXT while figure 2.11 shows an example light curve of a X-ray outburst from the black hole candidate soft X-ray transient GS 2000+25. Many SXTs exhibit recurrent outbursts with intervals ranging from several months to tens of years, however there is no fixed periodicity of recurrence. The X-ray outbursts are thought to be caused by thermal instability in the accretion disk (e.g. Van Paradijs 1996) and sudden increase of mass accretion onto the compact object, which could be a neutron star or a black hole, the latter is more common. They are usually accompanied by strong optical outbursts, considered to be due to reprocessing of the X-rays in the accretion disk. Radio outbursts are often observed and in some cases even relativistic jets are seen. This evidence is consistent with that of an eruptive mass ejection occurring as a result of sudden mass accretion.

It is worth pointing out that the X-ray outbursts from SXTs have similarities to those from dwarf novae, which are a subclass of cataclysmic variable systems, but with some important differences. One is that the timescales in dwarf novae are much shorter; a dwarf novae outburst lasts a few days and typically recurs every few weeks, whereas SXT outbursts last months with typical recurrence times of years.

2.3 Fast X-ray transients

Fast X-ray Transients (FXTs) are among the most extreme examples of variability in the X-ray sky. They have been observed with many X-ray satellites and are defined as transient X-ray sources lasting less than a day (see Heise & in't Zand 2004 for a detailed review). They occur at unpredictable locations and times so they are very difficult to detect and study using traditional narrow field X-ray instruments. However, detectors having a sufficiently wide field of view are particularly suited to detect fast X-ray transient sources. The larger the field of view of an instrument, the greater the chance of serendipitously detecting a short duration random event, such as a FXT. To date, a few hundred FXTs have been observed by such wide field X-ray instruments, from Ariel–V to the Wide Field Cameras on board BeppoSAX, although their all-sky rate is believed to be of the

order of several thousands per year.

The data on these X-ray sources are limited and many of them lack the identification of counterparts at other wavelengths. As a consequence, not too much is known about FXTs. In fact, less than a half of all reported FXTs have been optically identified with stellar flares originating in galactic coronal sources such as RS CVn binaries, dMe-dKe flare stars, Algol-type binaries, W UMa systems and young T Tauri stars (Pye & McHardy 1983, Ambruster et al. 1986, Castro-Tirado et al. 1999). In galactic coronal sources, the rotational energy creates magnetic fields which in turn causes coronal activity through the annihiliation of these fields, and so subsequently the X-ray flares. However, FXTs are a heterogeneous collection of objects showing large diversity of observational characteristics such as light curves and spectra. The latter vary substantially, from hard (kT ~ 20 keV) to soft spectra with black body temperatures in the range 0.87 – 2.3 keV. All this seems to suggest that FXTs are caused by more than one physical mechanism, in fact many unidentified FXTs do not appear to be coronal events. Other progenitors have been suggested such as dwarf novae, ordinary or anomalous type I X-ray bursts, BL Lac objects, X-ray flashes (Hoffman et al. 1978, Lewin & Joss 1981).

2.3.1 The first detections of FXTs

FXTs were detected by the very first X-ray satellite Uhuru (also known as the Small Astronomical Satellite SAS-1) launched in December 1970. Subsequently, Ariel–V (launched in October 1974) and HEAO–1 (launched in August 1977) effectively recognized them as a class of X-ray transients. At the time of these early X-ray missions, they were indicated as transient X-ray sources lasting one or two satellite orbits, the orbital period of low earth satellites being ~ 1.5 hours. They tended to be seen once and never again, with no detectable quiescent emission. Moreover, since most of them were detected off the galactic plane, they were also referred to as High Latitude Transients.

Ariel–V scanned the entire sky for 5.5 years, during which 27 FXTs were detected in the energy band 2–18 keV (Pye & McHardy 1983), the highest peak flux was ~ 5×10^{-9} erg cm^{-2} s^{-1}. Six identifications were with RS CVn-like systems, three with Be stars, one with a BL Lac and a M-giant system, respectively. The remaining sources were unidentified. RS CVn systems are slightly evolved binaries (luminosity class IV-V) formed by a cool giant/subgiant star with an active corona and a less massive companion (a late G-dwarf). They are in a close synchronous orbit with typical periods in the range 1–14 days. Figure 2.12 shows a collage of X-ray light curves of some FXTs detected by Ariel–V, the time resolution is one satellite orbit (~ 100 minutes). A typical RS CVn light curve is

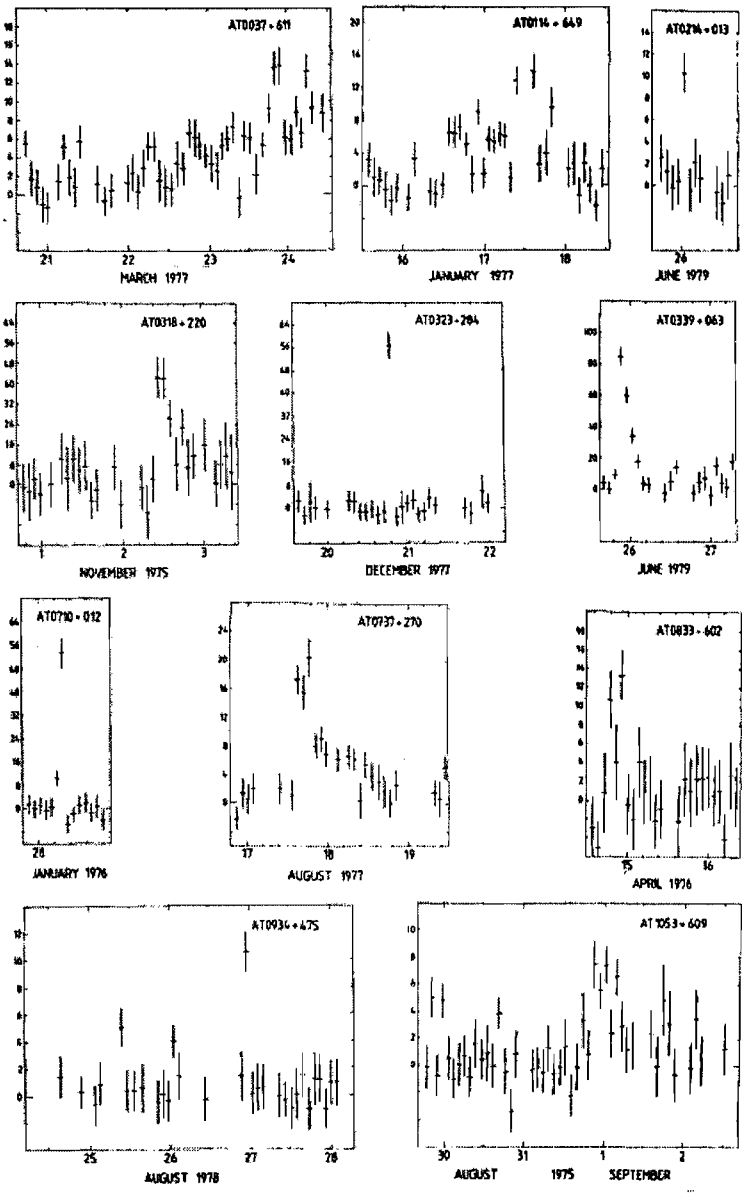

Figure 2.12: Collage of X-ray light curves of FXTs detected by Ariel–V (2–18 keV). Each data point represents an interval of ~ 100 minutes (one satellite orbit). Picture taken from Pye & Mchardy (1983).

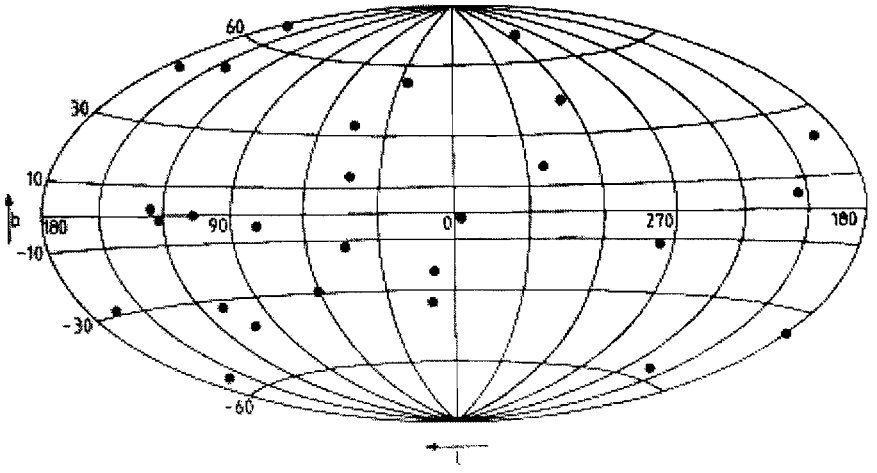

Figure 2.13: Distribution in the sky in galactic coordinates of FXTs detected by Ariel–V. Picture taken from Pye & McHardy (1983).

sharply peaked, with a fast rise and a slower decay. Figure 2.13 shows the distribution in the sky in galactic coordinates of all FXTs detected by Ariel–V. We can note that they are isotropically distributed and there is no confinement on the galactic plane.

The A-1 instrument on board HEAO–1 (0.5–20 keV) detected 10 FXTs with peak fluxes up to $\sim 4\times10^{-9}$ erg cm^{-2} s^{-1} (Ambruster et al. 1986). One was identified with a RS CVn-like system and 3 with coronal flares from dMe–dKe, which are active cool M or K dwarf stars with Balmer lines in emission. The A-2 instrument (2–60 keV) provided the detection of 8 further FXTs, 6 of them identified with flares from dMe–dKe stars (Connors et al. 1986).

Greiner et al. (2000) searched the ROSAT PSPC (Position Sensitive Proportional Counter) all sky survey data archive and found 23 FXTs with peak fluxes and durations in the range 10^{-10}–10^{-9} erg cm^{-2} s^{-1} (0.1–2.4 keV) and 10 seconds–few hours, respectively. They stated a stellar flare origin for many, if not all, of them. It is worth pointing out that this ROSAT survey was sensitive to FXTs fainter than those reported by previous X-ray missions, however it suffered from a much smaller field of view and bias towards much softer events.

2.3.2 FXTs in the BeppoSAX era

Many of the FXTs detected by the previously cited X-ray missions are still unidentified, mainly because of their poor angular resolution which prevented the search for counterparts at other wavelengths. In the absence of identifications, FXTs remained essentially an enigmatic class for a long time.

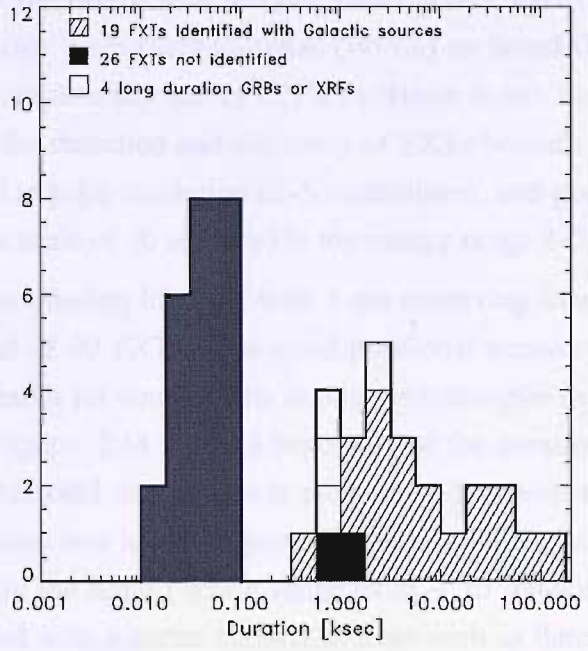

Figure 2.14: Histogram of durations of FXTs detected by WFCs. The distribution appears to be bimodal. The long duration events are galactic coronal sources, the short duration events are X-ray flashes. Picture taken from Heise & in't Zand (2004).

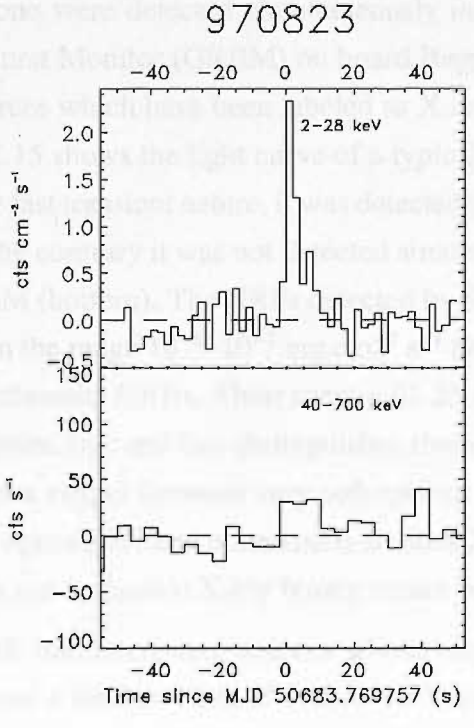

Figure 2.15: WFCs (top, 2–28 keV) and GRBM (bottom, 40–700 keV) light curves of a XRF detected on 23 August 1997. Picture taken from Heise & in't Zand (2004).

With the advent of the BeppoSAX satellite (launched in 1996) this situation significantly changed. The two Wide Field Cameras (WFCs) on board BeppoSAX performed the most recent and complete sky survey of FXTs (Heise & in't Zand 2004). They were particularly suited to the detection and discovery of FXTs because of their large field of view (40°×40°), good angular resolution (2–5 arcminutes), and good sensitivity ($\sim 10^{-8}$ erg cm^{-2} s^{-1} on a time scale of 10 seconds) in the energy range 2–25 keV.

During the six year mission lifetime, with a net observing time of 10^8 seconds, the WFCs detected a total of 49 FXTs. The good positional accuracy and sensitivity permitted a successful search for counterparts at other wavelengths as well as the detection of quiescent fluxes. Figure 2.14 shows a histogram of the duration of the 49 FXTs detected by WFCs. A bimodal distribution is evident, with a peak around a few minutes and another peak around one hour. In particular, there are a total of 21 long duration events (hatched area in the figure) which range from $\sim$ 30 minutes to $\sim$ 55 hours. All but two were identified with galactic coronal sources such as flare stars, algol systems, CVn systems. The short duration events are 24 and last from $\sim$ 10 seconds to no more than $\sim$ 15 minutes. None of them was identifiable with any coronal source or known X-ray object of any type. Neither are these events counterparts of conventional gamma-ray bursts (GRBs) because none were detected simultaneously in the energy band 40–700 keV by the Gamma-ray Burst Monitor (GRBM) on board BeppoSAX. They constitute a new class of transient sources which have been labeled as X-ray Flashes XRFs (Heise & in't Zand 2004). Figure 2.15 shows the light curve of a typical XRF detected on August 1997. We can note its very fast transient nature, it was detected by the WFCs in the energy band 2–28 keV (top), on the contrary it was not detected simultaneously at higher energy (40-700 keV) by the GRBM (bottom). The XRFs detected by the WFCs are bright X-ray sources with peak fluxes in the range 10^{-8}–10^{-7} erg cm^{-2} s^{-1} (2–28 keV), the same range as the X-ray afterglow of classical GRBs. Their spectra (2–25 keV) are non thermal, being typically fitted by a power law, and this distinguishes them from type I X-ray bursts. The power law photon index ranges between very soft spectra ($\Gamma \sim 3$) to hard ($\Gamma \sim 1.2$). The absence of quiescent optical/infrared counteparts implies X-ray to optical ratios R_{xo} > 100. This criterion rules out a possible X-ray binary nature for XRFs.

The XRFs are enigmatic and interesting sources whose origin is still unknown. Observationally, they constitute a distinct class of fast X-ray transient sources. As already stated before, they did not trigger the GRBM on board BeppoSAX, however they share several properties with classical GRBs such as isotropic spatial distribution, non thermal emission, non recurrence, lack of quiescent emission. All these aspects strongly suggest an extragalactic origin for XRFs and possibly point to a close connection with GRBs, the

main distinguishing property being the softness of their spectrum. The key question is if XRFs and GRBs are the same and only appear different because of geometrical reasons (for example a different viewing angle in the beamed emission) or if they are intrinsically distinct. To date, the few and sparse available data suggest a common origin for cosmic explosions that manifest themselves as XRFs and GRBs.

2.4 Gamma-ray bursts

Gamma-ray bursts (GRBs) are sudden, intense flashes of γ-rays releasing a tremendous amount of energy (10^{51}–10^{54} erg s^{-1}), larger than that of any other type of source in the Universe and second only to the Big Bang (see Meszaros 2001 and Zhang 2006 for a review). GRB durations span about 5 orders of magnitude, from 0.01 to 1000 s, their distribution displays a clear bimodality, with short bursts (durations $\sim$ 0.2 s) comprising around 25% of the total, and long bursts (durations $\sim$ 20 s) comprising the remainder. GRBs were first discovered in the 1960's by the U.S. Air Force military satellites Vela, devoted to the detection of eventual secret nuclear explosions violating the nuclear test ban treaty. Only after several years, in 1973, they were publically announced as a scientific discovery (Klebesadel et al. 1973). After their discovery, for the following 20 years, GRBs remained a mystery although hundreds of them were detected. The accuracy of their position, furnished by gamma-ray satellites, was very poor; moreover after a short time they were no longer detectable. The GRBs decay was so fast and the position uncertainty so large that no search for delayed emission in other wavelengths could be successfully attempted.

A major advance occurred in 1991 thanks to the Burst and Transient Experiment (BATSE) onboard the Compton Gamma-Ray Observatory (CGRO). BATSE was an all-sky monitor which detected $\sim$ 3,000 GRBs. BATSE showed that they were isotropically distributed in the sky, strongly suggesting an extragalactic cosmological origin. Each GRB has a unique light curve and spectrum. A sample variety of light curves of GRBs observed by BATSE are shown in figure 2.16. Despite the improvements achieved with BATSE, the detection of counterparts of GRBs remained unfulfilled.

The major breakthrough occurred in 1997 thanks to the BeppoSAX satellite, which discovered for the first time several fading X-ray signals from GRBs, detected only a few hours after they occurred (Costa et al. 1997). These X-ray afterglows, lasting typically for weeks, made possible the optical and radio detection of afterglows which in turn enabled the measurement of redshift, the identification of host galaxies, and the confirmation that GRB were, as suspected, at cosmological distances.

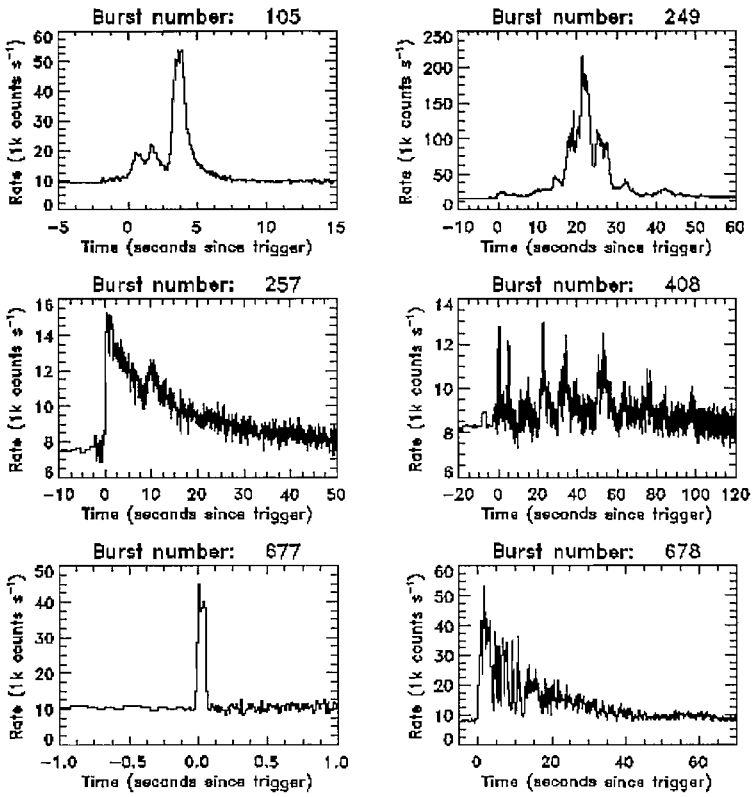

Figure 2.16: A sample variety of light curves of GRBs observed by BATSE.

The mechanism causing the phenomenon of GRBs is still a matter of debate. However, some basic characteristics are well understood. The so called relativistic fireball shock model (see references in Meszaros 2001) provides a framework for the starting energy, the expansion of the GRB, and the time involved in reaching the afterglow phase (see figure 2.17). In its most schematic view, a "hidden central engine" emits shells of matter (plasma) into the interstellar medium with relativistic bulk Lorentz factors. If the central engine emits shells with different velocities, a faster shell can reach a slower one and produce a shock. According to the relativistic fireball shock model, γ-rays are produced as a result of the collisions of shells of matter, however the fireball medium does not allow them to escape until it has cooled just enough to become transparent. At this point the photons race outward in the direction of motion of the jet, just ahead of the lead shock front. This is the γ-ray burst. The afterglow results when material in the fireball interacts with the material in the interstellar medium to create a wide array of less energetic photons. Initially X-rays are produced, then as the shells of matter bump into each other, they lose their kinetic energy and the resulting energies decrease, from visible light to eventually radio waves.

As for the "hidden central engine", at the moment there are two major theoretical

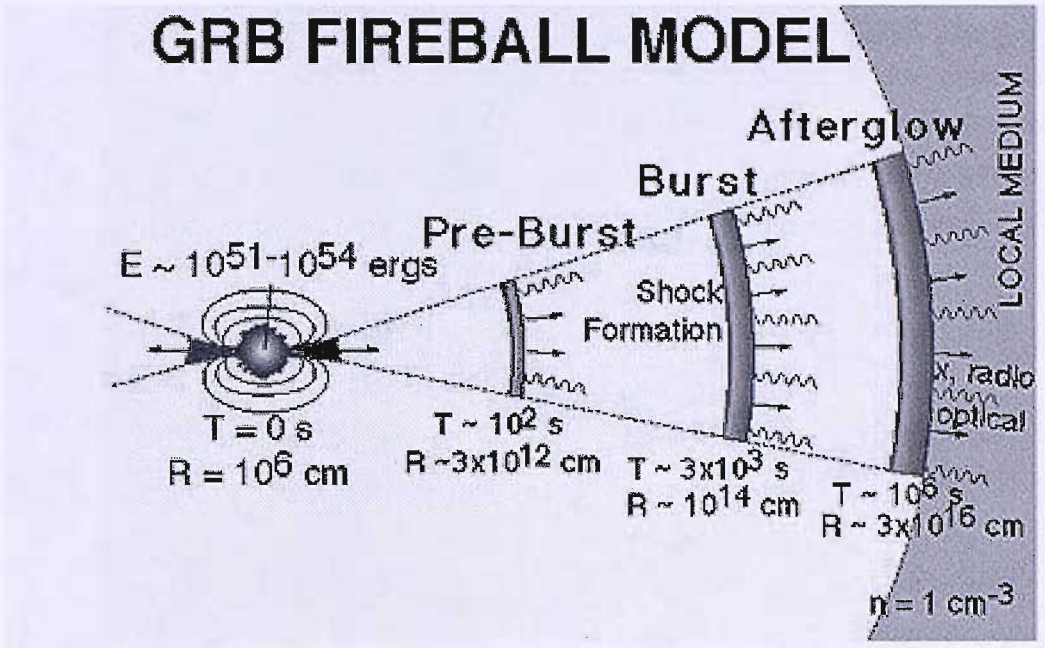

Figure 2.17: Schematic view of the relativistic fireball shock model for GRBs.

models (see references in Meszaros 2001). The first involves the coalescence of two compact objects such as neutron stars or black holes. The second, the so called hypernova or collapsar model, is more popular and convincing. The core of a supermassive rapidly rotating star collapses into a black hole, while two powerful jets of matter and energy are boosted into space in opposite directions. Internal shocks in the jets and their interaction with circumstellar material create the γ-ray burst. This model helps to explain why GRBs often occur in star-forming regions, where massive stars still reside at the end of their relatively short lives. Moreover, it is supported by the evidence of a few GRBs observed to coincide with supernova explosions.

2.5 Active Galactic Nuclei

An Active Galactic Nucleus (AGN) is a compact region at the centre of a galaxy which produces more radiation than the rest of the galaxy itself, over some or all of the electromagnetic spectrum. The source of this emission is believed to be the accretion of material onto a supermassive black hole ($\sim 10^8$ $M_\odot$) at the centre of the galaxy. Risaliti & Elvis (2004) reported a detailed multiwavelength review of AGN. A large number of different types and sub-types of AGNs are known, based upon their radio, optical, X-ray properties. A schematic view of the "AGN bestiary" is shown in figure 2.18.

AGNs are generally divided into two main categories according to their radio emission:

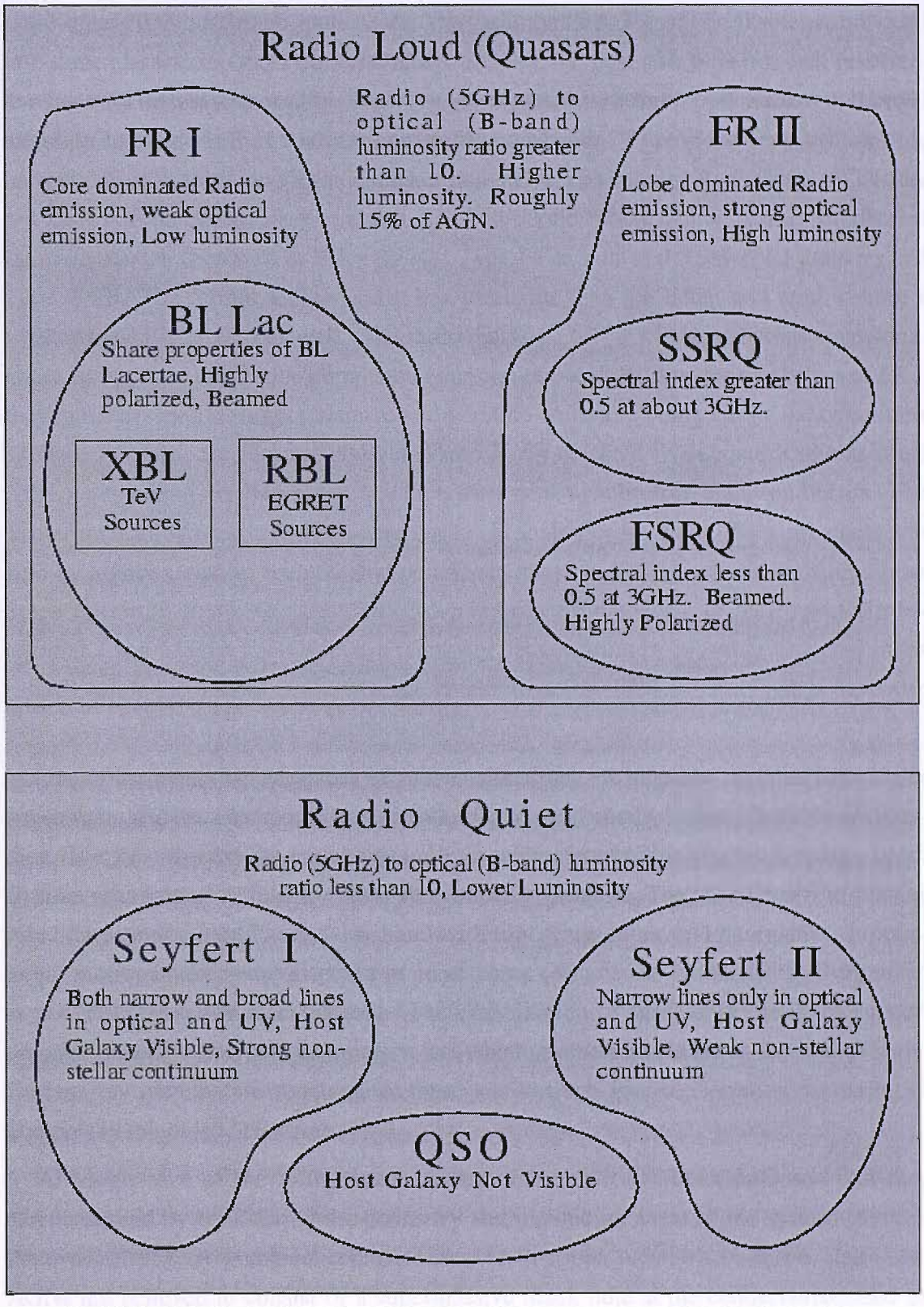

Figure 2.18: Schematic view describing the classification scheme for AGNs.

radio quiet AGN and radio loud AGN. The radio quiet AGN can be further subdivided into three classes. In Quasi Stellar Objects (QSOs), the host galaxy is not well resolved, leaving only the nucleus visible. Type I Seyferts generally exhibit both narrow and broad emission lines, as well as a strong non-stellar continuum. Type II Seyferts exhibit only narrow emission lines, and have a weaker non-stellar continuum. Radio quiet AGNs are not known to be strong γ-ray emitters. The radio loud AGNs can be mainly subdivided into two classes (Fanaroff & Riley 1974). Type I Fanaroff and Riley (FR) galaxies and Type II FR. The former are generally less luminous than the latter, and tend to have a weaker optical emission as well. The radio emission of FR I is classified as core dominated, as opposed to the lobe dominated emission of FR II. BL Lac are a subclass of FR I, they generally exhibit highly beamed and variable emission, being strong γ-ray emitters as well. BL Lacs are further subdivided into X-ray selected (XBL) and Radio-selected (RBL), depending on the energy in which their peak synchrotron emission occurs. Flat Spectrum Radio Quasars (FSRQs) are the FR II analog of BL Lacs. They are characterized by highly variable, beamed, and polarized emission. FSRQs are distinguished from Steep Spectrum Radio Quasars (SSRQs) primarily by the shape of their spectrum between 2.7 and 5 GHz. FSRQs have a relatively flat spectrum in this range (spectral index α<0.5), while the indices for SSRQs are greater than 0.5. BL Lacs and FSRQs have also been grouped into a class of objects called Blazars.

One of the main characteristics of AGNs is that they are variable, on wide time scales (from years and decades to minutes and hours) and in all energy ranges (from γ-rays to radio). The X/γ-rays exhibit variability on time scales shorter than any other energy band. Blazars are, among AGNs, the most dramatically variable. They are known to display rapid flares in the hard X-ray/γ-ray band with timescales of several hours/days, superluminal motions have been observed in some cases (Wagner & Witzel 1995, Brinkmann et al. 2005, Foschini et al. 2006). The combination of these characteristics support the argument of relativistic beaming in jets which are pointing close to the line of sight. Gamma-ray photons are produced in these jets through inverse Compton scattering of photons by relativistic electrons.

Although each of the AGN types appears different, it has been proposed that they can be unified by considering the geometry and inclination angle of the system (Urry & Padovani 1995). A graphical representation of this idea is shown in figure 2.19. All AGNs are believed to consist of a supermassive black hole at the centre surrounded by an accretion disk and a hot corona. Outside of this there is a molecular torus of cold material. Depending on the presence or not of a jet in the system, then the AGN would appers as radio loud or quiet. FR I radio loud AGN are viewed close to the jet axis and

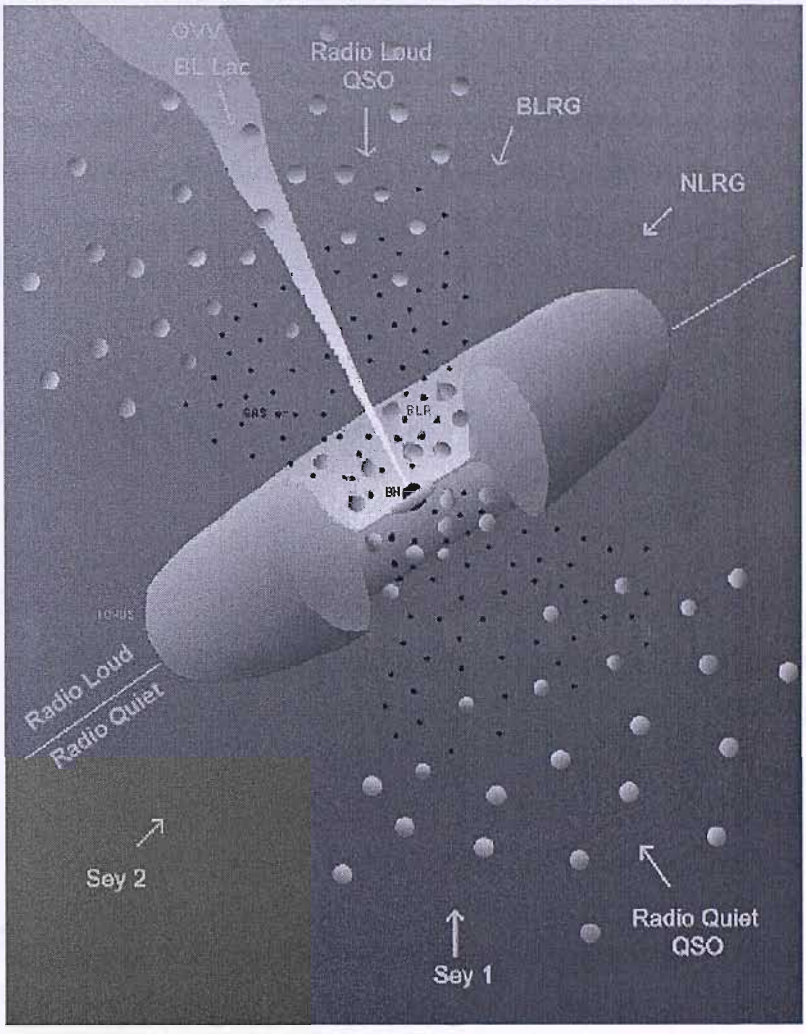

Figure 2.19: Unification model of AGN (picture credit ESA/ISDC).

in Seyfert I the broad line emission from the inner parts of the system can be observed. FR II radio loud AGN are not viewed close to the jet axis. In Seyfert II the broad line emission is obscured by the optically thick torus, only the narrow line emission region can be observed.

2.6 Summary

It is evident that the high energy sky is transient in nature, with a zoo of astrophysical objects appearing and then disappearing in a wide range of timescales, from few seconds to years. Thanks to INTEGRAL's wide FOV and good sensitivity, this mission offers an excellent capability in detecting transient sources. It should be possible to improve the understanding of these objects through a study of their high energy behaviour.

Chapter 3

The INTEGRAL gamma-ray satellite

Science is a wonderful thing if one
does not have to earn one's living at it.
– Albert Einstein

3.1 The INTEGRAL mission

The European satellite INTEGRAL (INTErnational Gamma-Ray Astrophysics Laboratory) is an astronomical satellite for observations of the sky in the soft γ-ray regime 15 keV–10 MeV (Winkler et al. 2003). It was launched on 17 October 2002 by a Russian PROTON rocket and placed in a 72 hour highly eccentric orbit with a perigee of $\sim$ 10,000 km, an apogee of $\sim$ 154,000 km and an inclination of 51.6 degrees. This keeps INTEGRAL above the proton radiation belts which consist of subatomic particles that are trapped by the Earth's magnetic field. Passage through proton belts would increase the background in the γ-ray instruments onboard the satellite, reducing their sensitivity.

INTEGRAL scientific goals are achieved through fine spectroscopy, imaging capability and accurate positioning of celestial sources. The fine imaging capability within a large field of view (FOV) permits an accurate location and hence identification of the γ-ray sources with counterparts at other wavelengths. Moreover, it provides considerable serendipitous science, which is very important for an observatory-class mission. The fine spectroscopy, over the entire energy range, permits spectral features to be uniquely identified and line profiles to be determined for physical studies of the source region.

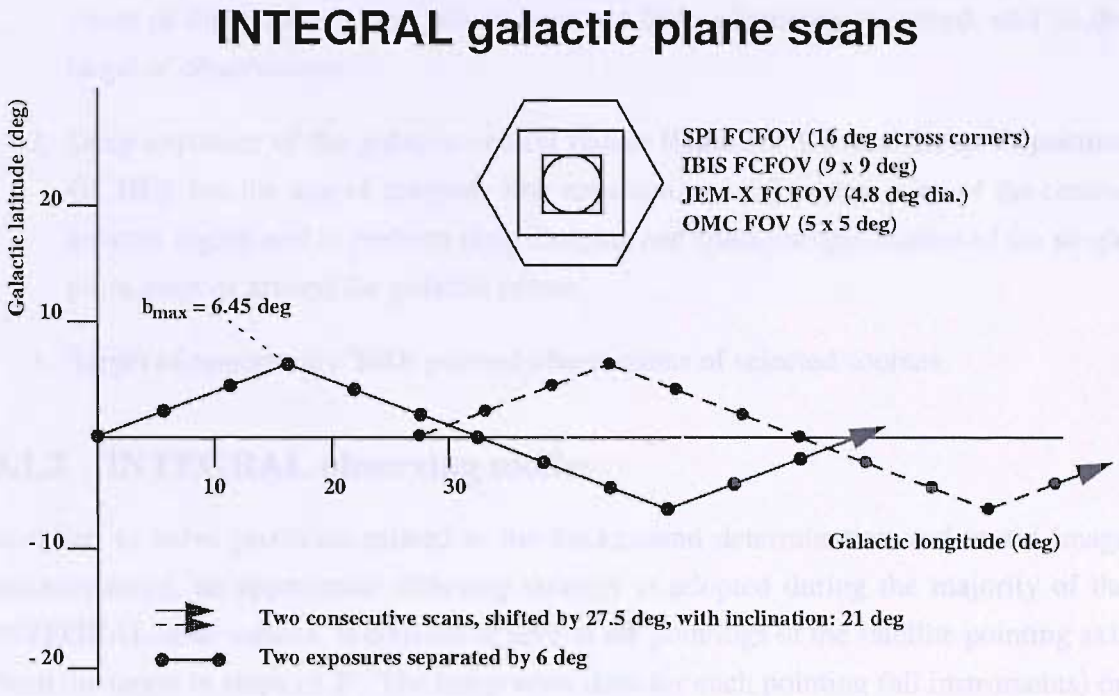

Figure 3.1: Schematic view of two consecutive Galactic Plane Survey (GPS) scans. The scans are performed by executing a "slew and stare" manoeuvre of the spacecraft, resulting in 20 to 55 different pointings (staring) separated by 6°. The extremes in latitude of the pointings are at |b| = 6°.45 and follow a saw-tooth pattern inclined at 21° to the galactic equator. Each subsequent scan will be shifted by 27°.5 in galactic longitude. Each pointing lasts about 2200 sec, while the slew lasts about 200 sec.

3.1.1 INTEGRAL observing program

Most of the observing time (65% of the total time in year 1, 70% year 2, 75% year 2+) is devoted to the scientific community. Proposals for observations are selected on their scientific merit by a single Time Allocation Committee. These selected observations are the basis of the General Programme. The remaining fraction of the observing time is the Core Programme (Winkler 2001), reserved for scientific institutes which have developed and delivered instruments as well as for the data centre (guaranteed PI time). During all the nominal period of the mission, the Core Programme consists of three parts with a dedicated exposure time per year:

1. Frequent scans of the galactic plane (**Galactic Plane Survey, GPS**): provide periodic monitoring to search for transient sources and monitor the persistent ones. The scans are performed weekly with a "slew and stare " manoeuvre of the spacecraft along the season visible part of the galactic plane, within a galactic latitude of ±10° (see figure 3.1). Moreover, for the period of mission extension, specific interesting

zones of the galactic plane, which have not been adequately surveyed, will be the target of observations.

2. Deep exposure of the galactic central radian (**Galactic Central Deep Exposure, GCDE**): has the aim of mapping line emission and diffuse emission of the central galactic region and to perform deep imaging and spectroscopic studies of the single point sources around the galactic centre.

3. Target of opportunity **ToO**: pointed observations of selected sources.

3.1.2 INTEGRAL observing modes

In order, to solve problems related to the background determination and to aid image reconstruction, an appropriate dithering strategy is adopted during the majority of the INTEGRAL observations. It consists of several off-pointings of the satellite pointing axis from the target in steps of 2°. The integration time for each pointing (all instruments) on the raster is flexible in the range 0.5–1 hour. The integration time is adjusted in a way so that multiples of a complete dither pattern are always executed for each observation. The satellite will continuously follow one dither pattern throughout one observation. Two different dither patterns are used as the operational baseline:

- Rectangular dithering (baseline): this mode consists of a square pattern (see figure 3.2) centred on the nominal target location (1 source on-axis pointing, 24 off-source pointings, each 2° apart, in a rectangular pattern). This mode is used for multiple point sources in the FOV, sources with unknown locations, and extended diffuse emission.

- Hexagonal dithering: this mode consists of a hexagonal pattern (see figure 3.2) centred on the nominal target location (1 source on-axis pointing, 6 off-source pointings, each 2° apart, in a hexagonal pattern). It will only be used for a single, strong, known point source, where no significant contribution from out-of-view sources is expected. Experience from earlier observations has shown that this is not very often fulfilled (e.g. because of transient sources).

Because of the pointing-slew-pointing dithering nature of INTEGRAL operations, each observation of a celestial target is actually comprised of numerous individual pointings and slews. In addition, there are periods within a given sequence where scheduled observations occur, i.e. engineering windows, yet the instruments still acquire data. All these data acquisition periods are refereed to as Science Windows (ScWs). Pointing (fixed

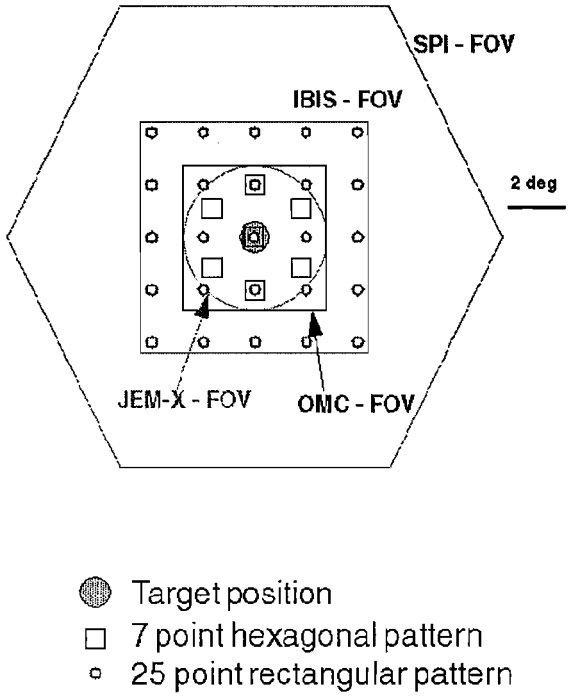

Figure 3.2: Dither patterns adopted for INTEGRAL observations: rectangular dithering and hexagonal dithering.

orientation), Slew (changing orientation), and Engineering (undefined orientation) windows are all special cases of a Science Window. The duration of a pointing ScW is typically ~ 2000 seconds. It is worth noting that a small fraction of the INTEGRAL observations are performed in staring mode, where the telescope axis is kept fixed on a target without dithering.

3.2 The INTEGRAL payload

The INTEGRAL gamma-ray observatory carries three co-aligned coded mask telescopes: the imager IBIS (Ubertini et al.2003), the spectrometer SPI (Vedrenne et al. 2003) and the X-ray monitor JEM-X (Lund et al. 2003). The optical monitor OMC (Mas-Hesse et al. 2003), in optical Johnson V-band, complements the payload. The instruments of the payload cover a wide energy band, from the soft X-rays to the soft γ-rays (3 keV–10 MeV). All of them are co-aligned with overlapping fully coded field of views, ranging from 4.8° diameter (JEM–X) to 9°×9° (FCFOV IBIS) and 16° corner-to-corner (SPI). They operate simultaneously, so an observer receives data from all instruments. Figure 3.3 illustrates the main components of INTEGRAL. The next sections will give an overview of each instrument. Particular attention will be paid to the IBIS telescope, whose data are the particular interest of this thesis.

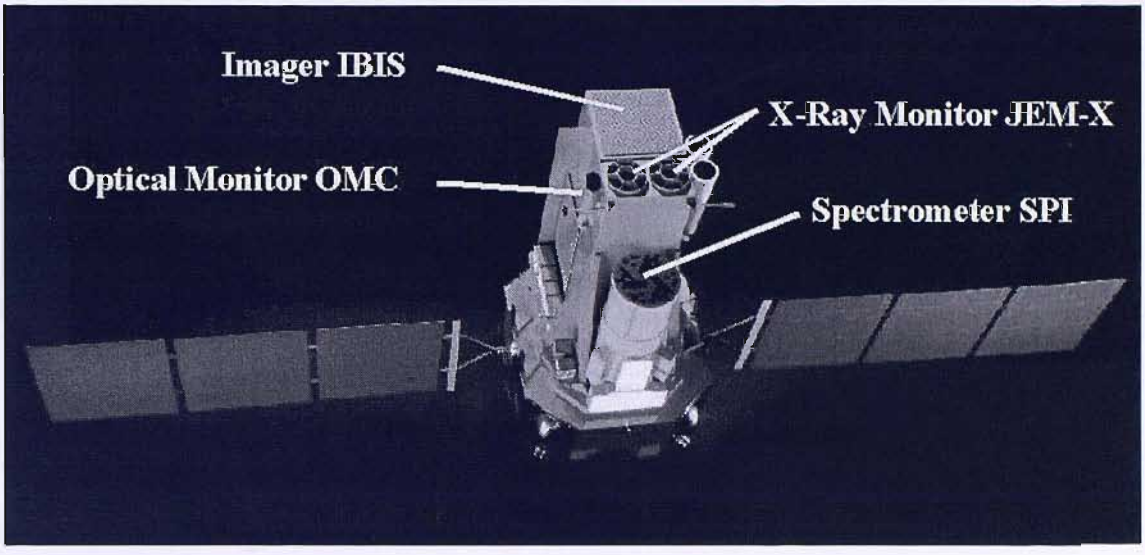

Figure 3.3: The INTEGRAL satellite.

Table 3.1: An overview of the IBIS scientific capabilities.

Energy Range	15 keV–10 MeV
Continuum sensitivity, at 3σ and 10^6s integration (ph cm^{-2} s^{-1} keV^{-1})	2.3×10^{-6} @ 100 keV 1.6×10^{-6} @ 1 MeV
Line sensitivity, at 3σ and 10^6s integration (ph cm^{-2} s^{-1})	1.8×10^{-5} @ 100 keV 3.8×10^{-4} @ 1 MeV
Energy Resolution (FWHM %)	8 % at 100 keV 10% at 1 MeV
Angular resolution (FWHM)	~ 12′
Point Source Location Accuracy (90 % error radius)	30” @ 100 keV (50 σ source) 3’ @ 100 keV (5 σ source) 5’-10’ @ 1 MeV (5 σ source)
Timing accuracy	61 μs - 1 hr
Field of View	8.6°×8.6° (fully coded) 29°×29° (zero response)

3.2.1 IBIS, the gamma-ray imager

IBIS (Imager on Board the Integral Satellite) is designed for the fine imaging (12 arcmin Full Width Half Maximum) and precise location (30 arcsec for strong sources) of soft γ-ray sources in the energy range 15 keV–10 MeV. The fully coded field of view (FCFOV) is 9°×9°, the partially coded field of view (PCFOV) is 30°×30° (full width at zero response) and 19°×19° (full width at half response), respectively. Table 3.1 lists the principal IBIS scientific capabilities.

IBIS consists of two pixellated detector planes separated by 10 cm and placed in parallel beneath a coded mask aperture system. The telescope shielding is composed of a combined collimator and a VETO assemblage. A representation of the detector arrangement is shown in figure 3.4.

The two pixellated detectors composing IBIS are:

- **ISGRI (Integral Soft Gamma-Ray Imager)**: constitutes the upper detector layer, covering the energy range 15 keV–1 MeV (Lebrun et al. 2003). It consists of 16,384 cadmium telluride semiconductor crystal detectors organised in 8 modules, each containing 32×64 pixels. Each pixel size is 2×2×4 mm^3 which enables high spatial resolution images to be obtained.

- **PICsIT (Pixilated CsI Telescope)**: provides the lower layer covering the energy range 170 keV–10 MeV (Labanti et al. 2003). It is made up of 4,096 caesium iodide crystal scintillators divided into 16 modules.

IBIS can detect photons in three modes: detection on ISGRI, detection on PICsIT, and detection on the two layers (Compton mode).

Two shields protect IBIS from external radiation (see figure 3.4). The passive collimating system consists of two subsystems based on tungsten and lead as passive material: the "hopper" (truncated pyramid on the top of the ISGRI detector) and a "tube" made of four walls with a profile that ideally join the hopper top part to the mask sides. This creates a passive shield able to reduce the celestial diffuse background component, it becomes transparent above 200 keV. The active shield, the VETO system, is composed of 16 independent modules, each made of 2 large BGO crystals. This ensures rejection of the background events and shields the underneath and sides of the telescope to the top level of the ISGRI detector.

The IBIS coded mask (see figure 3.5) is a square array of 9,025 cells in a MURA (Modified Uniformly Redundant Array) configuration. Half of the cells are in tungsten (16 mm thickness) offering a minimum opacity of $\sim$ 70% at 3 MeV. The other half of

the cells are "open", with an off-axis transparency of 60% at 20 keV. The coded mask projects a shadowgram onto the detector plane and images of the sky are reconstructed by decoding the detector shadowgram with the mask pattern.

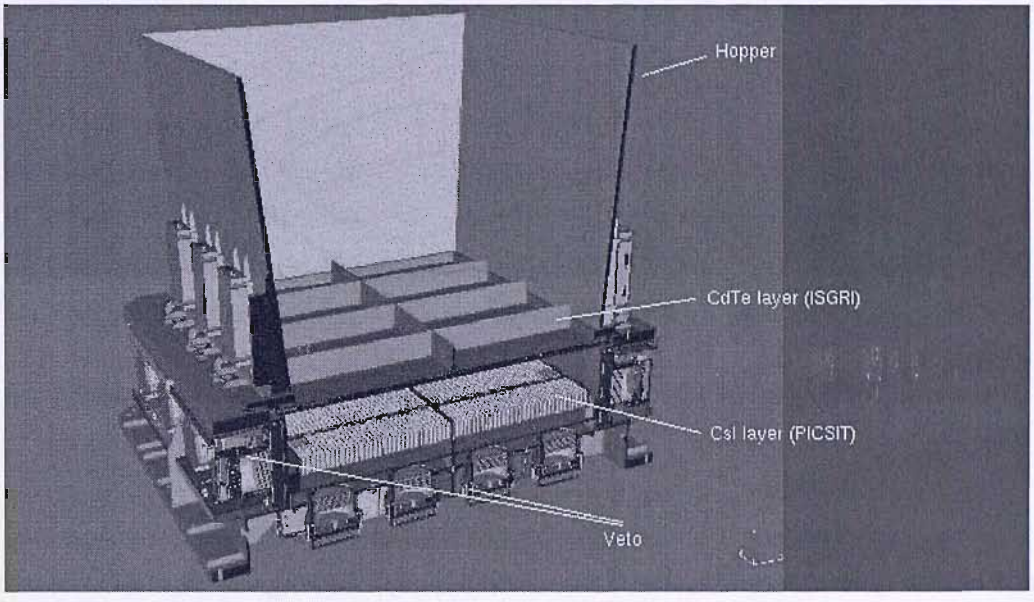

Figure 3.4: Scheme of the IBIS instrument showing the PICsIT and ISGRI detector planes and shielding systems. Above the detector planes is the lower part of the collimating system (hopper).

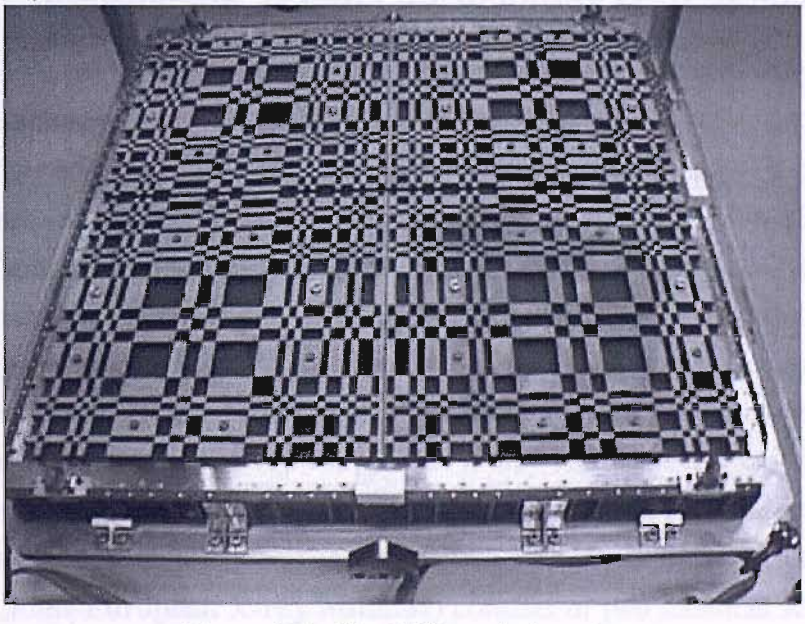

Figure 3.5: The IBIS coded mask.

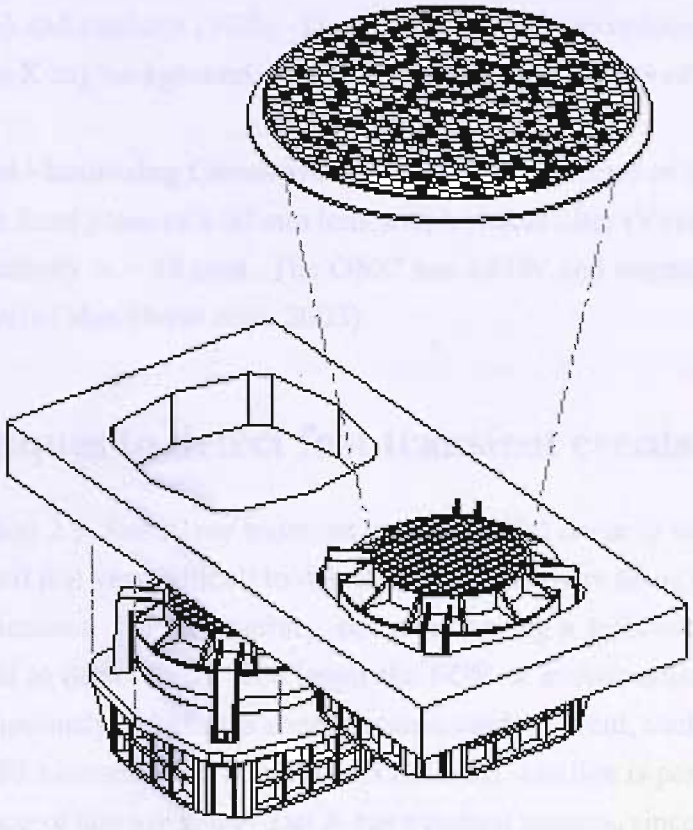

Figure 3.6: Overall design of JEM–X, showing the two units, with only one of the two coded masks.

3.2.2 The spectrometer SPI and the monitors JEM–X and OMC

The INTEGRAL payload is complemented by three further instruments: the spectrometer SPI and two monitoring cameras, JEM–X (X-ray) and OMC (optical).

SPI (SPectrometer on INTEGRAL) provides fine spectral analysis of γ-ray point sources as well as extended sources, over the energy range 200 keV–8 MeV. The fully coded FOV and the angular resolution are 16° and 2°, respectively. SPI consists of an array of 19 individual hexagonal high purity germanium detectors. The SPI coded mask is placed 1.7 meters above them. It is composed by 127 hexagonal cells in a HURA (Hexagonal Uniformly Redundant Array) pattern with a 120° rotational symmetry. Sixty-three cells are opaque to γ-rays (95% at 1 MeV), they are made of 3 cm thick tungsten. The remaining sixty-four cells are transparent (80% at 60 keV). Emission lines from radioactive nuclei are some of the main observational targets of the spectrometer SPI.

JEM–X (Joint European X-ray Monitor) consists of two identical X-ray monitors (JEM–X1 and JEM–X2) covering the energy range 3–35 keV (Lund et al. 2003). The FCFOV of each instrument is 4°.8, the angular resolution is $3'$. The coded mask (HURA pattern) is placed 3.4 meters above the detectors which are collimated gas chambers filled

with xenon (90%) and methane (10%). The collimator helps to reduce events caused by the cosmic diffuse X-ray background. Figure 3.6 is a schematic view of the overall design of JEM–X.

OMC (Optical Monitoring Camera) employes a CCD detector of 1024×1024 pixels. It is located in the focal plane of a 50 mm lens with a visible filter (V) centred on 550 nm. The limiting sensitivity is ~ 18 mag. The OMC has a FOV and angular resolution of 5° and 23″ respectively (Mas-Hesse et al. 2003).

3.3 Techniques to detect fast transient events with IBIS

As stated in section 2.3, fast X-ray transient events (FXTs) occur at unpredictable locations and times and it is very difficult to detect and observe them using traditional narrow FOV X-ray instruments. On the contrary, detectors having a sufficiently wide FOV are particularly suited to detect them. The larger the FOV of an instrument, the greater the chance of serendipitously detecting a short duration random event, such as a FXT.

The IBIS/ISGRI instrument on board the INTEGRAL satellite is particularly suited to the detection of new or already known fast X-ray transient sources, since it provides a very powerful combination of a large FOV (PCFOV of 30°×30°, full width at zero response), good sensitivity, fine angular resolution and wide energy range. All are indispensable characteristics for the detection of fast X-ray transient events. To this aim, a vast dataset of ISGRI data, spanning more than three years of INTEGRAL observations, has been inspected. Specifically, the ScWs dataset belongs to the Core Program data (GPS and GCDE) from revolution 46 (end of February 2003) to 429 (mid-April 2006) inclusive as well as to all public data released up to revolution 260. This implies a total of ~ 20,000 ScWs in the ISGRI dataset. Each ScW has been analysed using the imaging components of the OSA 5.1 software. Subsequently, a proprietary tool was used to search each ScW, and provide a cross-correlated list of all excesses above 5σ (20–30 keV) found in one or more ScWs. The search was initially performed in the energy band 20–30 keV; but when an excess was found a check was made for the detection at higher energies and in the previous and subsequent ScWs, when available. This approach is very efficient in unveiling fast X-ray transient events lasting only a few hours since the search occurs at ScW level, on the same timescale as the outbursts themselves. Integrating for longer time periods (e.g. several days, weeks or months) just degrades the signal-to-noise of the detection to a much smaller value, eventually precluding the discovery of the fast X-ray transient events.

At the preliminary level of inspection, approximately 1,000 resulting excesses were

found. It is important to point out that all of them were carefully studied in order to reject false detections and so to identify them as real fast X-ray transient sources. False excesses can be due to noisy pixels, structures, bad source cleaning (due to "moving" telescope or "bad" input catalog), background noise or ghosts. As the coded mask aperture is symmetric, up to eight source ghosts can be produced by a source. They are distributed at the corners ($\sim 14°.7$) and midpoints ($\sim 10°.5$) of a square with sides of length $\sim 21°$ centred on the real source. To prevent this, a catalog of X/γ-ray sources (input catalog) likely to be visible is provided to the OSA software to allow it to clean ghost sources. However, the OSA software occasionally fails and leaves the ghosts or may keep a ghost and remove the real source. In this context, each resulting excess was carefully studied to reject false detections. A visual inspection was performed, in order to reject a likely ghost, confirm the excess had an appropriate point spread function and that it was unaffected by source structures. After rejecting many false detections, all the remaining excesses (a few hundred in total) displayed a recurrence nature, being detected by INTEGRAL more than once. This strongly suggested their real nature to be fast X-ray transients. Their position was correlated with all X/γ-ray and radio catalogs from the HEASARC database to find counterparts at other wavelengths. By doing so, a total of 14 X/γ-ray sources were found, displaying fast X-ray outbursts on very short timescales, typically a few hours. Each outburst from each source was studied in detail by performing an ISGRI and, when possible, JEM–X timing and spectral analysis. To this aim, two versions of the OSA software were used: initially OSA 4.2 and subsequently OSA 5.1. Checks were performed on some outbursts by analyzing them with both versions of OSA. As result, their spectral and temporal characteristics were effectively the same. The difference between the two versions of the OSA software was mainly related to the fact that OSA 5.1 provided a much faster and stable data analysis tool than OSA 4.2. The spectral and timing results on each outburst from each source are presented in Chapter 4 and 5. It is worth pointing out that almost all the fast outbursts presented in this thesis are newly discovered, they have never been reported in the literature before. Due to possible cross-talk between objects in the same FOV, the variability pattern of all other bright sources in the FOV was also investigated, as well as the source of interest. All sources have shown different time variability indicating that the light curves obtained for the sources of interest and presented in this thesis are reliable.

The sensitivity limit for a persistent source detected at 5σ level (20–30 keV) in one ScW of $\sim$ 2000 seconds is $\sim$ 25 mCrab or $\sim 1.2{\times}10^{-10}$ erg cm^{-2} s^{-1}. In the case of an outburst visible in more than one consecutive ScW, we can assume our detection limit is again $\sim$ 25 mCrab, which now refers to the average flux of the outburst during the ScW

containing the peak.

The dataset of ~20,000 ScWs used for the analysis, although being highly inhomogeneous in both extent and exposure, covers ~ 70% of the sky at a level of at least 10 ksec, as can be seen from the exposure map shown in figure 3.7. Moreover, we can note that the galactic center is particularly well covered, with an exposure time of at least 3 Ms. As for the the galactic plane, most of it is covered with an exposure time of at least 1 Ms.

Figure 3.8 shows the angular distribution off the galactic plane of the central pointing direction of all (~ 20,000) ScWs in the dataset. Their strong concentration towards the galactic plane ($|b| \leq 5°$) rather than medium or high galactic latitude is clearly evident.

3.4 Summary

This chapter has introduced the INTEGRAL gamma-ray satellite. Specifically, it has shown that the IBIS instrument on board INTEGRAL is particularly suited to detect fast transient events thanks to its large field of view, good sensitivity, fine angular resolution and wide energy range. The capability of IBIS in detecting fast X-ray transient sources will be demonstrated in chapter 4 and chapter 5.

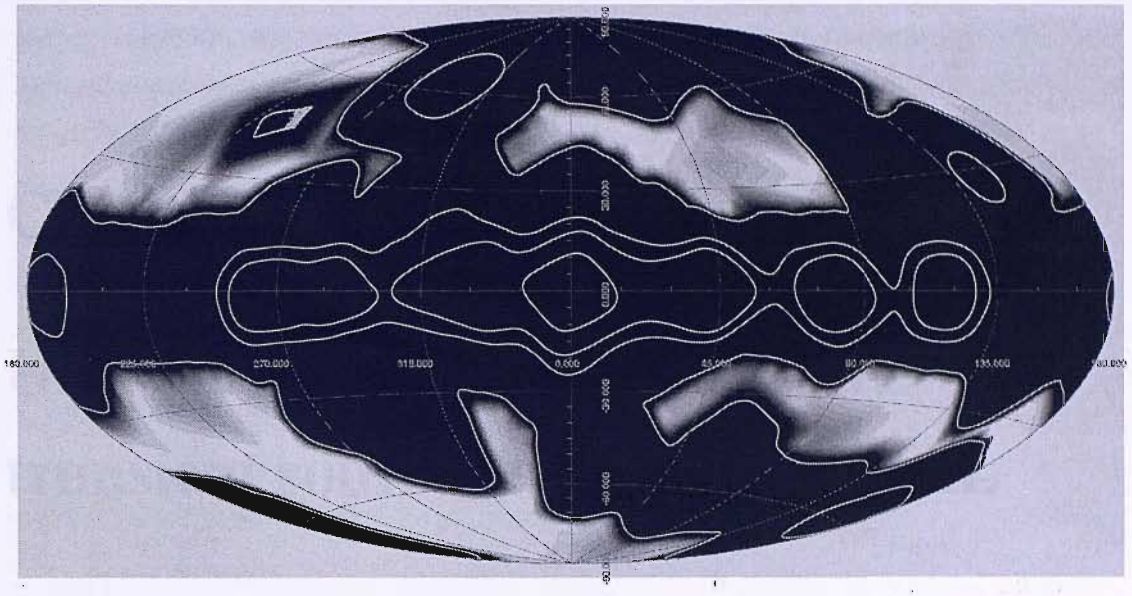

Figure 3.7: The exposure map for the dataset. Contour levels are at 10 ksec, 500 ksec, 1 Ms and 3 Ms.

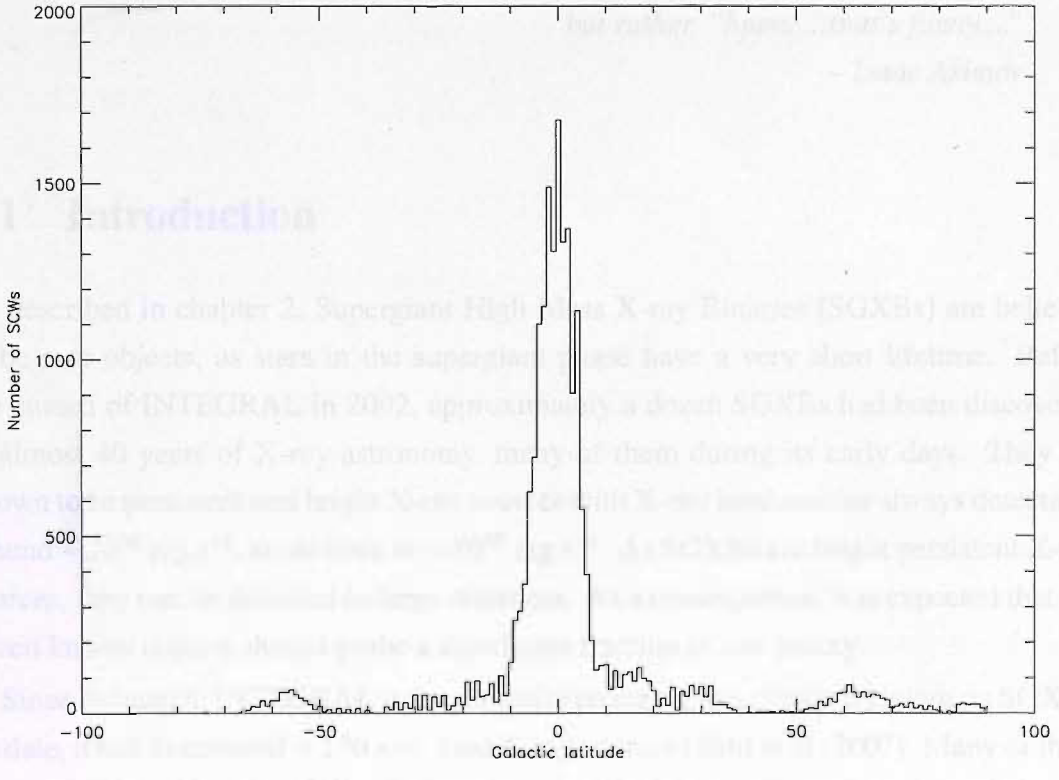

Figure 3.8: The number of ScWs belonging to the dataset versus galactic latitude of their pointing.

Chapter 4

Unveiling supergiant fast X-ray transient sources with INTEGRAL

The most exciting phrase to hear in science,
the one that heralds new discoveries,
is not Eureka! (I found it!)
but rather, "hmm.... that's funny...."
– Isaac Asimov

4.1 Introduction

As described in chapter 2, Supergiant High Mass X-ray Binaries (SGXBs) are believed to be rare objects, as stars in the supergiant phase have a very short lifetime. Before the launch of INTEGRAL in 2002, approximately a dozen SGXBs had been discovered in almost 40 years of X-ray astronomy, many of them during its early days. They are known to be persistent and bright X-ray sources with X-ray luminosities always detectable around $\sim 10^{36}$ erg s^{-1}, some even at $\sim 10^{38}$ erg s^{-1}. As SGXBs are bright persistent X-ray sources, they can be detected to large distances. As a consequence, it is expected that the dozen known objects should probe a significant fraction of our galaxy.

Since its launch, INTEGRAL is dramatically changing this classical picture on SGXBs. To date, it has discovered ~ 170 new hard X-ray sources (Bird et al. 2007). Many of them are characterized by absorbed hard spectra, with little or no emission in the soft X-rays because of heavy absorption by the interposing material. This, together with their often transient nature, explains why they have not been detected by any previous X-ray mission. As discussed by Dean et al. (2005), most of the newly discovered INTEGRAL

sources should be High Mass X-ray Binaries (HMXBs). This picture has been supported by several optical identifications with transient Be HMXBs or bright persistent SGXBs exhibiting a huge intrinsic and local extinction (Walter et al. 2006). In principle, the properties of the latter do not appear to be extremely different from those of classical persistent SGXBs, except for the much higher absorption which explains why they were not detected earlier. Besides the highly absorbed persistent SGXBs, more interestingly INTEGRAL is playing a key role in discovering a new class of SGXBs with an X-ray behaviour completely different and never seen before. They have been dubbed Supergiant Fast X-ray Transients; SFXTs (Negueruela et al. 2006a, Sguera et al. 2007, Sguera et al. 2006, Sguera et al. 2005) and escaped detection by previous X-ray satellites mainly because of their fast X-ray transient behaviour. In fact, most of the time SFXTs are undetectable and then occasionally they undergo fast X-ray outbursts lasting less than a day, typically only a few hours. The next section extensively reports on INTEGRAL results pertaining to 8 firm SFXTs: XTE J1739−302, IGR J17544−2619, AX J1841.0-0536, AX J1845.0−0433, SAX J1818.6−1703, IGR J11215−5952, IGR J16465−4507 and IGR J08408−4503.

4.2 Firm supergiant fast X-ray transients detected by INTEGRAL

4.2.1 XTE J1739−302=IGR J17391−3021

4.2.1.1 Archival X-ray observations of the source

This source can be considered the prototype of SFXTs since it was the first object of this class to be recognized. XTE J1739−302 (Smith et al. 1998) was the brightest source in the galactic center region while active at the time of the RXTE discovery (12 August 1997), with a flux of 3×10^{-9} erg cm^{-2} s^{-1} (2–25 keV). The source was only observed by RXTE in that one day, it was not detectable 9 days earlier or 2, 8 and 16 days later. The spectrum (2–25 keV) during the bright state was well described by a thermal bremsstrahlung model with kT $\sim$ 12 keV, furthermore no statistically significant periodicities have been found from 0.01 to 1000 Hz. At the time of the discovery, Smith et al. (1998) tentatively identify XTE J1739−302 as a Be/X-ray transient, even if its outbursts (constrained by RXTE observations to be more than a few hours but less than a day) were much shorter than those typical of Be/X-ray transients.

ASCA detected XTE J1739−302 on 11 March 1999 (Sakano et al. 2002). The light curve (2–10 keV) initially showed null flux, then suddenly the source flared up reaching

the peak after ~ 4 minutes and it dropped to zero flux level with the same timescale as the flare-rise. Then the source flared up again, this second flare was characterized by an almost identical profile except for the peak flux which was about half of that of the first flare. The 2–10 keV ASCA spectrum of XTE J1739–302, accumulated during the flaring period, was a hard and absorbed power law (Γ ~0.8, N_H ~ 3×10^{22} cm^{-2}). ASCA timing analysis did not find any significant pulsations, which is consistent with the RXTE results by Smith et al. (1998). This ASCA observation provided the lowest limit for the quiescent luminosity of XTE J1739–302 which is equal to 7×10^{32} erg s^{-1} (2–10 keV).

Recently, a Chandra observation of the source provided a very accurate position at RA=17^h 39^m 11.58^s Dec=-30° 20′ 37.6″ with an accuracy better than a few arcseconds (Smith et al. 2006a). This permited an unambigous identification of its optical/infrared counterpart with a very bright and reddened object catalogued in the USNO–B1.0 as well as 2MASS catalog. Optical and infrared spectroscopy (Negueruela et al. 2006b) revealed it as a late type O8Iab(f) supergiant star at a distance of ~ 2.3 kpc. Both spectra are very similar to those of classical wind fed persistent SGXBs, there is nothing in it that can provide a clue or explanation to the completely different X-ray behaviour of XTE J1739–302.

An interesting property of XTE J1739–302 is that its absorption column density is not only larger than the galactic one along the line of sight, but is also variable. It ranges, at different times, from ~ 3 to ~ 38 $\times10^{22}$ cm^{-2} (Smith et al. 2006a).

4.2.1.2 Archival INTEGRAL observations of the source

The fast transient source IGR J17391–3021 was discovered in outburst by INTEGRAL on 26 August 2003 at 18:49 UTC (Sunyaev et al. 2003a) with a flux level of 70 mCrab (18–50 keV). The maximum flux (150 mCrab) was detected on 27 August 2003 at 00:44 UTC, when the source was also detected in the energy range 50–100 keV at a level of 50 mCrab. The total length of the outburst was less than a day. The 20–100 keV spectrum of IGR J17391–3021 at the maximum of the outburst was well fit by an optically thin thermal bremsstrahlung model with kT~22 keV (Lutovinov et al. 2005b). The IGR source position reported by Sunyaev et al. (2003a), which has an error circle radius equal to 3′, is located ~1′.5 from the Chandra location of the known transient XTE J1739–302, which has a position accuracy better than a few arcseconds (Smith et al. 2006a). The RXTE satellite pointed to IGR J17391–3021 ~ 35 hours after the time quoted as the beginning of the previous cited outburst detected by INTEGRAL, but no detection was reported. This implied an upper limit to the source flux of ~ 3 mCrab in the energy band 3–20 keV (Lutovinov et al. 2005b).

Table 4.1: Summary of ISGRI observations of outbursts of XTE J1739–302.

No.	Date	duration (hours)	energy band (keV)	flux at the peak (mCrab)	luminosity peak (10^{36} erg s^{-1})	ref
1	22 March 2003	~ 2	20–60	~ 210	~ 1.6	[1]
2	26 August 2003	~ 14	18–60	~ 120		[2]
3	6 September 2003	~ 7	18–60	~ 60		[2]
4	9 March 2004		20–30	~ 280	~ 0.8	[1]
5	10 March 2004	~ 1.5	20–30	~ 250	~ 0.7	[1]
6	21 August 2004		20–60	~ 480	~ 3.5	[1]
7	31 August 2004	~ 6	20–60	~ 210	~ 1.5	[1]

[1] This PhD thesis; [2] Lutovinov et al. (2005b)

4.2.1.3 Analysis of newly discovered outbursts by INTEGRAL

This section reports on 5 newly discovered fast outbursts of IGR J17391–3021 detected by INTEGRAL. All of them are listed in Table 4.1 (No. 1, 4, 5, 6, 7) together with all other detected outbursts by INTEGRAL and already reported in the literature (No. 2, 3). It is worth pointing out that the ISGRI analysis of outburst No. 1 in table 4.1 enabled a more accurate IGR J17391–3021 position (RA=17^h 39^m 12.24^s Dec=-30° 20′ 52.8″, error circle radius 36″) than that reported by Sunyaev et al (2003a) when the source was discovered. This improved position is now located ~ 17″ from the Chandra location of XTE J1739–302, fully confirming that IGR J17391–3021 and XTE J1739–302 are indeed the same source.

Outburst No. 1 in table 4.1 lasted ~ 2 hours, its 20–60 keV ISGRI light curve is shown in figure 4.1 with a bin time of 150 seconds. Three peaks are very evident. The first two had a very fast rise and decay as well as a similar total duration of ~ 20 minutes. The third peak lasted ~ 1 hour showing a fast rise followed by a slower decay. The source reached a maximum peak flux of ~ 210 mCrab or ~ 2.5×10^{-9} erg cm^{-2} s^{-1} (20–60 keV). Figure 4.2 shows the sequence of 3 consecutive ISGRI ScWs during which this outburst has been detected. It is worth noting that during two of them (specifically the second and the third ScW during which the source was detected) XTE J1739–302 was inside the JEM–X FOV so it was possible to obtain information at even lower energy. Figure 4.3 shows their JEM–X mosaic significance image in three different energy bands (4–10, 10–20, 15–35 keV) where XTE J1739–302 is clearly detected.

The combined JEM–X/ISGRI spectrum (3–80 keV) extracted during the outburst is best fit by a cutoff power law (χ^2_ν=1.25, 150 d.o.f.) with Γ=1.25±0.1 and cutoff energy

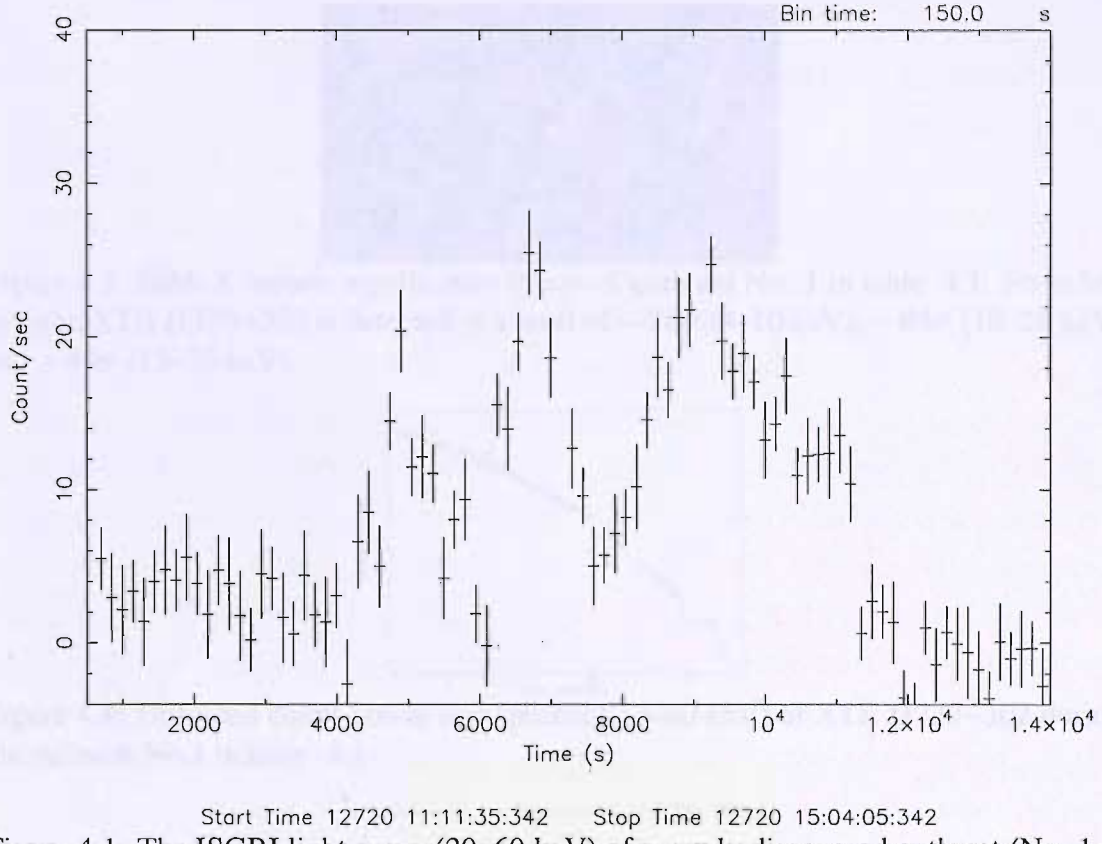

Figure 4.1: The ISGRI light curve (20–60 keV) of a newly discovered outburst (No. 1 in table 4.1) of XTE J1739−302.

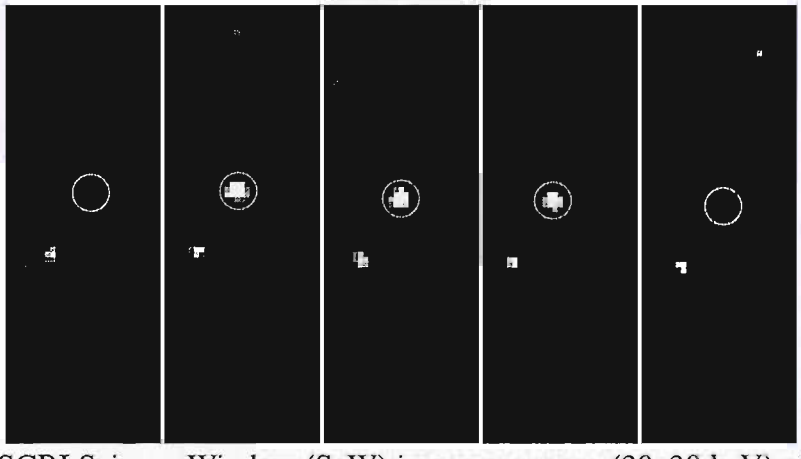

Figure 4.2: ISGRI Science Window (ScW) image sequence (20–30 keV) of a newly discovered outburst (No. 1 in Table 4.1) of XTE J1739−302 (encircled). The duration of each ScW is ~ 2000 s. The source was not detected in the first ScW (significance less than 2σ), then it was detected during the next 3 ScWs with a significance, from left to right, equal to 14σ, 16σ and 23σ, respectively. Finally in the last ScW the source was not detected (significance less than 2σ). A weak persistent source (1E 1740.7–2942) is also visible in the field of view

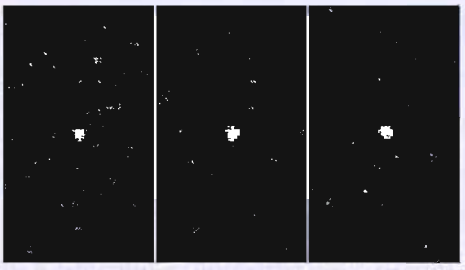

Figure 4.3: JEM–X mosaic significance image of outburst No. 1 in table 4.1. From left to right, XTE J1739−302 is detected at a level of ~ 78σ (4–10 keV), ~ 65σ (10–20 keV) and ~ 40σ (15–35 keV).

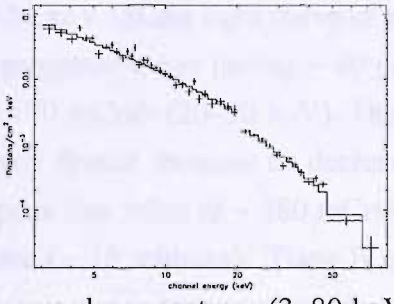

Figure 4.4: Unfolded cutoff power law spectrum (3–80 keV) of XTE J1739−302 during the outburst No.1 in table 4.1.

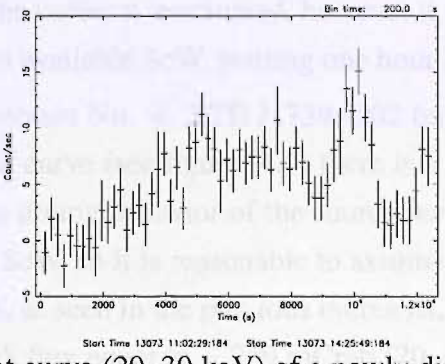

Figure 4.5: The ISGRI light curve (20–30 keV) of a newly discovered outburst (No. 4 in table 4.1) of XTE J1739−302.

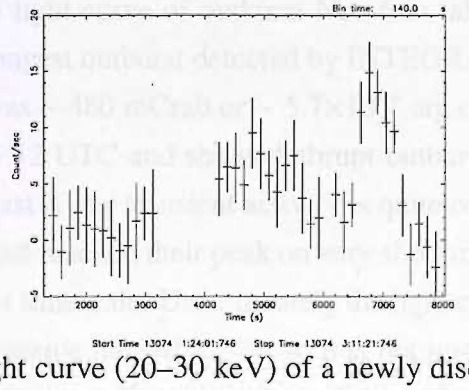

Figure 4.6: The ISGRI light curve (20–30 keV) of a newly discovered outburst (No. 5 in table 4.1) of XTE J1739−302

equal to $19^{+2.8}_{-2.3}$ keV (see figure 4.4). This spectral model is typical of an accreting neutron star in a HMXB. The absorption is not required by the data since the fit does not statistically improve by adding it to the cutoff power law. To account for a cross-calibration mismatch between the two instruments JEM–X/ISGRI, a constant in the fit has been introduced. When left free to vary it provided a value of 1.3±0.15. Moreover, an equally good fit is also provided by a thermal bremsstrahlung model (χ^2_ν=1.25, 151 d.o.f.) with kT=$21.5^{+2}_{-1.7}$ keV. The same thermal bremsstrahlung temperature kT was reported by Lutovinov et al. (2005b) during a different outburst (No.2 in table 4.1).

Figure 4.5 shows the 20–30 keV ISGRI light curve of outburst No.4 in table 4.1. It displayed at the beginning a progressive rise lasting ~ 80 minutes, during which the flux increased up to a value of ~ 170 mCrab (20–30 keV). Then it stopped rising and for ~ 50 minutes it did not show any drastic increase or decrease. Subsequently, the source flared up quickly reaching a peak flux value of ~ 280 mCrab and then it dropped with the same timescale as the rise-time (~ 15 minutes). There is evidence of a possible second flare but unfortunately the light curve is truncated at the end, at ~ 14:25 UTC, because the following 2 ScWs are not available for data analysis. In this case it is not possible to establish exactly when the outburst terminated, however it was verified that the source was not detected in the next available ScW, starting one hour later at 15:24:01 UTC.

About 12 hours after outburst No. 4, XTE J1739−302 turned on again (outburst No. 5 in table 4.1). In the light curve (see figure 4.6) there is a gap due to one unavailable ScW for data analysis. The timing behavior of the source seems to suggest that it turned on just during the missing ScW, so it is reasonable to assume the outburst start time at ~ 01:54:35 UTC. Once again, as seen in the previous outbursts, XTE J1739−302 showed a very quick flare with a peak flux equal to ~ 250 mCrab (20–30 keV), then it dropped to an undetectable flux level with the same timescale as the time-rise (~ 15 minutes).

The 20–60 keV ISGRI light curve of outburst No. 6 in table 4.1 is shown in figure 4.7. To date this is the strongest outburst detected by INTEGRAL from XTE J1739−302, the maximum peak flux was ~ 480 mCrab or ~ 5.7×10^{-9} erg cm^{-2} s^{-1} (20–60 keV). The source turned on at 05:25:12 UTC and showed abrupt outburst activity. As we can see from the light curve, the fast X-ray transient activity is quite complex. It is characterized by several sharp flares which reached their peak on very short timescale (few minutes) and then dropped with a similar timescale. Unfortunately the light curve is truncated at the end because the source went outside the IBIS FOV so it is not possible to constrain the total duration of the outburst activity. A Fourier analysis did not show any significant evidence of pulsations, however we note that the peaks are approximately separated by ~ 2000 s. The outburst No.1 in figure 4.1 also displayed this kind of behaviour. Unfortunately in

both cases the duration of the outburst is only a few times the putative period of 2000 s, so the detection of a longer outburst is needed to investigate any such periodicity in the light curve of XTE J1739−302. However, it could just be a typical timescale of whatever drives the outburst.

Figure 4.8 displays the 20–60 keV ISGRI light curve of the outburst No. 7 in table 4.1. It is mainly characterized by a very strong and fast flare which reached a peak flux of ~ 210 mCrab (20–60 keV) and then dropped in only ~ 20 minutes to an almost null value. During the strong flare, the source was in the JEM–X FOV so it was possible to extract a broad band JEM–X/ISGRI spectrum (3–60 keV). It is best fit by a single power law (χ^2_ν=0.9, 146 d.o.f.) with Γ=2.1±0.1 (see figure 4.9). An equally good fit is also provided by a bremsstrahlung model (χ^2_ν=0.88, 146 d.o.f.) with kT=23.5^{+4}_{-3} keV. It can be noted that before this fast and strong flare, the source showed a couple of smaller ones which reached a maximum peak flux of 70 mCrab (20–60 keV).

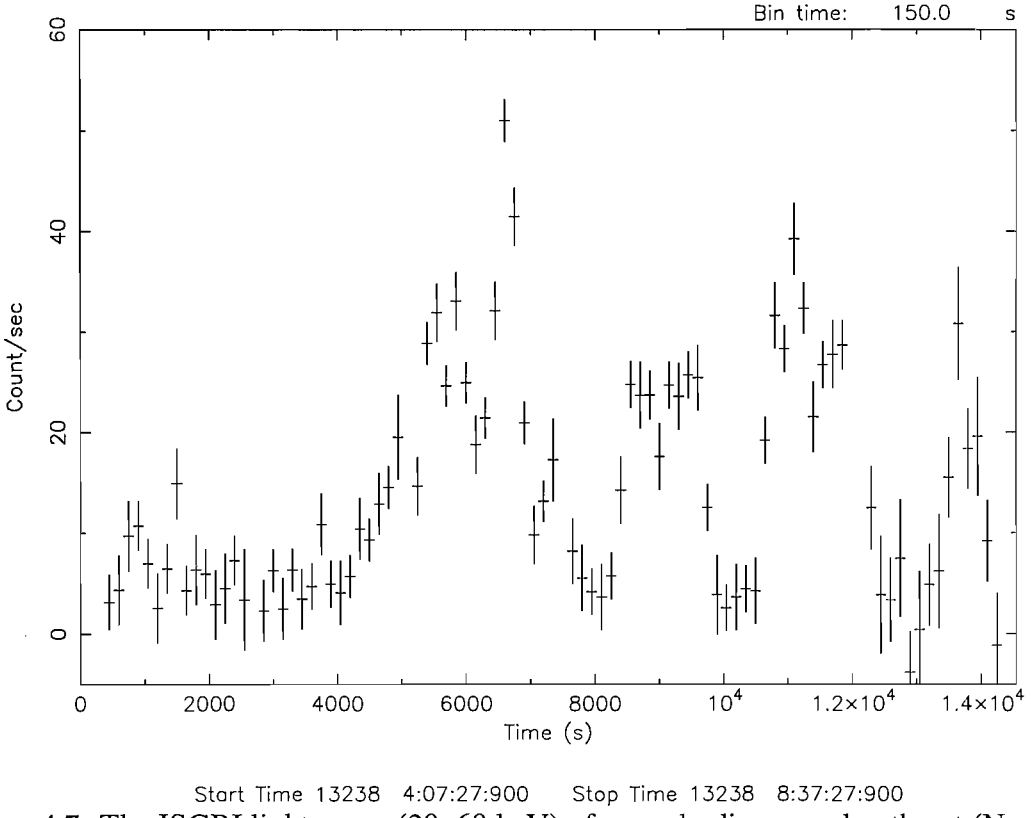

Figure 4.7: The ISGRI light curve (20–60 keV) of a newly discovered outburst (No. 6 in table 4.1) of XTE J1739−302.

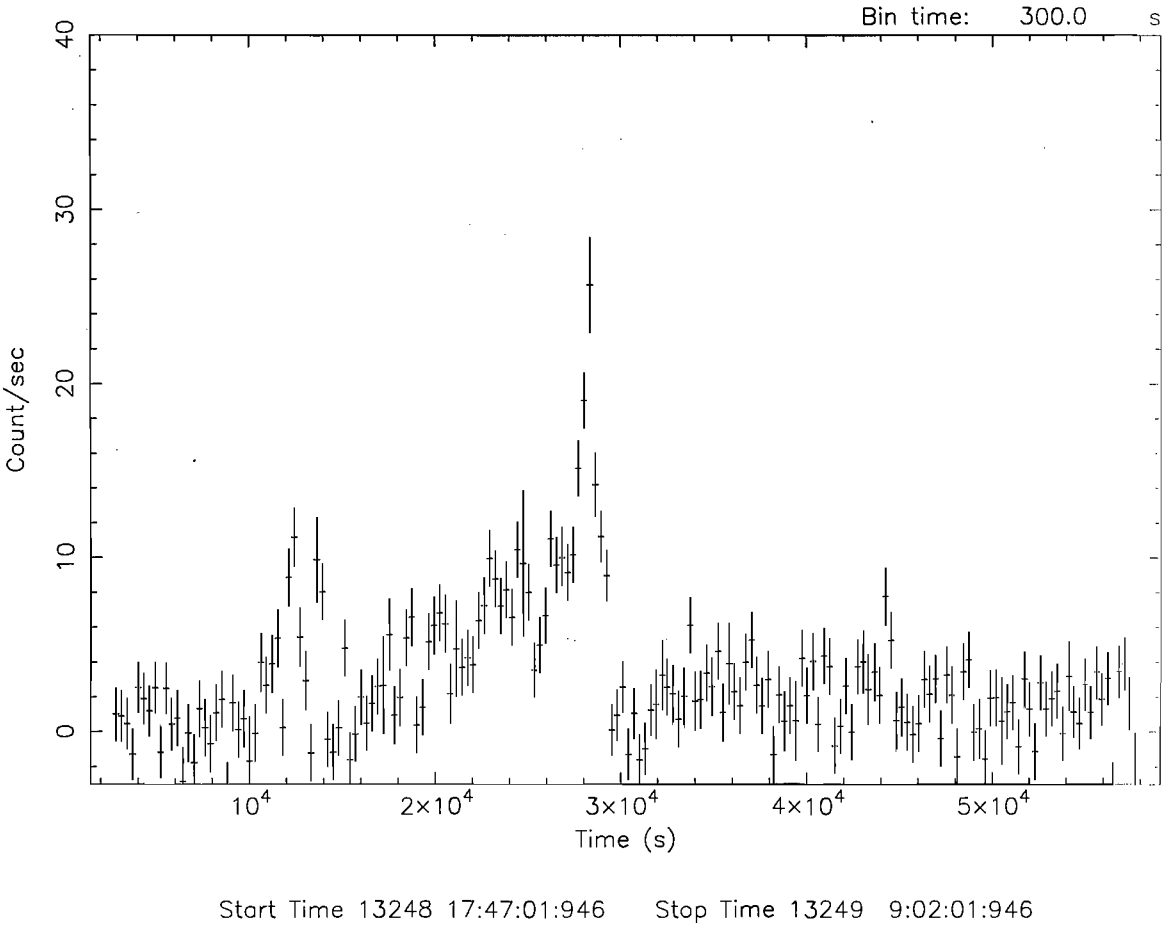

Figure 4.8: The ISGRI light curve (20–60 keV) of a newly discovered outburst (No. 7 in table 4.1) of XTE J1739–302.

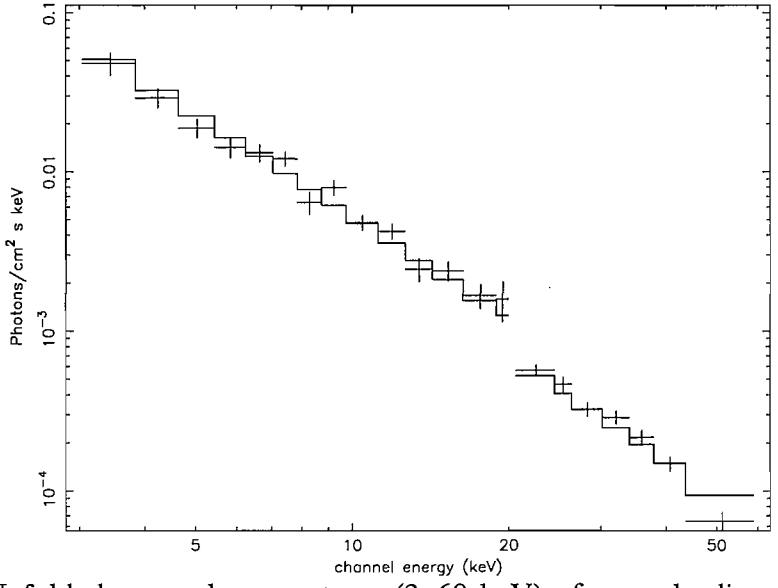

Figure 4.9: Unfolded power law spectrum (3–60 keV) of a newly discovered outburst (No. 7 in table 4.1) of XTE J1739–302.

4.2.2 IGR J17544–2619

4.2.2.1 Archival X-ray observations of the source

IGR J17544–2619 is a fast X-ray transient source discovered with INTEGRAL on 17 September 2003 at 01h10 UTC (Sunyaev et al. 2003b), when the source was active for ~ 2 hours. About 5 hours later the source turned on again undergoing another fast outburst activity (Grebenev et al. 2003). INTEGRAL detected another outburst on 8 March 2004 (Grebenev et al. 2004); the duration was ~ 10 hours.

In't Zand et al. (2004) analyzed archival BeppoSAX WFCs data revealing that IGR J17544–2619 was already detected in outburst five times from 1996 to 2000. The durations varied between 10 minutes and 8 hours while the peak fluxes were measured to be between 100 and 200 mCrab (2–28 keV).

XMM observed IGR J17544–2619 in quiescence and in outburst, during observations performed on March 17, September 11 and 17 2003 (Gonzalez-Riestra et al. 2004). The flux of the source in outburst was ~ 7.5×10^{-11} erg cm^{-2} s^{-1} (0.5–10 keV), it varied strongly on very short timescales (few minutes). The upper limit to the flux in quiescence was $\leq 5\times10^{-14}$ erg cm^{-2} s^{-1} (0.5–10 keV), which corresponds to a luminosity $\leq 5.6\times10^{31}$ erg s^{-1} (0.5–10 keV). The spectrum (2–10 keV) was hard, being best fit by an absorbed power law with variable absorption (N_H ~ 1.9–4.3 $\times10^{22}$ cm^{-2}). Chandra observed the source both in quiescence and outburst in the same observation, on 3 July 2004 (in't Zand 2005). The luminosity (0.5–10 keV) in quiescence was ~ 5×10^{32} erg s^{-1}. The spectrum during the outburst was hard and moderately absorbed (N_H ~ 1.4×10^{22} cm^{-2}) while it was softer in quiescence. In't Zand (2005) suggests that the accretor object is a neutron star. Both Chandra and XMM observations revealed that the absorption is variable, and hence it cannot be completely interstellar. They provided a very accurate positioning of the source. Inside its small error circle only one USNO star is present, which is also a 2MASS infrared source. Its optical/NIR spectroscopy allowed its identification as a blue O9Ib supergiant (25–28 $M_\odot$) located at ~ 3 kpc, in the Scutum–Crux arm of the Milky Way (Pellizza et al. 2006).

4.2.2.2 Analysis of newly discovered outbursts by INTEGRAL

This section reports on two newly discovered fast outbursts of IGR J17544–2619 detected by INTEGRAL. They are listed in table 4.2 (No. 4 and 5) together with three other outbursts (No.1, 2, 3) detected by INTEGRAL and already reported in the literature. None of the latter has been studied in detail so this section reports their ISGRI light curves and spectra for the first time.

Table 4.2: Summary of ISGRI observations of outbursts of IGR J17544−2619

No.	Date	duration (hours)	energy band (keV)	flux peak (mCrab)	luminosity peak (10^{36} erg s^{-1})	ref
1	17 Sep 2003 01h UTC	~ 2	20–40	~ 400	~ 3.2	[1]
2	17 Sep 2003 06h UTC	~ 8	25–50	~ 80		[2]
3	8 Mar 2004	~ 10	20–60	~ 240	~ 3	[3]
4	12 Mar 2005	~ 0.5	20–30	~ 150	~ 0.72	[4]
5	12 Mar 2006		20–40	~ 150	~ 1.2	[4]

[1] Sunyaev et al. (2003b); [2] Grebenev et al. (2003); [3] Grebenev et al. (2004); [4] this PhD thesis

Figure 4.10 shows the ISGRI light curve (20–40 keV) of the outburst which occurred on 17 September 2003 at 01:10 UTC (No.1 in table 4.2). The fast transient nature of the source is clearly evident with two strong flares characterized by a very quick rise and decay (few tens of minutes). The peak-flux and the peak-luminosity (20–40 keV) were ~ 400 mCrab and ~ 3.2×10^{36} erg s^{-1} respectively. A spectrum extracted during the outburst activity (20–60 keV) is best fit by a thermal bremsstrahlung model (χ^2_ν=1.004, d.o.f. 14) with kT=9±0.8 keV (see figure 4.11). This type of spectrum in the hard X-ray band is typical of binary systems with neutron stars. A thermal model such as black body provided instead a poor fit (χ^2_ν=1.9, 14 d.o.f.).

Figure 4.12 shows the ISGRI light curve (20–60 keV) of the outburst No.3 in table 4.2. Initially it was characterized by several very quick flares (few minutes timescales), then suddenly the source flared up in ~10 minutes to a 20–60 keV peak-flux of ~ 240 mCrab. Subsequently the flux dropped to a low level in ~ 20 minutes. A spectrum of this strong flare was extracted (20–60 keV), it was best fit by a thermal bremsstrahlung model with kT=9.5±0.9 keV (χ^2_ν=1.24, d.o.f. 14). However a reasonable fit was also provided by a black body model with kT=4.4±0.25 keV (χ^2_ν=1.4, d.o.f. 14).

Outburst No.4 in table 4.2 is a newly discovered one. It occurred on 12 March 2005 and it was detected in only one ScW. As we can see from its 20–30 keV ISGRI light curve (figure 4.13), the data are of poorer quality and do not allow any fast variability to be seen. The duration and the peak-flux were ~ 30 minutes and ~ 150 mCrab (20–30 keV) respectively. Although the source was detected in only one ScW, it was possible to extract a spectrum during the flare. The best fit model (20–40 keV) was provided by a black body with kT=2.9±0.4 keV (χ^2_ν=1.007, d.o.f. 8), the unfolded spectrum is shown in figure 4.14. However, even an optically thin thermal bremsstrahlung model provided a reasonable fit (kT=5±1 keV, χ^2_ν=0.8, d.o.f. 8).

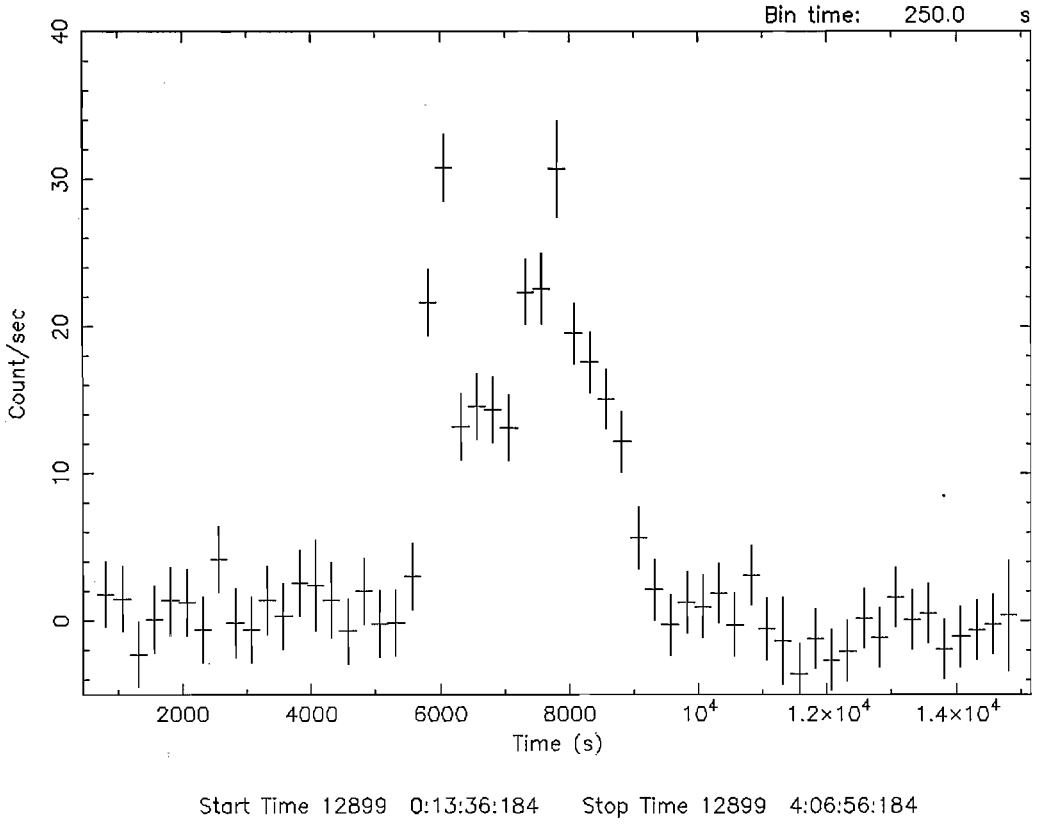

Figure 4.10: ISGRI light curve (20–40 keV) of the IBIS detection of IGR J17544−2619 on Sep 2003 01h10 UTC (outburst No. 1 in table 4.2).

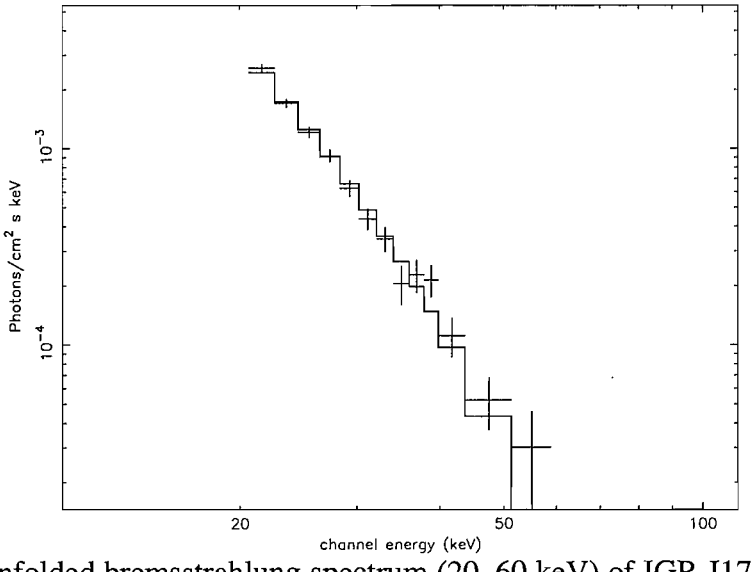

Figure 4.11: Unfolded bremsstrahlung spectrum (20–60 keV) of IGR J17544−2619 during the outburst No.1 in table 4.2.

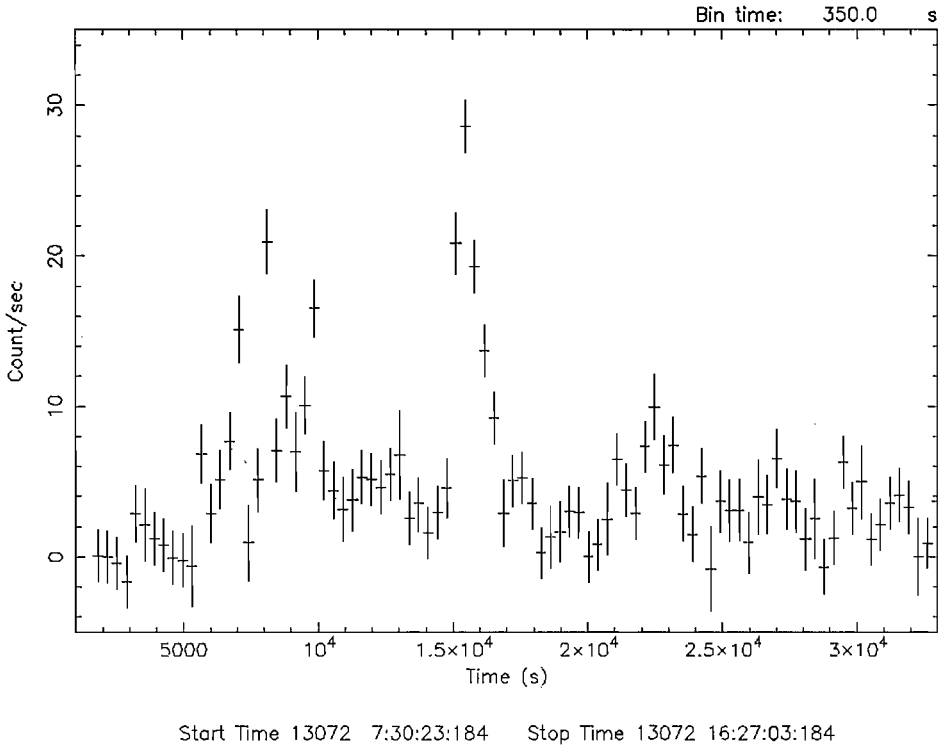

Figure 4.12: ISGRI light curve (20–60 keV) of the IBIS detection of IGR J17544–2619 on 2004 March 8 (outburst No. 3 in table 4.2).

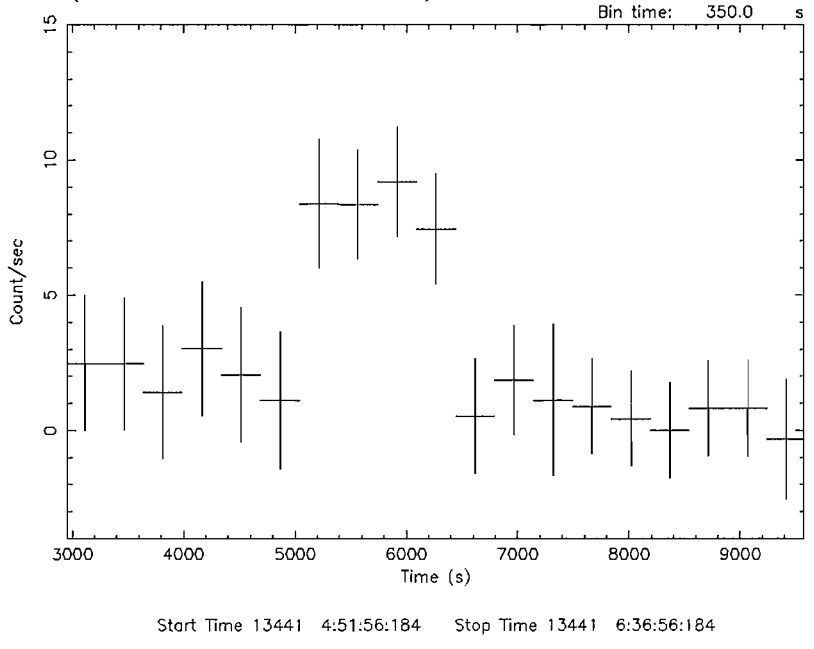

Figure 4.13: ISGRI light curve (20–30 keV) of the IBIS detection of IGR J17544–2619 on 12 March 2005 (outburst No. 4 in table 4.2).

The second newly discovered outburst (No. 5 in table 4.2) occurred on 12 March 2006 and its 20–40 keV light curve is shown in figure 4.15. We can note two prominent fast flares. Unfortunately the light curve is truncated at the beginning and at the end because the source was outside the IBIS FOV so it was not possible to constrain the duration of the outburst. The peak-flux (20–40 keV) was ~ 150 mCrab.

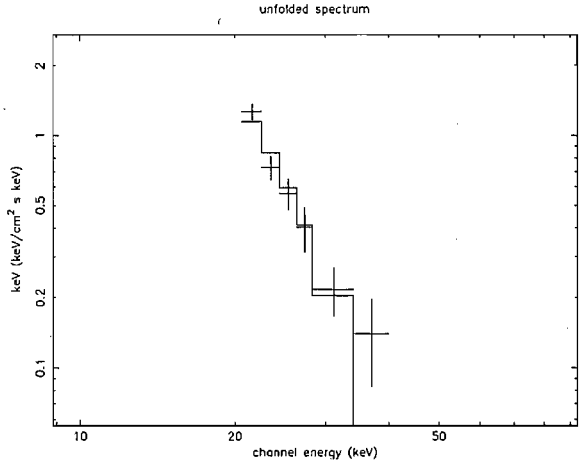

Figure 4.14: Unfolded black body spectrum (20–40 keV) of IGR J17544−2619 during the outburst that occurred on 12 March 2005 (No.4 in table 4.2).

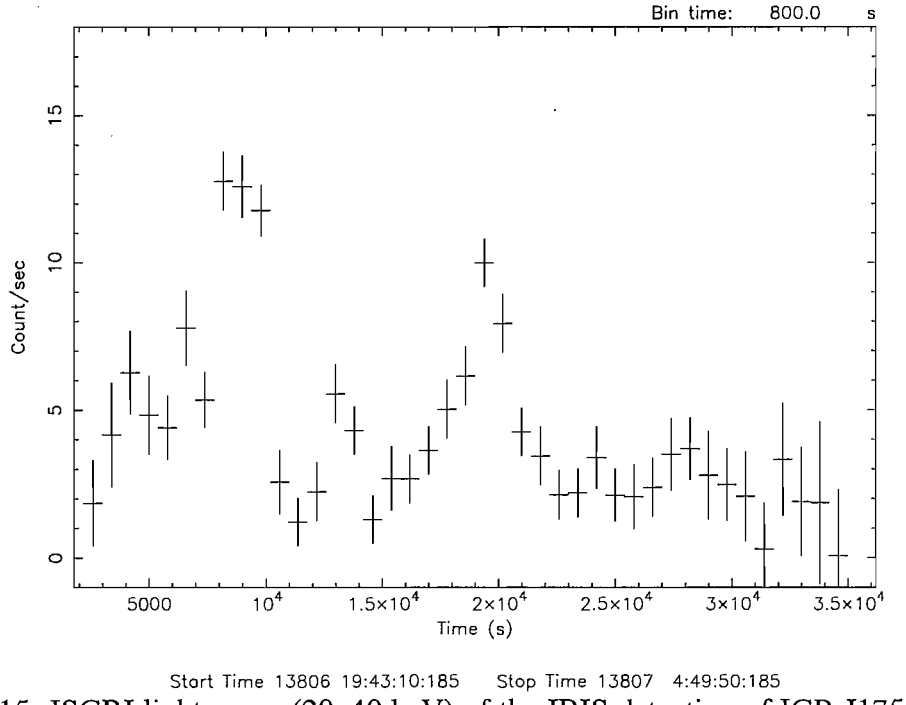

Figure 4.15: ISGRI light curve (20–40 keV) of the IBIS detection of IGR J17544−2619 on 12 March 2006 (outburst No. 5 in table 4.2).

Table 4.3: Summary of IBIS observations of outbursts of AX J1841.0-0536

No.	Date	duration (hours)	energy band (keV)	flux peak (mCrab)	ref
1	24 April 2003	~ 7	20–80	~ 120	[1]
2	6 May 2003	~ 1.1	20–80	~ 120	[1]
3	8 October 2004	~ 2.8	20–60	~ 130	[2]
4	20 April 2006	~ 55	20–40	~ 51	[1]

[1] this PhD thesis; [2] Rodrigueaz et al. (2004)

4.2.3 AX J1841.0–0536=IGR J18410–0535

4.2.3.1 Archival X-ray observations of the source

IGR J18410–0535 was discovered by INTEGRAL on 8 October 2004 as it was undergoing an outburst detected between 20–60 keV (Rodriguez et al. 2004). The nominal position of IGR J18410–0535 reported by Rodriguez et al. (2004) is in agreement with the Chandra location of AX J1841.0–0536 (Halpern & Gotthelf 2004a), indicating that they are the same object. The latter is a 4.74 s transient X-ray pulsar (Bamba et al. 2001) discovered by ASCA as a fast X-ray transient source in April 1994 and then detected again in October 1999. In both cases a noticeable feature was multiple fast flares during which the flux increased by one order of magnitude within only 1 hour. The ASCA X-ray spectrum (2–10 keV) was fit by an absorbed power law with $\Gamma \sim 1$, narrow Gaussian line centered at 6.4 keV and $N_H \sim 3\times10^{22}$ cm^{-2} (Bamba et al. 2001). A Chandra observation of AX J1841.0–0536 provided a spectrum well fit by an absorbed power law with $\Gamma \sim 1.35$ and $N_H = 6\pm1\times10^{22}$ cm^{-2} (Halpern et al. 2004b). The accurate Chandra position permitted the identification of its optical counterpart with a luminous supergiant star (Negueruela et al. 2006a). Infrared K-band spectroscopy (Nespoli et al. 2007) allowed its classification as a supergiant of spectral type B0I.

4.2.3.2 Analysis of newly discovered outbursts by INTEGRAL

This section describes 3 newly discovered fast outbursts of AX J1841.0–0536 detected by INTEGRAL. They are listed in table 4.3 (No. 1, 2, 4) together with the only other one already reported in the literature (No. 3). The latter has never been studied in detail, so a detailed timing and spectral analysis is reported for the first time.

The outburst No. 1 in table 4.3 occurred on 24 April 2003. It was detected in the energy band 20–80 keV, its duration was ~ 7 hours. As we can note in figure 4.16, the

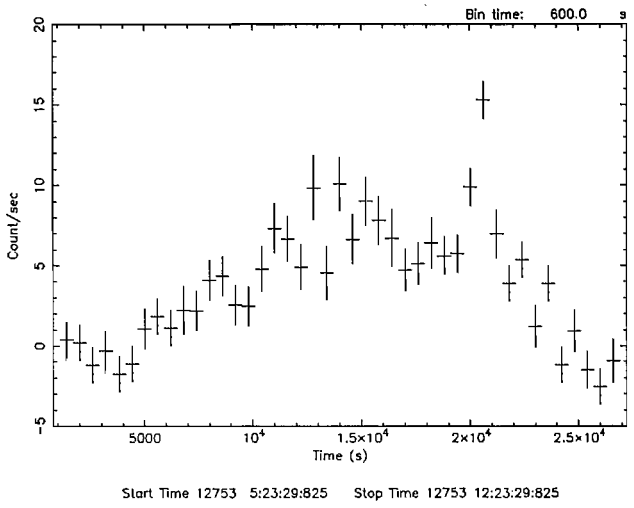

Figure 4.16: ISGRI light curve (20–80 keV) of AX J1841.0-0536 during outburst No. 1 in table 4.3.

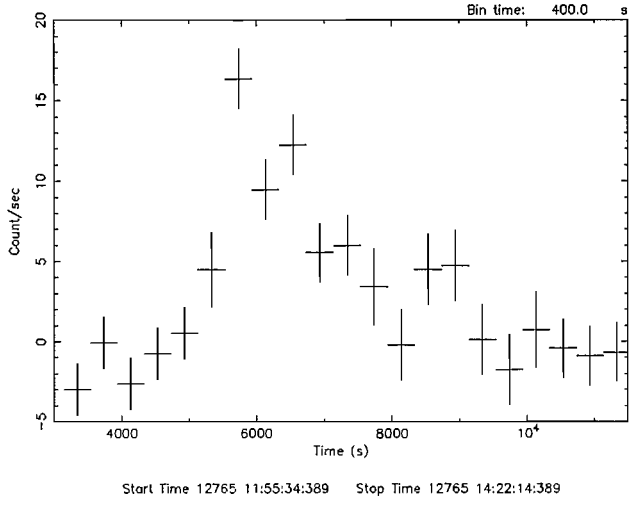

Figure 4.17: ISGRI light curve (20–80 keV) of AX J1841.0-0536 during outburst No. 2 in table 4.3.

light curve shows an evident fast transient activity, the peak-flux was ~ 120 mCrab (20–80 keV). A spectrum extracted during the outburst is best fit by a black body model with kT=8±0.9 keV (χ^2_ν=1.1, d.o.f. 19).

A second, shorter, outburst (~ 1.1 hours) occurred on 6 May 2003 (No.2 in table 4.3). Figure 4.17 shows its 20–80 keV light curve. Initially the flux was consistent with zero, then suddenly the source turned on, flared up and quickly reached a peak of ~ 120 mCrab in ~ 13 minutes. The flux then dropped to a low level in ~ 30 minutes and subsequently the source turned off. A spectrum was extracted during this outburst, the best fit (20–80 keV) is provided by a black body with kT=9±0.9 keV (χ^2_ν=1.45, d.o.f. 19). It is

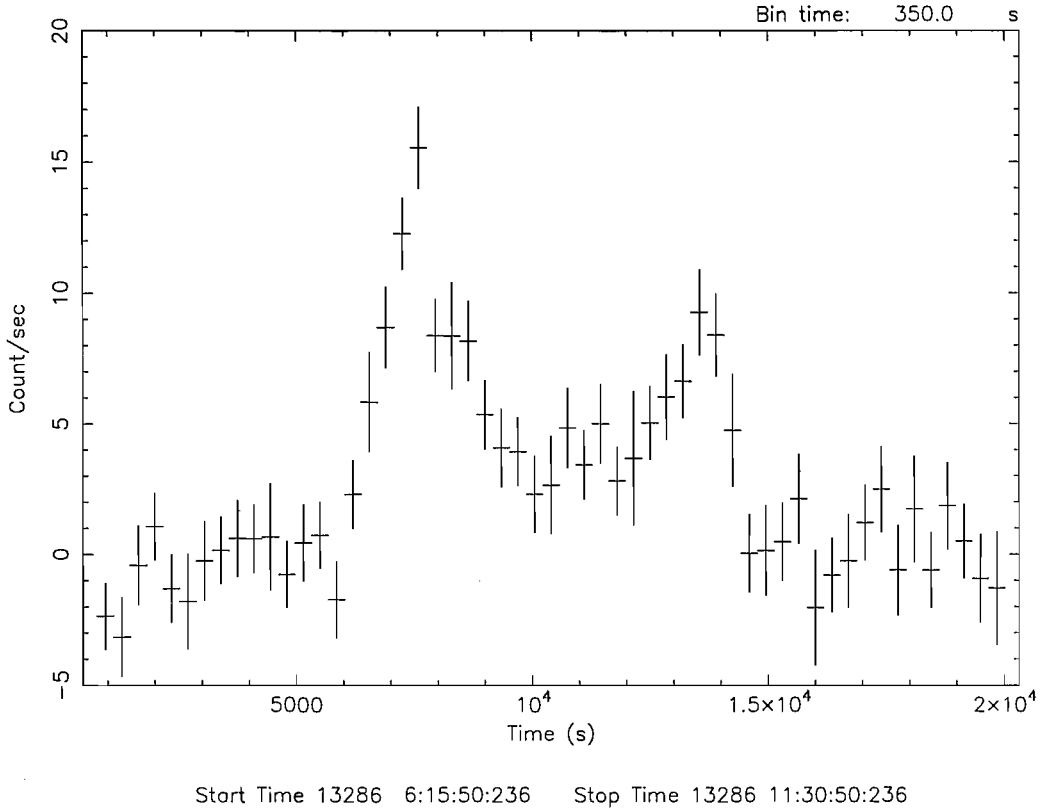

Figure 4.18: ISGRI light curve (20–60 keV) of AX J1841.0-0536 during outburst No. 3 in table 4.3.

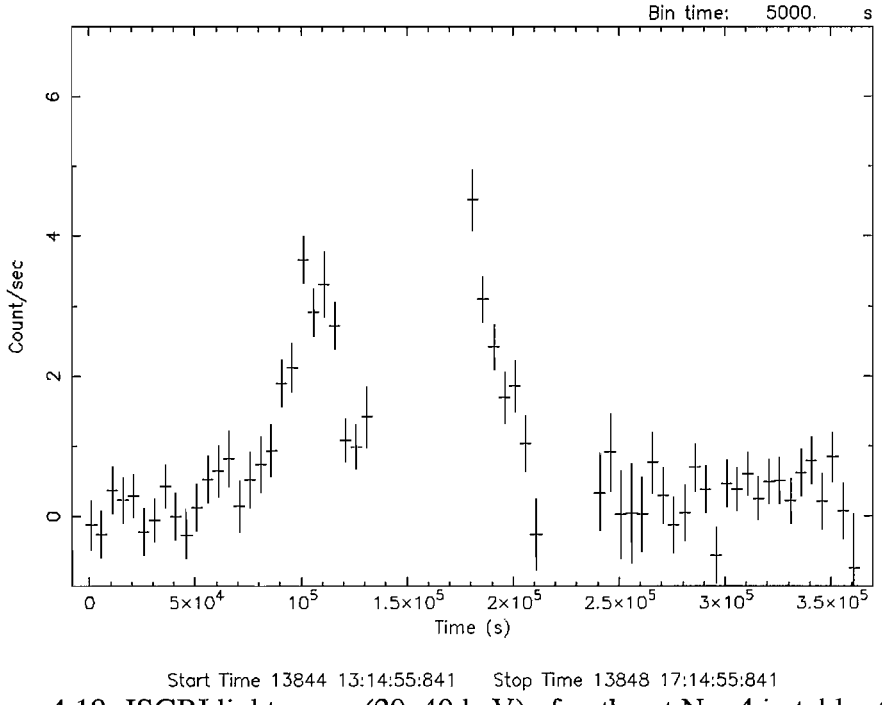

Figure 4.19: ISGRI light curve (20–40 keV) of outburst No. 4 in table 4.3.

worth noting that both previous outbursts (No. 1 and 2) are detected up to 80 keV. Their ISGRI analysis provided a refined position of IGR J18410−0535 (RA=18^h 40^m 57.6^s, Dec=-05° 35′ 38″, 1′.2 error radius) which is located ~ 40″ from the Chandra position of AX J1841.0−0536, fully confirming that they are indeed the same source.

The outburst No.3 in table 4.3 has been already reported in the literature by Rodriguez et al. (2004) when the source was discovered, but it was never studied in detail. Here the timing and spectral analysis is reported for the first time. As we can note in the light curve in figure 4.18, the fast transient behaviour of AX J1841.0-0536 is very evident. It is characterized by two prominent flares. The first one is the strongest, it reached in only ~ 30 minutes a peak flux of ~ 130 mCrab (20–60 keV). A spectrum extracted during the total outburst activity (20–100 keV) is best fit by a black body model (χ^2_ν=1.18, d.o.f. 25) with kT=$7.7^{+0.7}_{-0.6}$ keV. An equally good fit is obtained using a thermal bremsstrhalung with kT=32^{+9}_{-6} keV.

The light curve of outburst No. 4 in table 4.3 is shown in figure 4.19. We note that there are two gaps. The first one (~ 10 hours) is due to visibility constraints between two consecutive INTEGRAL revolutions. The second one (~ 4 hours) is due to a few ScWs not available for data analysis. Nevertheless, the fast outburst activity of the source is evident. It was mainly characterized by two prominent flares, the total duration of the outburst activity was ~ 55 hours. The maximum peak flux was ~ 50 mCrab (20–40 keV).

4.2.4 AX J1845.0−0433=IGR J18450−0435

4.2.4.1 Archival X-ray observations of the source

The X-ray transient AX J1845.0−0433 was discovered in the Scutum arm region on 1993 October 18 during an ASCA observation lasting ~ 16 hours (Yamauchi et al. 1995). Its 2–10 keV ASCA light curve is shown in figure 4.20. In the initial ~ 9 hours, the source was in a very faint quiescent state with a 0.7–10 keV flux of ~ 3×10^{-12} erg cm^{-2} s^{-1}, then suddenly it flared up reaching a peak flux of ~ 10^{-9} erg cm^{-2} s^{-1} in less than 20 minutes. Subsequently the source was characterized by several other flares with timescales of a few tens of minutes, continuing until the end of the observation. Optical and infrared measurements of the ASCA error circle (1 arcmin radius) of AX J1845.0−0433 were performed by Coe et al. (1996). The only object of interest is an O9.5I supergiant star which was proposed by Coe et al. (1996) as the optical counterpart. Its estimated distance is ~ 3.6 kpc, consistent with that derived from ASCA X-ray measurements. However Coe et al. (1996) pointed out that the error on the distance could be large, mainly because of the uncertainty in the reddening law. With these assumptions, the quiescent and the peak

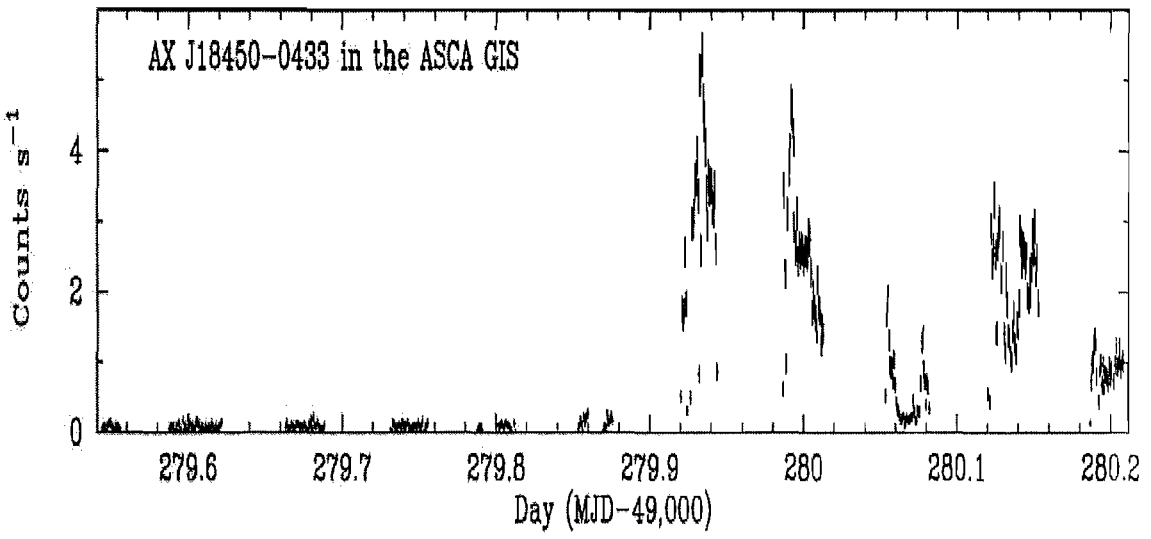

Figure 4.20: ASCA light curve (2–10 keV) of AX J1845.0-0433 when the source was discovered in 1993.

luminosity (0.7–10 keV) of the source measured by ASCA were 4.6×10^{33} erg s^{-1} and 1.5×10^{36} erg s^{-1}. The ASCA X-ray spectrum of the flare state was fit by an absorbed power law with $\Gamma\sim1$ and $N_H=3.6\pm0.3\times10^{22}$cm^{-2}; no coherent pulsation was found in the range from 125 ms to 4096 s (Yamauchi et al. 1995).

Since the ASCA discovery, no further outburst activity has been reported from the source by any X-ray mission. The fast X-ray transient behaviour of AX J1845.0–0433 as well as its likely, but not entirely definitive, association with a supergiant star, suggest its classification as a possible member of the recently newly discovered class of SFXTs.

Recently, Halpern et al. (2006) noted that AX J1845.0–0433 is very likely the same object as IGR J18450–0435. Using the precise position of its optical counterpart, AX J1845.0–0433 is located 2′.3 off the IBIS position of IGR J18450–0435 reported by Bird et al. (2006), slightly outside the ISGRI error circle. IGR J18450–0435 was first discovered by INTEGRAL during a survey of the Sagittarius arm tangent region in the spring 2003 (Molkov et al. 2004) at an average flux of 1.5±0.3 mCrab (18–60 keV).

4.2.4.2 Analysis of newly discovered outbursts by INTEGRAL and *Swift*

As stated before, the only X-ray detection of AX J1845.0–0433 in outburst dates back to 1993. No X-ray mission provided a regular monitoring of the Scutum arm region, which is essential to detect fast X-ray transient activity from a source like AX J1845.0–0433. Whereas, the INTEGRAL satellite is regularly monitoring the Scutum arm region.

This section reports on renewed fast outburst activity from AX J1845.0–0433 discov-

Table 4.4: Summary of INTEGRAL, *Swift* and ASCA observations of outbursts of AX J1845.0−0433

Obs	Date	energy band (keV)	peak flux (erg cm^{-2} s^{-1})	peak lum (erg s^{-1})	Γ	N_H (cm^{-2})	ref
ASCA	18 Oct 1993	0.7–10	1×10^{-9}	1.5×10^{36}	$1^{+0.07}_{-0.07}$	$3.6\pm0.3\times10^{22}$	[2]
ISGRI	28 Apr 2005	20–40	4.5×10^{-10}	7×10^{35}	$2.5^{+0.6}_{-0.5}$		[1]
JEM–X	28 Apr 2005	3–10	4.8×10^{-10}	7.4×10^{35}			[1]
Swift XRT	11 Nov 2005	0.2–10	2.3×10^{-10}	3.6×10^{35}	$0.75^{+0.1}_{-0.1}$	$1.6\pm0.18\times10^{22}$	[1]
Swift XRT	5 Mar 2006	0.2–10	1.1×10^{-10}	2×10^{35}	$0.85^{+0.3}_{-0.3}$	$2.3\pm0.7\times10^{22}$	[1]
ISGRI	20 Apr 2006	20–40	6×10^{-10}	9.3×10^{35}	$2.9^{+0.9}_{-0.7}$		[1]

[1] this PhD thesis, [2] Yamauchi et al. 1995

ered by INTEGRAL and also on results of two archival *Swift* XRT observations of the source, which permitted a refined source position to be obtained. Table 4.4 provides a summary of the characteristics of the newly discovered outbursts from AX J1845.0−0433, together with the only other one already reported in the literature and detected by ASCA.

The region of the sky containing AX J1845.0−0433 was observed by INTEGRAL for a total of ~ 2 Ms. In almost all ScWs, the source was well below a 5σ detection level (20–40 keV), and only in two ScWs in revolution 310 and one ScW in revolution 429 was it significantly detected at ~ 6σ level (20–40 keV). The analysis showed that these detections corresponded to fast flares reaching their peak in a few tens of minutes and then dropping on the same timescale.

Figure 4.21 displays the 20–40 keV light curve of IGR J18450−0435 from ~ 25^{th} to ~ 30^{th} April 2005 (data belonging to revolutions 309, 310 and 311); each data point represents the average flux during one ScW. The temporal gaps are due to the fact that the source is not always in the IBIS FOV. As we can see, at the beginning of the light curve (during revolution 309) the source showed no evident outburst activity. Subsequently, during revolution 310, the source turned on, displaying evident flaring activity (highlighted in the box in figure 4.21). Unfortunately, shortly afterwards the source went outside the IBIS FOV so the light curve is truncated. It is not possible to constrain the overall duration of the outburst activity and we cannot exclude the possibility that further flares took place. Finally, IGR J18450−0435 was again in the IBIS FOV during the next revolution (311) only in the first 3 ScWs and then went outside its FOV (see the three points at the end of light curve in figure 4.21).

Figure 4.22 shows an expanded and more detailed view of the flaring activity highlighted in the box in figure 4.21, plotted with a bin period of 900 s, compared to the 2000 s used in figure 4.21. As we can see, the source underwent two fast flares (number

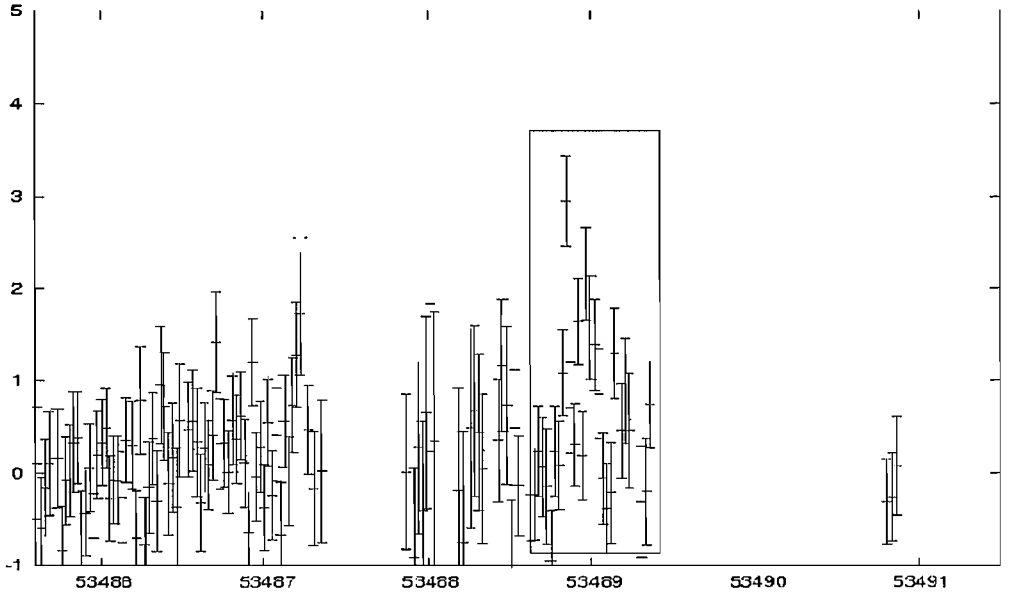

Figure 4.21: ISGRI light curve (20–40 keV) of a newly discovered outburst of AX J1845.0–0433 on 28 April 2005. Time axis is in MJD. Each data point represents the average flux during one ScW (~2000 seconds).

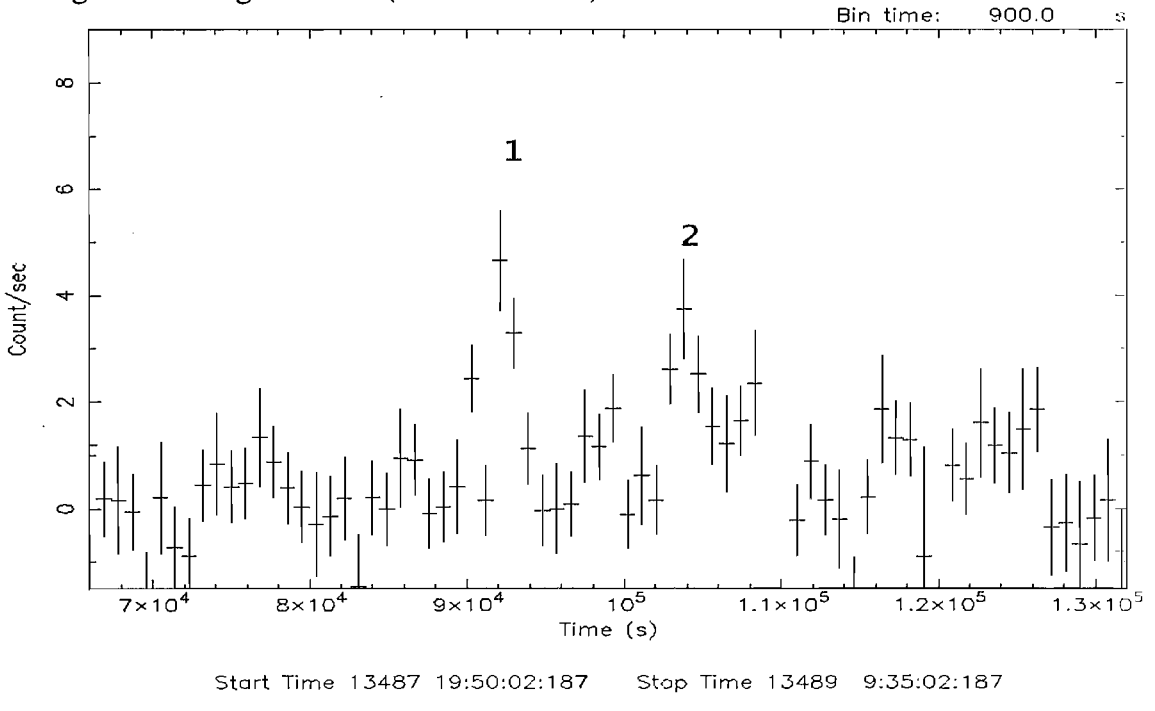

Figure 4.22: Expanded view of the light curve of the outburst activity from AX J1845.0–0433 highlighted in the box in figure 4.21. The bin time is 900 s

1 and 2 in figure 4.22) with timescales of a few tens of minutes on 28 April 2005 at ~ 19:40 UTC. The first flare reached a peak flux of ~ 60 mCrab (20–40 keV). Assuming a distance of 3.6 kpc, the 20–40 keV peak luminosity is ~ 7×10^{35} erg s^{-1}, in agreement with typical outburst luminosities of SFXTs. After the second flare, the source seemed to show no further X-ray flaring activity. However, as we stated before, the light curve is unfortunately truncated at the end because the source went outside the IBIS FOV. The INTEGRAL observation coverage since the source turned on up to the end of the light curve is ~ 11 hours.

The first flare (No. 1 in figure 4.22) is also covered with JEM–X data. The 3–10 keV peak flux and peak luminosity were ~ 32 mCrab and ~ 7.4×10^{35} erg s^{-1}, respectively. The latter is similar to that measured by ASCA in 1993. The combined JEM–X and ISGRI spectrum (3–100 keV) during the first flare was reasonably fit by a single power law (χ^2_ν=1.12, 156 d.o.f.) with $\Gamma=2.5^{+0.6}_{-0.5}$. The fit improved adding a black body to the power law (χ^2_ν=1.02, 154 d.o.f.), the best fit parameters being $kT=2^{+0.7}_{-0.5}$ keV and $\Gamma=1.7^{+0.7}_{-0.8}$. To account for a cross-calibration mismatch between the two instruments we have introduced a constant in the fit, which, when left free to vary, provides a value of $0.02^{+0.08}_{-0.016}$. An equally good fit (χ^2_ν=1.02, 154 d.o.f.) was also achieved using a Bulk Motion Comptonization model (BMC), the model parameters are the characteristic black body temperature of the soft photon source kT_{col} and a spectral energy index α. This model reproduces rather well the whole spectrum (χ^2_ν=1.02, 154 d.o.f.) both at high and low energies (see figure 4.23), without the addition of other components. The best fit parameters are $kT_{col}=1.7^{+0.8}_{-0.3}$ keV and $\alpha=0.9^{+0.9}_{-0.6}$, respectively. An acceptable fit was also achieved using a thermal bremsstrahlung model (χ^2_ν=1.09, 171 d.o.f.) with $kT=19^{+15}_{-7}$ keV.

The analysis of this first flare enabled the determination of an ISGRI position for IGR J18450–0435 (RA=18^h 45^m $03^s.3$ DEC=-04° 34′ 05″.5, error radius of 2.′4) which is located 0′.5 from the optical counterpart of AX J1845.0–0433. This fully confirms that AX J1845.0–0433 and IGR J18450–0435 are indeed the same source.

Figure 4.24 displays the 20–40 keV ISGRI light curve (1000 seconds bin time) of IGRJ18450–0435 during the outburst that occurred on 20 April 2006. As we can note, it strongly resembles the light curve of the previous flaring activity in figure 4.22. Most of the time the source did not show any relevant outburst activity, with a count rate less than 1 count/sec, however several very quick flares (labeled from A to E in figure 4.24) appeared on a timescale of tens of minutes. Their peak flux never reached a value greater than ~ 30 mCrab (20–40 keV). Moreover, a noticeable very fast and strong flare (No. 1 in figure 4.24) occurred on ~ 9:30 UTC 20 April 2006. It reached a peak flux of ~ 80 mCrab or 6×10^{-10} erg cm^{-2} s^{-1} (20–40 keV) in ~ 30 minutes and then it dropped

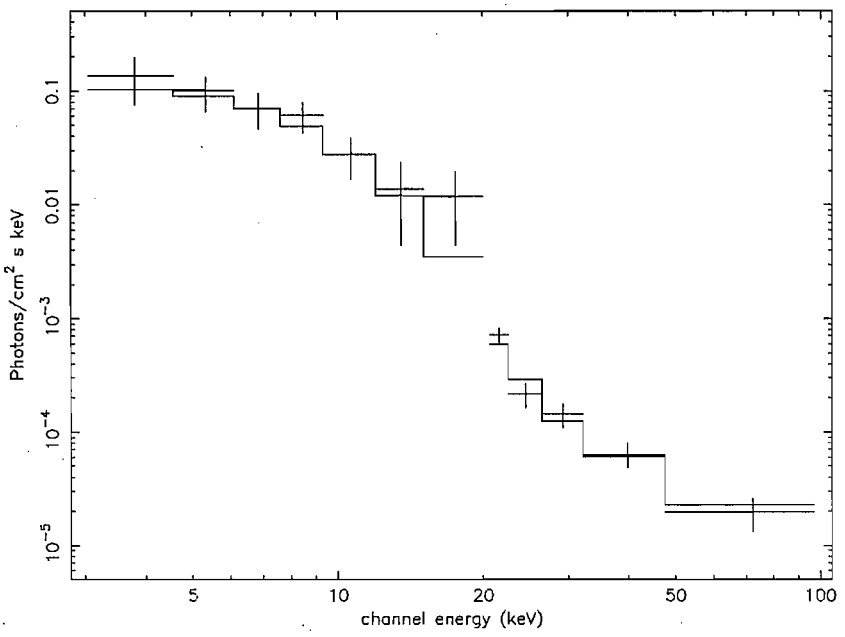

Figure 4.23: Unfolded Bulk Motion Comptonization (BMC) spectrum (3–100 keV) of AX J1845.0–0433 during the flare that occurred on 28 April 2005.

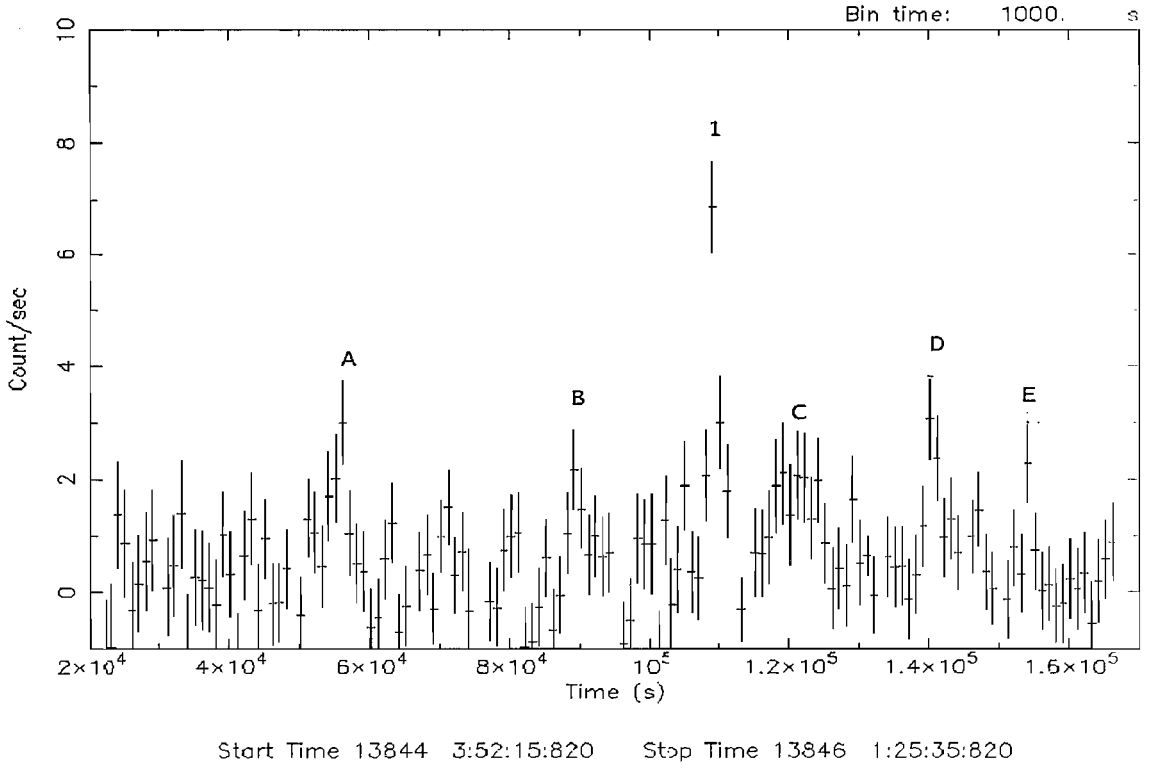

Figure 4.24: ISGRI light curve (20–40 keV) of a newly discovered outburst of AX J1845.0–0433 occurred on 20 April 2006.

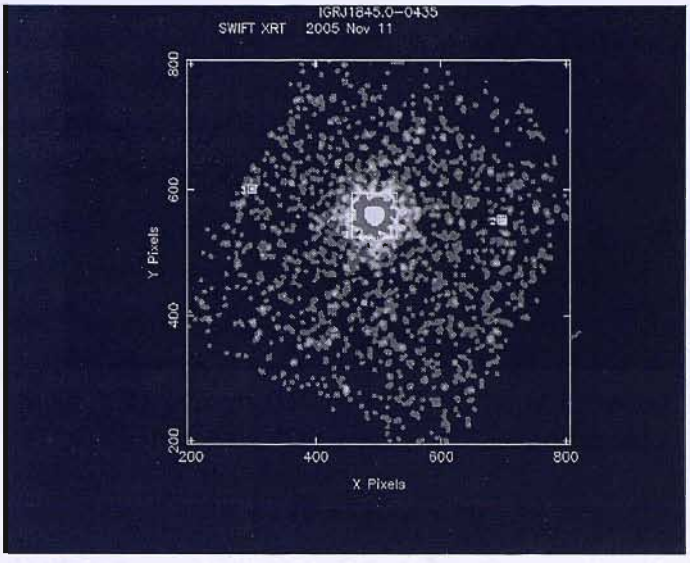

Figure 4.25: *Swift* XRT image (0.2–10 keV) of the observation of AX J1845.0–0433 performed on 11 November 2005. The source is clearly detected at $\sim 68\sigma$ at the center of the field of view.

with the same timescale. The 20–40 keV peak luminosity is $\sim 9.3\times10^{35}$ erg s^{-1}. These values are slightly greater than the previous ones relating to the flaring activity detected by INTEGRAL about one year before. The light curve in figure 4.24, pertaining to rev 429, is truncated at the beginning and at the end. A search for more flaring activity before and after this revolution did not give any results. An ISGRI spectrum was extracted during this fast flare (20–100 keV), the best fit (χ^2_ν=1.18, 24 d.o.f.) was provided applying a single power law with $\Gamma=2.9^{+0.9}_{-0.7}$. However a BMC model also provided a good description to the data (χ^2_ν=1.2, 22 d.o.f.)

Swift XRT observed several times the region of the sky including IGR J18450–0433. However, a search of the *Swift* XRT data archive revealed that the source was positively detected only in two occasions: 11 November 2005 and 5 March 2006. The XRT collected data for a total exposure time of 4.6 ks and 4.8 ks. Unfortunately in both the observations the source was outside the IBIS FOV so we had no simultaneous ISGRI data.

Figure 4.25 shows the 0.2–10 keV image of the observation of AX J1845.0–0433 performed by *Swift* XRT on 11 November 2005. The source is clearly detected at $\sim 68\sigma$ at the center of the field of view. The *Swift* XRT analysis provided a very accurate position of AX J1845.0–0433 (RA=$18^h\ 45^m\ 01.^s9$ Dec=-04° 33′ 57″.6) which is located 4″.7 from the supergiant star proposed by Coe et al. (1996) as its optical counterpart. This fully confirms the supergiant HMXB nature of AX J1845.0–0433.

Figures 4.26 and 4.27 show the 0.2–10 keV XRT light curve of IGR J18450–0433 during the observations performed on 11 November 2005 and 5 March 2006, respectively.

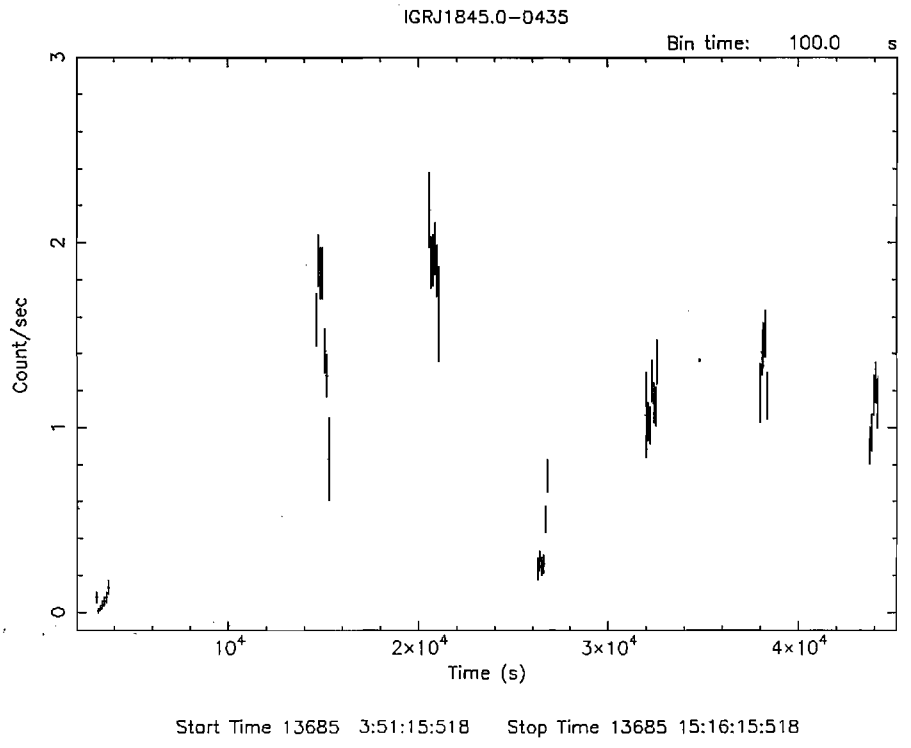

Figure 4.26: *Swift* XRT light curve (0.2–10 keV) during the observation on 11 November 2005.

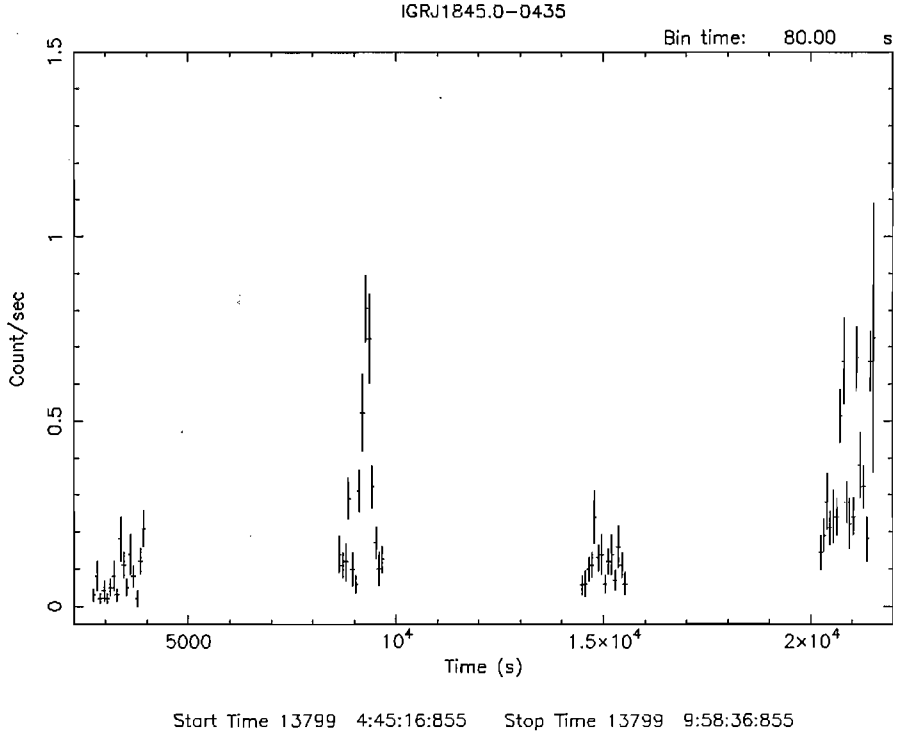

Figure 4.27: *Swift* XRT light curve (0.2–10 keV) during the observation on 5 March 2006.

We note that the temporal coverage is not continuous, there are significant gaps in both the light curves due to visibility constraints. In spite of that, the fast flaring behaviour of the source is evident, especially during the observation performed on 5 March 2006 (figure 4.27). On this occasion, initially the source displayed a very low count rate, close to zero. Subsequently, it underwent a very fast flare reaching in only 4 minutes a peak flux and a peak luminosity of $\sim 1.1\times10^{-10}$ erg cm^{-2} s^{-1} and $\sim 2\times10^{35}$ erg s^{-1}, respectively (0.2–10 keV). Then the flux dropped again to a very low level with the same fast timescale. The spectrum (0.2–8 keV) extracted during the observation 5 March 2006 is well fit by an absorbed power law (χ^2_ν=0.63, 41 d.o.f) with Γ=0.85±0.3 and N_H equal to $2.3\pm0.7\times10^{22}$ cm^{-2}. The average 0.2–8 keV flux is $\sim 2\times10^{-11}$ erg cm^{-2} s^{-1}. However a good fit is also provided by a black body model (χ^2_ν=0.7, 42 d.o.f) with kT=2.4±0.2.

In the light curve in figure 4.26 (11 November 2005), initially the source is characterized by a count rate less than 0.1 count/s, then it flared up quickly reaching a peak flux and peak luminosity of $\sim 2.3\times10^{-10}$ erg cm^{-2} s^{-1} and $\sim 3.6\times10^{35}$ erg s^{-1}, respectively (0.2–10 keV). The spectrum (0.2–10 keV) is best fit by an absorbed power law (χ^2_ν=1.28, 166 d.o.f.) with Γ=0.75±0.1 and $N_H=1.6\pm0.18\times10^{22}$ cm^{-2}. The latter is in agreement with the galactic absorption along the line of sight ($N_H=1.58\times10^{22}$ cm^{-2}). A simple power law or thermal models, such as blackbody or bremsstrahlung, instead provided very poor fits. The 0.2–10 keV average flux is $\sim 1.3\times10^{-10}$ erg cm^{-2} s^{-1}, which is an order of magnitude higher than that during the other observation.

Fast X-ray transient activity has been detected from the source in ASCA, *Swift* and INTEGRAL observations lasting only a few hours. Since INTEGRAL is regularly monitoring the Scutum arm region, further IBIS detections of AX J1845.0–0433 in outburst are not unexpected. This could allow us to search for recurrence time and in turn further insights into the system geometry.

4.2.5 SAX J1818.6–1703

4.2.5.1 Archival X-ray observations of the source

SAX J1818.6–1703 is a fast transient X-ray source discovered with the WFCs onboard BeppoSAX on 11 March 1998 (in't Zand et al. 1998). It turned on at 19:12:00 UTC and peaked quickly (20:38:24 UTC) at a level of 100 mCrab (2–9 keV) and 400 mCrab (9–25 keV). During the last 40 minutes of the BeppoSAX observation the source intensity decreased to an undetectable flux level. The duration of this outburst was $\sim$ 2 hours, marking the fast transient nature of the source. The WFC BeppoSAX position of the source is RA=18^h 18^m 39^s DEC=-17° 03′ 06″ (error circle radius of 3′). Although the

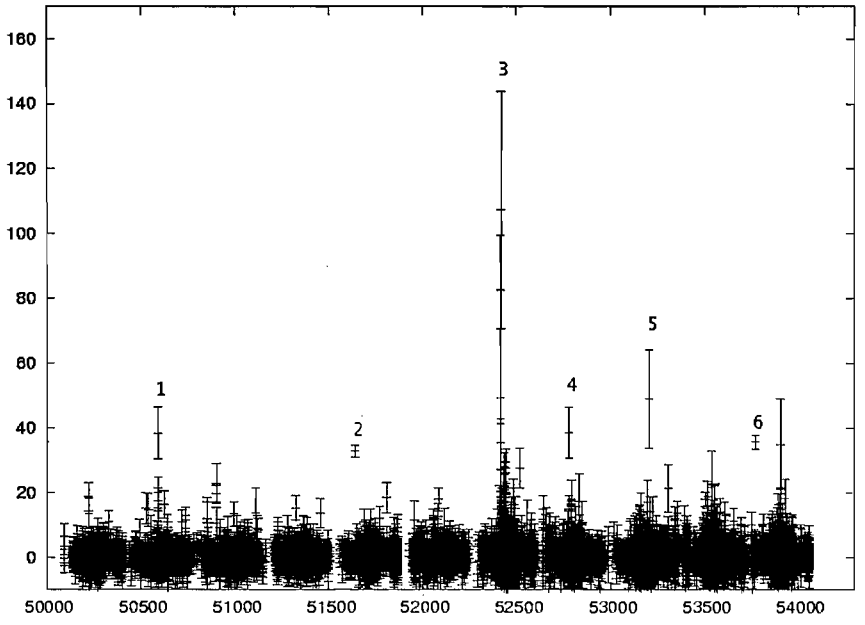

Figure 4.28: RXTE ASM dwell by dwell light curve (2–12 keV) of SAX J1818.6–1703 from 1996 to 2006. In the light curve 30 c s^{-1} is equivalent to a flux of ~ 400 mCrab. Time axis is in MJD. The six outbursts detected by RXTE, with a flux greater than 400 mCrab, are indicated by the numbers from 1 to 6.

WFCs were operational up to April 2002, monitoring the galactic bulge once per week, no more outbursts of SAX J1818.6–1703 detected by BeppoSAX have been reported in the literature.

On 19 September 2006, Chandra observed the area of the sky containing the error circle of SAX J1818.6–1703 for 9.8 ksec (in't Zand et al. 2006). A source was detected at RA=18^h 18^m $37^s.89$ Dec=-17° 02′ 47″.9 with an error circle of 0″.6, it was not undergoing any major outburst activity. Its spectrum (0.5–10 keV) was fit by an absorbed power law with Γ=1.9±0.3 and N_H=6±0.7×10^{22} cm^{-2}. The average 0.5–10 keV flux was ~ 7.5×10^{-12} erg cm^{-2} s^{-1}.

An investigation of the RXTE ASM (All Sky Monitor) data archive provided a light curve (2–12 keV) of SAX J1818.6–1703 from 1996 to 2006 (see figure 4.28), which shows at least 6 outbursts having a flux greater than ~ 400 mCrab (see numbers in figure 4.28).

4.2.5.2 Analysis of newly discovered outbursts by INTEGRAL

This section reports on detections by INTEGRAL of 4 newly discovered outbursts from SAX J1818.6–1703, which are the first to be reported since its discovery with BeppoSAX in 1998. Their times are listed in table 4.5 together with their duration, energy range over

Table 4.5: Summary of newly discovered outbursts of SAX J1818.6–1703 by INTEGRAL

No.	Date	Duration (hours)	Energy Range (keV)	peak–flux (mCrab)	ref
1	9 Sep 2003	~ 14	20–100	446	[1],[2]
2	9 Oct 2003	~ 1	20–60	120	[1]
3	10 Oct 2003	~ 3	20–30	185	[1]
4	3-4 Oct 2004		20–40	70	[1]

[1] this PhD thesis; [2] Grebenev et al. (2005)

which they have been detected and fluxes at the peak.

The outburst No. 1 in table 4.5 was independently found and studied also by Grebenev et al. (2005). It occurred on 9 September 2003, its 20–100 keV ISGRI light curve is shown in figure 4.29 with a bin time of 250 seconds. It is truncated at the end because the source went outside the IBIS FOV. Very strong and fast outburst activity lasting ~ 14 hours is clearly evident, it was characterized by 2 prominent flares. After the second flare the source was still characterized by a very low level of activity but it did not display flares, then the intensity decreased to an undetectable flux level towards the end of the light curve. Figure 4.30 shows an expanded view of the two flares displayed in the light curve in figure 4.29, highlighting their complex time strucuture. Note that the bin time in figure 4.29 (250 s) is different from that in figure 4.30 (100 s). In the case of the first flare, as we can note from figure 4.30, its rise can be divided into two different parts showing a different temporal behaviour. Initially, from point A to B, the rise is characterized by a gradual increasement lasting ~ 13 minutes. Then suddenly, from point B to C, it reached a peak flux of 446 mCrab or 7.6×10^{-9} erg cm^{-2} s^{-1} (20–100 keV) in only ~ 5 minutes. As for the decay, the flux quickly dropped from point C to D while on the contrary from point D to E it showed a kind of plateau phase for ~ 1 hour. Subsequently, the flux dropped to zero flux level (point F) in ~ 75 minutes. Then, the source underwent three very fast flares during which the flux quickly increased and then decreased never dropping to a zero value. The flares 1 and 2 (see figure 4.30) are characterized by a rise as well as decay lasting ~ 6.5 minutes, their peak-fluxes (20–100 keV) are ~250 mCrab and ~345 mCrab. The flare 3 (see figure 4.30) showed a very quick rise lasting ~1.5 minutes and the peak-flux (20–100 keV) is ~ 375 mCrab. This is followed by a longer and gradual decay (~ 30 minutes) after which the flux dropped to a zero value. There is some indication of another possible quick flare (number 4 in figure 4.30).

A spectrum extracted during the total outburst activity of the source can not be fit by any spectral model such as power law, black body, thermal bremsstrahlung or Comp-

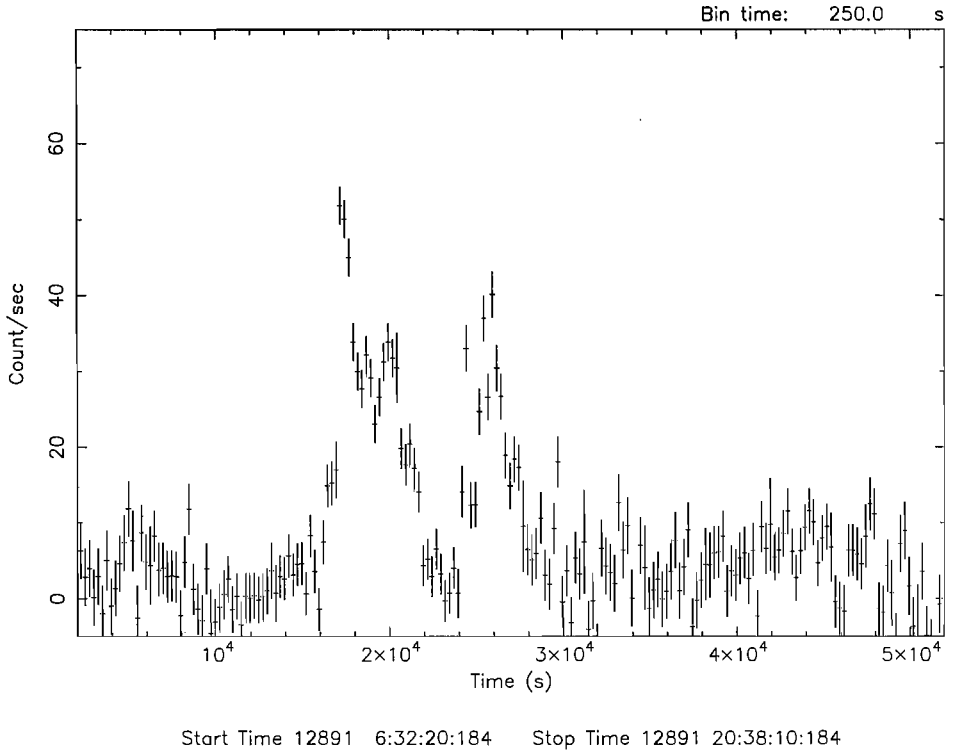

Figure 4.29: ISGRI light curve (20–100 keV) of a newly discovered outburst (No.1 in table 4.5) of SAX J1818.6–1703.

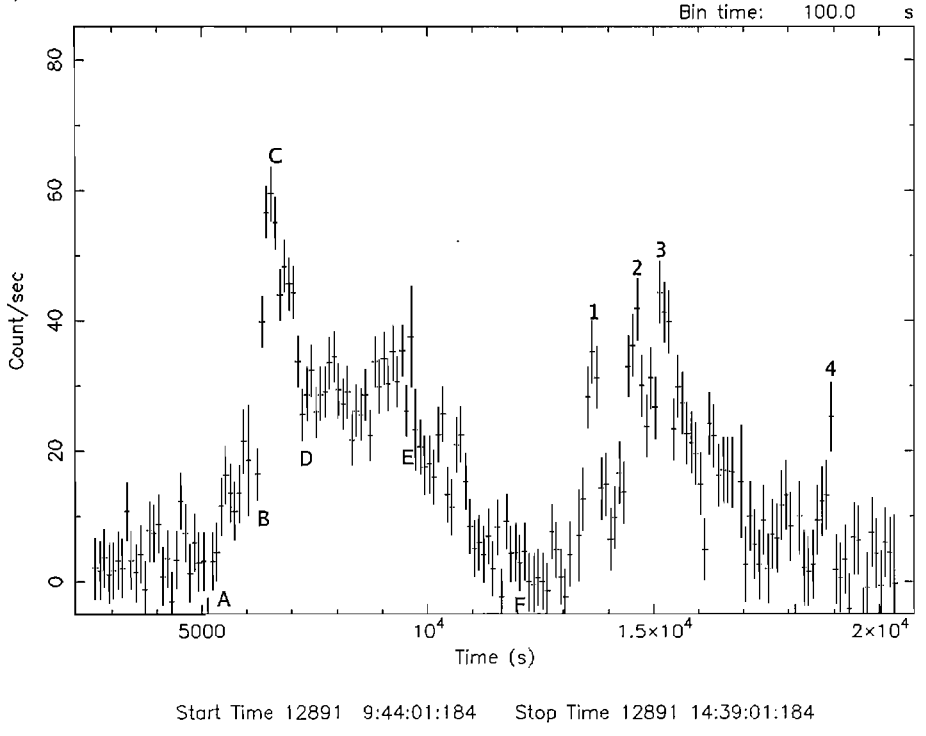

Figure 4.30: Expanded view of the light curve (20–100 keV) of the outburst from SAX J1818.6–1703 showed in figure 4.29

tonized models. All provided very poor fits with a χ^2_ν greater than 3. This could be due to the fact that the extracted spectrum is the sum of very different spectral states. In fact, as we can note from figure 4.30, the outburst activity of the source is complex with several different flares. Bearing this in mind, the best approach for a spectral analysis is to extract spectra for characteristic flux levels: rise (from point A to C) and decay (from point C to D). As for the 20–100 keV spectrum extracted during the rise, the black body model gives a reasonable description (χ^2_ν=1.18, 24 d.o.f.) with a temperature of 7.1±0.5 keV. A thermal bremsstrahlung provides an equally good fit (χ^2_ν=0.9, 24 d.o.f.) with kT=25^{+5}_{-4} keV. The 20–100 keV spectrum extracted during the decay is well fit by a thermal bremsstrahlung (χ^2_ν=1.18, 24 d.o.f.) with kT=26.5±2.5 keV as well as a Comptonized model CompST (χ^2_ν=1.15, 23 d.o.f.) with kT=$12.1^{+3.9}_{-2.1}$ keV. Whereas, a black body model provides a very poor fit.

The ISGRI analysis of this outburst (No. 1 in table 4.5) enabled a more accurate source position than that reported by in't Zand et al. (1998) when the source was discovered by BeppoSAX. The new ISGRI refined position is RA=18^h 18^m 38.28^s Dec =-17° 03′ 12.5″, error radius of 42″.

Outburst No. 2 in table 4.5 was detected by ISGRI on 9 October 2003 in 2 consecutive ScWs. The 20–60 keV ISGRI light curve is shown in figure 4.31, the peak flux was ~ 120 mCrab. The 20–60 keV spectrum extracted during this outburst is best fit by thermal models such as black body (χ^2_ν=1.27, 14 d.o.f., kT=$6^{+0.85}_{-0.75}$ keV) or bremsstrahlung (χ^2_ν=1.24, 14 d.o.f., kT=$17^{+6.5}_{-4.3}$ keV). The unfolded black body spectrum is shown in figure 4.32. However a reasonable fit is also provided by a single power law (χ^2_ν=1.34, 14 d.o.f., Γ=3.2±0.5)

Outburst No. 3 in table 4.5 was detected only ~1.5 days later than No. 2. It was observed in 6 consecutive ScWs (20–30 keV). Figure 4.33 shows its ISGRI light curve (20–30 keV), while figure 4.34 shows the sequence of consecutive ScWs (20–30 keV) during which it was observed. The source turned on at 21:50:45 UTC 10 October 2003 and subsequently peaked after ~ 35 minutes at a level of ~ 185 mCrab. Subsequently the intensity decreased to an undetectable flux level on 11 October 2003 01:00:12 UTC.

The light curve of outburst No. 4 in table 4.5 is shown in figure 4.35. It is truncated at the end, the source was active for ~ 9 hours then it went outside the IBIS FOV. The source is detected at ~ 6σ level (20–40 keV) in a mosaic significance map of all ScWs during which it was detected.

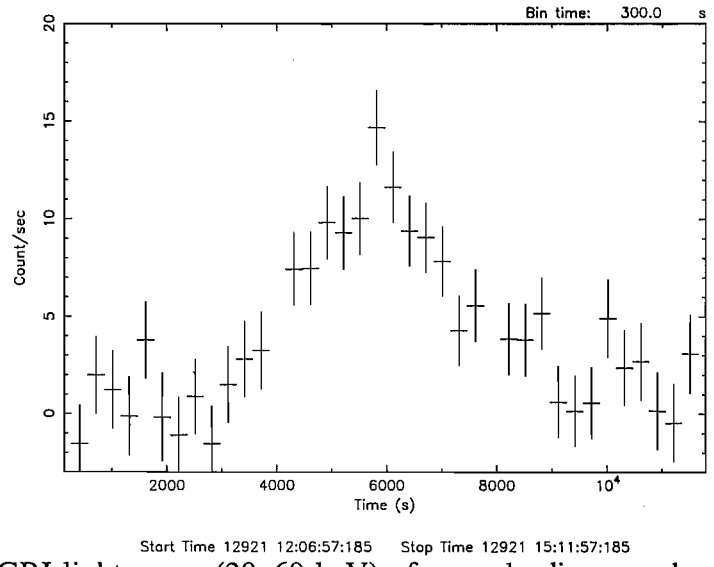

Figure 4.31: ISGRI light curve (20–60 keV) of a newly discovered outburst (No. 2 in table 4.5) of SAX J1818.6–1703.

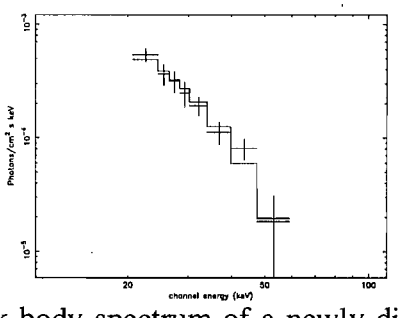

Figure 4.32: Unfolded black body spectrum of a newly discovered outburst (No. 2 in table 4.5) of SAX J1818.6–1703.

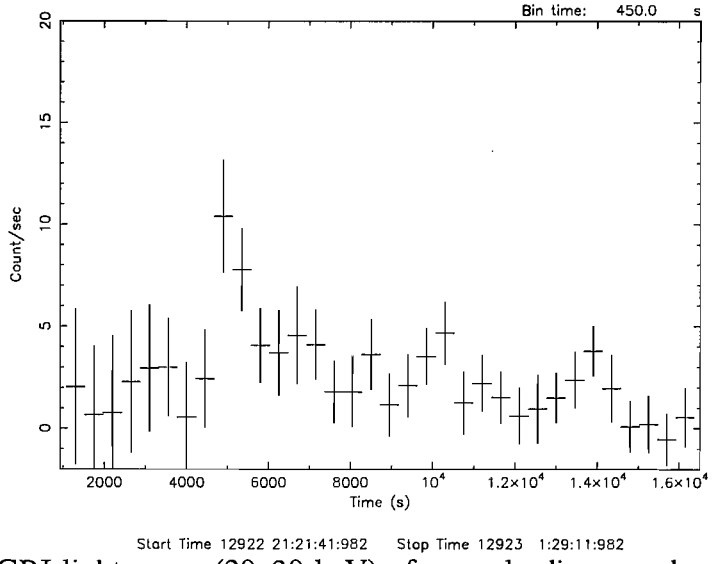

Figure 4.33: ISGRI light curve (20–30 keV) of a newly discovered outburst (No. 3 in table 4.5) of SAX J1818.6–1703.

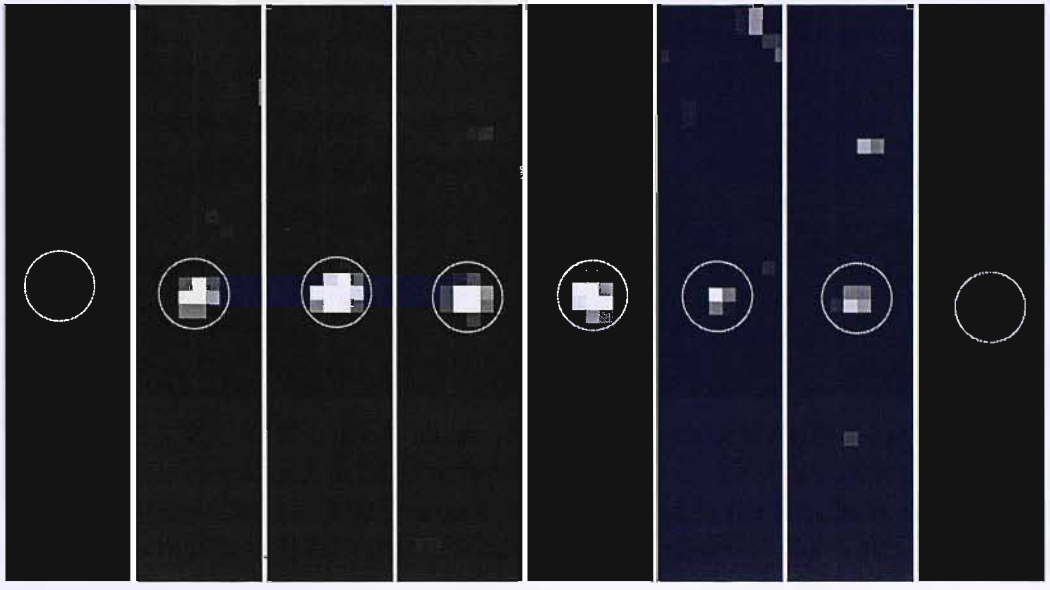

Figure 4.34: ISGRI Science Window (ScW) image sequence (20–30 keV) of a newly discovered outburst (No.3 in table 4.5) of SAX J1818.6–1703 (encircled). The duration of each ScW is ~ 2000 s. The source was not detected in the first ScW on the left (significance less than 1σ), then it was detected during the next 6 ScWs with a significance, from left to right, equal to 5σ, 10.5σ, 7.5σ, 7σ, 5σ and 4.5σ, respectively. Finally in the last ScW the source was not detected (significance less than 2σ).

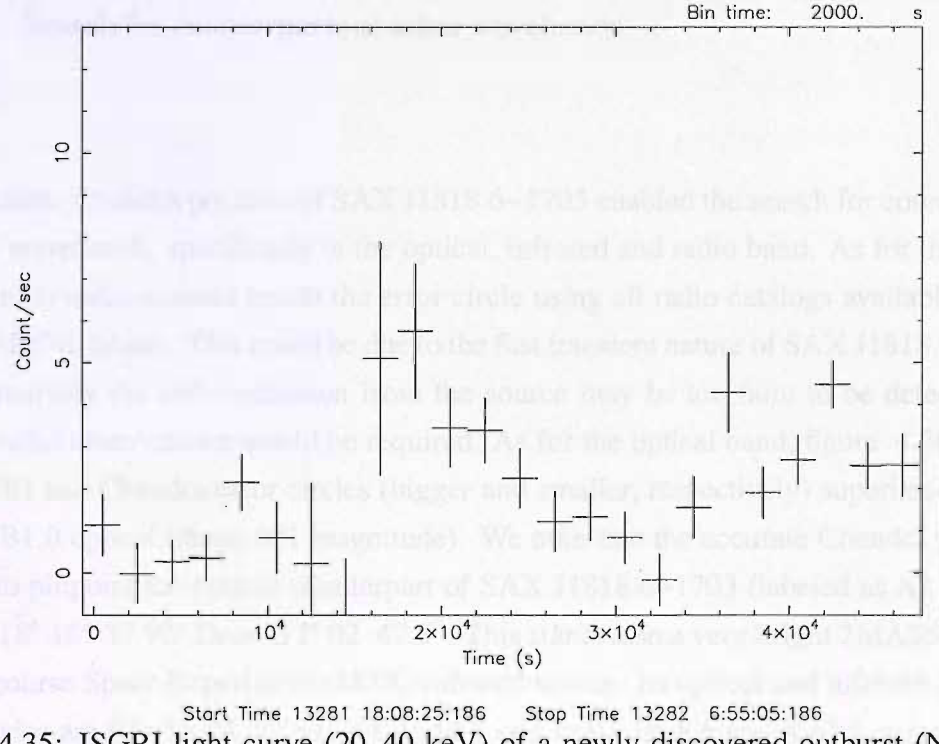

Figure 4.35: ISGRI light curve (20–40 keV) of a newly discovered outburst (No. 4 in table 4.5) of SAX J1818.6–1703.

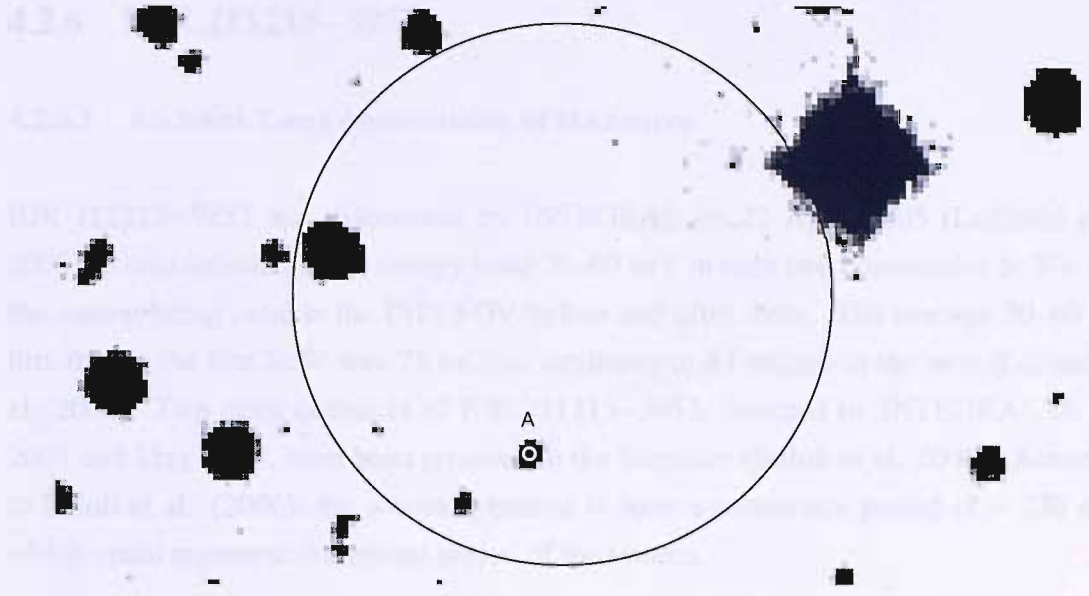

Figure 4.36: USNO R1 optical image superimposed on the ISGRI error circle of SAX J1818.6−1703 (the bigger one, radius of 42″) and on the Chandra error circle (the smaller one, in white, radius of 0″.62).

4.2.5.3 Search for counterparts at other wavebands

The accurate Chandra position of SAX J1818.6−1703 enabled the search for counterparts at other wavebands, specifically in the optical, infrared and radio band. As for the latter, there are no radio sources inside the error circle using all radio catalogs available in the HEASARC database. This could be due to the fast transient nature of SAX J1818.6−1703 or alternatively the radio emission from the source may be too faint to be detected, so deeper radio observations would be required. As for the optical band, figure 4.36 shows the ISGRI and Chandra error circles (bigger and smaller, respectively) superimposed on USNO B1.0 optical image (R1 magnitude). We note that the accurate Chandra position allows to pinpoint the optical counterpart of SAX J1818.6−1703 (labeled as A), located at RA=18^h 18^m 37.92^s Dec=-17° 02′ 47.5″. This star is also a very bright 2MASS as well as Midcourse Space Experiment (MSX) infrared source. Its optical and infrared 2MASS magnitudes are R1=16.84, R2=17.44, I=14.7 and J=10, H=8.6 and K=7.8, respectively. Low resolution spectroscopy of this optical object was obtained by Negueruela et al. (2006c). It turned out to be a supergiant star of spectral type O9–B1I. A high resolution optical spectrum is required to better constrain its optical characteristics.

4.2.6 IGR J11215–5952

4.2.6.1 Archival X-ray observations of the source

IGR J11215–5952 was discovered by INTEGRAL on 22 April 2005 (Lubinski et al. 2005). It was detected in the energy band 20–60 keV in only two consecutive ScWs, with the source being outside the IBIS FOV before and after them. The average 20–60 keV flux during the first ScW was 75 mCrab, declining to 44 mCrab in the next (Lubinski et al. 2005). Two other outbursts of IGR J11215–5952, detected by INTEGRAL on July 2003 and May 2004, have been reported in the literature (Sidoli et al. 2006). According to Sidoli et al. (2006), the source appeared to have a recurrence period of ~ 330 days, which could represent the orbital period of the system.

RXTE and *Swift* XRT ToO observations detected IGR J11215–5952 in outburst, exactly when predicted by the ephemeris of Sidoli et al. (2006), on mid March 2006 and at the beginning of February 2007 (Smith et al. 2006b, Romano et al. 2007, Sidoli et al. 2007, Mangano et al. 2007, Swank et al. 2007). As for the detection on March 2006, the lower and upper limits to the total duration of the outburst activity are 2 and 3.4 days, respectively. Figure 4.37 shows its 2–10 keV RXTE light curve. The peak flux was ~ 2×10^{-10} erg cm^{-2} s^{-1}, which corresponds to a peak luminosity of ~ 10^{36} erg s^{-1} (Smith et al. 2006b). From the RXTE analysis, a possible pulsation period of ~ 195 seconds was suggested by Smith et al. (2006b). The outburst on February 2007 was detected by RXTE and *Swift*. On 4–8 of February the source was mostly quiescent, then on 9 February it underwent a very bright flare (see light curve in figure 4.38). The peak flux measured by *Swift* XRT was ~ 2×10^{-10} erg cm^{-2} s^{-1} (1–10 keV), which corresponds to a peak luminosity of ~ 7×10^{35} erg s^{-1} (Mangano et al. 2007). The *Swift* XRT spectrum was best fit by a power law (Γ=0.93±0.2) absorbed with a column density of $1.02^{+0.4}_{-0.3}\times10^{22}$ cm^{-2}. The RXTE study of this flare confirmed the detection of pulsations at 186.78±0.3 seconds.

The *Swift* XRT observations of IGR J11215–5952 provided a very accurate position (RA=11^h 21^m 46.9^s Dec=-59° 51′ 42″, error radius of 5″) which allowed the identification of its optical counterpart (Steeghs et al. 2006). It is a star known as HD 306414 and classified as B1Ia-type supergiant (Vijapurkar & Drilling 1993). Masetti et al. (2006a) performed an optical follow-up observation of HD 306414 and the spectrum indicates that it is an early B-type luminous star in agreement with the B1Ia spectral type classification of Vijapurkar & Drilling (1993). Its distance (~ 6.2 kpc) is compatible with a location in the far end of the Carina Arm.

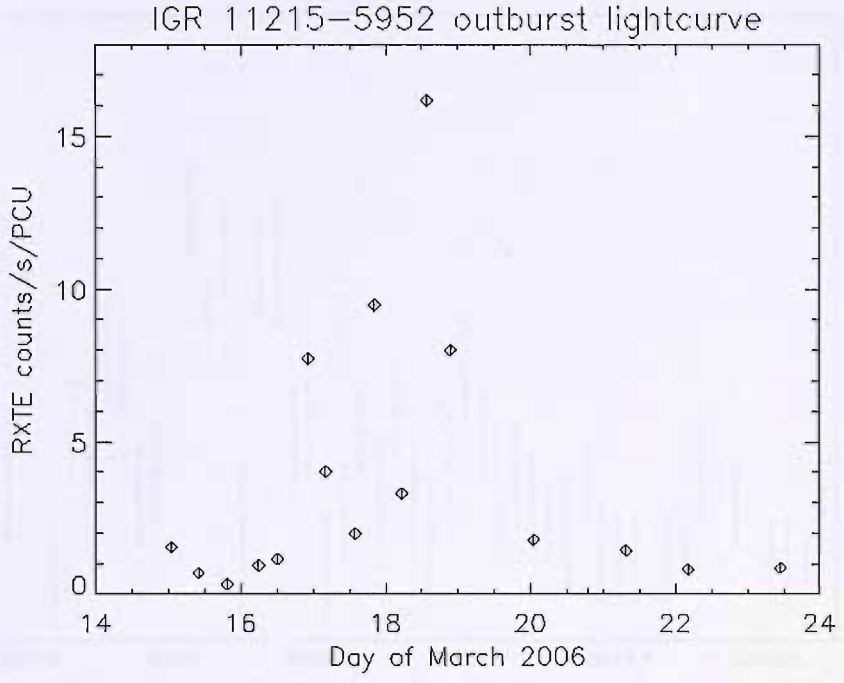

Figure 4.37: RXTE light curve (2–10 keV) of IGR J11215−5952 in outburst on March 2006 (Credit:Smith at al. 2006b).

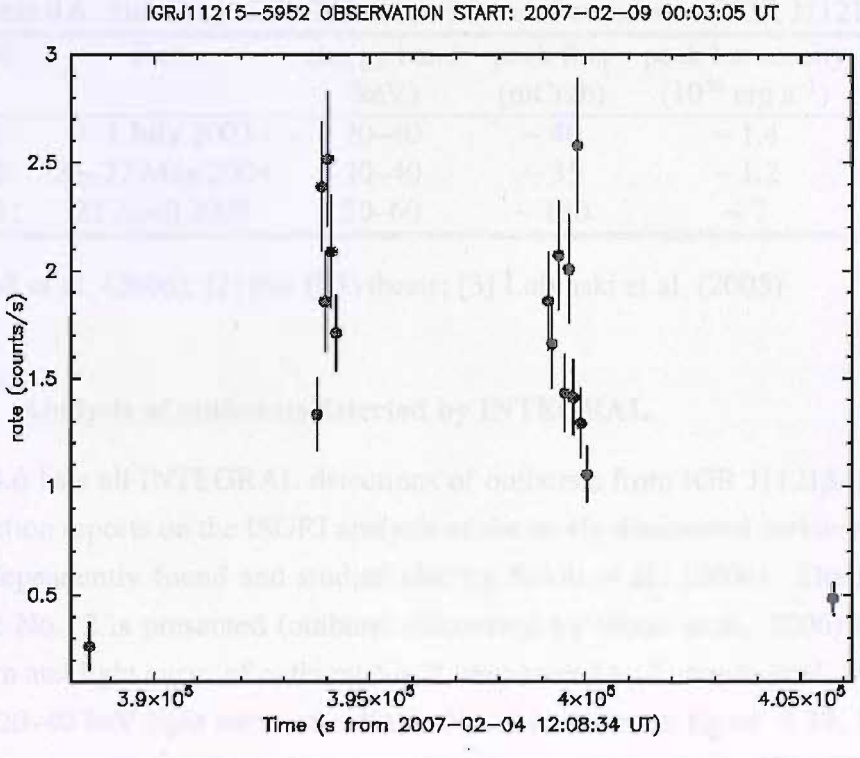

Figure 4.38: *Swift* XRT light curve (1–10 keV) of IGR J11215−5952 in outburst on February 2007 (Credit:Mangano at al. 2007).

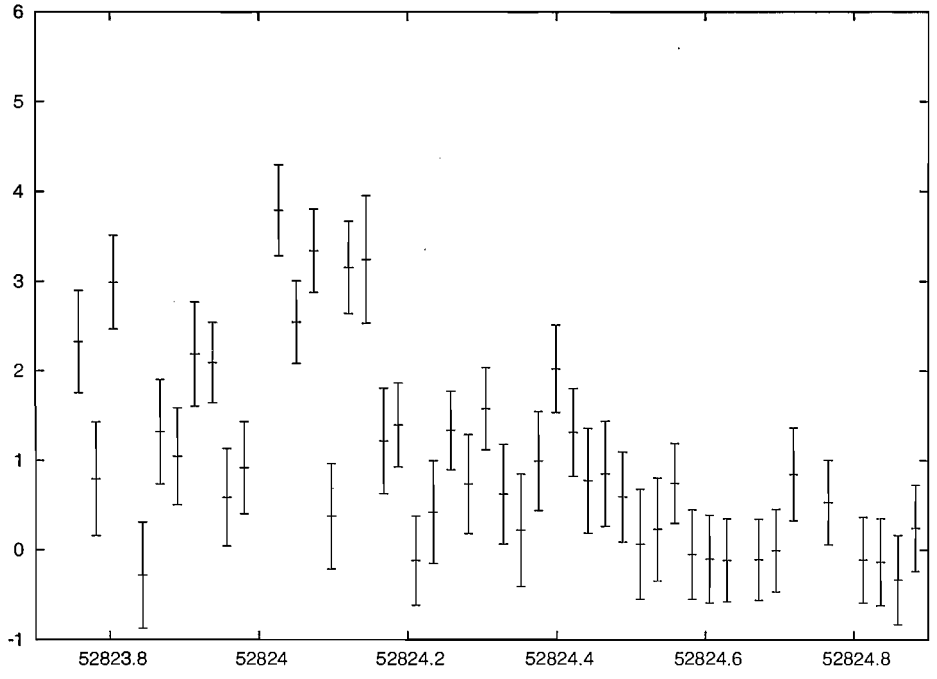

Figure 4.39: ISGRI light curve (20–40 keV) of outburst No. 1 in table 4.6. Time axis is in MJD. Each data point represents the average flux during one ScW (~2000 seconds).

Table 4.6: Summary of ISGRI observations of outbursts of IGR J11215−5952

No.	Date	energy band (keV)	peak flux (mCrab)	peak luminosity (10^{36} erg s^{-1})	ref
1	3–4 July 2003	20–40	~ 40	~ 1.4	[1],[2]
2	26–27 May 2004	20–40	~ 35	~ 1.2	[1]
3	22 April 2005	20–60	~ 130	~ 7	[3]

[1] Sidoli et al. (2006); [2] this PhD thesis; [3] Lubinski et al. (2005)

4.2.6.2 Analysis of outbursts detected by INTEGRAL

Table 4.6 lists all INTEGRAL detections of outbursts from IGR J11215−5952, to date. This section reports on the ISGRI analysis of the newly discovered outburst No. 1, which was independently found and studied also by Sidoli et al. (2006). The light curve of outburst No. 2 is presented (outburst discovered by Sidoli et al. 2006) as well as the spectrum and light curve of outburst No. 3 (discovered by Lubinski et al. 2005).

The 20–40 keV light curve of outburst No. 1 is shown in figure 4.39. It is truncated at the beginning and at the end because the source was outside the IBIS FOV. As we can note, the source was already active when it entered the IBIS FOV. The peak flux and peak luminosity (20–40 keV) are ~ 40 mCrab and ~ 1.4×10^{36} erg s^{-1}. The spectrum during the outburst activity can be reasonably described (χ^2_ν=0.9, d.o.f. 14) by an optically thin

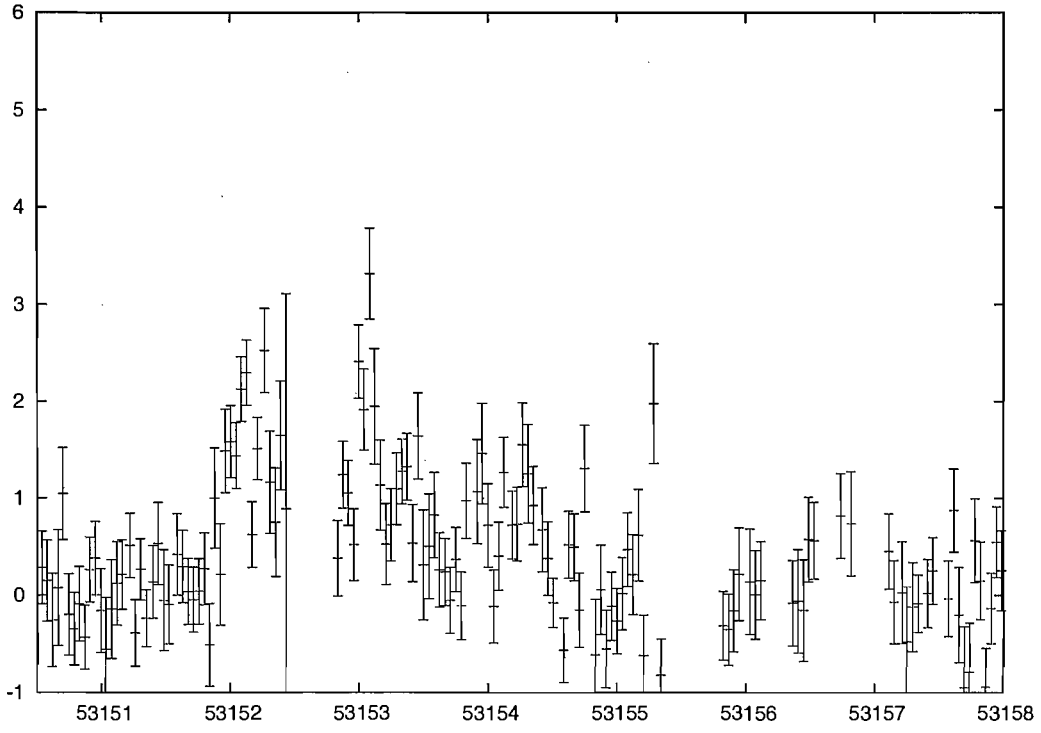

Figure 4.40: ISGRI light curve (20–40 keV) of outburst No. 2 in table 4.6. Time axis is in MJD. Each data point represents the average flux during one ScW (~2000 seconds).

thermal bremsstrahlung model with kT=$19^{+5}_{-3.5}$ keV. However, a reasonable fit was also achieved using a black body model with kT=6.2±0.6 keV (χ^2_ν=1.4, d.o.f. 14).

Figure 4.40 displays the 20–40 keV light curve of outburst No. 2. It is truncated at the beginning and at the end because the source was outside the IBIS FOV. The outburst activity is evident through the presence of several flares. The maximum peak flux was ~ 35 mCrab (20–40 keV), which implies a peak luminosity of ~ 1.2×10^{36} erg s^{-1}.

Finally, the 20–60 keV ISGRI light curve of outburst No. 3 is shown in figure 4.41. Again it is truncated at the beginning and at the end because the source was in the IBIS FOV only during two consecutive ScWs. No strong flares are evident, the source was very bright with a 20–60 keV peak flux of ~ 130 mCrab, which implies a peak luminosity of ~ 7×10^{36} erg s^{-1}. The 20–100 keV spectrum of the source is best fit by a single power law (χ^2_ν=1.2, d.o.f. 24) with Γ=3.2±0.25 (see figure 4.42). A reasonable fit is also achieved with a thermal bremsstrahlung (χ^2_ν=1.4, d.o.f. 24) with kT=$18.5^{+3.5}_{-2.5}$ keV. A black body is not a good description to the data (χ^2_ν=2).

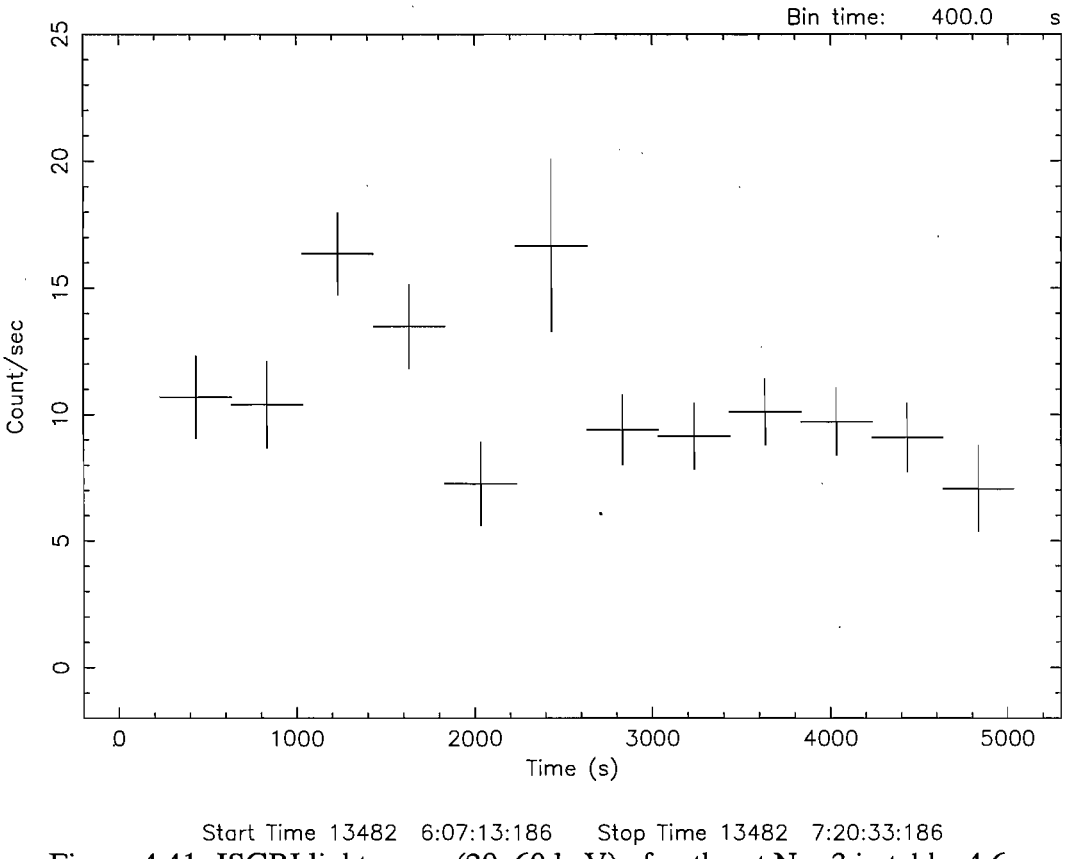

Figure 4.41: ISGRI light curve (20–60 keV) of outburst No. 3 in table 4.6.

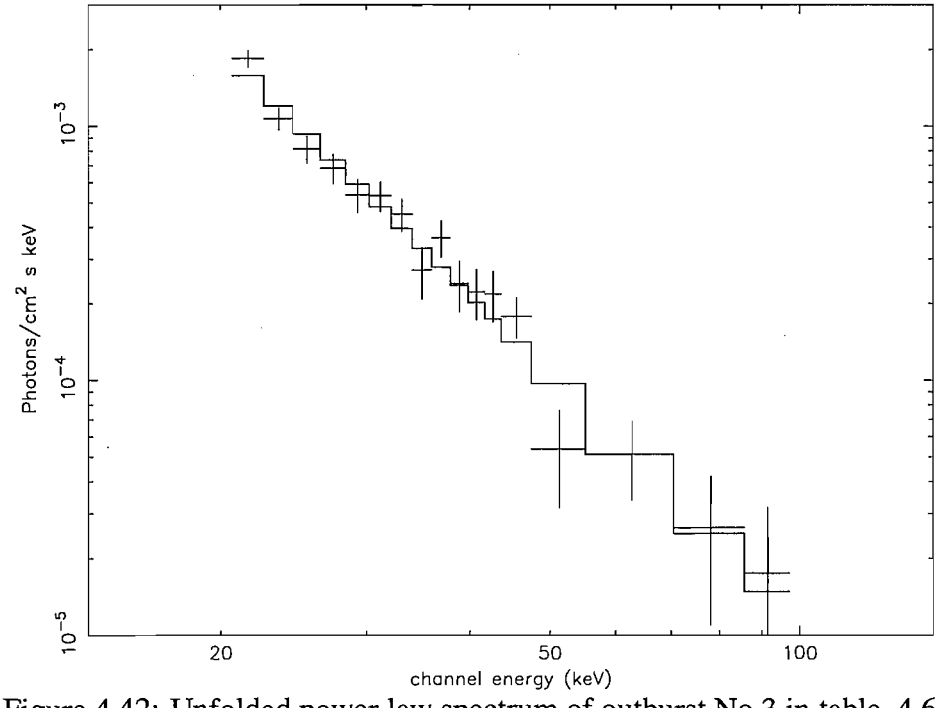

Figure 4.42: Unfolded power law spectrum of outburst No.3 in table 4.6.

Table 4.7: Summary of INTEGRAL observations of outbursts of IGR J16465−4507

No.	Date	energy band (keV)	peak flux (mCrab)	ref (discovery)
1	9 August 2004	20–40	~ 50	[1]
2	7 September 2004	20–30	~ 94	[2]

[1] this PhD thesis; [2] Lutovinov et al. (2004)

4.2.7 IGR J16465−4507

4.2.7.1 Archival X-ray observations of the source

IGR J16465−4507 was discovered by INTEGRAL on 6–7 September 2004 (Lutovinov et al. 2004) with an average flux of ~ 9 mCrab (18–60 keV). A strong flare was detected on 7 September ~ 12:00 UTC with an higher average flux of ~ 28 mCrab. To date this is the only detection by INTEGRAL of the source in outburst, no further flaring activity has been reported in the literature.

A XMM ToO observation of the source was performed on 14 September 2004, about a week after its discovery (Walter et al. 2006, Zurita et al. 2004). The source was faint with a 4–10 keV flux of ~ 3×10^{-12} erg cm^{-2} s^{-1}, which is ~ 100 times smaller than the flux during the flare detected by INTEGRAL. The timing analysis of the XMM data allowed the discovery of pulsations at 227±5 seconds. The combined ISGRI and XMM data, although not simultaneous, were fit by an absorbed black body plus a Comptonized model CompTT (Walter et al. 2006). The absorbing column density is high (N_H=60±10×10^{22} cm^{-2}), exceeding by far the galactic absorption along the line of sight (N_H ~ 1.6×10^{22} cm^{-2}). The XMM observation provided a very accurate source position (RA=16^h 46^m 35.5^s Dec=-45° 07′ 04″, uncertainty 4″). Only one object is contained inside the XMM error circle, it is a very bright infrared 2MASS as well as optical USNO B–1.0 source. Optical spectroscopy of this object (Negueruela et al. 2006a, Negueruela et al. 2005, Smith 2005) revealed that it is a reddened early type supergiant. Unfortunately the signal to noise of the optical spectrum is not good enough to allow an exact spectral classification. It is compatible with a luminous supergiant star in the range B0–B1, probably a B0.5I.

4.2.7.2 Analysis of the outbursts detected by INTEGRAL

Table 4.7 lists all INTEGRAL detections of outbursts from IGR J16465–4507. In this section the temporal and spectral analysis of the already discovered outburst No. 2 is re-

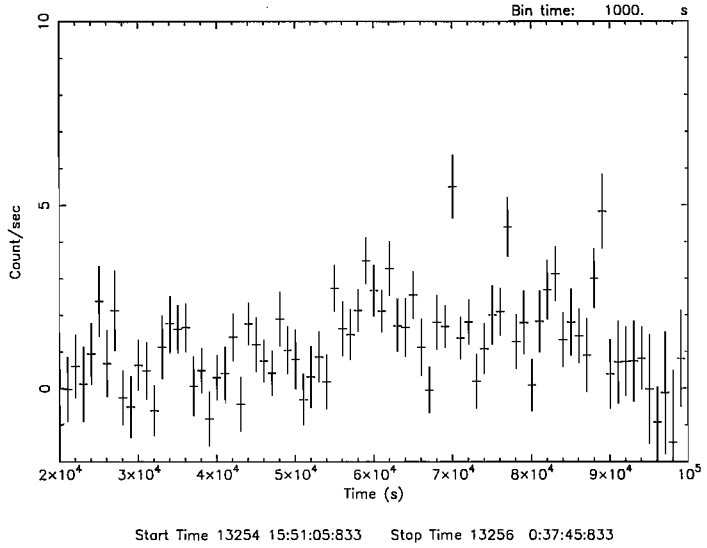

Figure 4.43: ISGRI light curve (20–30 keV) of outburst No.2 in table 4.7.

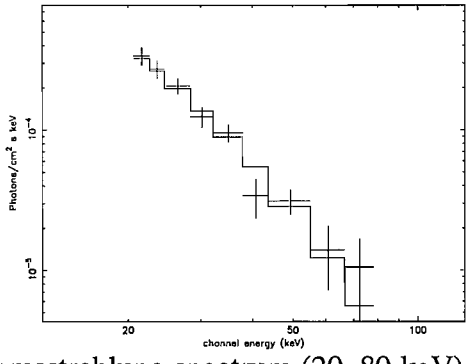

Figure 4.44: Unfolded bremsstrahlung spectrum (20–80 keV) of IGR J16465–4507 during outburst No. 2 in table 4.7.

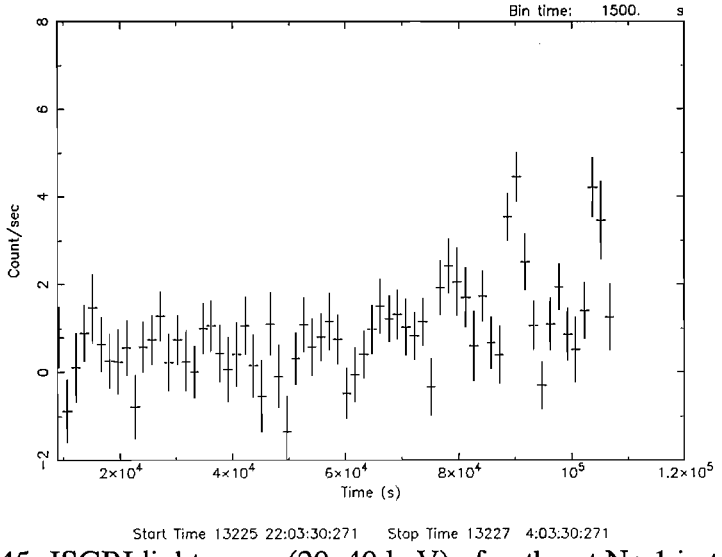

Figure 4.45: ISGRI light curve (20–40 keV) of outburst No.1 in table 4.7.

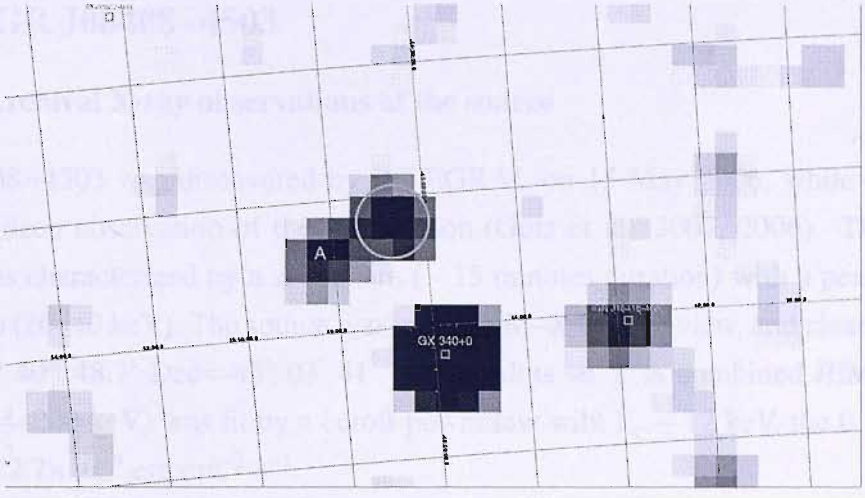

Figure 4.46: ISGRI mosaic significance map (17–40 keV) of ScWs during which outburst No. 1 was detected. IGR J16465–4507 is encircled in the picture, it was detected at a level of $\sim 13\sigma$.

ported. Moreover, a possible newly discovered outburst, not reported yet in the literature, is investigated (No. 1 in table 4.7).

Figure 4.43 shows the 20–30 keV light curve of IGR J16465–4507 at the time of its discovery (outburst No. 2 in table 4.7). It is truncated at the end because the source was outside the IBIS FOV. The outburst activity is evident especially towards the end of the light curve, where three fast flares took place on timescale of ~ 15 minutes. The peak flux is ~ 94 mCrab (20–30 keV). A spectrum (20–80 keV) is best fit by a thermal bremsstrahlung model (χ^2_ν=1.1, d.o.f. 19) with kT=$21^{+6.5}_{-4.5}$ keV (see figure 4.44). A black body gives a χ^2_ν=1.5 (d.o.f. 19) with kT=6.6±0.7 keV.

Outburst No. 1 is a newly discovered one and it is the second ever detected from IGR J16465–4507. Figure 4.45 shows the 20–40 keV ISGRI light curve from 8 August 2004 ~ 22:00 UTC to 10 August 2004 ~ 04:00 UTC. It can be noted that at the beginning there is no detection, then towards the end of the observation the source turned on displaying a couple of fast flares with peak flux of ~ 50 mCrab (20–40 keV). Unfortunately no further data exist due to the fact that the source went outside the IBIS FOV. A search for outburst activity when it was again in the IBIS FOV did not give any positive results. Figure 4.46 shows the ISGRI mosaic significance map (17–40 keV) of all ScWs during which outburst No. 1 was detected. IGR J16465–4507 (encircled in the figure) is detected at a level of ~ 13σ (17–40 keV). The other nearby detected source, labelled as A, is located ~ 18 arcminutes from IGR J16465–4507.

4.2.8 IGR J08408–4503

4.2.8.1 Archival X-ray observations of the source

IGR J08408–4503 was discovered by INTEGRAL on 15 May 2006, while it was performing a deep observation of the Vela region (Gotz et al. 2007, 2006). The outburst activity was characterized by a short flare (~ 15 minutes duration) with a peak flux of ~ 250 mCrab (20–40 keV). The source was in the JEM–X field of view, and clearly detected at RA=08^h 40^m 48.7^s Dec=-45° 03′ 41″ (error radius 46″). A combined JEM–X/ISGRI spectrum (4–200 keV) was fit by a cutoff power law wiht E_c ~ 12 keV, the 0.1–100 keV flux was ~ 2.7×10^{-9} erg cm^{-2} s^{-1}.

A *Swift* XRT ToO observation of IGR J08408–4503 was performed on 22 May 2006, just a few days after its discovery (Kennea & Campana 2006). A faint source was detected inside the JEM–X error circle at RA=08^h 40^m 47.97^s Dec=-45° 03′ 29.8″ (error radius of 5.4″). The source had faded significantly since its discovery, the X-ray flux was ~ 2×10^{-13} erg cm^{-2} s^{-1} (0.5–10 keV). It could be that this detection by *Swift* XRT represents the quiescent X-ray emission from IGR J08408–4503.

Subsequent to the discovery of IGR J08408–4503, Mereghetti et al. (2006) reported another fast outburst from the source detected by INTEGRAL on 1 July 2003 (~ 2 hours duration).

Swift BAT detected again the source in outburst on 4 October 2006 (Gotz et al. 2007). The broad band spectrum 0.3–100 keV was best fit by an absorbed cutoff power law with Γ~0.1 and E_c~15keV. The hydrogen column density was found to be $1\pm0.3\times10^{21}$ cm^{-2}, compatible with the galactic value along the line of sight. Other spectral models, such as black body or bremsstrahlung, were not a good description to the spectrum.

The *Swift* XRT observations of IGR J08408–4503 provided a very accurate position which can be used to find counterparts in the optical and infrared wavebands. Figure 4.47 shows the *Swift* XRT error circle of IGR J08408–4503 superimposed on the 2MASS infrared J band image. As we can note, the X-ray source is associated with a very bright infrared object, its magnitudes are J=6.93, H=6.88 and K=6.8. As for the optical waveband, the *Swift* XRT refined position allowed to pinpoint a USNO–B1.0 star as counteraprt as well (Masetti et al. 2006b, Barba et al. 2006). This star, known also as HD 74194, is a supergiant of spectral type O8.5 Ib(f). The distance, as calculated from its parallax listed in the Hipparcos catalogue (Perryman et al. 1997), is 2.77 kpc. This gives a peak luminosity of the outburst, when the source was discovered by INTEGRAL, of ~ 1.7×10^{36} erg s^{-1} (20–40 keV). The 0.5–10 keV quiescent luminosity from the *Swift* XRT observation is equal to ~ 2×10^{32} erg s^{-1}.

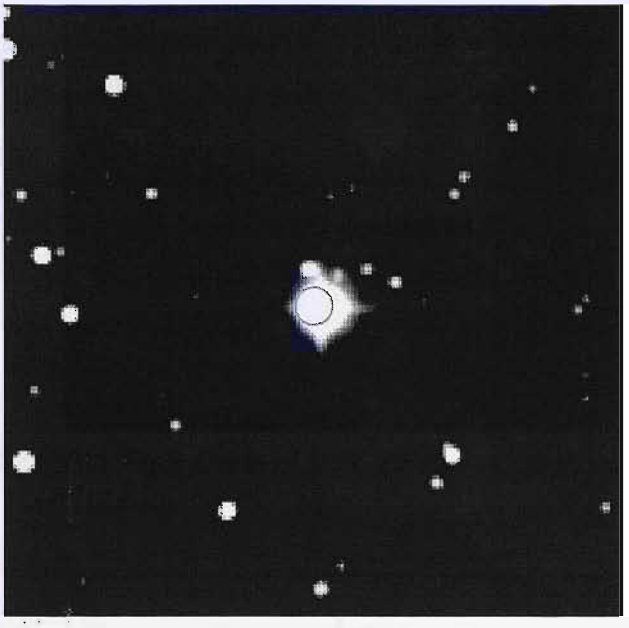

Figure 4.47: *Swift* XRT error circle of IGR J08408−4503 superimposed on the 2MASS infrared image band (J band).

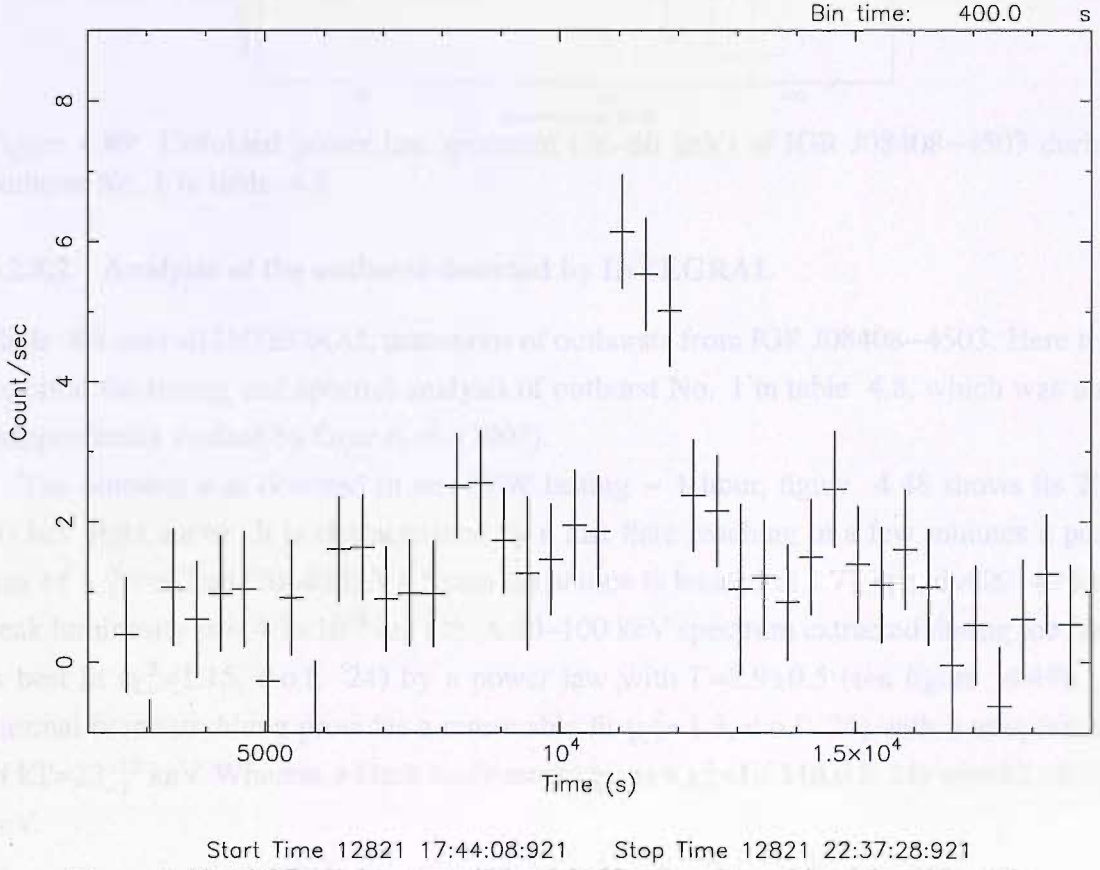

Figure 4.48: ISGRI light curve (20–40 keV) of outburst No. 1 in table 4.8.

Table 4.8: Summary of INTEGRAL observations of outbursts of IGR J08408−4503

No.	Date	Duration (hours)	energy band (keV)	flux peak (mCrab)	luminosity peak (10^{36} erg s^{-1})	ref (discovery)
1	1 July 2003	~ 1	20–40	~ 70	0.47	[1]
2	15 May 2006	~ 1	20–40	~ 250	1.7	[2]

[1] Mereghetti et al. (2006); [2] Gotz et al. (2007)

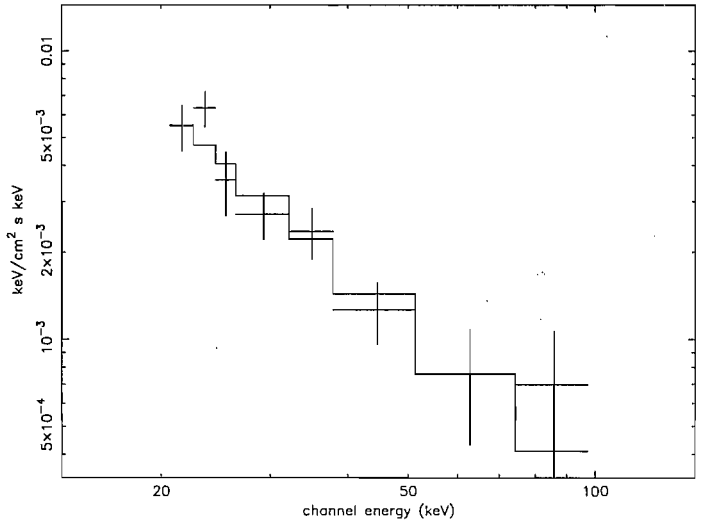

Figure 4.49: Unfolded power law spectrum (20–80 keV) of IGR J08408−4503 during outburst No. 1 in table 4.8.

4.2.8.2 Analysis of the outburst detected by INTEGRAL

Table 4.8 lists all INTEGRAL detections of outbursts from IGR J08408−4503. Here it is reported the timing and spectral analysis of outburst No. 1 in table 4.8, which was also independently studied by Gotz et al. (2007).

The outburst was detected in one ScW lasting ~ 1 hour, figure 4.48 shows its 20–40 keV light curve. It is characterized by a fast flare reaching in a few minutes a peak flux of ~ 70 mCrab (20–40 keV). Since the source is located at 2.77 kpc, the 20–40 keV peak luminosity is ~ 4.7×10^{35} erg s^{-1}. A 20–100 keV spectrum extracted during the flare is best fit (χ^2_ν=1.15, d.o.f. 24) by a power law with Γ=2.9±0.5 (see figure 4.49). A thermal bremsstrahlung provides a reasonable fit (χ^2_ν=1.3, d.o.f. 24) with a temperature of kT=23^{+13}_{-7} keV. Whereas a black body model gives a χ^2_ν=1.55 (d.o.f. 24) with kT=6.5^{+1}_{-1} keV.

Chapter 5

Candidate Supergiant Fast X-ray transients

If we knew what we were doing,
it wouldn't be called research, would it?
– Albert Einstein

5.1 Introduction

As described in chapter 4, INTEGRAL is discovering a growing number of SGXBs which display fast X-ray outbursts with a duration of typically a few hours. They have been labelled as Supergiant Fast X-ray Transients (SFXTs). Their X-ray behaviour is very different from that seen from classical persistent SGXBs.

This chapter reports on INTEGRAL results on a sample of 6 unidentified hard X-ray sources: IGR J16479–4514, IGR J17407–2808, AX J1749.1–2733, IGR J11321–5311, IGR J18483–0311 and AX J161929–4945. They display an X-ray behaviour similar to that of SFXTs, so they can be considered candidate SFXTs even if their optical counterpart has not yet been identified with a supergiant star.

Table 5.1: Summary of INTEGRAL observations of outbursts of IGR J16479–4514.

No.	Date	duration (hours)	energy band (keV)	peak-flux (mCrab)	peak-luminosity (10^{36} erg s^{-1})	ref (discovery)
1	5 Mar 2003	~ 3.5	20–30	~ 850	16 ⋆	[1]
2	28 Mar 2003	~ 1.5	20–30	~ 40†		[1]
3	21 Apr 2003	~ 0.5	20–30	~ 160†		[1]
4	8–10 Aug 2003					[2]
5	14 Aug 2003		20–30	~ 44†		[1]
6	11 Aug 2004	~ 11	20–80	~ 140		[1]
7	7 Sep 2004	~ 2	20–60	~ 80		[1]
8	16 Sep 2004	~ 2.5	20–60	~ 120		[1]
9	4 Apr 2005	~ 2.5	20–60	~ 60	3 ⋆	[1]
10	12 Aug 2005		20–60	~ 120		[1]
11	30 Aug 2005	~ 0.5	20–60	~ 240		[1]

[1] This PhD thesis; [2] Molkov et al. (2003a)
Note: ⋆ = assuming a distance of 6 kpc since its location in the Norma spiral arm
Note: † = average flux (20–30 keV) during the outburst

5.2 Candidate SFXTs observed with INTEGRAL

5.2.1 IGR J16479–4514

5.2.1.1 Archival X-ray observations of the source

IGR J16479–4514 was discovered by INTEGRAL during observations of the galactic center region performed between 8–10 August 2003 (Molkov et al. 2003a). The measured average fluxes were 12 mCrab and 8 mCrab in the energy bands 18–25 keV and 25–50 keV, respectively. Up to now, this was the only detection by INTEGRAL of the source to be reported in the literature. Its discovery was reported as an average detection and no analysis at the Science Window level was performed, hence the fast transient nature of the source was not unveiled. Lutovinov et al. (2005) published a broad band energy spectrum of IGR J16479–4514 (1–100 keV) using non simultaneous ISGRI data and archival ASCA data. It is described by a power law model modified by a cutoff at high energies and the photoabsorption at soft X-rays. The best fit parameters are Γ=1.4±0.8, N_H~1.2×10^{23} cm^{-2} and a high energy cut-off of E_c~32 keV. Based on these spectral characteristics as well as on its location in the Norma spiral arm, Lutovinov et al. (2005) argue that IGR J16479–4514 should be a neutron star HMXB.

On 30 August 2005, the *Swift* Burst Alert Telescope (BAT) was triggered by a strong flare. The *Swift* spacecraft slewed in less than 2 minutes to the position of the detected

flare and the *Swift* X-ray Telescope (XRT) detected a bright variable source at RA=16^h 48^m 07^s, Dec=-45° 12′ 05.8″with an error circle of 6″ (Kennea et al. 2005). This position is fully compatible with the ISGRI location of IGR J16479–4514. The flare in the BAT light curve lasted ~ 400 seconds and was detected in the energy band 15–50 keV. The XRT light curve, which covered ~ 30 ks, showed 2 other bright fast flares. The spectrum of the source was fit by an absorbed power law (Γ=1.1±0.25, N_H=6.4±0.9×10^{22} cm^{-2}) with a 0.5–10 keV flux of 3.8×10^{-11} erg cm^{-2} s^{-1} (Kennea et al. 2005). The *Swift* UV/optical telescope (UVOT) detected a faint object (RA=16^h 48^m 06.8^s, Dec=-45° 12′ 08″) inside the XRT error circle (Kennea et al. 2005). It was visible only in the V band with a magnitude of 20.4±0.4. This optical source is catalogued in the USNO–B1.0 catalog with I and R1 magnitudes of 16.7 and 18.36, respectively. It is the only USNO–B1.0 object located inside the *Swift* XRT error circle, further optical follow-up is required to unveil its nature.

IGR J16479–4514 was also detected with a low X-ray flux by XMM, at a position compatible with that of *Swift* XRT (Walter et al. 2006). The intrinsic absorption, as derived from the XMM observation, is 7.7±1.7×10^{22} cm^{-2}; it exceeds the galactic absorption along the line of sight which is ~ 2×10^{22} cm^{-2}.

5.2.1.2 Analysis of newly discovered outbursts by INTEGRAL

This section reports on 10 newly discovered fast X-ray outbursts of IGR J16479–4514 detected by INTEGRAL. All of them last only a few hours, marking the very fast transient nature of the source. They strongly resemble those detected from the known SFXTs, so IGR J16479–4514 can be considered a reliable candidate, even if its optical counterpart has not been yet identified with a supergiant star. All the newly discovered fast X-ray outbursts are listed in table 5.1 together with the only detection of IGR J16479–4514 already reported in the literature (No. 4 in table 5.1).

Outburst No. 1 in table 5.1 is particularly interesting, being by far the brightest one to be detected, to date. Its ISGRI light curve (20–30 keV) is shown in figure 5.1. Initially the source flux was consistent with zero, then suddenly IGR J16479–4514 turned on at 13:36:37 UTC 5 March 2003. It flared up reaching in only ~ 5 minutes a peak flux of ~ 850 mCrab or ~ 3.8×10^{-9} erg cm^{-2} s^{-1} (20–30 keV). Then it dropped to a very low flux level in ~ 25 minutes and it continued to be characterized by a very low flux showing some secondary very small peaks. At 16:58:30 UTC the source completely turned off. Being located in the direction of the Norma region, an active star formation region, we can assume a distance for IGR J16479–4514 of ~ 6 kpc. This implies a 20–30 keV luminosity of ~ 1.6×10^{37} erg s^{-1}. Figure 5.2 shows an expanded view of the flare in

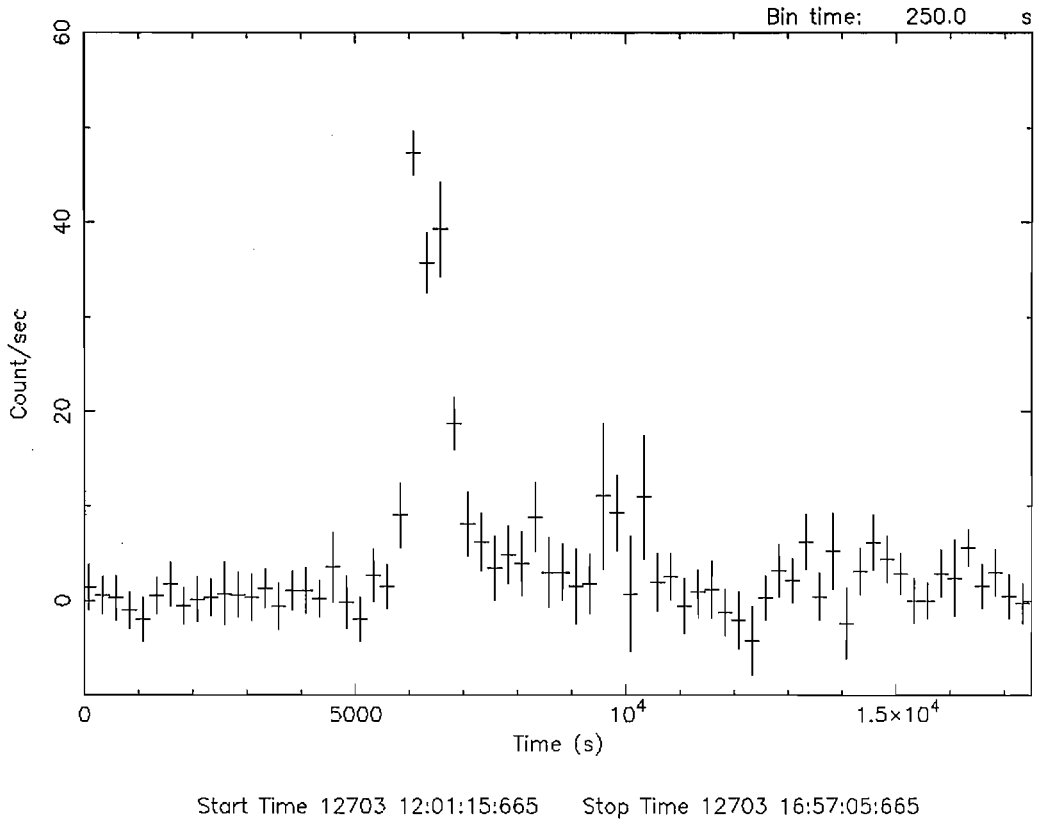

Figure 5.1: The ISGRI light curve (20–30 keV) of a newly discovered outburst (No. 1 in table 5.1) of IGR J16479–4514.

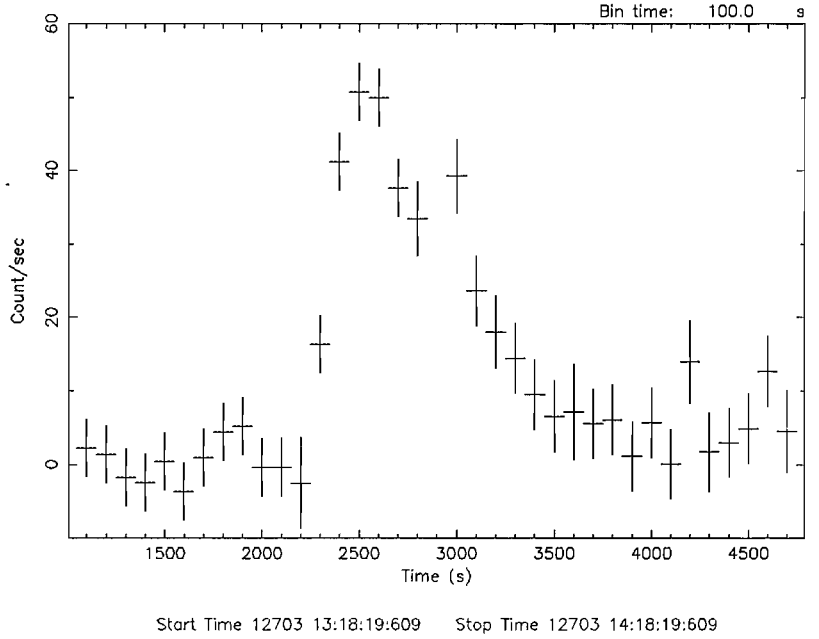

Figure 5.2: Expanded view of the light curve (20–30 keV) of the outburst from IGR J16479–4514 showed in figure 5.1

figure 5.1, binned in 100 s periods, compared to the 250 s used in figure 5.1. There is evidently a very fast rise of the flare followed by a slower kind of exponential decay. An exponential function $F=F(0)e^{-t/\tau}$ was fit to the observed flux count rate during the decay. This gave a χ^2_ν=0.8 for 15 d.o.f. and τ=15±9 minutes, so it is reasonable to assert an exponential behavior for the decay of the outburst.

It can be noted in figure 5.2 that, at first glance, the temporal behavior of outburst No. 1 (very rapid rise lasting ~ 5 minutes followed by a slower exponential decay lasting ~ 25 minutes) seems to recall a thermonuclear type I X-ray burst. About 40% of the LMXBs in our galaxy show type I X-ray bursts, which are explained as energy release by rapid nuclear fusion of material on the surface of a neutron star. Thus a type I X-ray burst is thought to identify the source emitting it unambiguously as a LMXB containing a neutron star. Normally they are characterized by rise times lasting from less than a second to ~ 10 s, followed by a slower exponential decay lasting from 10 s to minutes. During the decline they also show cooling of the characteristic temperature of the X-ray spectrum which is attributed to cooling of the neutron star surface. Some rare longer type I X-ray bursts have been detected in few other LMXBs. In order of decreasing duration, some examples are: 4U1708-23, ≃25 min (Hoffman et al. 1978, Lewin et al. 1984); 4U1724-307, ≥10 min (Swank et al. 1977); 3A1715-321, ≥4.5 min (Tawara et al. 1984). Typical type I X-ray outburst spectra are well described by a black body emission with temperature of ~2–3 keV. The temperature increases during the outburst rise (reflecting the heating of the neutron star surface) and decreases during the decay (due to subsequent cooling). A detailed spectral analysis of outburst No. 1 was performed to confirm or exclude an eventual type I X-ray burst origin. To this aim, a spectrum was extracted during the rise as well as during the exponential decay. This approach is necessary to find evidence of an eventual cooling of the characteristic temperature of the X-ray spectrum, which would be a clear signature of a type I X-ray burst. As for the 20–60 keV spectrum extracted during the rise, the best fit is a black body (χ^2_ν=1.6, d.o.f. 14) with kT= 6.8±0.6 keV. Other spectral models, such as thermal bremsstrahlung or Comptonization models, provided instead very poor fits with a χ^2_ν greater than 1.9. The 20–60 keV spectrum extracted during the exponential decay can be fit by a black body (χ^2_ν=1.5, d.o.f. 14) with kT= 6.4±0.3 keV (see figure 5.3). Firstly, we can note that the temperatures of the black body emission during the rise and the exponential decay are comparable within the errors of the measurements. The statistics are not good enough to find evidence of a possible cooling. However, the black body spectrum is characterized by a temperature higher than that typical of type I X-ray bursts (~2–3 keV). In the light of the findings reported above, a type I X-ray burst origin for the outburst No. 1 should be excluded.

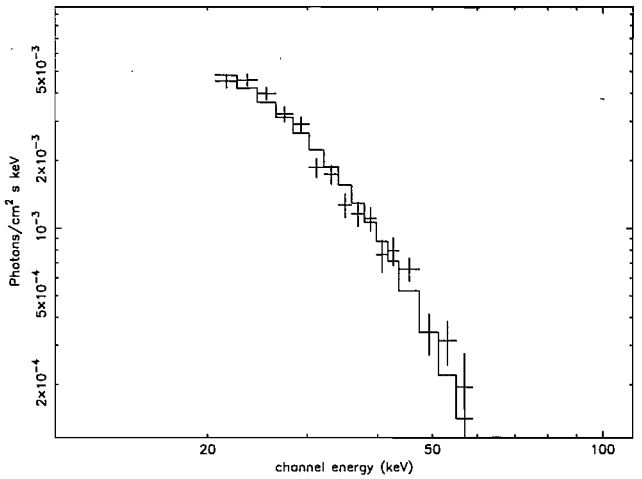

Figure 5.3: Unfolded black body spectrum (20–60 keV) of IGR J16479–4514 during the decay of outburst No.1 in table 5.1

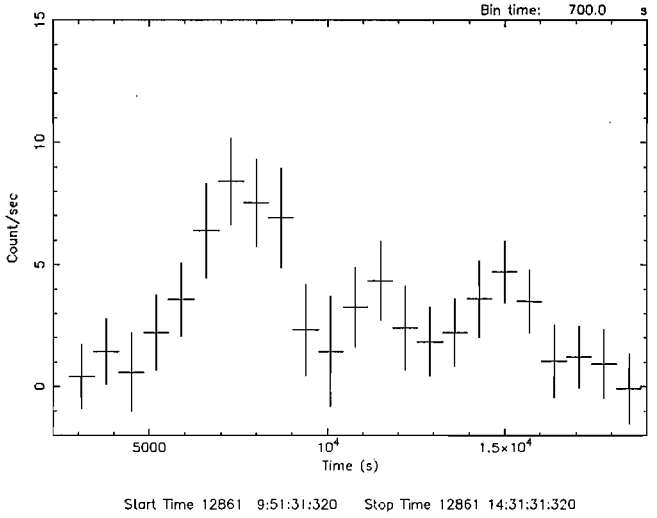

Figure 5.4: The ISGRI light curve (20–30 keV) of the detection of IGR J16479–4514 on 10 August 2003 (No.4 in table 5.1).

Outbursts No. 2 and No. 3 in table 5.1 were detected in only a few ScWs (3 and 1, respectively). Their average flux during the outburst activity was ~ 40 mCrab (20–30 keV) and ~ 160 mCrab (20–30 keV), respectively.

The outburst No. 4 was reported by Molkov et al. (2003a) as an average detection when the source was discovered by INTEGRAL, hence the fast X-ray transient nature of the source was not unveiled. Performing an analysis at the ScW level, here the ISGRI light curve on 10 August 2003 is reported for the first time. The fast X-ray transient behaviour is clearly evident (see figure 5.4). The duration of the outburst was ~ 3.5 hours with a 20–30 keV peak flux of ~ 150 mCrab.

On 14 August 2003 at ~ 00:20 UTC, IGR J16479–4514 turned on again (outburst No. 5 in table 5.1). It remained in the IBIS FOV during 3 consecutive ScWs and then it went outside of it. Because of this it was not possible to constrain a duration for the outburst activity. The average flux was ~ 44 mCrab (20–30 keV).

Figure 5.5 shows the 20–80 keV ISGRI light curve of outburst No. 6. The source turned on at ~ 06:30 UTC on 11 August 2004 and it turned off ~ 11 hours later. The outburst activity was mainly characterized by 3 very fast flares, the maximum peak flux was ~ 140 mCrab (20–80 keV).

The ISGRI light curve of outburst No. 7 is shown in figure 5.6. We can note that the source suddenly underwent flaring activity on 7 September 2004 at ~ 01:50 UTC. The duration was no longer than ~ 2 hours, the peak flux was ~ 80 mCrab (20–60 keV).

The outburst No. 8 is shown in figure 5.7, it was detected ~ 9 days later than No. 7 and it is characterized by one single strong flare with similar timescales during the rise and the decay. The duration and peak flux are ~ 2.5 hours and ~ 120 mCrab (20–60 keV), respectively. An ISGRI spectrum extracted during this outburst is equally well fit (20–60 keV) by a black body model (kT=7.4±0.5 keV, χ^2_ν=0.95, d.o.f. 14) or by a single power law (Γ=2.6±0.2, χ^2_ν=1.06, d.o.f. 14).

The outburst No. 9 occurred on 4 April 2005 and it is shown in figure 5.8. The duration and peak flux are ~ 2.5 hours and ~ 60 mCrab (20–60 keV), respectively.

The outburst No. 10 (see figure 5.9) was detected on 12 August 2005 starting at ~ 18:40 UTC. At the beginning the outburst activity (20–60 keV) is characterized by two very fast flares lasting no longer than few tens of minutes and reaching a maximum peak flux of ~ 120 mCrab. Towards the end of the light curve, the source was still on although it did not show any fast strong flare. Unfortunately the light curve is truncated at the end because the source went outside the IBIS FOV so the total duration of the outburst activity can not be constrained.

Finally, figure 5.10 shows the 20–60 keV ISGRI light curve of outburst No. 11 in table 5.1. It was detected on 30 August 2005 in only one ScW which started at 03:54:36 UTC and finished at 04:24:36. We note that the source was characterized by a fast flare with timescale of few tens of minutes. It reached a maximum peak flux of ~ 240 mCrab (20–60 keV). A spectrum extracted during the outburst is best fit by a single power law (χ^2_ν=0.72, d.o.f. 14) with Γ=2.4±0.4. However an equally good fit is also provided by a black body (χ^2_ν=0.68, d.o.f. 14) with kT=8±1 keV (see figure 5.11). It is worth pointing out that during this outburst the source was in the fully coded field of view of the JEM–X telescope but the source was not significantly detected in any of the following energy band:3–6, 6–10, 10–15 and 15–34 keV.

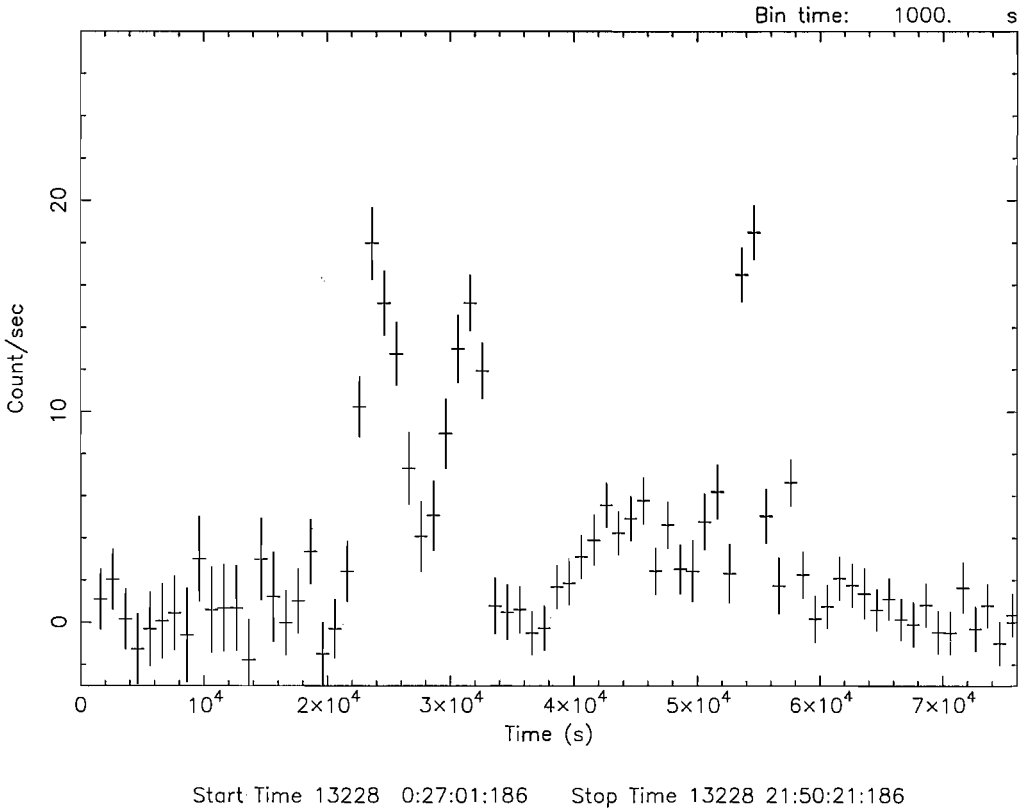

Figure 5.5: The ISGRI light curve (20–30 keV) of the detection of IGR J16479–4514 on 11 August 2004 (No.6 in table 5.1).

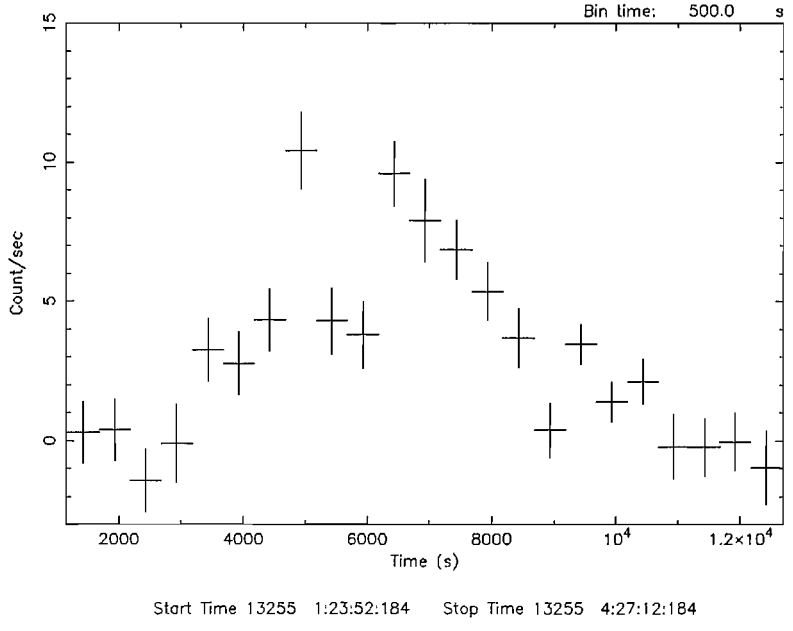

Figure 5.6: The ISGRI light curve (20–40 keV) of the detection of IGR J16479–4514 on 7 September 2004 (No.7 in table 5.1).

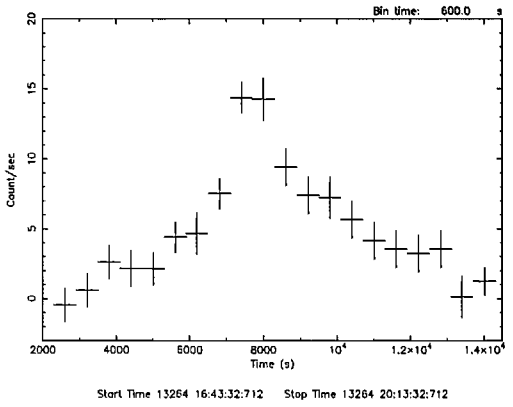

Figure 5.7: The ISGRI light curve (20–60 keV) of outburst No. 8 (in table 5.1) of IGR J16479–4514.

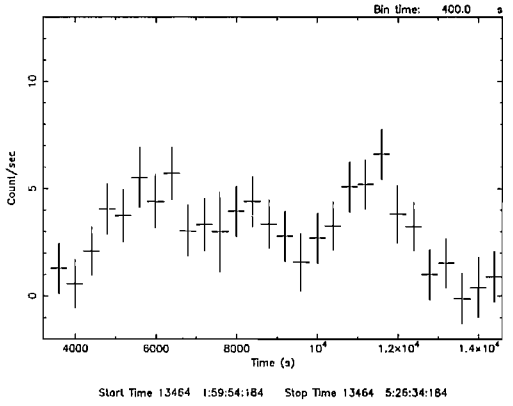

Figure 5.8: The ISGRI light curve (20–60 keV) of outburst No. 9 (in table 5.1) of IGR J16479–4514.

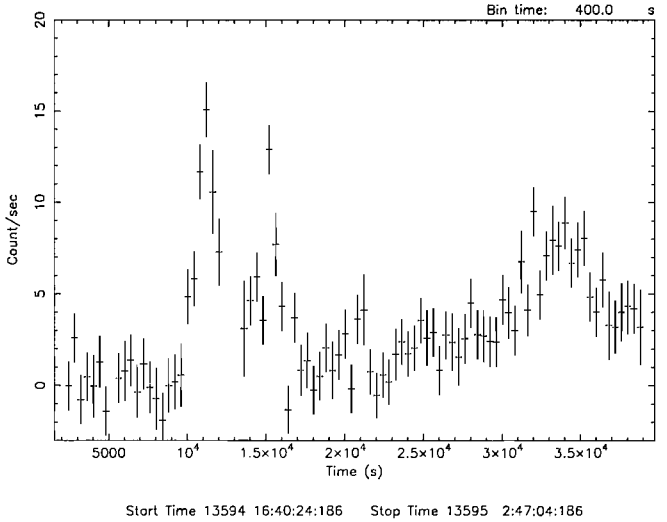

Figure 5.9: The ISGRI light curve (20–60 keV) of the detection of IGR J16479–4514 on 12 August 2005 (No.10 in table 5.1).

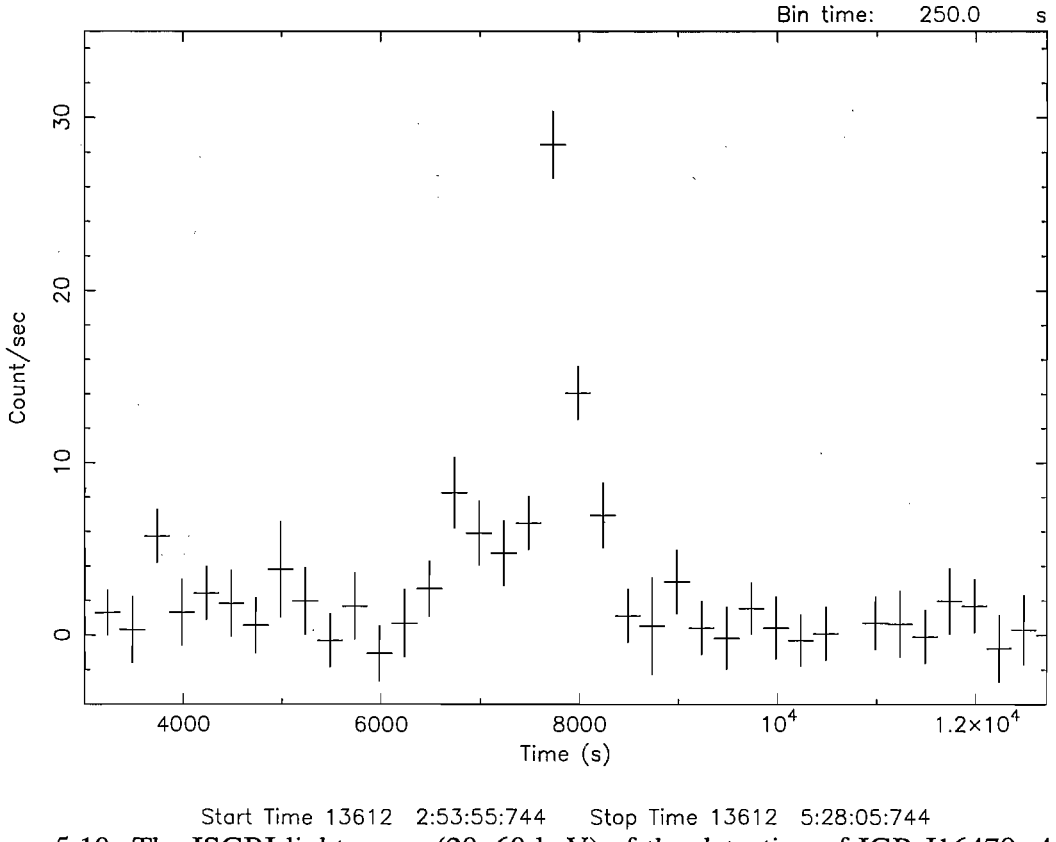

Figure 5.10: The ISGRI light curve (20–60 keV) of the detection of IGR J16479–4514 on 30 August 2005 (No.11 in table 5.1).

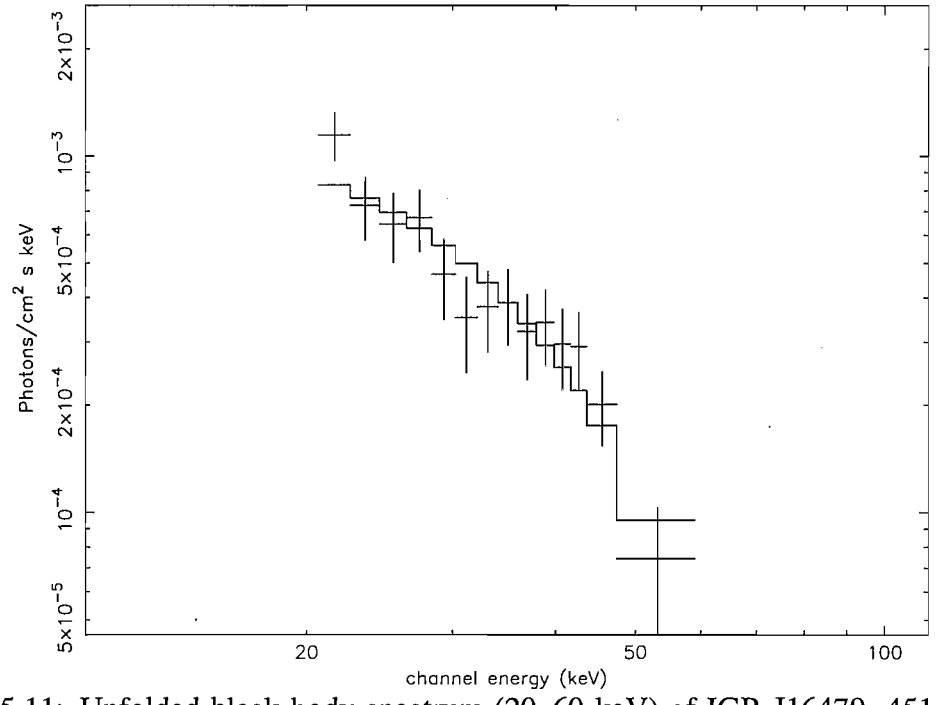

Figure 5.11: Unfolded black body spectrum (20–60 keV) of IGR J16479–4514 during the outburst No. 11 in table 5.1.

Table 5.2: USNO–B1.0 optical sources located inside the ROSAT error circle of IGR J17407–2808.

No. USNO–B1.0	RA (J2000)	DEC (J2000)	B1	R1	B2	R2	I
1	17 40 40.84	-28 08 52.7		17.41	18.54	17.19	14.52
2	17 40 41.12	-28 08 53.0		16.90			17.28
3	17 40 41.16	-28 08 56.1	19.97	17.78			25.24
4	17 40 41.40	-28 09 00.6	14.90	13.79	15.71	14.04	12.42
5	17 40 42.05	-28 08 40.2	15.74	14.22	17.58	14.96	12.79

5.2.2 IGR J17407–2808

5.2.2.1 Archival X-ray observations of the source

IGR J17407–2808 was discovered on 9 October 2004 (Kretschmar et al. 2004b) as it was undergoing strong X-ray outburst activity characterized by several flares detected in the 20–60 keV band. The nominal position is (J2000) RA=17^h 40^m 42^s Dec=-28° 08′ 00″ with an error circle of 2′.3 radius. The most energetic flare was strong enough to trigger an automatic alert message of the INTEGRAL Burst Alert System IBAS (Gotz et al. 2004) but the position consistency with the X-ray source SBM2001 10 (50″ angular separation between them) and soft spectrum excluded a gamma-ray burst origin for IGR J17407–2808. SBM2001 10 is a faint unidentified X-ray source listed in the ROSAT catalog of sources in the galactic center region (Sidoli et al. 2001) with a position of (J2000) RA=17^h 40^m 41.2^s Dec=-28° 08′ 50″ (error circle of 16″ radius). The ROSAT count rate is equal to 3.73±1.2 cts $ksec^{-1}$ (0.1–2.4 keV).

An investigation of the RXTE All Sky Monitor (ASM) data archive provided a light curve (2–12 keV) of IGR J17407–2808 from 1996 to 2006, which is shown in figure 5.12. It can be noted that outbursts from IGR J17407–2808 are rare but not unusual. There are at least 7 outbursts (labelled with numbers in figure 5.12) having a peak flux greater than ~ 250 mCrab (2–12 keV).

As stated before, the ROSAT error circle of IGR J17407–2808 has a radius of 16″, which is not sufficiently small so as to find an optical/infrared counterpart using archival catalogs. From an investigation with the HEASARC database, there are too many 2MASS infrared sources (13 in total) located inside the ROSAT error box. As for the optical waveband, there are 5 stars catalogued in the USNO–B1.0 catalog. Their equatorial coordinates are listed in table 5.2 together with their magnitudes. A much smaller error circle is strongly needed in order to pinpoint the optical/infrared counterpart of IGR J17407–2808.

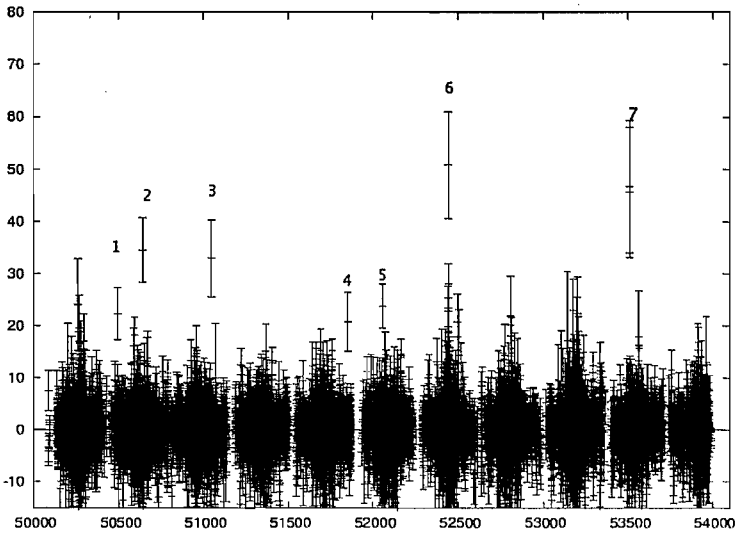

Figure 5.12: RXTE ASM dwell by dwell light curve (2–12 keV) of IGR J17407–2808 from 1996 to 2006. In the light curve 20 c s^{-1} is equivalent to a flux of 250 mCrab. Time axis is in MJD. The seven outbursts detected by RXTE, with a flux greater than 250 mCrab, are indicated in the light curve by means of numbers from 1 to 7.

Table 5.3: Summary of ISGRI observations of outbursts of IGR J17407–2808.

No.	Date	duration (hours)	energy band (keV)	peak-flux (mCrab)	ref (discovery)
1	20 Mar 2003	~ 0.5	20–30	~ 140	[1]
2	9 Oct 2004	~ 3 minutes	20–60	~ 805	[1], [2]

[1] This PhD thesis; [2] Kretschmar et al. (2004)

5.2.2.2 Analysis of newly discovered outbursts by INTEGRAL

Table 5.3 reports a list of all outbursts of IGR J17407–2808 detected by INTEGRAL, to date. Outburst No. 1 is a newly discovered one. On the contrary, outburst No. 2 was already reported in the literature when the source was discovered, however it has never been studied in detail. Here its ISGRI light curve and spectral analysis is reported for the first time.

Outburst No. 1 was detected on 20 March 2003 in only 1 ScW, the duration was ~ 30 minutes. The 20–30 keV ISGRI light curve is shown in figure 5.13. The flaring activity is evident, being characterized by a fast rise (~ 6 minutes) followed by a slower decay (~ 25 minutes), the peak flux is ~ 140 mCrab (20–30 keV). A spectrum extracted during this flare is best fit by a black body (χ^2_ν=1.26, d.o.f. 8) with kT=$4.8^{+1.5}_{-1}$ keV (see figure 5.14). However, an equally good fit is also obtained using a thermal bremsstrahlung model (χ^2_ν=1.3, d.o.f. 8) with kT=$11.5^{+13.7}_{-4.5}$ keV.

Figure 5.15 shows the 20–60 keV ISGRI light curve (bin time of 25 seconds) of outburst No. 2. Three prominent very fast flares, lasting no more than a few minutes, are clearly visible. In particular the last flare is very strong, it reached a peak-flux of ~ 805 mCrab or 9.5×10^{-9} erg cm^{-2} s^{-1} (20–60 keV), its duration was ~ 1 minute. A significance image as well as a spectrum of IGR J17407−2808 have been extracted during this fast and strong flare lasting only ~ 1 minute. Figure 5.16 shows the 20–60 keV ISGRI significance image (69 seconds exposure time), IGR J17407−2808 is clearly detected at a level of ~ 15σ. As for the spectrum (20–60 keV), it is best fit by a thermal bremsstrahlung model (χ^2_ν=0.78, d.o.f. 14) with kT=$23^{+7}_{-4.5}$ keV (see figure 5.17). However a black body model also gave a reasonable fit (kT=7±0.7 keV, χ^2_ν=1.3, d.o.f. 14). The ISGRI analysis of this flare provided a source position (J2000, RA=17^h 40^m 40.08^s Dec=-28° 08′ 24″, error radius of 1′.7) which is located 30″ from the ROSAT source SBM2001 10.

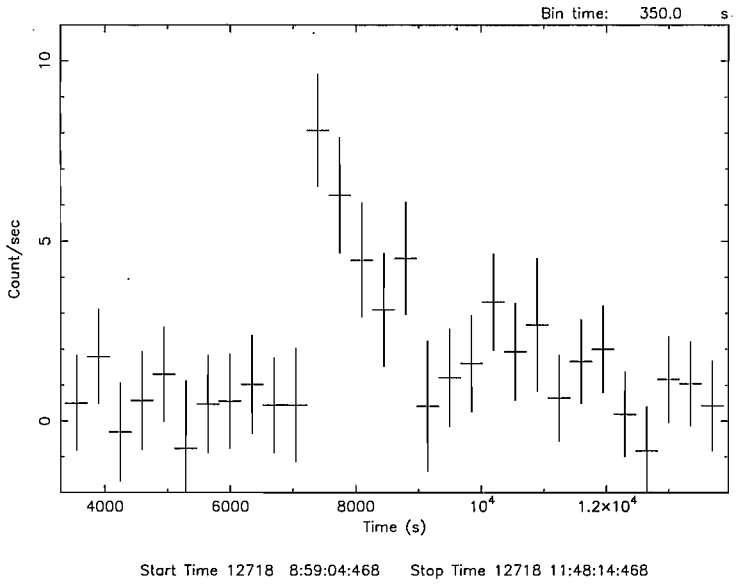

Figure 5.13: The ISGRI light curve (20–30 keV) of the detection of IGR J17407−2808 on 20 march 2003 (No.1 in table 5.3).

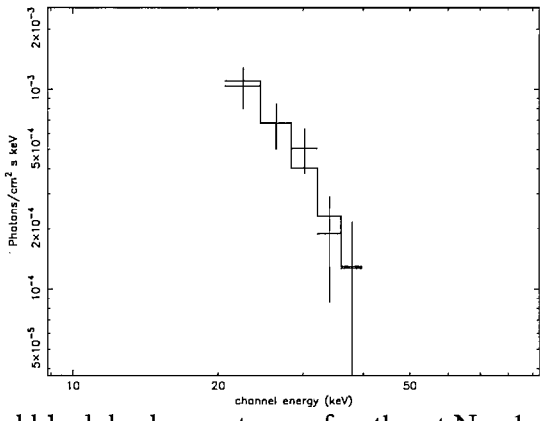

Figure 5.14: Unfolded black body spectrum of outburst No. 1 of IGR J17407−2808

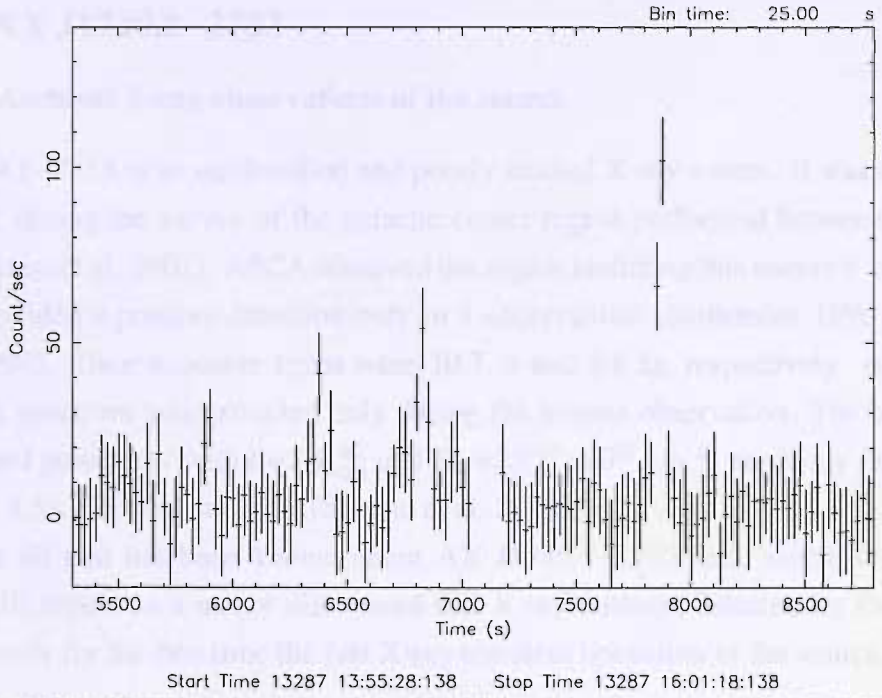

Figure 5.15: The ISGRI light curve (20–60 keV) of the detection of IGR J17407–2808 on 9 October 2004 (outburst No.2 in table 5.3).

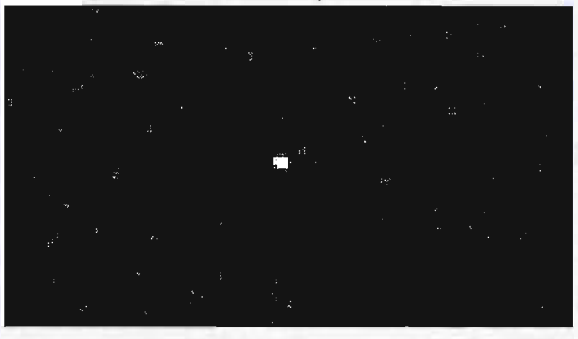

Figure 5.16: ISGRI 20–60 keV significance image extracted during the strongest flare in figure 5.15 (69 seconds exposure time). IGR J17407–2808 is clearly detected at a level of $\sim 15\ \sigma$.

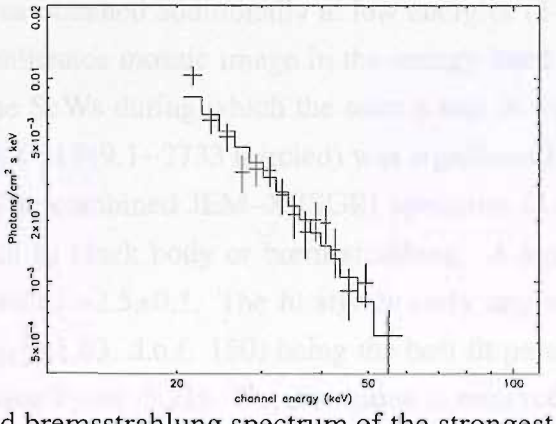

Figure 5.17: Unfolded bremsstrahlung spectrum of the strongest flare in figure 5.15.

5.2.3 AX J1749.1–2733

5.2.3.1 Archival X-ray observations of the source

AX J1749.1–2733 is an unidentified and poorly studied X-ray source. It was discovered by ASCA during the survey of the galactic center region performed between 1993 and 1999 (Sakano et al. 2002). ASCA observed the region including this source 6 times, however it provided a positive detection only in 3 observations (September 1996 and 1997, March 1998). Their exposure times were 10.7, 6 and 8.8 ks, respectively. A meaningful ASCA spectrum was extracted only during the longest observation. The best fit was an absorbed power law with $\Gamma=2.1^{+4.7}_{-2.6}$ and $N_H=25^{+57}_{-21}\times10^{22}$ cm^{-2}, the X-ray flux (0.7–10 keV) was 1.5×10^{-12} erg cm^{-2} s^{-1} (Sakano et al. 2002).

This is all that has been known about AX J1749.1–2733 until recently. The next section will report on a newly discovered fast X-ray outburst detected by INTEGRAL which unveils for the first time the fast X-ray transient behaviour of the source.

5.2.3.2 Analysis of a newly discovered outburst by INTEGRAL

Figure 5.18 shows the 20–60 keV ISGRI light curve of the newly discovered fast X-ray outburst from AX J1749.1–2733 detected by INTEGRAL. Each data point in the light curve represents the average flux during one ScW (~2000 seconds). As we can clearly note, at the beginning the source is not detected. Then suddenly, on 9 September 2003 ~ 07:40 UTC, it turned on undergoing a fast flare (duration ~ 1.3 days) after which it turned off again. Figure 5.19 shows an expanded and more detailed view of the flaring activity, plotted with a bin period of 800 s, compared to the 2000 s used in figure 5.18. The maximum peak flux was ~ 65 mCrab (20–60 keV).

During part of its outburst activity, AX J1749.1–2733 was in the JEM–X FOV so spectral information was obtained additionally at low energies (3–20 keV). Figure 5.20 shows the JEM–X significance mosaic image in the energy band 10–20 keV, it was obtained mosaicing all the ScWs during which the source was in the JEM–X FOV during the outburst activity. AX J1749.1–2733 (circled) was significantly detected at a level of ~ 40σ (10–20 keV). The combined JEM–X/ISGRI spectrum (3–80 keV) cannot be fit by thermal models such as black body or bremsstrahlung. A single power law gives a χ^2_ν=1.22 (d.o.f. 151) with $\Gamma=2.5\pm0.1$. The fit significantly improves adding an absorption to the power law (χ^2_ν=1.03, d.o.f. 150) being the best fit parameters $\Gamma=2.7\pm0.1$ and $N_H=21^{+11}_{-8}\times10^{22}$ cm^{-2} (see figure 5.21). The absorption is required by the data at 99.99% confidence level using the F-test, it exceeds the galactic absorption along the line of sight which is $N_H=1.6\times10^{22}$ cm^{-2}. This suggests that most of the low energy absorption is

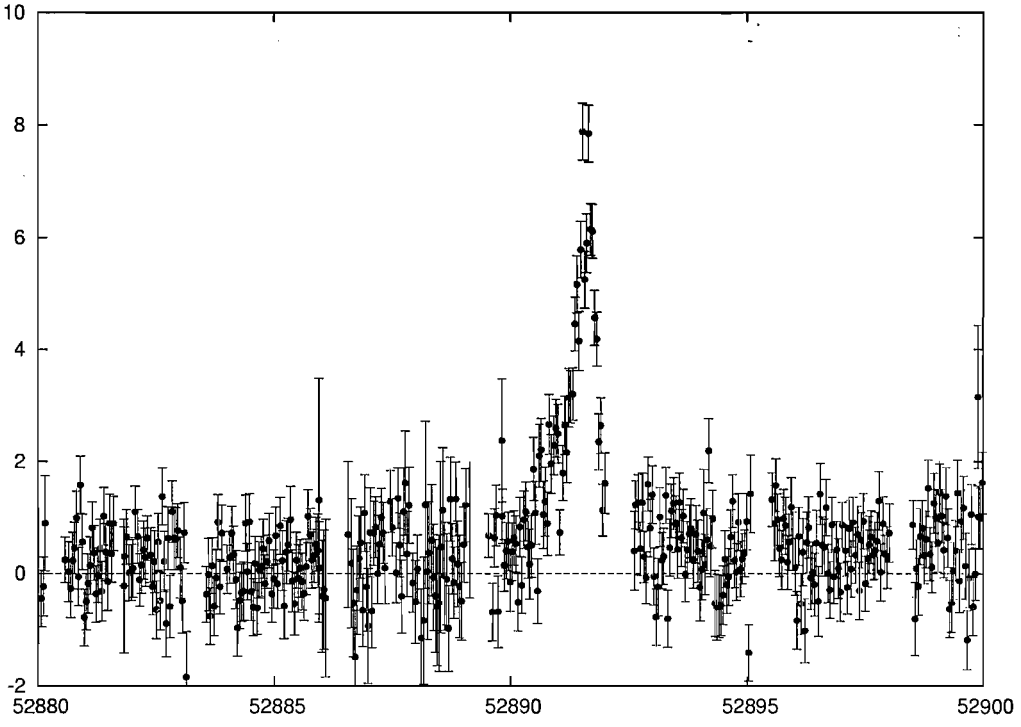

Figure 5.18: ISGRI light curve (20–60 keV) of AX J1749.1−2733 during the newly discovered outburst occurred on 9 September 2003. Time axis is on MJD. Each data point represents the average flux during one ScW (~2000 seconds).

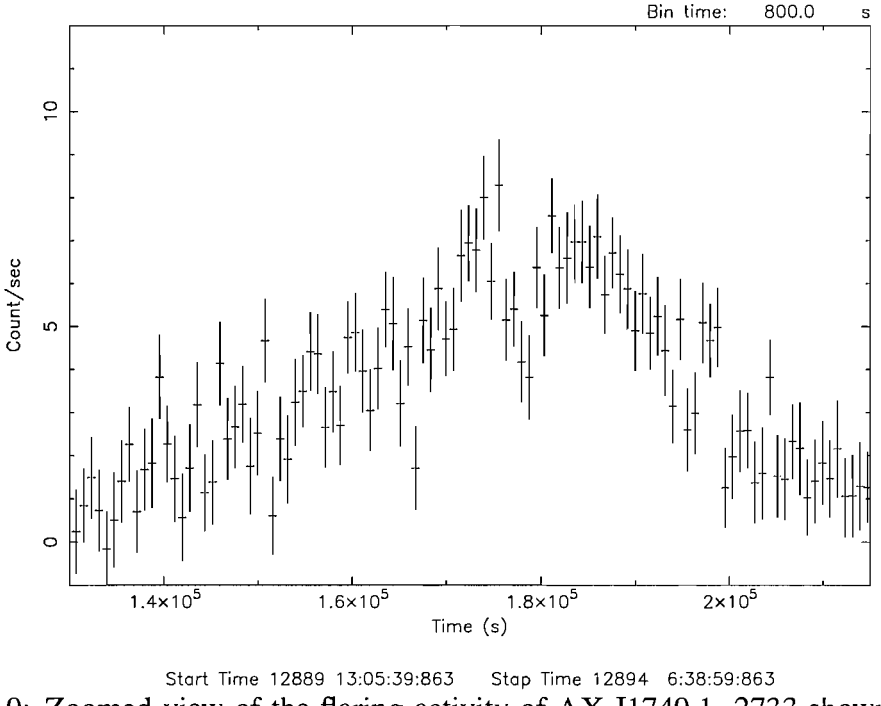

Figure 5.19: Zoomed view of the flaring activity of AX J1749.1−2733 shown in figure 5.18. Note that the bin time is smaller than that in figure 5.18.

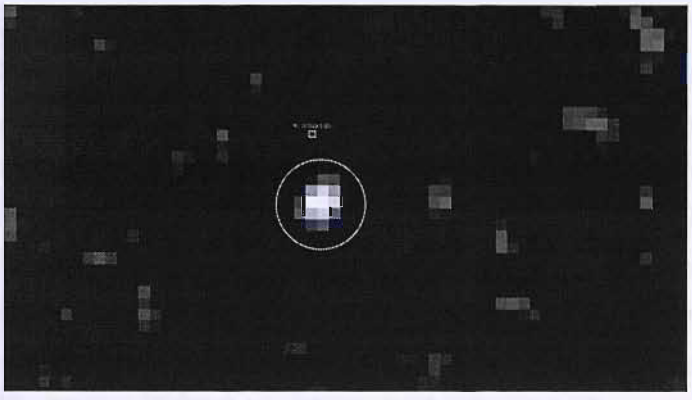

Figure 5.20: JEM–X significance mosaic map in the energy band 10–20 keV. AX J1749.1–2733 is circled in the map, detected at $\sim 40\sigma$ level.

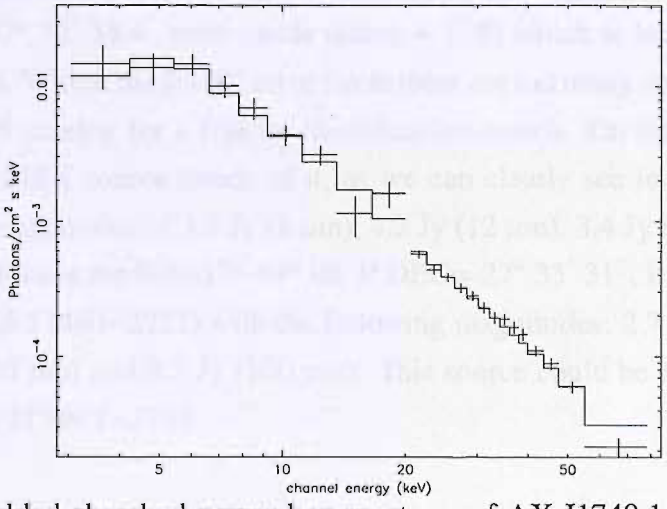

Figure 5.21: Unfolded absorbed power law spectrum of AX J1749.1–2733 (3–80 keV) during the outburst occurred on 9 September 2003.

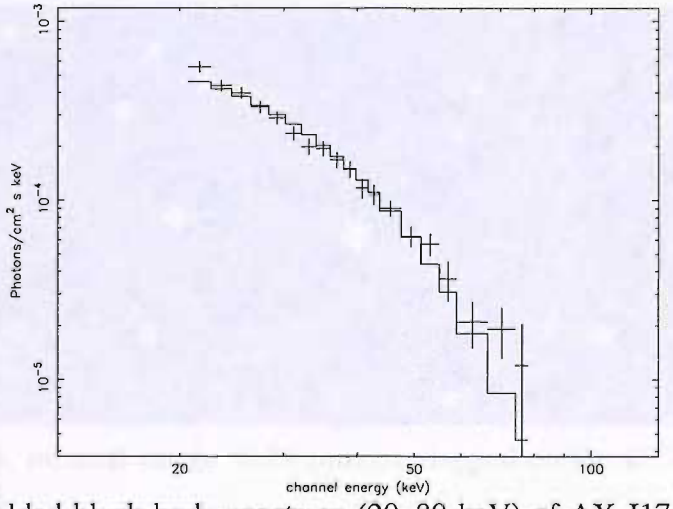

Figure 5.22: Unfolded black body spectrum (20–80 keV) of AX J1749.1–2733 during the outburst that occurred on 9 September 2003.

intrinsic to the source, moreover its high value could explain why the source has not been detected by JEM–X in the softer band 4–10 keV. To account for a cross-calibration mismatch between the two instruments, a constant has been introduced in the fit, which when left free to vary provides a value of 1.1±0.2. It is worth pointing out that an equally good fit to the broad band spectrum is also achieved using a cut off power law model (χ^2_ν=0.98, d.o.f. 150) with Γ=1.5±0.3 and cut off energy equal to 30^{+12}_{-7}. In this case the absorption is not required by the data. As for the 20–80 keV ISGRI spectrum, it can be fit by thermal models such as black body (χ^2_ν=1.16, d.o.f.19, kT=7.7±0.3) or bremsstrahlung (χ^2_ν=0.4, d.o.f.19, kT=$28^{+3.5}_{-3}$). Figure 5.22 shows the unfolded black body spectrum.

The analysis of this outburst provided an ISGRI position of AX J1749.1–2733 (RA=17^h 49^m 07.2^s Dec=-27° 32′ 38.4″ error circle radius ~ 1′.8) which is located 42″ from the ASCA coordinates. Within the ISGRI error circle there are too many optical sources listed in the USNO–B1.0 catalog for a fruitful identification search. On the contrary, there is only one infrared MSX source inside of it, as we can clearly see in figure 5.23. It is very bright, with magnitudes of 3.2 Jy (8 μm), 4.2 Jy (12 μm), 3.4 Jy (15 μm) and 3.6 Jy (21 μm). Its coordinates are RA=17^h 49^m 08.3^s DEC=-27° 33′ 31″, it is also an infrared IRAS object (IRAS 17460–2732) with the following magnitudes: 2.7 Jy (12 μm), 2.5 Jy (25 μm), 3.8 Jy (60 μm) and 4.3 Jy (100 μm). This source could be a potential infrared counterpart of AX J1749.1–2733.

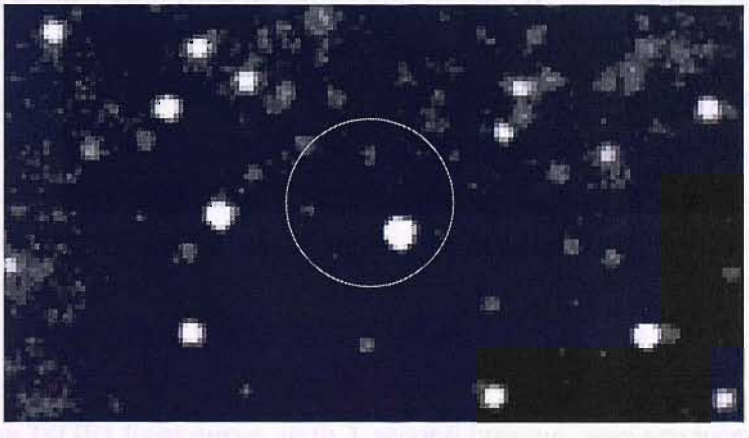

Figure 5.23: MSX infrared image (8.28 μm) overlapped on the ISGRI error circle of AX J1749.1–2733

5.2.4 IGR J11321−5311

5.2.4.1 Archival X-ray observations of the source

The hard X-ray transient IGR J11321−5311 was discovered by INTEGRAL during deep observations of the Crux spiral Arm on June 2005 (Krivonos et al. 2005). It was active for a few hours with average fluxes of ~ 30 mCrab (17–60 keV) and ~ 90 mCrab (60–200 keV). Subsequently, the flux diminished below ~ 3 mCrab (17–60 keV). To date, INTEGRAL is the only satellite which detected IGR J11321−5311, once and never again. All that has been known about this source until recently is listed above, only its discovery has been reported in the literature and no detailed study has never been performed. The next section provides, for the first time, a detailed timing and spectral analysis of the source.

5.2.4.2 Analysis of the outburst detected by INTEGRAL

IGR J11321−5311 was clearly detected by INTEGRAL in 4 consecutive ScWs in the energy range 20–300 keV. Figure 5.24 shows their significance map sequence. The source was not detected in the first ScW, then it was detected during the next 4 ScWs with a significance, from left to right, equal to 12σ, 8σ, 5σ and 4σ, respectively. Finally, in the last ScW the source turned off. Summing the 4 ScWs in a mosaic, IGR J11321−5311 is detected at ~ 18σ level in the energy band 20–300 keV and ~ 8σ level in 100–300 keV. Figure 5.25 shows the 20–300 keV light curve. We assume the beginning of the first ScW during which the source was significantly detected as being the start time of the outburst and similarly the burst stop time to be the end of the last ScW during which the source was significantly detected. As we can note from the light curve, initially the source is not detected. Then it turned on at 21:59:49 UTC (27 June 2005) reaching in only ~ 1 hour a peak flux of ~ 77 mCrab or ~ 2.1×10^{-9} erg cm^{-2} s^{-1} (20–300 keV). Subsequently, the flux gradually decreased and then the source turned off on 28 June 2005 at 01:22:33 UTC. The duration of the total outburst activity was ~ 3.5 hours, whereas the flare lasted ~ 1.5 hours. Figure 5.26 shows the light curve in two different energy bands (20–100 keV and 100–300 keV) and their ratio, which suggests a possible spectral evolution of the source during the outburst.

A fine timing ISGRI light curve, with 1 second binning, was produced in the 20–100 keV band using the OSA ii-light tool. Then, it was searched for evidence of any pulsations in the 1–1000 second range using the Lomb-Scargle periodogram method; no clear signal was detected. Using a Monte-Carlo approach, it was possible to assess the data quality of the fine timing light curve and our sensitivity to periodic signals. Simulated light curves

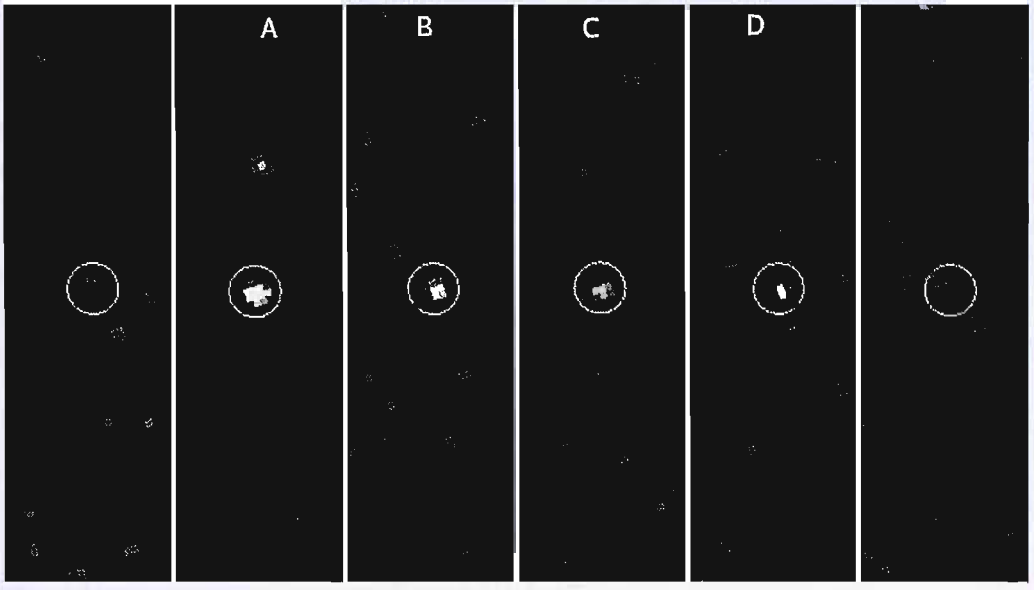

Figure 5.24: ISGRI ScW significance image sequence (20–300 keV) of the outburst from IGR J11321−5311 (encircled). The source was not detected in the first ScW, then it was detected during the next 4 ScWs with a significance, from left to right, equal to 12σ, 8σ, 5σ and 4σ, respectively. Finally in the last ScW there is no detection.

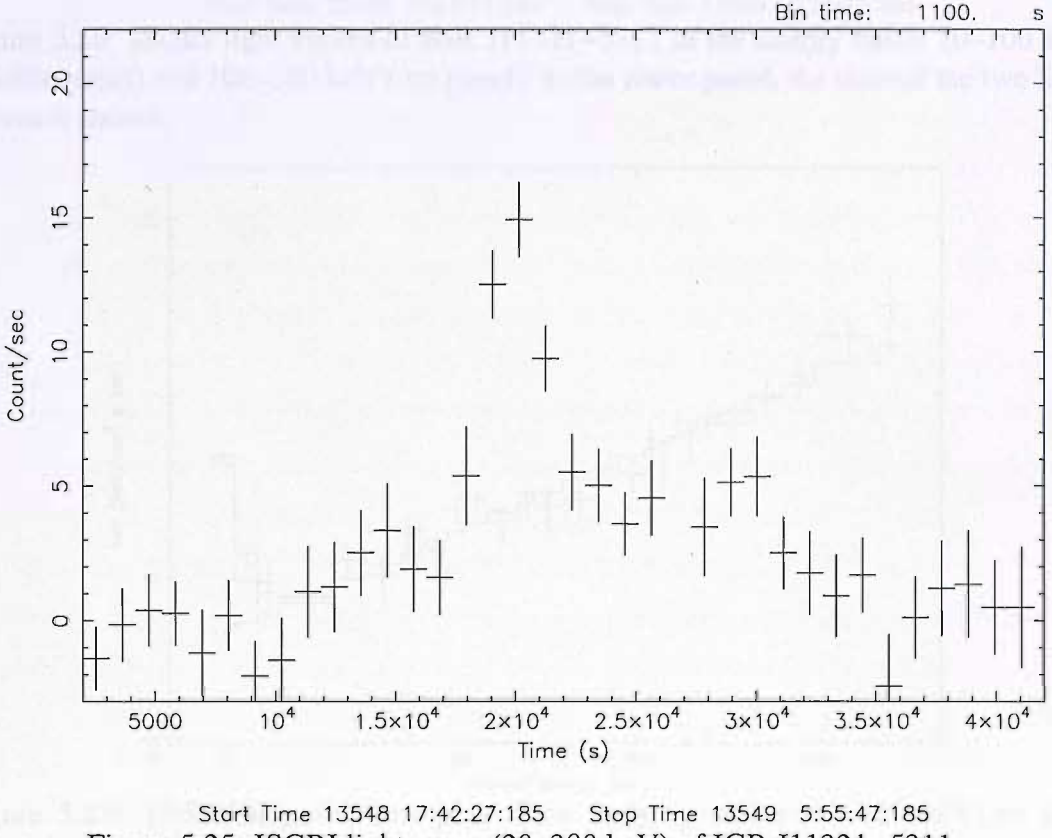

Figure 5.25: ISGRI light curve (20–300 keV) of IGR J11321−5311.

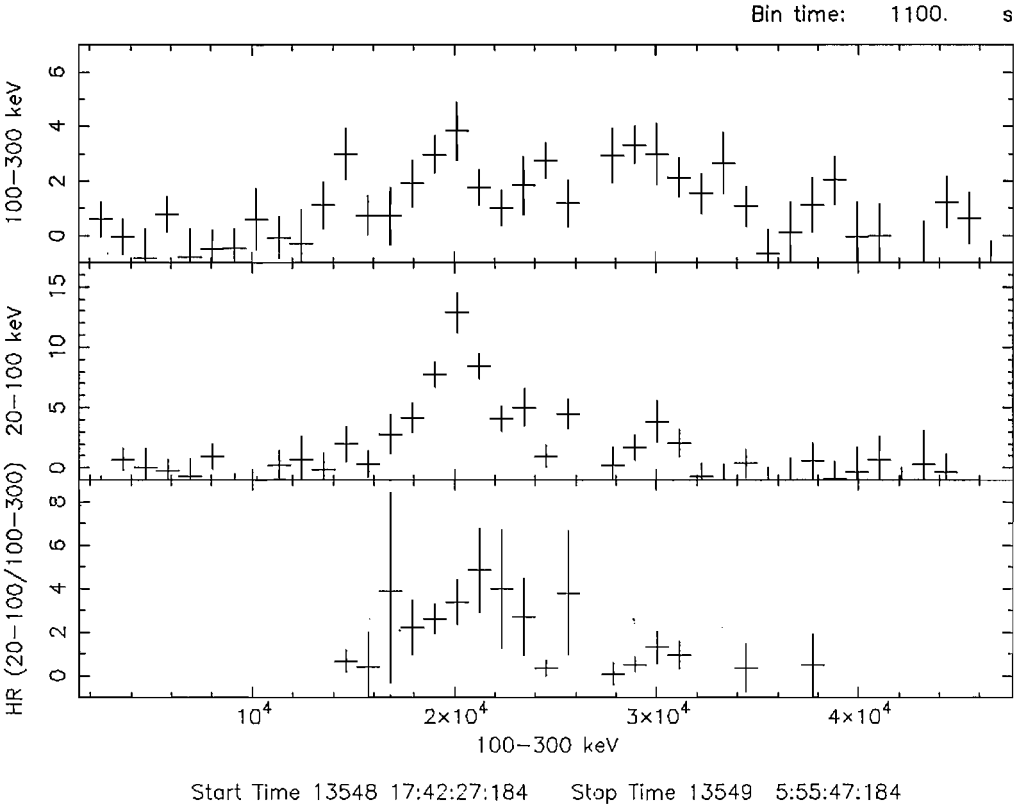

Figure 5.26: ISGRI light curves of IGR J11321−5311 in the energy bands 20–100 keV (middle panel) and 100–300 keV (top panel). In the lower panel, the ratio of the two light curves is shown.

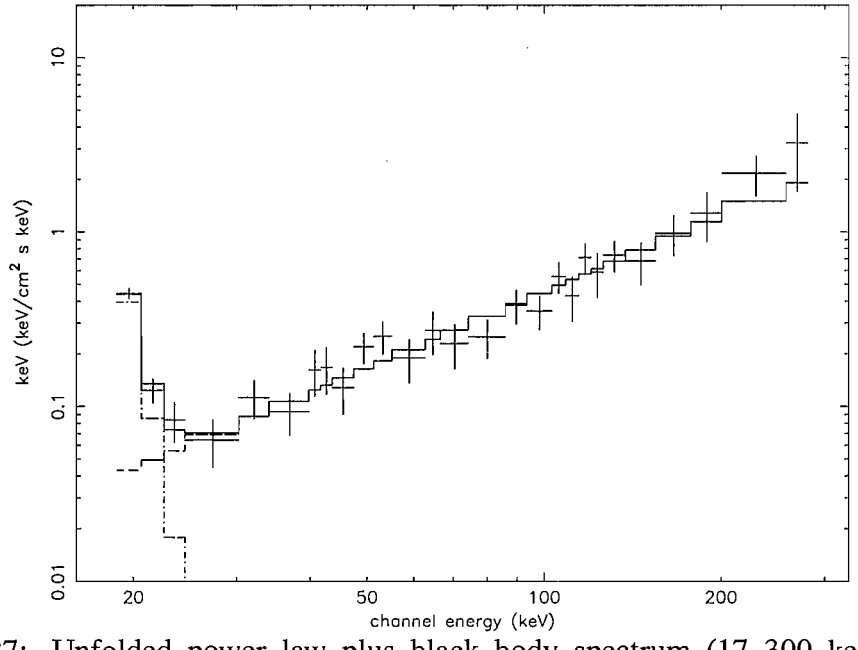

Figure 5.27: Unfolded power law plus black body spectrum (17–300 keV) of IGR J11321−5311 extracted during its total outburst activity.

were generated which had the same sampling and statistical properties of the data but which had a sinusoidal modulation of ~10 seconds introduced. The results of the Monte-Carlo simulations found that to detect 100% pulsed emission a signal strength ~3 times stronger than that of the data was required; 50% pulsed emission required a signal ~9 times stronger. The implication of the Monte-Carlo results is that the statistical quality of the ISGRI data is insufficient to detect pulsations.

The spectrum extracted from the sum of the four ScWs (A,B,C and D in figure 5.24) during which the source was detected is best fit (17–300 keV) by a power law plus a black body model (χ^2_ν=0.8, d.o.f.46) with Γ=0.55±0.18 and kT=$1^{+0.2}_{-0.3}$ keV. Other spectral models, such as black body or bremsstrahlung, do not provide a good fit to the data. The unfolded spectrum is displayed in figure 5.27, it does not show any break up to 300 keV. A spectral analysis at ScW level has been performed searching for a possible spectral evolution. Spectra extracted from ScW A and B (see figure 5.24) are very similar, being both best fit by a power law plus a black body model (17–300 keV) with almost identical values of the best fit parameters. It was so reasonable to extract a spectrum from the sum of ScWs A+B to obtain a better model fit. In this case, the best fit parameters of the power law plus black body best fit (χ^2_ν=0.8, d.o.f. 46) are Γ=1±0.17 and kT=$0.9^{+0.44}_{-0.25}$ keV. Whereas the best fit parameters concerning the spectrum extracted from the sum of ScW C and D (see figure 5.24) are Γ=–$0.36^{+0.18}_{-0.44}$ and kT=$1^{+0.3}_{-0.3}$ keV (χ^2_ν=0.55, d.o.f.46). The spectrum of IGR J11321−5311 during the final part of its outburst activity is much harder than that pertaining to the beginning of the outburst. This can be clearly noted in figure 5.28 which shows the two spectra extracted from the sum of ScW A+B and C+D, and in figure 5.29 which displays their confidence countour levels for the photon index and the normalization costant of the power law. IGR J11321−5311 was unfortunately outside the narrower JEM–X FOV so that it is not possible to add any information at lower energies.

The position of IGR J11321−5311, taken from the ScW that had the most significance detection, is RA=11 32 08.52, Dec=-53 11 32.8, error radius=2′.1. The source is located off the galactic plane (b=7°.847) and far away from the galactic center.

IGR J11321−5311 was not reported in the third IBIS catalog (Bird et al. 2007) which covered ~ 3.5 years of INTEGRAL observations, from October 2003 to May 2006, during which the region of the sky including IGR J11321−5311 was observed for a total of ~ 1.15 Ms. It worth pointing out that the third IBIS catalog input dataset did not include the INTEGRAL data pertaining to the detection of the source here discussed, since they were not public at the time. It was possible to infer a 2σ IBIS upper limit on the quiescent flux of IGR J11321−5311, equal to ~ 0.5 mCrab or 3.4×10^{-12} erg cm^{-2} s^{-1} (20–40 keV). Recently, *Swift* XRT performed two targeted observations of IGR J11321−5311 (expo-

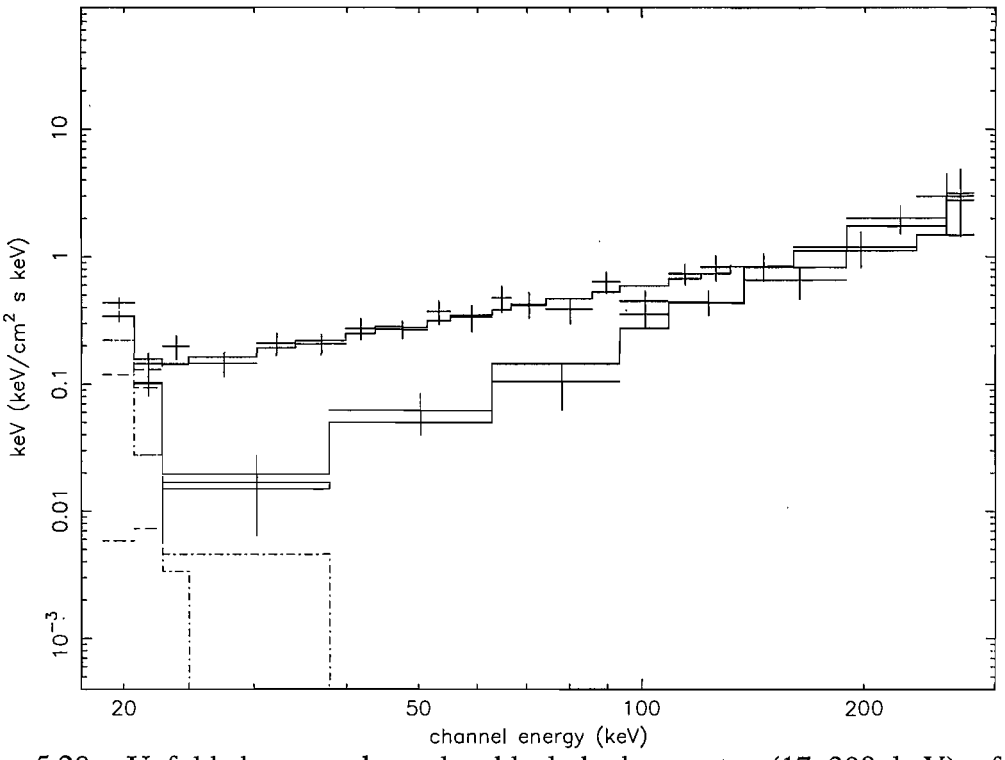

Figure 5.28: Unfolded power law plus black body spectra (17–300 keV) of IGR J11321−5311 extracted from the sum of ScW A and B (top), C and D (bottom).

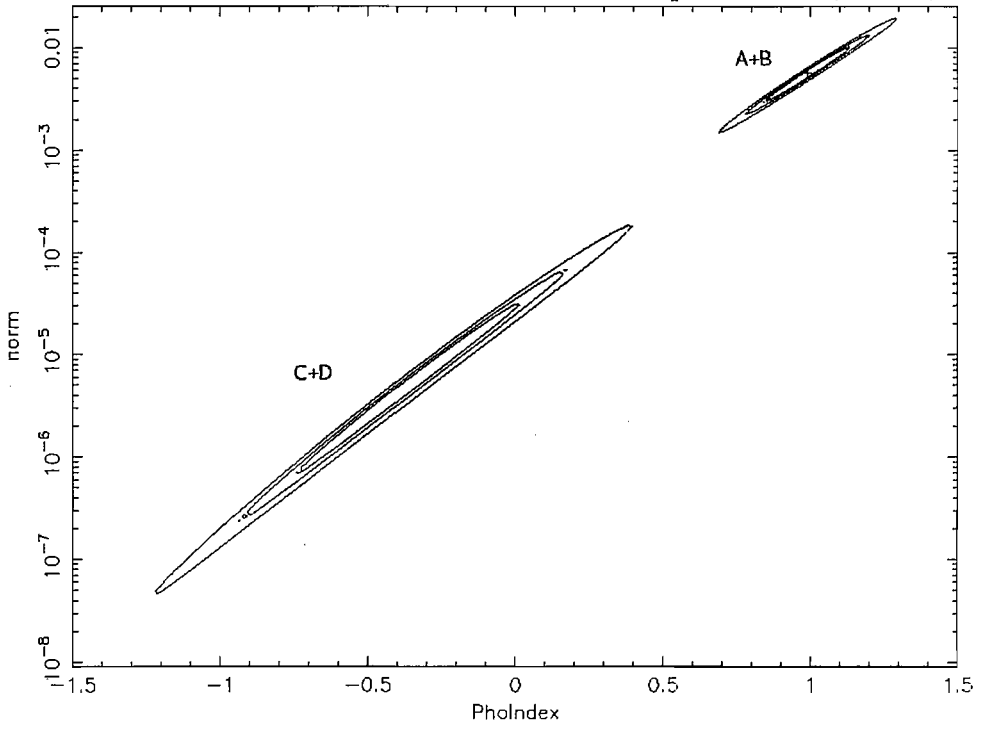

Figure 5.29: Confidence countour levels for the photon index and the normalization costant of the power law model pertaining the spectra extracted from the sum of ScW A+B and C+D.

sure time of ~ 2.5 and 3.3 ks), but no X-ray objects were detected inside the ISGRI error box, as it can be seen in figure 5.30 and figure 5.31 (Landi et al. 2007). A *Swift* XRT upper limit to the flux of ~ 8.8×10^{-14} erg cm^{-2} s^{-1} (0.2–10 keV) was derived. Moreover, the source has been targeted several times by the RXTE satellite, but detections were never reported. IGR J11321−5311 seems to spend a considerable fraction of its time in quiescence.

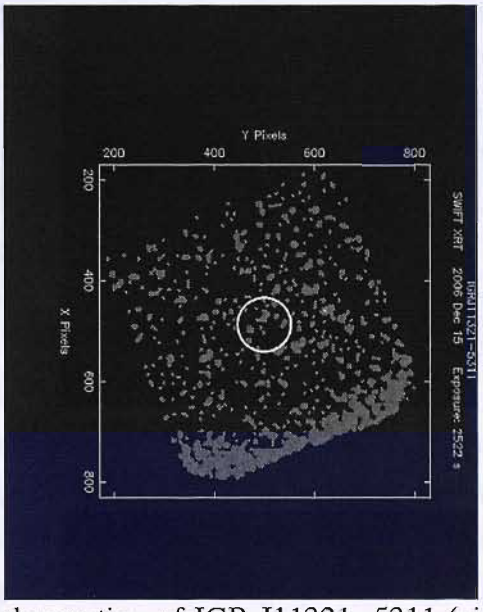

Figure 5.30: *Swift* XRT observation of IGR J11321−5311 (circled) on December 2006 (0.2–10 keV).

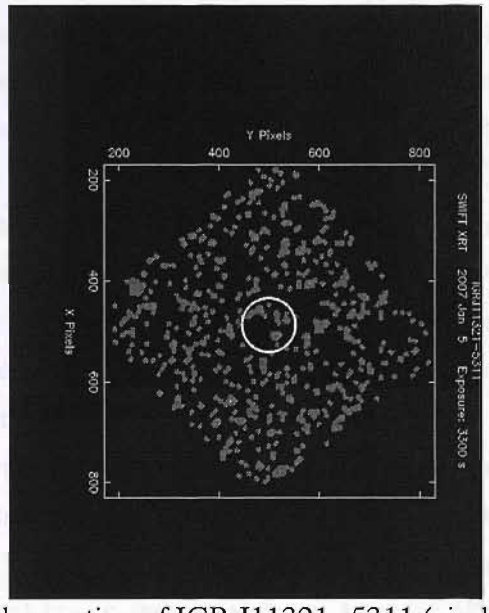

Figure 5.31: *Swift* XRT observation of IGR J11321−5311 (circled) on January 2007 (0.2–10 keV).

5.2.4.3 Discussion

No previously known X-ray, gamma-ray or radio sources are located inside the ISGRI error circle of IGR J11321−5311, using all the available catalogs in the HEASARC database. As for the optical and infrared band, the ISGRI error circle is naturally too large for a fruitful identification using catalogs such as USNO–B1.0 or 2MASS. A much more refined source position is strongly needed to this aim. It is worth pointing out that Negueruela & Schurch (2007) used existing photometric catalogs to search for early type stars within the error circles of unidentified X-ray source believed to be HMXBs. Their method proved to be very efficient at finding reddened OB stars, resulting in the detection of the counterpart to several unidentified X-ray sources. However, no suitable candidates were found in the field of IGR J11321−5311 (Negueruela & Schurch 2007).

Even if the observational data about IGR J11321−5311 are few, all the finding previously reported may furnish hints on its possible nature. The temporal and spectral behaviour of the source are reminiscent of outburst characteristics from two different class of hard X-ray emitters: Black Hole transients and Magnetars.

IGR J11321−5311 could be a new member of the Anomalous X-ray Pulsars (AXPs) group. A review by Kaspi (2006) outlines the recent observational progress on temporal and spectral behaviour of the seven, possibly nine AXPs so far detected. They have pulsation periods ranging from 6 to 12 s, large period derivatives ($\sim 10^{-13}$–10^{-10} ss^{-1}), very strong magnetic fields (0.6–7.1$\times 10^{14}$ G) and some of them are situated inside supernova remnants. Their relatively high X-ray luminosity ($\sim 10^{34}$–10^{36} erg s^{-1}) cannot be accounted for by rotational energy losses, moreover no convincing evidence for a companion star has been found for any of them. Many observational properties support the idea that AXPs are magnetars, isolated neutron stars powered by the decay of their huge magnetic fields. Spectra in the traditional X-ray band (0.5–10 keV) are well described by two components; a blackbody (kT~0.3–0.6 keV) due to internal heating caused by the intense magnetic field decay plus a relatively steep power law ($2<\Gamma<4$) resulting from resonant scattering of the thermal seed photons off magnetospheric currents in the twisted magnetoshere. The softness of the spectra predicts non detections above 10 keV, however recent INTEGRAL observations showed that some AXPs are very hard X-ray emitters with spectra extending well above 100 keV and characterized by no break up to 300 keV (Kuiper et al. 2006). Moreover, their pulsed spectra are exceptionally hard with photon index in the range from -1 to 1, while the photon index of the total spectra (sum of pulsed and unpulsed components) are in the range from 1 to 1.4 (Kuiper et al. 2006). Until recently AXPs were believed to be steady X-ray emitters, but one of the lately most interesting discoveries is the range and diversity of their X-ray variability properties in pulsed

and persistent emission. AXPs show long term flux variations, pulse profile changes, short term variability such as outbursting behaviour. A short outburst has been fortuitously detected from the AXP 1E 2259+589 (Kaspi et al. 2003, Woods et al. 2004). It lasted a few hours and it was accompanied by dramatic hardening of the spectrum. In the light of the finding reported above, the flaring behaviour and the spectral characteristics of IGR J11321−5311, with no break up to 300 keV and hardening of the spectrum, could resemble those of AXPs.

An alternative to the AXP scenario is a black hole (BH) transient nature. Here a few BHs, showing short and peculiar outbursts, are reported: SAX J1819.3−2525, XTE 0421+560 and Cyg X−1. The X-ray transient SAX J1819.3−2525 (see in't Zand et al. 2000 and Revnivtsev et al. 2002a,b for a review), subsequently to its discovery with BeppoSAX in February 1999, showed a weak X-ray activity and soft spectrum until September 1999, when a series of very bright and short X-ray flares occurred within less than 1.5–2 days. They reached a level of about 12 Crab (2–10 keV) during the brightest one, the X-ray flux then rapidly decreased and the source totally disappeared within 0.3 day. Spectra accumulated during the peak are reminiscent of a black hole, when in the low state, with $\Gamma<2$, cut-off at energy 100–200 keV and pronounced fluorescent Fe line at 6.4 keV. XTE J0421+56/CI Cam is a peculiar system consisting of a Be star and, more probably, a black hole. This X-ray transient was detected in 1998 by RXTE (Smith et al. 1998), brightened very quickly up to 2 Crab a few hour after discovery and decayed exponentially with a very short e-folding time (0.6 day). The 20–100 keV BATSE data on the decline are consistent with a power law with a photon number index of −3.9, while there is marginal evidence of a harder spectrum during the rise and/or peak (Belloni et al. 1999). In the case of Cyg X-1, seven episodes of strong hard X-ray emission occurred whitin 9 years (Golenetskii et al. 2003). These outbursts have duration up to ~8 hours and reached peak fluxes of 3×10^{-7} erg cm^{-2} s^{-1} (15–300 keV). All the spectral characteristics of the above black hole outburst examples do not show the peculiarity of IGR J11321−5311, i.e. flat spectral index and lack of any spectral break up to 300 keV. Moreover, the duration of the outburst detected by INTEGRAL from IGR J11321−5311 (~ 3.5 hours) is too short when compared to typical transient activity of accreting black hole binaries, which is of the order of months.

The location of IGR J11321−5311 off the galactic plane (b=7°.85) could suggest an AGN nature. However, blazars are known to display flares with timescales of days or weeks, significatly longer than the flare detected from IGR J11321−5311 (~ 5500 seconds). A possible very short hard X-ray flare (~ 2000 seconds duration) was reported only in one case, the blazar NRAO 530 (Foschini et al. 2006). Moreover, blazars are

known to be strong radio sources, but none are located inside the ISGRI error circle of IGR J11321−5311 using all the radio catalogs available in the HEASARC database. However, it is worth to remind that the region of the sky including IGR J11321−5311 has not yet be covered by deep radio surveys (e.g. NVSS).

Further detections of IGR J11321−5311 by INTEGRAL or other X-ray missions, as well as multiwavelength observations, could be very useful to shed more light on this enigmatic and very interesting hard X-ray transient source.

5.2.5 IGR J18483−0311

5.2.5.1 Archival X-ray observations of the source

IGR J18483−0311 was discovered by INTEGRAL during observations of the galactic center field performed between 23–28 April 2003 (Chernyakova et al. 2003). The source was reported as a detection with an average flux of ~10 mCrab and ~5 mCrab in the energy bands 15–40 keV and 40–100 keV, respectively. A possible X-ray outburst was observed on 26 April, when the X-ray flux increased to ~40 mCrab (15–40 keV). Subsequently to the discovery, Molkov et al (2003b) reported another detection of the source by INTEGRAL on 5 April 2003. Finally, IGR J18483−0311 has been detected by INTEGRAL at an average flux of 4.3±0.2 mCrab (18–60 keV) during a survey of the Sagittarius arm tangent region in the spring 2003 (Molkov et al. 2003c). Stephen et al. (2006) reported the association between IGR J18483−0311 and the ROSAT HRI source 1RXH J184817.3−031017. Two optical USNO−B1.0 objects were found within the ROSAT positional uncertainty; one of which is also a near−infrared (NIR) 2MASS source.

5.2.5.2 Analysis of newly discovered outbursts by INTEGRAL

With the aim of detecting new outbursts from IGR J18483−0311, an analysis at the ScW level of the deconvolved ISGRI shadowgrams has been performed. This section reports on the results of this search, which provided 5 newly discovered outbursts.

They are listed in table 5.4 together with the energy range of the detection, the peak and luminosity fluxes and duration of the outburst activity. Images from the X-ray monitor JEM−X were created for all 5 newly discovered outbursts. Only in one case (outburst No.1 in table 5.4) was the source inside the JEM−X FOV such that it was possible to extract a spectrum and a X-ray light curve.

Figure 5.32 shows the 20–100 keV ISGRI light curve of outburst No. 1. At the beginning there was no significant detection since the count rate was consistent with zero

Table 5.4: Summary of IBIS detections of newly discovered outbursts from IGR J18483−0311.

No.	Date	energy band (keV)	peak flux (mCrab)	peak luminosity ★ (erg s^{-1})	duration (days)
1	19 April 2006	20–100	~ 120	~ 7.8×10^{36}	~ 1.8
2	5 September 2004	20–60	~ 95	~ 4.4×10^{36}	~ 0.46†
3	26 April 2004	20–60	~ 80	~ 3.6×10^{36}	~ 3.5
4	18 March 2004	20–40	~ 135	~ 4×10^{36}	~0.33†
5	11 May 2003	20–60	~ 75	~ 3.2×10^{36}	~1.3†

† = lower limit on the duration.
★ = assuming a distance of ~ 5.7 kpc (see Section 5.2.5.7).

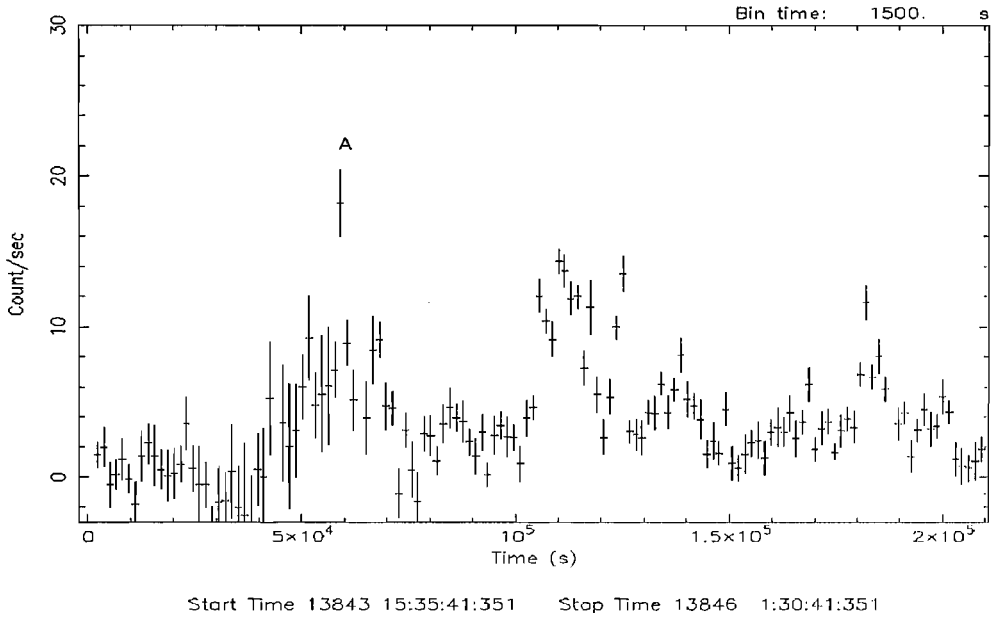

Figure 5.32: ISGRI light curve (20–100 keV) of a newly discovered outburst of IGR J18483−0311 that occurred in April 2006 (No.1 in table 5.4).

count/sec, then suddenly on 19 April 2006 ~04:50 UTC the source turned on. Initially, the outburst activity was characterized by a prominent flare (labeled as A in figure 5.32) which reached a peak flux of ~ 120 mCrab or 2.04×10^{-9} erg cm^{-2} s^{-1} (20–100 keV) in a few hours and then dropped with the same timescale. This first flare was followed by several others, then the source turned off. The duration of the total outburst activity was ~1.8 days.

All the ScWs during which the source was detected by ISGRI were combined into a single mosaic significance map. IGR J18483−0311 was detected at ~50σ (20–100 keV), and its coordinates (J2000) are RA=18^h 48^m 15.07^s, Dec=-03° 10′ 17″, with an error

radius of 1.′4.

The combined JEM–X/ISGRI spectrum (3–50 keV) from the whole duration of the outburst No.1 is best fit by an absorbed cutoff power law (χ^2_ν=1.19, 140 d.o.f.) with Γ=1.4±0.3, cutoff energy equal to $22^{+7.5}_{-4.5}$ keV and $N_H=9^{+5}_{-4}\times10^{22}$ cm^{-2}. The latter exceeds the galactic absorption along the line of sight (1.6×10^{22} cm^{-2}) suggesting that most of the low energy absorption is intrinsic to the source. Figure 5.33 displays the absorbed cutoff power law unfolded spectrum, while figure 5.34 shows the contours plot for the photon index and the cutoff energy. To account for a cross-calibration mismatch between the two instruments, we have introduced a constant in the fit, which when left free to vary provides a value of 1.3±0.15. It is worth pointing out that a similar good fit (χ^2_ν=1.2, 141 d.o.f.) is also provided by an absorbed bremsstrahlung with kT=$21.5^{+2.5}_{-2}$ keV and $N_H=7.5^{+2.5}_{-2}\times10^{22}$ cm^{-2}. The latter is compatible within the uncertainties with the value obtained from the absorbed cutoff power law spectral model.

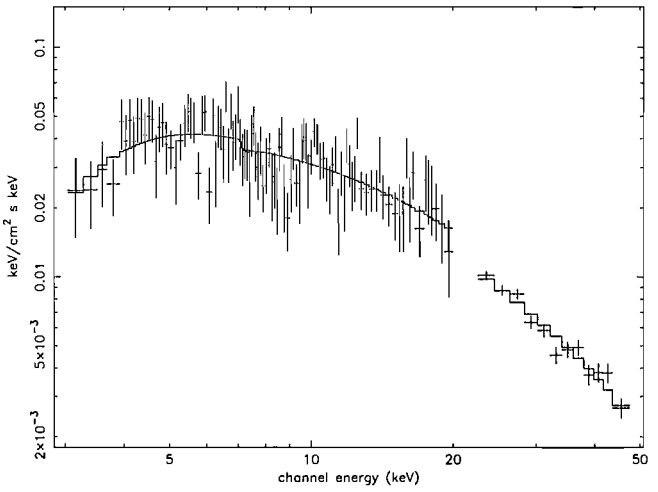

Figure 5.33: Unfolded JEM–X and ISGRI spectrum (3–50 keV) of IGR J18483–0311 during outburst No.1 in table 5.4.

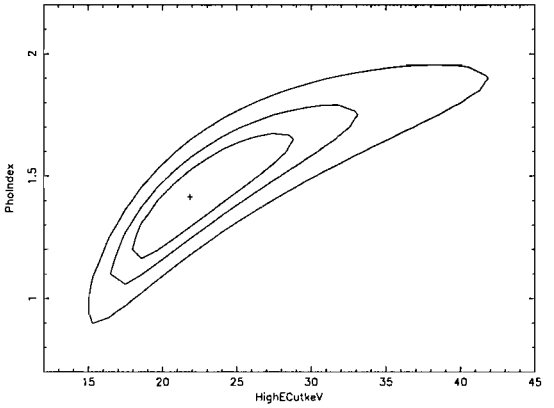

Figure 5.34: Confidence contours level for the photon index and the cutoff energy from the spectral analysis of the outburst No.1 in table 5.4.

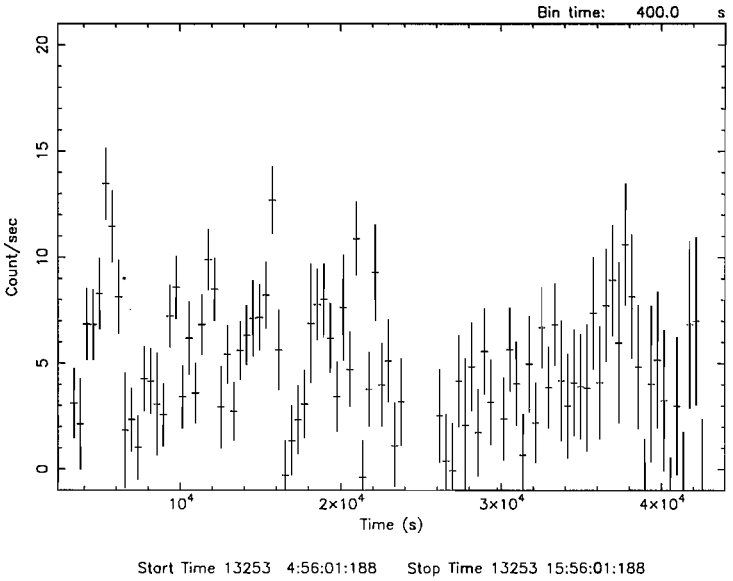

Figure 5.35: ISGRI light curve (20–60 keV) of a newly discovered outburst of IGR J18483–0311 that occurred in September 2004 (No.2 in table 5.4).

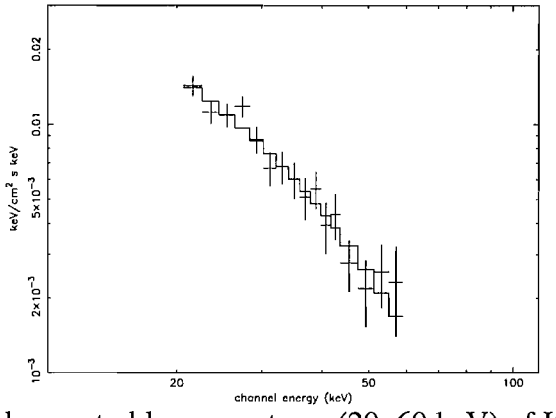

Figure 5.36: Unfolded bremsstrahlung spectrum (20–60 keV) of IGR J18483–0311 during outburst No.2 in table 5.4.

Figure 5.35 shows the 20–60 keV ISGRI light curve of outburst No.2. It started on 5 September 2004 at ~ 04:50 UTC and it ended on the same day at ~ 16:00 UTC. It is truncated at the beginning and at the end because the source was outside the IBIS FOV, so it is not possible to constrain a total duration for the outburst activity. The source was in the IBIS FOV for ~ 11 hours, its light curve is characterized by several fast flares on timescales of few tens of minutes which reached a maximum peak flux (20–60 keV) of ~ 95 mCrab or ~ 1.1×10^{-9} erg cm^{-2} s^{-1}. The 20–60 keV spectrum extracted during the whole outburst is well fit by thermal models such as black body (χ^2_ν=0.97, 14 d.o.f., kT=$6.5^{+0.45}_{-0.45}$ keV) or bremsstrahlung (χ^2_ν=0.61, 14 d.o.f., kT=20.6^{+4}_{-3} keV). A good fit is also provided by a simple power law with Γ=$2.9^{+0.25}_{-0.25}$ (χ^2_ν=0.74, 14 d.o.f.). Figure 5.36 shows the unfolded 20–60 keV bremsstrahlung spectrum.

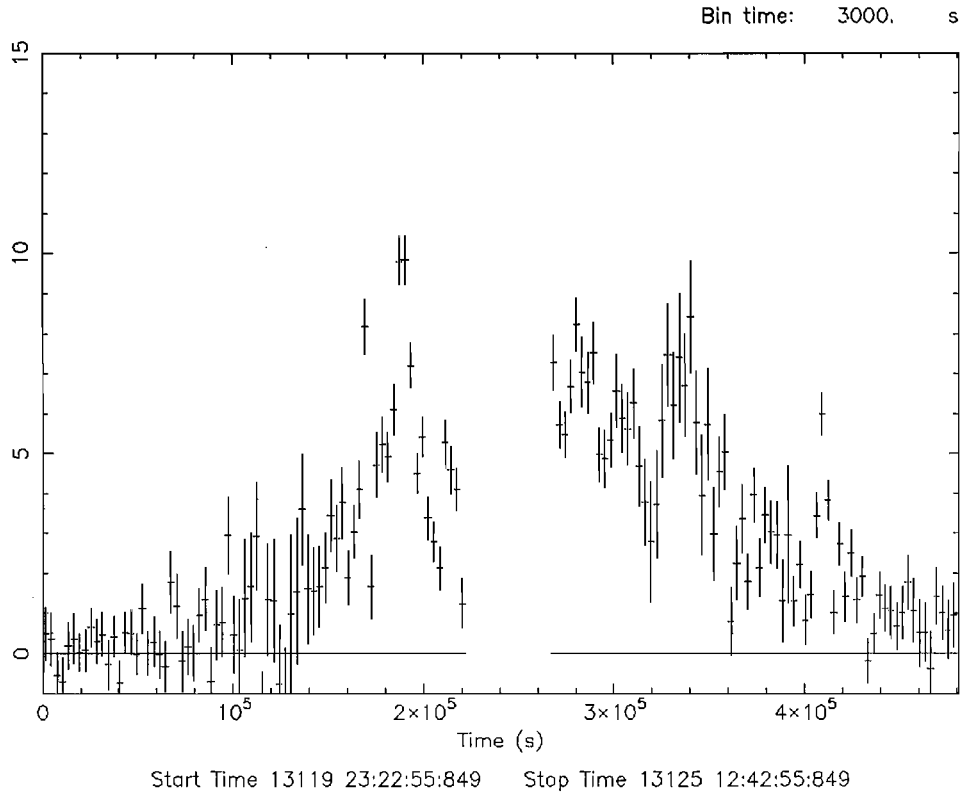

Figure 5.37: ISGRI light curve (20–60 keV) of a newly discovered outburst of IGR J18483–0311 that occurred in April 2004 (No.3 in table 5.4).

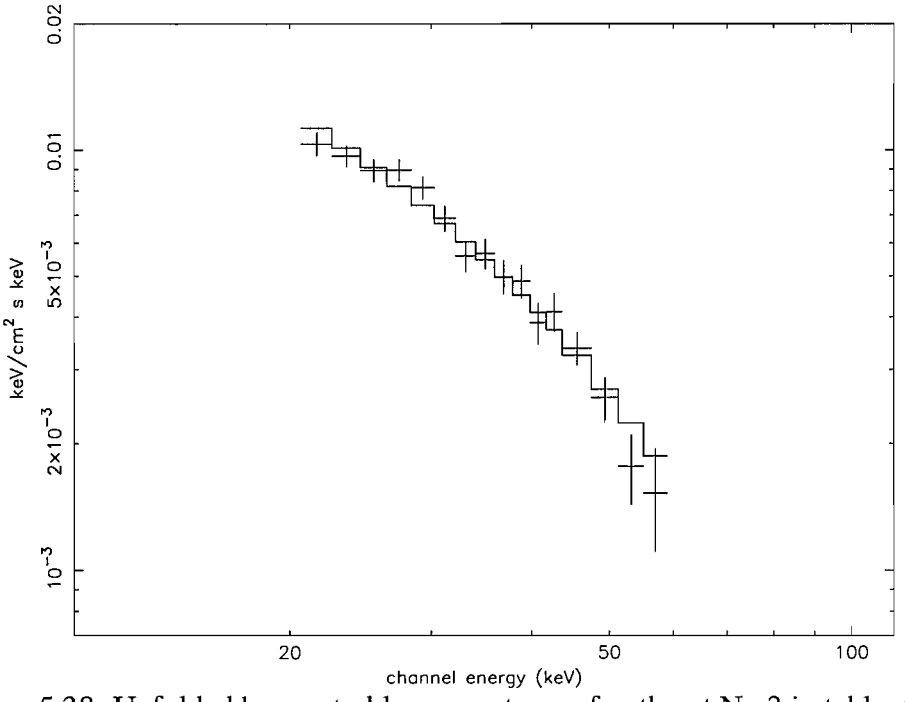

Figure 5.38: Unfolded bremsstrahlung spectrum of outburst No.3 in table 5.4.

Figure 5.37 displays the 20–60 keV light curve of outburst No.3 in table 5.4. The gap of ~ 13 hours is due to the visibility constraint between one INTEGRAL revolution and the next. In spite of that, the flaring activity of the source is very evident. Initially the flux was consistent with zero, then suddenly the source turned on at ~ 17:00 UTC on 26 April 2004. It reached a peak flux of ~ 80 mCrab (20–60 keV); the duration of the total outburst activity was ~ 3 days. A spectrum extracted during the whole outburst (20–60 keV) is equally best fit by a black body (χ^2_ν=0.95, 14 d.o.f., kT=$7.2^{+0.25}_{-0.25}$ keV) or bremsstrahlung (χ^2_ν=0.95, 14 d.o.f., kT=$25.2^{+2.5}_{-2.2}$ keV). A simple power law provides a bad fit (χ^2_ν=2.05, 14 d.o.f). Figure 5.38 shows the unfolded bremsstrahlung spectrum.

The ISGRI light curve (20–40 keV) of outburst No. 4 is shown in figure 5.39. The observation starts on 18 March 2004 at ~ 20:00 UTC. The beginning is truncated because the source was outside the IBIS FOV. Nevertheless, the decay of the flare is clear, in which the 20–40 keV flux dropped from ~ 135 mCrab (~ 1.02×10^{-9} erg cm^{-2} s^{-1}) to just a few mCrab in ~ 4 hours. This strongly suggests that the source was active before entering the IBIS FOV. Another flare is present in the light curve (labeled as A): it reached a peak flux of ~ 80 mCrab (20–40 keV) in ~ 1 hour and then dropped to an almost null flux with the same timescale. The remaining part of the light curve shows no flaring activity from the source. Reasonable fits were obtained by thermal models such as black body (χ^2_ν=0.85, 14 d.o.f., kT=$7.8^{+0.6}_{-0.6}$ keV) or bremsstrahlung (χ^2_ν=1.26, 14 d.o.f., kT=$32.5^{+10.5}_{-6.7}$ keV). Figure 5.40 shows the unfolded bremsstrahlung spectrum.

Finally, figure 5.41 shows the ISGRI light curve of outburst No.5 in table 5.4. It starts on 11 May 2003 at ~ 19:30 UTC and it ends on 13 May 2003 at ~ 02:30 UTC. It is truncated at the beginning and at the end because the source was outside the IBIS FOV. The peak flux was ~ 75 mCrab (20–60 keV). The 20–60 keV spectrum of the whole outburst is best fit by a bremsstrahlung (χ^2_ν=1.1, 14 d.o.f) with kT=$22^{+2}_{-2.5}$ keV, on the contrary a black body is a very bad description to the data (χ^2_ν=3.2, 14 d.o.f). A reasonable fit is also provided by a simple power law (χ^2_ν=0.85, 14 d.o.f) with $\Gamma=2.9^{+0.15}_{-0.15}$. Figure 5.42 shows the unfolded 20–60 keV bremsstrahlung spectrum.

Table 5.5 is a summary of the spectral analysis of each newly discovered outburst. Outburst No.1 is the only one for which a broad band spectrum (3–50 keV) is available, the cutoff power law model constrains very well its spectral properties both at soft and hard X-rays, with best fit parameters $\Gamma=1.4\pm0.3$, $E_c=22^{+7.5}_{-4.5}$ keV and $N_H=9^{+5}_{-4}\times10^{22}$ cm^{-2}. Moreover, it can be noted that a bremsstrahlung model provided a good description of all 5 outbursts with a similar temperature kT in the range 20–32 keV. A black body gave good fits for the outbursts No. 2, 3 and 4 with a similar temperature kT in the range 6.5–7.5 keV, but is unacceptable in the case of the outbursts No. 1 and 5. Finally, a simple power

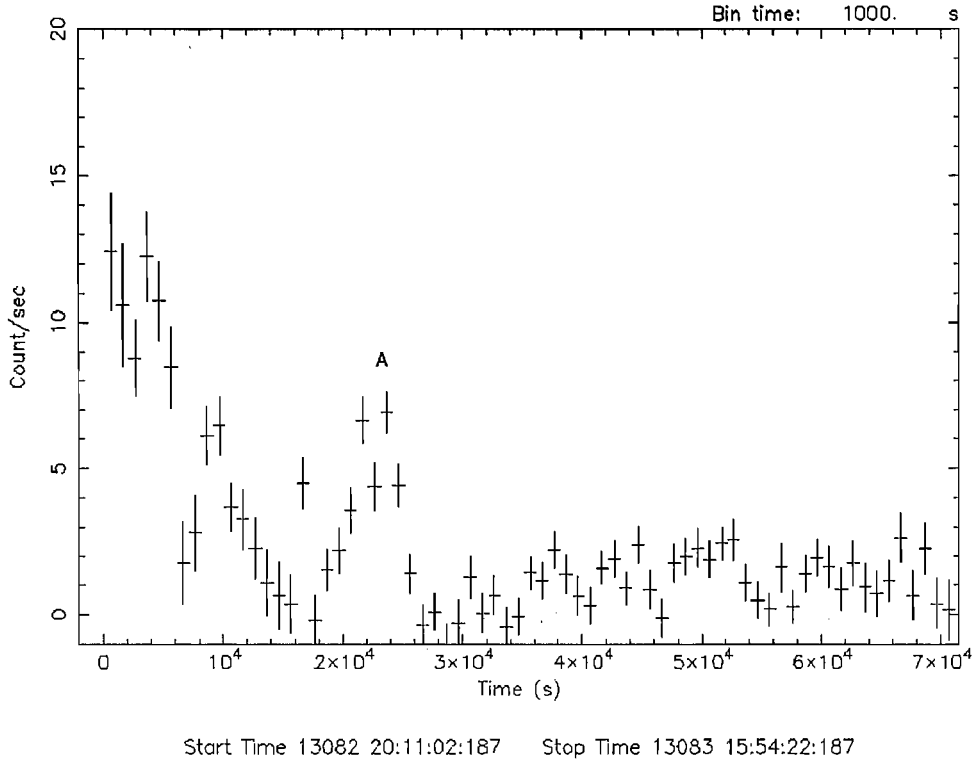

Figure 5.39: ISGRI light curve (20–40 keV) of a newly discovered outburst of IGR J18483−0311 that occurred in March 2004 (No. 4 in table 5.4).

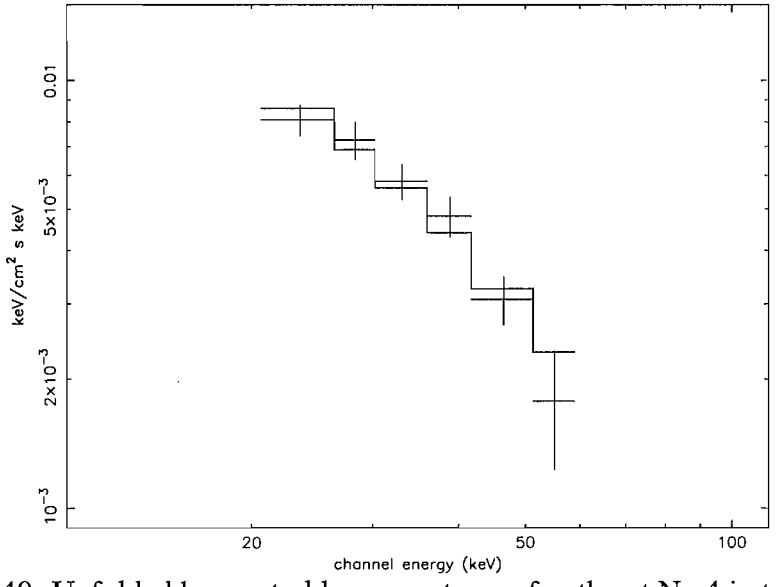

Figure 5.40: Unfolded bremsstrahlung spectrum of outburst No.4 in table 5.4.

law described well the spectra of outburst No. 2 and 5 providing the same value of the photon index (~2.9). Whereas, outbursts No. 3 and 4 could not be described by a simple power law.

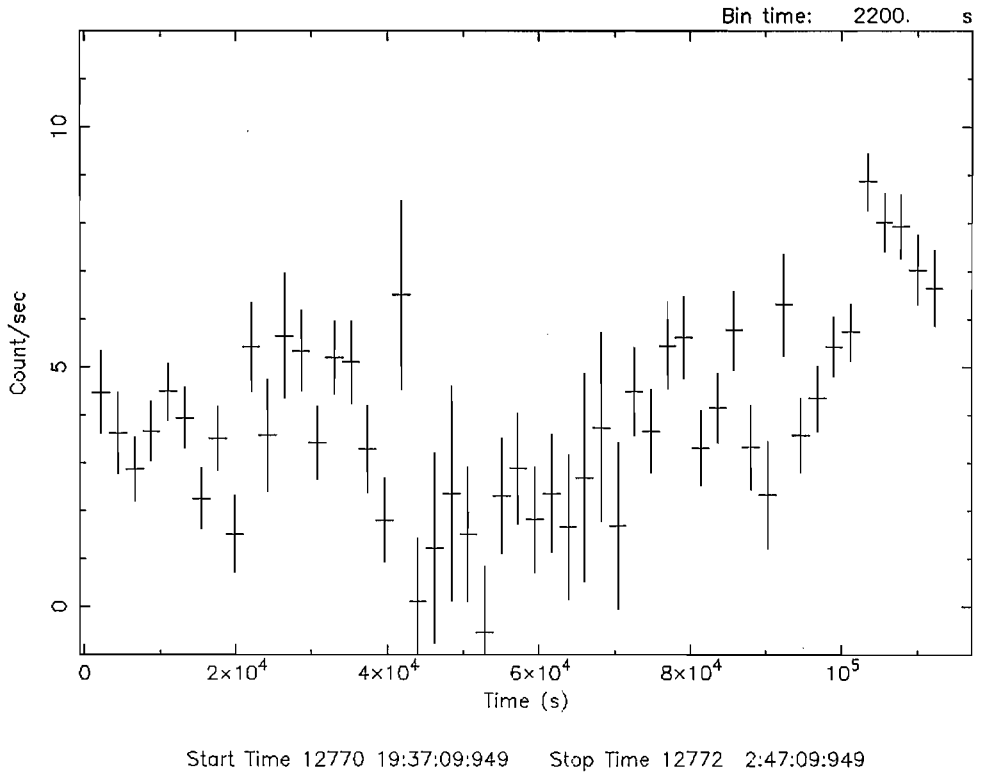

Figure 5.41: ISGRI light curve (20–60 keV) of a newly discovered outburst of IGR J18483–0311 that occurred in May 2003 (No. 5 in table 5.4).

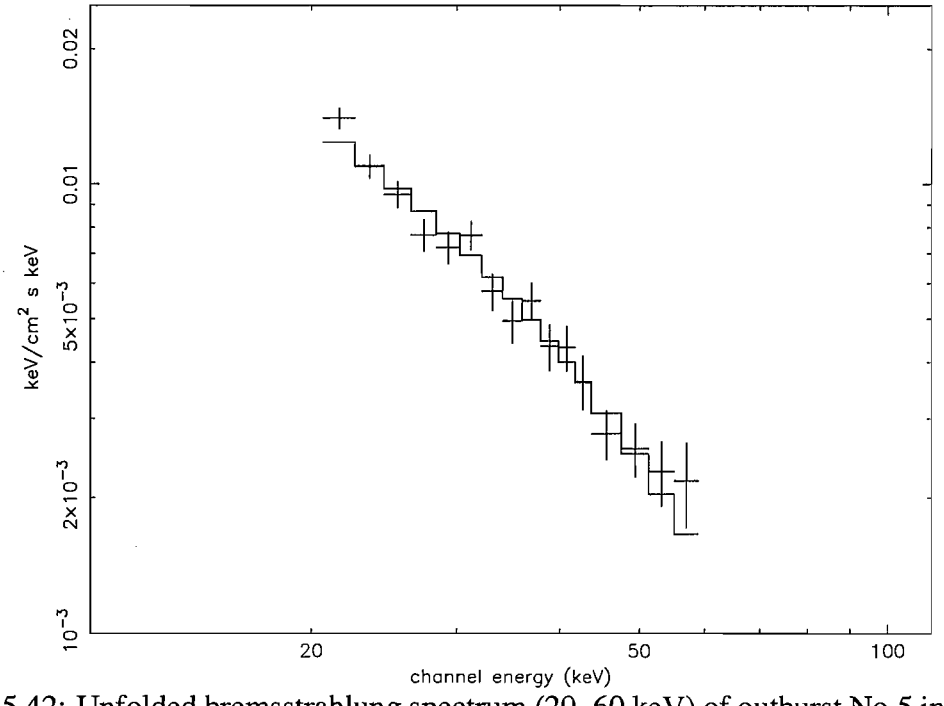

Figure 5.42: Unfolded bremsstrahlung spectrum (20–60 keV) of outburst No.5 in in table 5.4.

Table 5.5: Summary of spectral analysis of the 5 newly discovered outbursts from IGR J18483−0311. The name of the spectral models are written in XSPEC terminology.

Model	parameter	outburst No.1 (3–50 keV)	outburst No.2 (20–60 keV)	outburst No.3 (20–60 keV)	outburst No.4 (20–60 keV)	outburst No.5 (20–60 keV)
wa+cutoffpl	$N_H(10^{22}$ cm$^{-2})$	9^{+5}_{-4}				
	Γ	1.4±0.3				
	E_c (keV)	$22^{+7.5}_{-4.5}$				
	χ^2_ν(d.o.f.)	1.19 (140)				
wa+bremss	$N_H(10^{22}$ cm$^{-2})$	$7.5^{+2.5}_{-2}$				
	kT (keV)	$21.5^{+2.5}_{-2}$				
	χ^2_ν(d.o.f.)	1.2 (141)				
bremss	kT (keV)	$26^{+3.3}_{-2.5}$	20.6^{+4}_{-3}	$25.2^{+2.5}_{-2.2}$	$32.5^{+10.5}_{-6.7}$	$22^{+2}_{-2.5}$
	χ^2_ν(d.o.f.)	1.49 (142)	0.61 (14)	0.95 (14)	1.26 (14)	1.1 (14)
bb	kT (keV)		$6.5^{+0.45}_{-0.45}$	$7.2^{+0.25}_{-0.25}$	$7.8^{+0.6}_{-0.6}$	
	χ^2_ν(d.o.f.)	4.86 (142)	0.97 (14)	0.95 (14)	0.85 (14)	3.23 (14)
po	Γ		$2.9^{+0.25}_{-0.25}$			$2.9^{+0.15}_{-0.15}$
	χ^2_ν(d.o.f.)	2.65 (142)	0.74 (14)	2.05 (14)	1.59 (14)	0.85 (14)

5.2.5.3 Recurrence timescale

A long term light curve of IGR J18483–0311 was created, covering a time interval from MJD 52704 (March 2003) to MJD 53846 (end of April 2006). Subsequently, a search was made for any evidence of periodicity which would indicate the recurrence timescale of its transient activity. The flux of IGR J18483–0311 was extracted from each ISGRI pointing where the source was within 12° of the centre of the FOV, producing a long term light curve of the source on the ScW timescale. A 12° limit was applied because the off-axis response of ISGRI is not well modelled at large off-axis angles and this introduces a systematic error in the measurement of source fluxes, thus generating problems in the detection of periodic signals (Hill, 2006). The 20–40 keV long term light curve was then searched for periodicities using the Lomb-Scargle periodogram method by means of the fast implementation of Press & Rybicki (1989) and Scargle (1982). The resulting power spectrum is shown in figure 5.43; the peak power of 165.7 corresponds to a frequency of 0.0540 days^{-1}. This frequency equates to a period of 18.52 days with a theoretical Lomb-Scargle error of ± 0.01 days. The error on the angular frequency is given by Horne & Baliunas (1986).

$$\delta\omega = \frac{3\pi\sigma_N}{2\sqrt{N}TA} \tag{5.1}$$

where $\sigma_N{}^2$ is the variance of the noise, N is the number of data points, T is the total length of the data set and A is the amplitude of the signal given by:

$$A = 2\sqrt{\frac{z_0\sigma_s^2}{N}} \tag{5.2}$$

where z_0 is the Lomb-Scargle power and $\sigma_s{}^2$ is the variance of the light curve. The period estimate was confirmed with a Monte-Carlo simulation. Each flux measurement was adjusted using Gaussian statistics within its individual error estimate to generate a simulated light curve of the source. The corresponding periodogram was produced and any detected periodicity recorded. 200,000 light curves were simulated in this fashion and it was found that 99.5% identified a periodicity centred at 18.52 days. The phase-folded 20–40 keV lightcurve of IGR J18483–0311 is shown in figure 5.44. A clear flare-like profile is apparent, with the source being predominantly undetected and then briefly flaring to a detectable level. The average duration of an outburst can be seen to be of the order of 3 days (FWHM). This is consisted with the measured durations for outburst No. 1 and 3 in table 5.4.

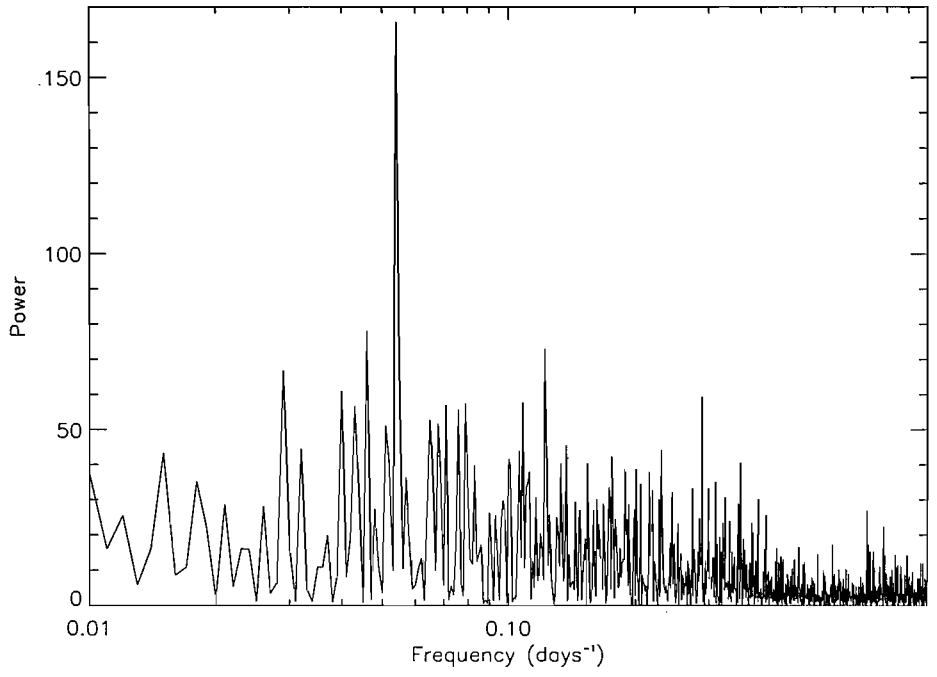

Figure 5.43: Lomb-Scargle periodogram generated from the 20–40 keV light long term curve of IGR J18483–0311

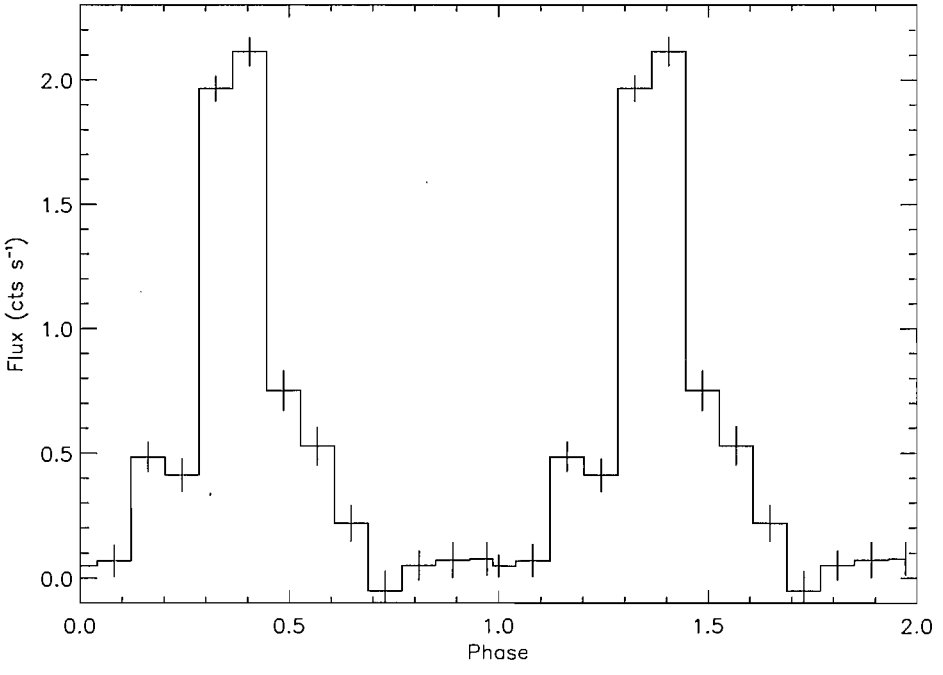

Figure 5.44: The phase-folded 20–40 keV light curve of IGR J18483–0311. The data are folded on a period of 18.52 days.

5.2.5.4 Looking for missed outbursts

Table 5.6: Analysis of the 20–40 keV long term light curve of IGR J18483−0311 around the expected start time of outbursts based upon the 18.52 days periodicity. For the outburst numbers not listed there was no significant coverage of the source by INTEGRAL around those times.

Out. No.	Expected start time (MJD)	INTEGRAL coverage (MJD)	Comments
1	~ 52714.48	52714.99– 52715.63	Low level of outburst activity (peak flux ~ 20 mCrab)
2	~ 52733	52734.92– 52735.61	Molkov et al. 2003b (peak flux ~ 40 mCrab)
3	~ 52751.52	52753.04– 52757.50	Outburst-discovery of the source†
4	~ 52770.04	52770.80– 52772.08	Outburst discussed in this paper (No.5 in table 5.4)
21	~ 53084.88	53082.85– 53083.62	Outburst discussed in this paper (No.4 in table 5.4)
23	~ 53121.92	~ 53121.7★	Outburst discussed in this paper (No.3 in table 5.4)
30	~ 53251.56	53253.20–53253.60	Outburst discussed in this paper (No.2 in table 5.4)
62		~ 53844.2★	Outburst discussed in this paper (No.1 in table 5.4)

★ = start time of the outburst
† = (Chernyakova et al. 2003)

The detected periodicity of ~ 18.52 days indicates the recurrence timescale of outbursts from IGR J18483−0311, we can then search for additional weaker outbursts in the INTEGRAL observations. Between the first and last observation analysed (52704 – 53846 MJD) 62 outbursts may have occurred. Using the measured start time (MJD~53844.2) of outburst No. 1 in table 5.4 and the periodicity of 18.52 days, the full long term light curve of IGR J18483−0311 was examined around the predicted outburst start times. The results of this examination are shown in Table 5.6. Of the 62 potential outbursts, only 8 were well covered by INTEGRAL observations, either in part or fully. For the outburst numbers not listed there was no significant coverage of the source by INTEGRAL around those times. These 8 include the 5 large brightest outbursts reported in table 5.4 and discussed in section 5.2.5.2, two outbursts with a low level of activity and the outburst when the source was discovered by Chernyakova et al. (2003). It should be noted that all but one the outbursts listed in table 5.6 occured when expected, based upon the 18.52 day periodicity. The only exception (No. 21 in table 5.6 or No.4 in table 5.4) occured at least 2 days earlier than expected. This may in part be explained by the difficulty in identifying a period when each outburst has a unique shape, moreover only 2 out of 5 outbursts detected by IBIS have been seen for their entire duration. Consequently the statistical error assigned to the 18.52 days period is likely to be underestimate. However, it might also indicate that the outbursting behaviour of the source is only semi-regular,

implying that there may be something which modulates the outburst time scale beyond the mechanism that produces the periodicity. This behaviour could be similar to that observed in Be X-ray transients in which the outbursts are associated with both the orbital period of the system and with the size of the disk around the Be star.

5.2.5.5 Searching for a pulse period

Fine timing resolution ISGRI light curves were constructed for the duration of the two brightest outbursts (No. 1 and No. 4) in table 5.4. The *ii–light* tool in OSA5.1 was used to generate light curves of IGR J18483–0311 in the 20–40 keV band using data from IBIS. The light curves were searched for pulsations using the Lomb-Scargle periodogram method with no positive results.

However, IGR J18483–0311 was also inside the JEM–X FOV during part of the outburst No.1 in table 5.4. Consequently, a 5 seconds bin time light curve was produced in the 4–20 keV. This light curve was also searched for periodicities using the Lomb-Scargle method; the resulting power spectrum is shown in figure 5.45. The peak power of 130.8 corresponds to a frequency of 0.04750 Hz. The error on this measurement is calculated using equations 5.1 & 5.2. The corresponding period is 21.0526 ± 0.0005 seconds; the 1^{st}, 2^{nd} and 3^{rd} harmonics of this period are also evident in the power spectrum.

Folding the JEM–X light curve on the 21.0526 s yields the pulse-period phase-folded light curve shown in figure 5.46. This periodicity could be attributed to the spin period of an X-ray pulsar located within the system. The pulse fraction, $(I_{max} - I_{min})/I_{max}$, where I_{max} and I_{min} are the maximum and minimum count rates respectively, is ~ (65±10) %.

5.2.5.6 *Swift* observations and results

In this section X-ray observations acquired with the XRT (X-ray Telescope) on board the *Swift* satellite are reported. A search of the XRT data archive revealed that *Swift* carried out 2 observations of IGR J18483–0311, on 16 February 2006 and 5 March 2006. Unfortunately in both observations the source was outside the IBIS FOV. The XRT collected data for a total exposure time of 8 ks and 5.6 ks, respectively.

First of all, the *Swift* XRT analysis of IGR J18483–0311 provided a very accurate source position (RA=18^h 48^m 17.17^s, Dec=-03° 10′ 15.54″, J2000) being the error radius equal to 3″.3.

As for the observation of 16 February 2006 (OBS1), it was possible to extract a meaningful spectrum only in the energy range 1–7 keV. Above 7 keV and below 1 keV the statistics were not good enough to perform a spectral analysis. The spectrum 1–

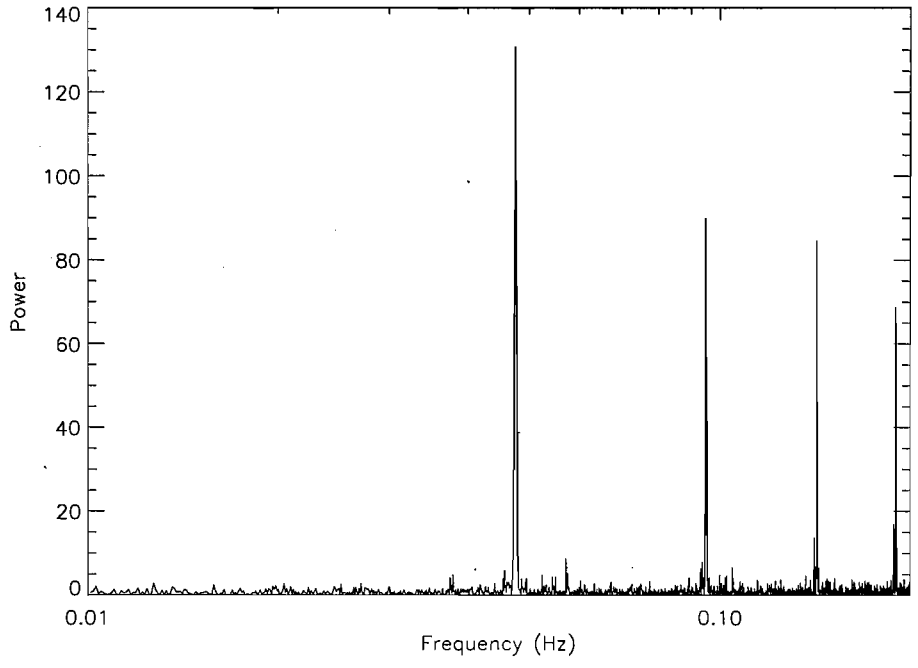

Figure 5.45: Lomb-Scargle periodogram generated from the JEM–X 4–20 keV light curve of IGR J18483–0311 during the outburst No.1 in table 5.4. The periodicity at 0.04750 Hz is clearly apparent, as are the 1^{st}, 2^{nd} and 3^{rd} harmonics.

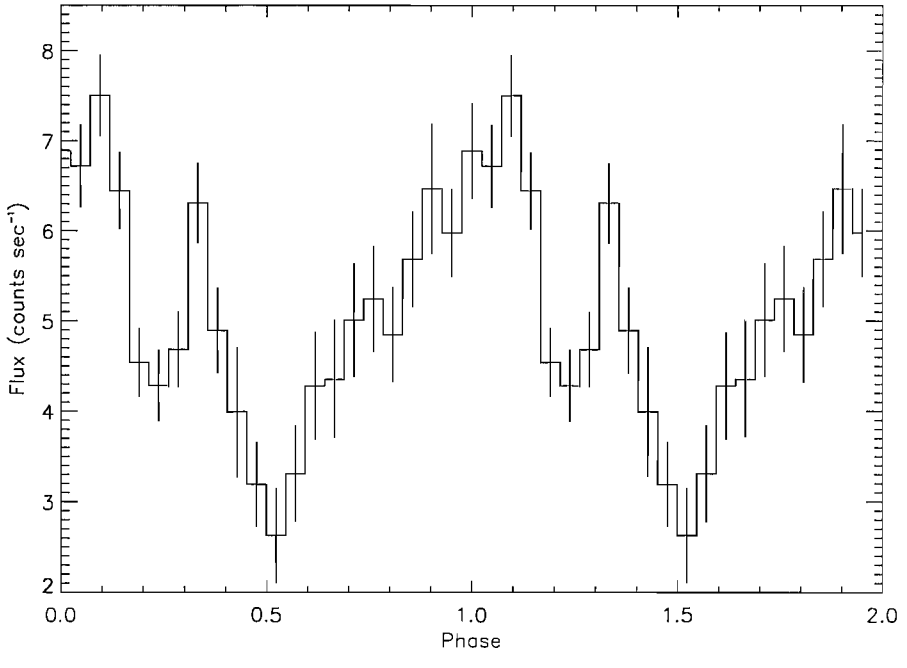

Figure 5.46: The phase-folded 4–20 keV light curve of IGR J18483–0311. The data are folded on a period of 21.0526 seconds.

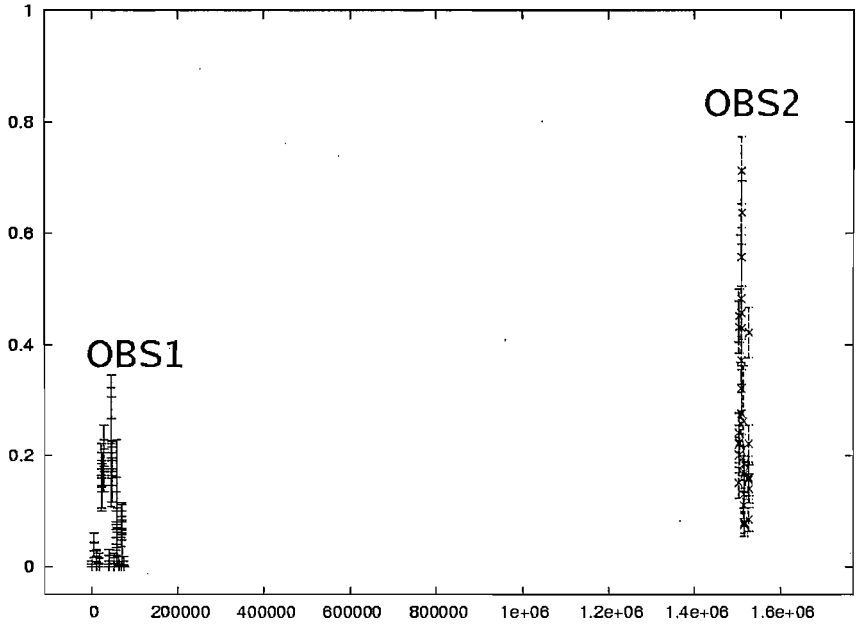

Figure 5.47: *Swift* XRT light curve (0.2–10 keV) light curve of the two *Swift* XRT observations. The bin time is 200 seconds. Time axis is in seconds, counted from the beginning of the first *Swift* XRT observation. Flux axis is in count/sec.

7 keV is best fit by an absorbed power law (χ^2_ν=1.38, 38 d.o.f) with Γ=1.7±0.7 and N_H=$6.3^{+2.4}_{-1.8}\times10^{22}$ cm^{-2}. Thermal models such as black body or bremsstrahlung provide very bad fits with a χ^2_ν greater than 2. The spectrum (1–10 keV) extracted during the observation of 5 March 2006 (OBS2) is best fit by an absorbed power law (χ^2_ν=1.009, 67 d.o.f) with Γ=1.3±0.25 and N_H=4.8±0.9×10^{22} cm^{-2}. Thermal models such as black body or bremsstrahlung are a bad description to the data. Table 5.7 provides a list of the characteristics of the two *Swift* XRT observations of IGR J18483−0311. In order to check for variability in the spectral index between the two *Swift* observations, both absorbed power law spectra have been fit fixing the N_H to the average value found from the previous spectral analysis (N_H=5.55×10^{22} cm^{-2}). By doing so, no variability has been found since the photon index assumed an identical value of 1.5±0.25 (OBS1) and 1.5±0.13 (OBS2), respectively.

Taking into account the *Swift* XRT spectra of IGR J18483−0311, we extrapolated its flux in the ROSAT energy range 0.1–2 keV. A count rate of cps~0.00046 was obtained, which is ~ 30 times smaller than that of the ROSAT HRI source (cps=0.0139) associated to IGR J18483−0311 according to Stephen et al. (2006). This, together with the huge absorption of IGR J18483−0311 as measured with INTEGRAL and *Swift* XRT, casts some doubt on a possible association between the ROSAT HRI source and IGR J18483−0311.

Table 5.7: Summary of *Swift* XRT observations of IGR J18483−0311.

Obs date (MJD)	closest expected outburst (MJD)	energy band (keV)	average flux (erg cm^{-2} s^{-1}	average lum$\star$ (erg s^{-1})	Γ	N_H (cm^{-2})
53782	~ 53788.64	0.2–7	~ 4.3×10^{-12}	~ 1.67×10^{34}	1.7±0.7	$6.3^{+2.4}_{-1.8}\times10^{22}$
53799	~ 53807.16	0.2–7	~ 2.2×10^{-11}	~ 8.55×10^{34}	1.3±0.25	$4.8\pm0.9\times10^{22}$

$\star$ = assuming a distance of ~ 5.7 kpc (see Section 5.2.5.7)

Figure 5.47 shows the 0.2–10 keV light curve of the two *Swift* XRT observations, OBS1 and OBS2 (bin time 200 seconds). The time axis is in unit of seconds, counted from the beginning of OBS1. The flux axis is in unit of count/sec. We can note some variabilty, the source during OBS2 is slightly brighter than OBS1. However, it is evident that in both occasions the source was faint and in a low state. Fine timing resolution light curves of both *Swift* XRT observations were searched for pulsations using the Lomb-Scargle method but no positive results were obtained, probably the statistics were not good enough because of the short exposure time of the observations and the low state of the source.

It is worth pointing out that the two *Swift* observations occurred several days before the closest expected outburst of IGR J18483−0311, based upon the 18.52 days periodicity (see table 5.7). Assuming that the *Swift* source is associated with IGR J18483−0311, the *Swift* XRT detections probably represent its quiescence emission. However, we cannot entirely exclude that the *Swift* source is not associated with IGR J18483−0311, since *Swift* did not observe it during an outburst.

5.2.5.7 An highly reddened star as optical counterpart of IGR J18483−0311

Stephen et al. (2006) reported the association between IGR J18483−0311 and the ROSAT HRI source 1RXH J184817.3−031017. Two optical USNO–B1.0 sources were found within the ROSAT positional uncertainty, one of which is an highly reddened object. As we can note in figure 5.48, the *Swift* XRT observations of IGR J18483−0311 furnished a very accurate source position which allows us to identify this highly reddened object, located at RA=$18^h\ 48^m\ 17.2^s$, Dec=-03° 10′ 16.5″ (J2000), as the likely optical counterpart of IGR J18483−0311. Its optical and NIR magnitudes extracted from the USNO–B1.0 and 2MASS catalogues, respectively, are R = 19.26, I = 15.32, J = 10.74, H = 9.29 and K = 8.46. This indicates an extremely reddened object, and the optical/NIR color indices of this source strongly resemble those of a heavily absorbed early-type star, similar to the

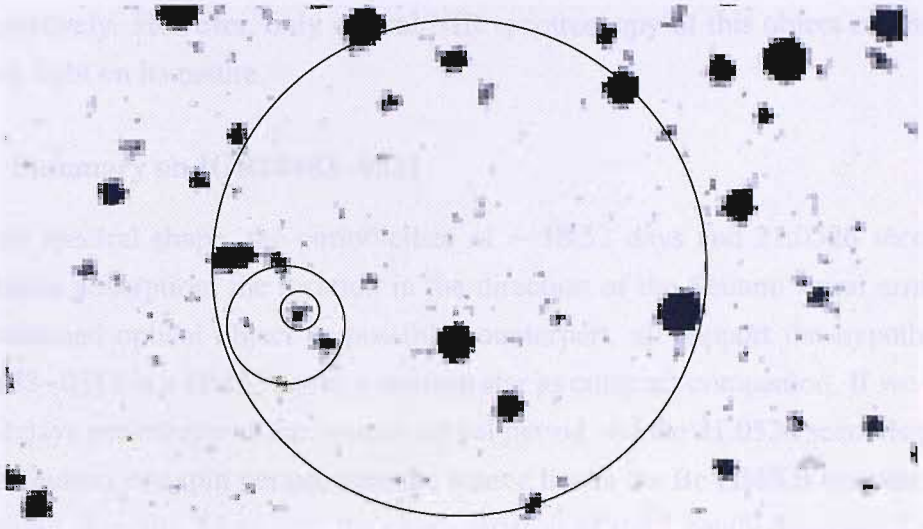

Figure 5.48: USNO B1.0 optical field image (R2 magnitude). The circles represent, from larger to smaller, the ISGRI error circle of IGR J18483–0311 (Bird et al. 2006), ROSAT (Stephen et al. 2006) and *Swift* (this PhD thesis). As we can note, the accurate *Swift* position allow us to identify the likely optical counterpart for IGR J18483–0311.

case of 2RXP J130159.6–635806 = IGR J13020–6359 (Chernyakova et al. 2005), identified as a HMXB by Masetti et al. (2006c). Indeed, assuming the Milky Way extinction law (Cardelli et al. 1989), we find that the optical/NIR color indices are consistent with those of a late O / early B-type star (Wegner 1994) suffering from a reddening of $A_V \approx$ 13 mag. This, using the formula of Predehl & Schmitt (1995), implies a column density of $N_H \sim 2.3 \times 10^{22}$ cm^{-2}, which is lower than that inferred with the *Swift* and *INTEGRAL* spectral analysis results. This may indicate that part of the absorption detected in X–rays is local to the accreting object. Admittedly, if one considers the $R - I$ color index alone, one gets a higher V-band optical extinction ($A_V \approx 16$ mag); however, it should be noted that, for faint (>18) magnitudes, the photometry of USNO catalogues can have uncertainties as high as 1 mag or more (e.g. Masetti et al. 2003). Thus, we consider the A_V estimate obtained using the $IJHK$ magnitudes as a more correct one. Assuming then $A_V \approx$13 mag along the IGR J18483–0311 line of sight and a B0 spectral type for the companion star in this system, we can infer its distance, depending on the luminosity class (main sequence, giant or supergiant) of the star. We find that, for these three cases, a distance of ~2.1, ~3.5 and ~5.7 kpc, respectively, is found. The first (main sequence) case would place the system in the Sagittarius arm of the galaxy (e.g. Leitch & Vasisht 1998): this distance is however too close to justify the inferred optical absorption.

Thus, we consider it more likely that the secondary star is an early giant or supergiant: in this case the source would lie either in the near or in the far side of the Scutum-Crux

arm, respectively. However, only optical/NIR spectroscopy of this object can help us to shed more light on its nature.

5.2.5.8 Summary on IGR18483–0311

The X-ray spectral shape, the periodicities of ~ 18.52 days and 21.0526 seconds, the high intrinsic absorption, the location in the direction of the Scutum spiral arm and the highly reddened optical object as possible counterpart, all support the hypothesis that IGRJ18483–0311 is a HMXB with a neutron star as compact companion. If we interpret the 18.52 days periodicity as the system orbital period and the 21.0526 seconds periodicity as the neutron star spin period, then the source lies in the Be HMXB transients region of the Corbet diagram. Moreover, the characteristics of the 5 newly discovered outbursts and their regular recurrence at ~ 18.52 days strongly support a Be/X-ray transient HMXB nature. However, we can not entirely exclude a different nature for the source, that of supergiant fast X-ray transient, because of the temporal and spectral properties of the source, resembling those of already known SFXTs. The typical duration of the outburst activity of IGR J18483–0311 is a few days; this is somewhat longer than typical outbursts from SFXTs which are usually shorter than a day, typically a few hours; however outbursts from SFXTs lasting a few days are not unprecedented (Sidoli et al. 2006). It is worth bearing in mind that SFXTs are characterized by typical luminosity ratios L_{Max} / $L_{Min} \sim 10^4$. Assuming that the *Swift* XRT detection is associated with IGR J18483–0311 and it represents its quiescence emission, then its luminosity ratio is $L_{Max} / L_{Min} \sim 10^3$, an order of magnitude smaller than that typical of SFXTs. Spectroscopy of the optical/NIR counterpart of IGR J18483–0311 is thus essential to fully characterize this hard X-ray emitting object.

5.2.6 IGR J16195–4945=AX J161929–4945

5.2.6.1 Archival X-ray observations of the source

IGR J16195–4945 was discovered by INTEGRAL during Core Program observations accumulated between 27 February and 19 October 2003 (Walter et al. 2004), being detected with a significance of 10σ (20–40 keV). Subsequently, Sidoli et al. (2005) proposed the X-ray source AX J161929–4945 as its low energy counterpart. AX J161929–4945 was detected by ASCA only two times, on September 1994 and on September 1997, during the ASCA survey of the galactic ridge (Sugizaki et al. 2001). The ASCA spectrum (1–10 keV) during the observation in 1997 is well fit by an absorbed power law model with $\Gamma=0.6^{+0.8}_{-0.5}$ and a relatively high value of $N_H=12^{+8}_{-4}\times10^{22}$ cm^{-2} (Sidoli et al. 2005). Other

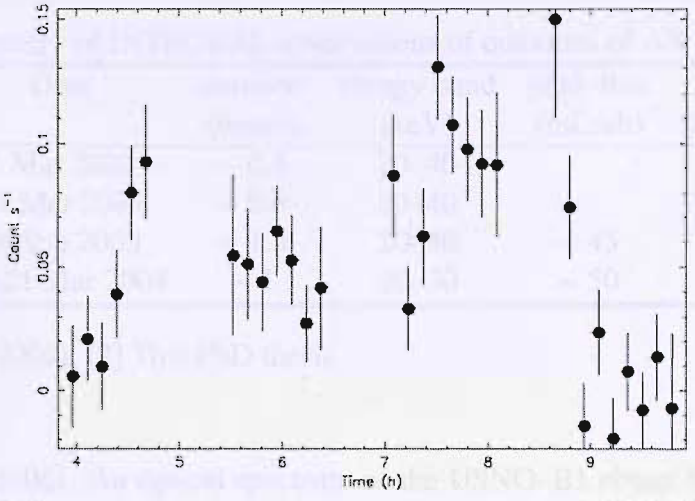

Figure 5.49: ASCA light curve (1–10 keV) of AX J161929–4945 during the observation on September 1997. Credit: Sidoli et al. (2005)

spectral models, such as black body or thermal bremsstrahlung, were not adequate to describe the spectrum (Sidoli et al. 2005). Figure 5.49 shows the ASCA light curve (1–10 keV) as taken from Sidoli et al. (2005). The bin size is 512 seconds. Variability can be noted on short timescales with several quick flares, the source went below the threshold of detectability at the beginning and at the end of the ASCA observation.

Analysing public INTEGRAL data, Sidoli et al. (2005) reported on IBIS detections of AX J161929–4945 in only 2 ScWs. The first ScW corresponds to a detection on 5 March 2003, the second on 14 March 2003. In both of them the average flux level was $\sim$ 17 mCrab (20–40 keV).

A $\sim$ 5 ks Chandra observation of the region detected a X-ray source located $1'.1$ from the best ASCA position of AX J161929–4945. It should be close enough to consider the association likely (Tomsick et al. 2006). The Chandra coordinates are RA=16^h 19^m 32.3^s Dec=-49° 44′ 30.7″ (error radius 0.″6). The 0.3–10 keV Chandra spectrum is best fit by an absorbed power law with $\Gamma=0.5^{+0.9}_{-0.7}$ and $N_H=7^{+5}_{-3}\times10^{22}$ cm^{-2}. The galactic absorption along the line of sight is 2.2×10^{22} cm^{-2} so the measured N_H suggests that the source is intrinsically absorbed. The precise Chandra position has been used to find counterparts at optical and infrared wavebands (Tomsick et al. 2006, Tovmassian et al. 2006). An infrared 2MASS source lies well inside the Chandra error circle. Whereas, an optical UNSO–B1.0 star lies just outside of it. Being $\sim$ 1″ apart, the USNO and 2MASS sources are not probably the same object. This may indicate the presence of a second optical source blended with the counterpart. The optical/infrared Spectral Energy Distribution (SED) of IGR J16195–4945 provides further evidence that there are two blended sources (Tomsick et al. 2006). Moreover, the SED indicates a likely HMXB nature for the source

Table 5.8: Summary of INTEGRAL observations of outbursts of AX J161929–4945.

No.	Date	duration (hours)	energy band (keV)	peak-flux (mCrab)	ref (discovery)
1	5 Mar 2003	~ 0.5	20–40		[1]
2	14 Mar 2003	~ 0.5	20–40		[1]
3	26 Sep 2003	~ 1.5	20–40	~ 45	[2]
4	20–21 Mar 2004	~ 1	20–30	~ 50	[2]

[1] Sidoli et al. (2005); [2] This PhD thesis

(Tomsick et al. 2006). An optical spectrum of the USNO–B1 object has been taken by Tovmassian et al. (2006), it is consistent with a late F type star and it strongly suggests that it is not the IGR J16195–4945 optical counterpart for several reasons. It should just be a nearby dwarf star (Tovmassian et al. 2006).

5.2.6.2 Analysis of newly discovered outbursts by INTEGRAL

Table 5.8 lists all outbursts detected by INTEGRAL, to date. The first two outbursts have been already reported in the literature by Sidoli et al. (2005). The remaining two are newly discovered and here their timing and spectral analysis is reported.

Outburst No. 3 in table 5.8 occurred on 26 September 2003 and its 20–40 keV light curve is shown in figure 5.50. It is truncated at the beginning and at the and because the source was outside the IBIS FOV. Although most of the time the source is not detected, a flare is particularly evident. Figure 5.51 shows a zoomed view of this flare with a smaller bin time (600 seconds) compared to that of figure 5.50 which is 2000 seconds. The duration and the peak flux of the flare are ~ 1.5 hours and ~ 45 mCrab (20–40 keV), respectively. Its spectrum is well fit by a black body (χ^2_ν=1.04, d.o.f. 14) with kT=$5.5^{+2}_{-1.5}$ keV (see figure 5.52).

Outburst No. 4 in table 5.8 has been detected in the energy range 20–30 keV only in 2 ScWs. Figure 5.53 shows their mosaic significance map, IGR J16195–4945 (circled) is detected at a level of ~ 6σ. From the 20–30 keV ISGRI light curve (figure 5.54), it can be noted that the source was active for no more than ~ 1 hour, reaching a peak flux of ~50 mCrab (20–30 keV). A spectrum extracted from the 2 ScWs during which the source was detected is best fit by a black body (χ^2_ν=1.38, d.o.f. 15) with kT=$5.2^{+1.4}_{-1.8}$ keV. However a simple power law (χ^2_ν=1.48, d.o.f. 15, Γ=$3.6^{+1.4}_{-1}$) and a thermal bremsstrahlung (χ^2_ν=1.43, d.o.f. 15, kT=$13^{+14}_{-5.5}$ keV) provide reasonable fits.

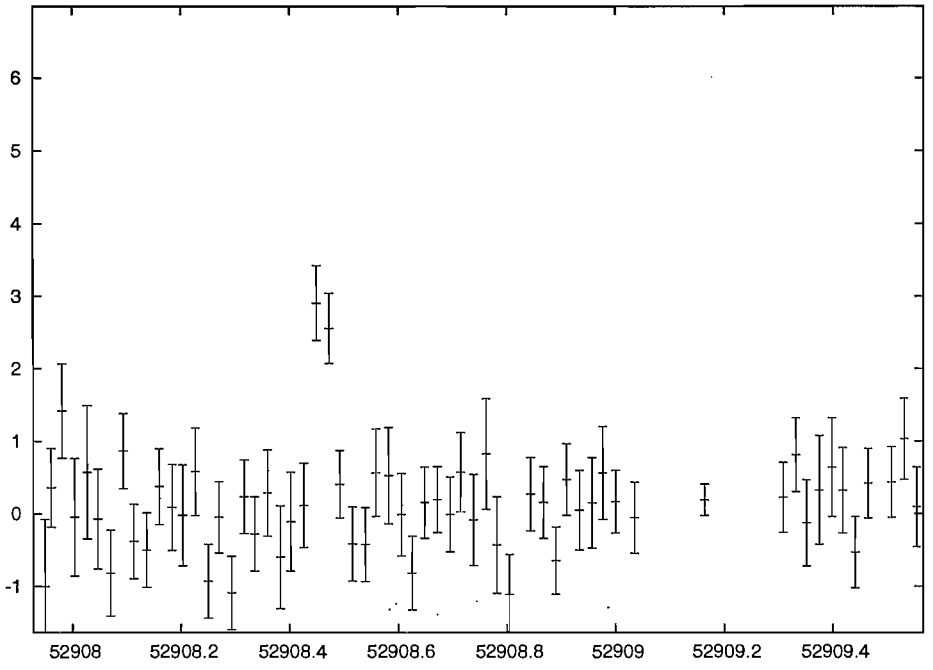

Figure 5.50: ISGRI light curve (20–40 keV) of AX J161929–4945 during the outburst occurred on 26 September 2003 (No. 3 in table 5.8). Time axis is in MJD. Each data point represents the average flux during one ScW (~2000 seconds).

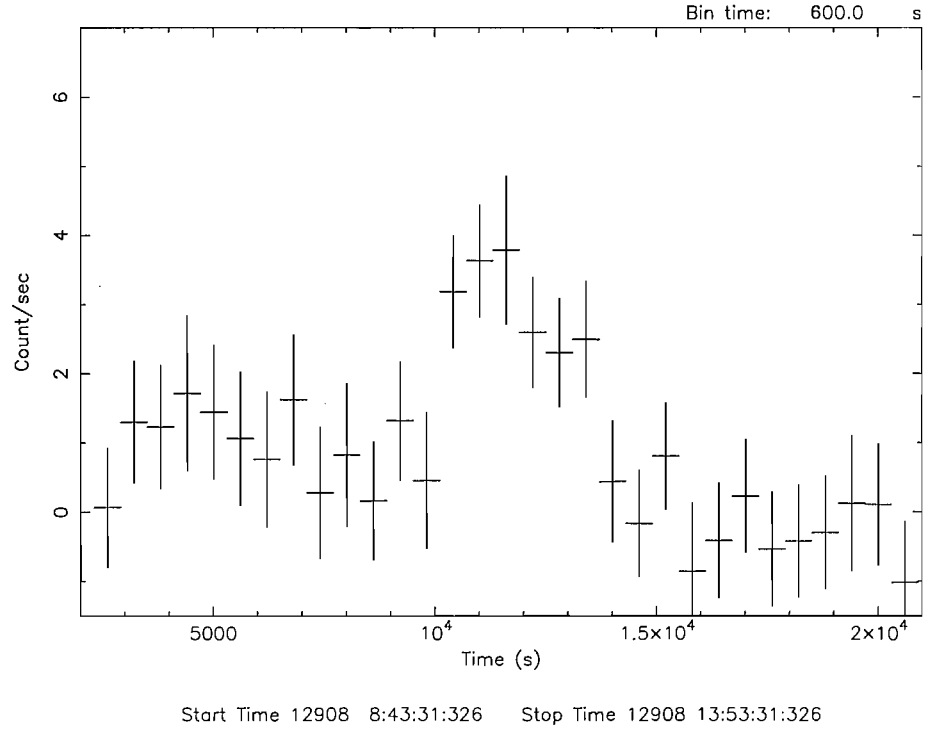

Figure 5.51: Zoomed view of the flare showed in figure 5.50. Note that the bin time is smaller than that in figure 5.50.

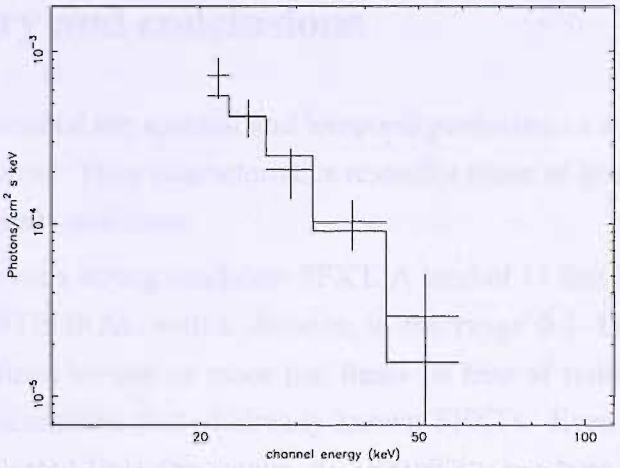

Figure 5.52: Unfolded black body spectrum (20–60 keV) of the outburst No. 3 in table 5.8.

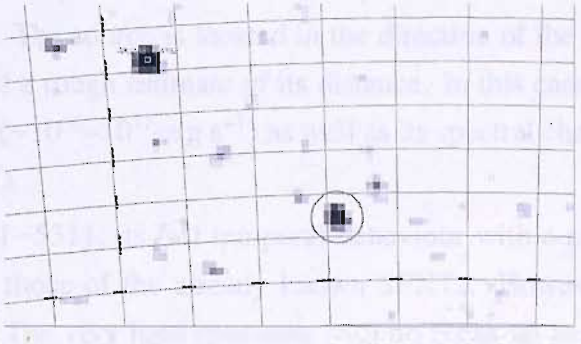

Figure 5.53: ISGRI mosaic significance map of AX J161929–4945 (circled) during outburst No. 4 in table 5.8. The source is detected at $\sim 6\sigma$ level (20–30 keV).

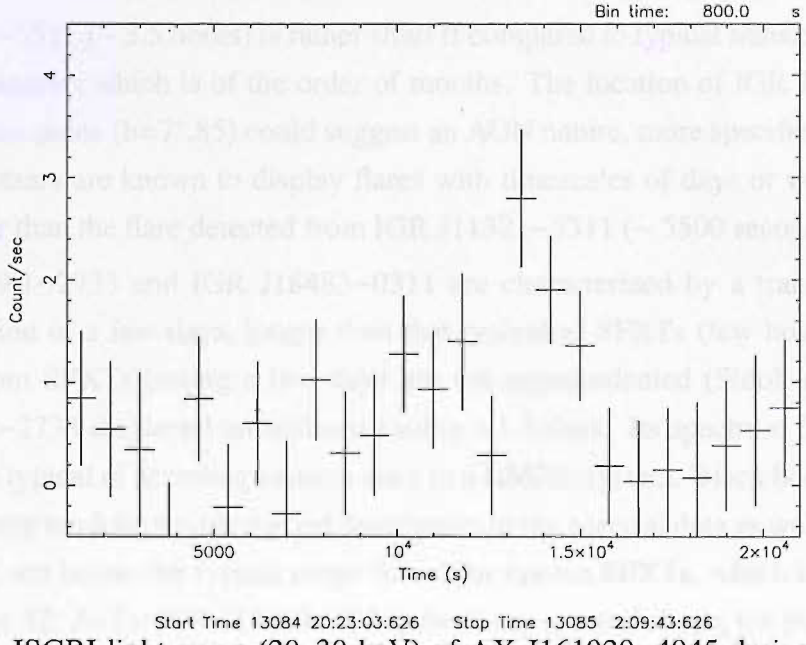

Figure 5.54: ISGRI light curve (20–30 keV) of AX J161929–4945 during the outburst No. 4 in table 5.8.

5.3 Summary and conclusions

This chapter has described the spectral and temporal properties of a sample of 6 unidentified hard X-ray sources. Their characteristics resemble those of firm SFXTs and so they can be considered good candidates.

IGR J16479–4514 is a strong candidate SFXT. A total of 11 fast X-ray outbursts have been detected by INTEGRAL with a duration in the range 0.5–11 hours. Their light curves are characterized by one or more fast flares on tens of minutes timescale. This behaviour strongly resembles that of already known SFXTs. Even if a total of 11 outbursts have been detected from the source, no periodicity has been found performing a Lomb-Scargle period analysis. The minimum temporal distance between two consecutive outbursts is ~ 9 days. The source is located in the direction of the Norma region, so ~ 6 kpc can be considered a rough estimate of its distance. In this case its peak luminosities are typical of SFXTs (~10^{36}–10^{37} erg s^{-1}) as well as its spectral characteristics (i.e. black body with kT~ 7 keV).

As for IGR J11321–5311, its fast temporal behaviour with a rapid flare lasting only few hours resembles those of the already known SFXTs. However, other possibilities can not be excluded. The very hard spectrum with no break up to 300 keV and the flaring behaviour are very typical of Anomalous X-ray Pulsars (AXPs). Another possibility could be that of a black hole transient. Nevertheless, the duration of the outburst from IGR J11321–5311 (~ 3.5 hours) is rather short if compared to typical transient activity of black hole binaries which is of the order of months. The location of IGR J11321–5311 off the galactic plane (b=7°.85) could suggest an AGN nature, more specifically a Blazar. However, blazars are known to display flares with timescales of days or weeks, significantly longer than the flare detected from IGR J11321–5311 (~ 5500 seconds).

AX J1749.1–2733 and IGR J18483–0311 are characterized by a transient activity with a duration of a few days, longer than that typical of SFXTs (few hours); however outbursts from SFXTs lasting a few days are not unprecedented (Sidoli et al. 2006). AX J1749.1–2733 displayed an outburst lasting ~1.3 days. Its spectrum fit by a cutoff power law is typical of accreting neutron stars in a HMXB system. Black body or thermal bremsstrahlung models provide a good description to the spectral data as well. Their temperatures kT are inside the typical range found for known SFXTs, which is $3<kT_{BB}<9$ and $9<kT_{BR}<32$. As for IGR J18483–0311, the X-ray spectral shape, the periodicities of 18.52 days and 21.0526 seconds, the high intrinsic absorption, the location in the direction of the Scutum spiral arm and the highly reddened optical object as possible counterpart, all support the hypothesis that IGR J18483–0311 is a HMXB with a neutron star as com-

pact companion. If we interpret the 18.52 days periodicity as the system orbital period and the 21.0526 seconds periodicity as the neutron star spin period, then the source lies in the Be HMXB transients region of the Corbet diagram. Moreover, the characteristics of the outbursts and their regular recurrence at 18.52 days strongly support a Be/X-ray transient HMXB nature. However, we can not entirely exclude a different nature for the source, that of supergiant fast X-ray transient.

IGR J17407–2808 and AXJ J161929–4945 are candiate SFXTs characterized by fast flares in the range 0.05–1.5 hours. Their spectra are well fit by black body or thermal bremsstrahlung models with temperatures kT inside the typical range found for known SFXTs, which is $3<kT_{BB}<9$ and $9<kT_{BR}<32$.

Chapter 6

Discussion and Conclusions

This thesis has presented results on fast transient soft γ-ray sources detected with the INTEGRAL satellite during $\sim$ 3 years of observations. In the light of all the findings reported in chapter 4 and 5, INTEGRAL is clearly playing a key role in unveiling a new class of SGXBs labelled as Supergiant Fast X-ray Transients; SFXTs. Most of the time these sources are undetectable, then occasionally they undergo fast X-ray outburst activity lasting less than a day, typically only a few hours. This kind of X-ray behaviour is very surprising since SGXBs were, until recently, only seen as bright persistent X-ray sources. To date, 8 SFXTs have been discovered and several optically unidentified X-ray sources have been proposed as candidate SFXTs, based on their fast X-ray transient behaviour. This is a very important achievement, in just a few years the number of SFXTs is already comparable to that of classical persistent bright SGXBs discovered in almost 40 years of X-ray astronomy.

INTEGRAL provided detections of all 8 known SFXTs, allowing a detailed study of their fast X-ray transient activity. In particular, 4 out of 8 are new hard X-ray sources discovered by INTEGRAL. The remainder were discovered by previous X-ray missions (ASCA, RXTE, BeppoSAX WFCs), however they were poorly known and studied. INTEGRAL has discovered many new fast X-ray outbursts from them, revealing or confirming their fast X-ray transient nature. Table 6.1 provides a summary of the known characteristics of the 8 firm SFXTs studied in this thesis (chapter 4). It lists distance, absorption and spin rate when available, number of outbursts detected by INTEGRAL, their duration, peak-flux, peak-luminosity, temperature of the black body and bremsstrahlung best fit spectra, photon index of the power law and cutoff energy of the cutoff power law best fit spectra. Table 6.2 provides a summary of known characteristics of a sample of 6 unidentified hard X-ray sources which have been studied in this thesis and considered to be candidate SFXTs (chapter 5). It lists spin rate and absorption when known, number of

outbursts detected by INTEGRAL, their duration, peak-flux, peak-luminosity, temperature of the black body and bremsstrahlung best fit spectra, photon index of the power law and cutoff energy of the cutoff power law best fit spectra.

Figure 6.1 shows the angular distribution off the galactic plane of the 8 firm SFXTs (horizontal hatched bars), of the 6 candidate SFXTs (filled black bars) and of all galactic HMXBs (empty white bars) as taken from the third IBIS/ISGRI γ-ray catalog (Bird et al. 2007). We can note that all 8 SFXTs are concentrated on the galactic plane, at $|b|<2^{\circ}$, as amply expected from the supergiant nature of their optical counterpart. In the case of the 6 candidate SFXTs, as far as we can tell from the very limited statistics, their density is clearly greater toward the galactic plane, 2/3 of them being at $|b|<1^{\circ}$. This is to be expected if they are HMXBs, due to the very young age of their progenitor stars. Unfortunately the numbers of our sample of sources are not sufficient to perform a reasonable and rigorous statistical analysis.

Figure 6.2 is an histogram of the duration of all outbursts detected by INTEGRAL from the 8 SFXTs (filled black bars) and from the 6 candidate SFXTs (diagonal hatched bars). In the case of SFXTs, all but two have a duration less than a day, being typically in the range 0.5–14 hours. The only two outbursts longer than usual are from AX J1841.0–0536 (~ 55 hours) and IGR J11215–5952 (~ 72 hours), respectively. The duration of the outbursts from candidate SFXTs is very similar to that of firm SFXTs. The majority of them have a duration in the range 0.05–11 hours. Only three outbursts are longer than a day (see figure 6.2); two have been detected from IGR J18483–0311 (43.2 and 84 hours) and one from AX J1749.1–2733 (31 hours).

As for the spectral characteristics of the fast X-ray outbursts, thermal models such as black body or bremsstrahlung provided a good description to almost all ISGRI spectra above 20 keV. Figure 6.3 shows the distribution of the temperature (kT) of the spectral fit using a bremsstrahlung model, pertaining the firm SFXTs (horizontal hatched bars) and the candidate SFXTs (filled black bars). As far as we can tell from the limited statistics, the former are in the range 9–32 keV, whereas the latter are in a very similar range, 11–33 keV. In particular, 2/3 of the total sample are in the range 20–25 keV. Figure 6.4 shows the distribution of the temperature (kT) of the spectral fit using a black body model, pertaining to the SFXTs (filled black bars) and the candidate SFXTs (horizontal hatched bars). The former are in the range 3–9 keV, whereas the latter are in a very similar range 5–8 keV. Unfortunately, the data are not sufficient to perform a reasonable and rigorous statistical analysis, we can just point out that 2/3 of the total sample have a temperature kT in the range 7–8 keV. By knowing the temperatures of the black body spectra as well as the peak luminosities, it was possible to calculate the radius of the emitting black body regions in

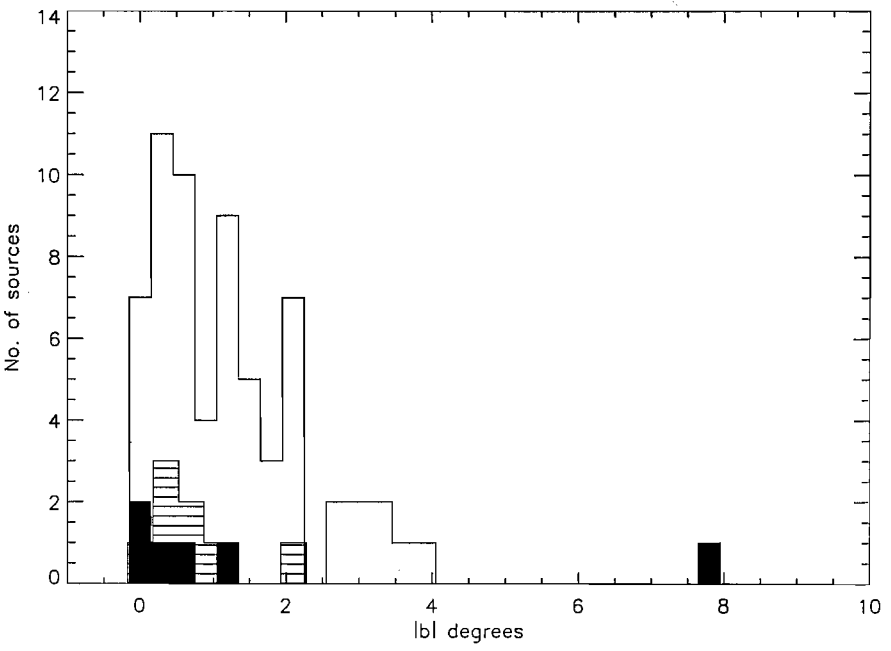

Figure 6.1: Angular distribution off the galactic plane of the 8 SFXTs reported in table 6.1 (horizontal hatched bars), of the 6 candidate SFXTs in table 6.2 (filled black bars) and of all galactic HMXBs (empty white bars) as taken from the third IBIS/ISGRI gamma-ray catalog (Bird et al. 2007).

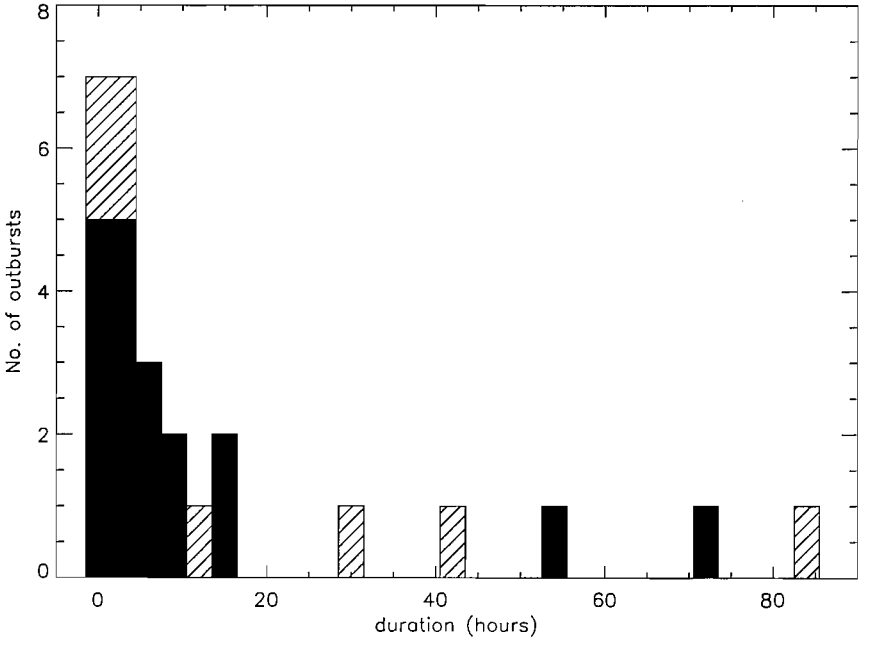

Figure 6.2: Duration of all outbursts detected by IBIS from the 8 SFXTs (filled black bars) and from the 6 candidate SFXTs (diagonal hatched bars).

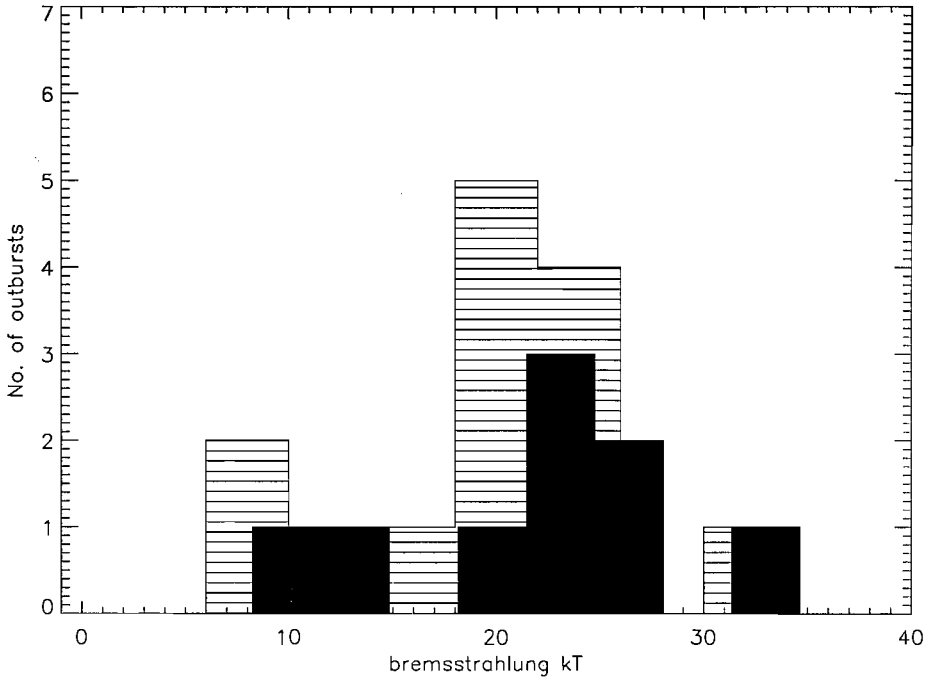

Figure 6.3: Distribution of the temperature kT of the bremsstrahlung spectra of the firm SFXTs (horizontal hatched bars) and of the candidate SFXTs (filled black bars).

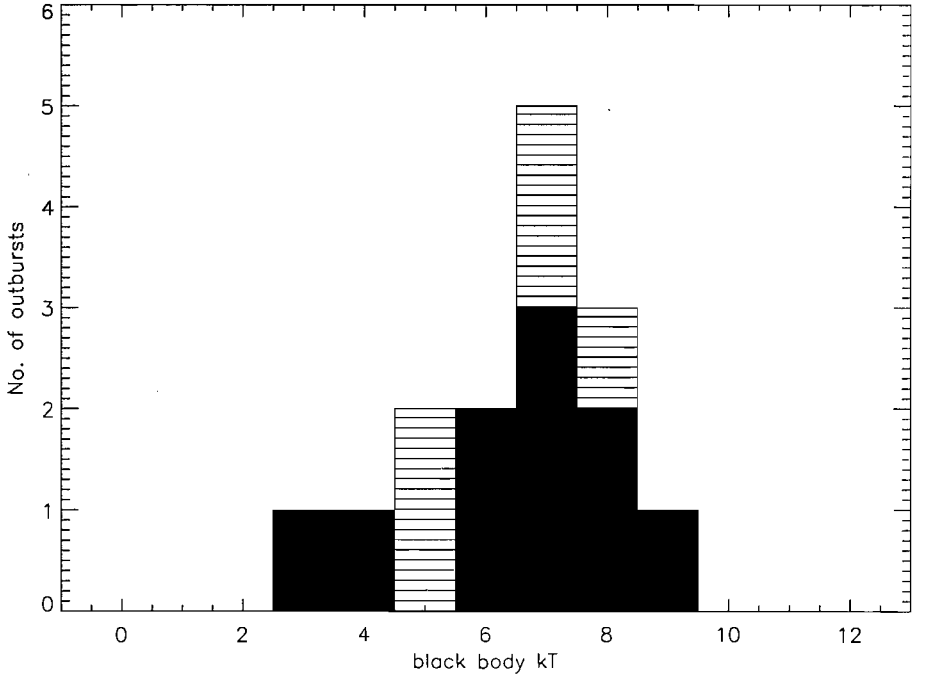

Figure 6.4: Distribution of the temperature kT of the black body spectra of the firm SFXTs (filled black bars) and of the candidate SFXTs (horizontal hatched bars).

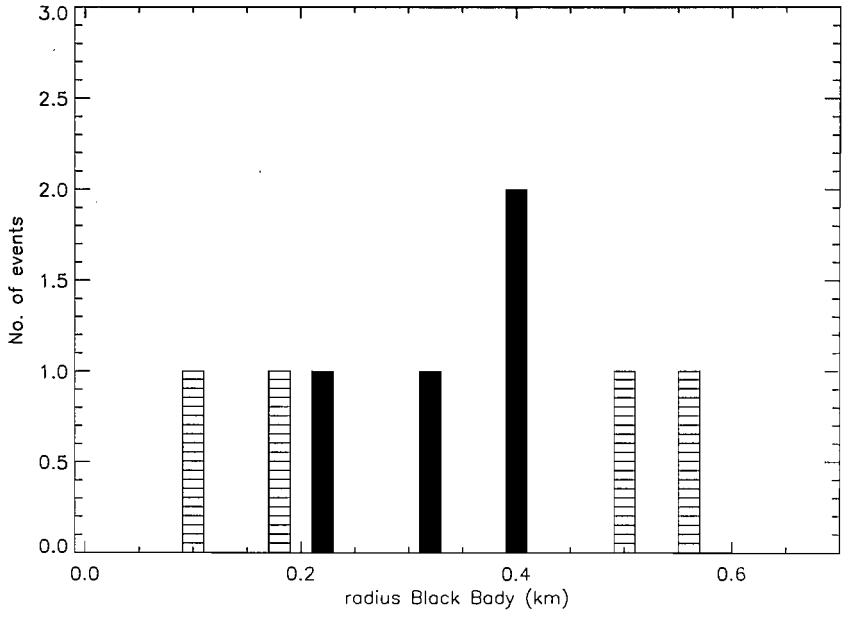

Figure 6.5: Distribution of the radius of the emitting black body regions (Km) of firm SFXTs with known distances (horizontal hatched bars) and unknown distances (filled black bars). For the latter, a rough estimation of the distance was obtained from their location in the direction of the galactic spiral arms Norma and Scutum (see table 6.1).

the case of the firm SFXTs IGR J16465–4507, AX J1841.0–0536, IGR J17544–2619, IGR J11215–5952 and IGR J08408–4503. It is worth pointing out that IGR J16465–4507 and AX J1841.0–0536 are the only sources for which the distance is still unknown. A rough estimation of their distance was obtained from their location in the direction of the galactic spiral arms Norma and Scutum, respectively (see table 6.1). Figure 6.5 shows the distribution of the calculated radius of the emitting black body regions. We can note that they are in the range 0.1–0.55 km. Such values suggest that the soft-γ ray emission from SFXTs probably originates in the polar cap region of a neutron star (see figure 6.6). The values of the radius of the polar cap regions have been then used to infer a rough estimation of their half-angular size, assuming a standard neutron star radius of 10 km. The half-angular sizes are found to be in the range 0°.5–3°.2. As comparison, the radius and half-angular size of the polar cap region of the Crab pulsar are $\sim$ 0.8 Km and $\sim$ 4°.6, respectively. They are slightly greater but still comparable to those found for SFXTs.

A simple power law was often, but not always, a good fit to the ISGRI spectra above 20 keV. Figure 6.7 displays the distribution of the photon index of the power law spectra of the firm SFXTs (horizontal hatched bars) and of the candidate SFXTs (filled black bars). It is worth pointing out that only 4 outbursts detected by ISGRI were also covered by JEM–X observations, providing broad band spectra (soft and hard X-rays). Two of them

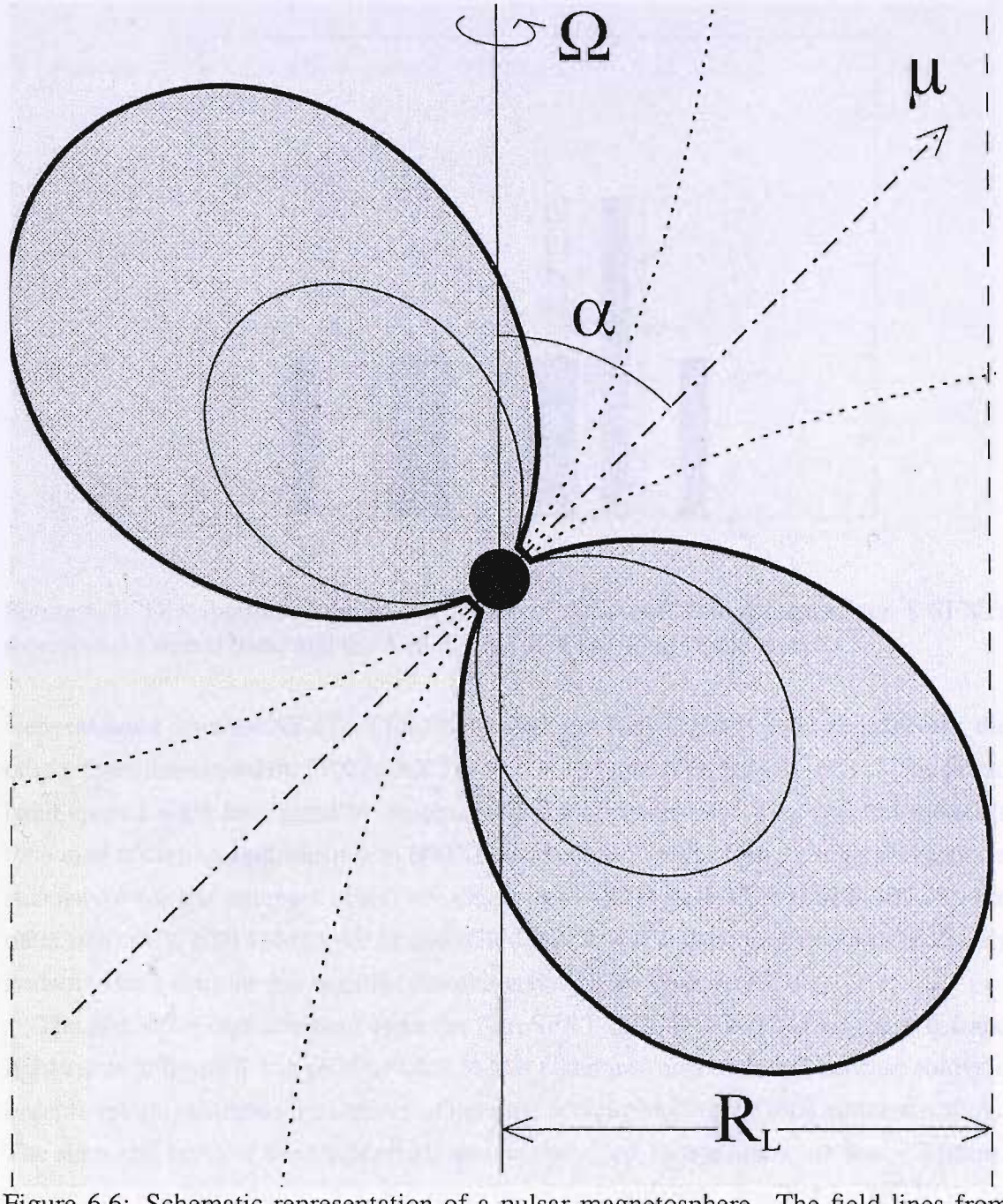

Figure 6.6: Schematic representation of a pulsar magnetosphere. The field lines from the magnetic dipole moment μ are inclined at angle α with the rotation axis. They will corotate with the pulsar at angular velocity Ω out to a radial distance R_L=c/ Ω where the field lines will be swept along at the speed of light c. Field lines which cross the light cylinder defined by R_L do not return to the surface of the neutron star, and are referred to as open field lines. Radiation escapes along these open field lines outside the shaded regions. The last closed magnetic field lines, which just touch the light cylinder, define the edge of the two polar cap regions on the neutron star surface.

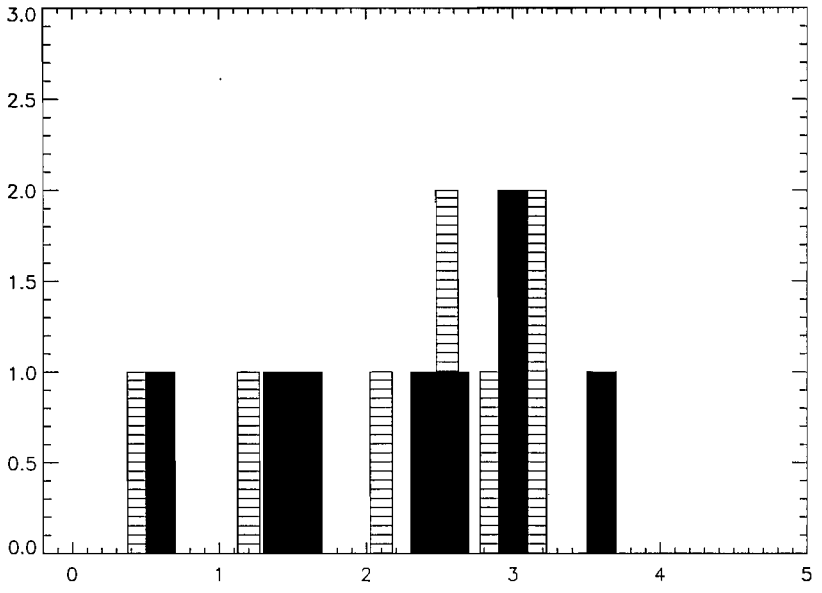

Figure 6.7: Distribution of the photon index of the power law spectra of the 8 SFXTs (horizontal hatched bars) and the 6 candidate SFXTs (filled black bars).

were detected from the SFXTs XTE J1739–302 and IGR J11215–5952 respectively, the others from the candidate SFXTs AX J1749.1–2733 and IGR J18483–0311. The broad band spectra were best fitted by an absorbed cutoff power law. This spectral model is typical of accreting neutron stars in HMXBs and consequently strongly suggest a neutron star nature for the compact object of AX J1749.1–2733 and XTE J1739–302. In the other two cases, IGR J18483–0311 and IGR J11215–5952, the compact object is already known to be a neutron star because pulsations have been discovered.

The fast X-ray outburst No.1 from the firm SFXT XTE J1739–302 (see table 6.1 and light curve in figure 4.1 in section 4.1.2.3) was taken into account as a best case study, in order to roughly estimate the amount of material accreted during the total outburst activity. The start–end times of this outburst are well constrained, its total duration was ~ 2 hours. As we can see from figure 6.2, the majority of fast outbursts detected by INTEGRAL had a typical duration of ~ 2 hours. Firstly, the total amount of energy released by the source during the outburst activity was calculated to be ~ 6.14×10^{39} erg. Then, assuming η=0.1 as the efficiency in the conversion of gravitational energy into X-rays for a neutron star, the amount of material accreted in ~ 2 hours was derived, which is ~ 6.8×10^{20} g or ~ 3.4×10^{-13} $M_{\odot}$. As a comparison, the mass loss rates through the stellar winds of supergiant stars are typically in the range 10^{-6}–10^{-8} $M_{\odot}$ per year.

The N_H value of some SFXTs (XTE J1739–302, AX J1841.0–0536, SAX J1818.6–1703, IGR J16465–4507 and IGR J11215–5952), as implied by X-ray spectral fits (see table

6.1), exceeds the galactic absorption along the line of sight. This strongly suggests a local intrinsic nature for most of the absorption. In the case of XTE J1739–302, which is better studied, the amount of absorbing material is strongly variable ($3–38\times10^{22}$ cm^{-2}), this is probably related to the orbital phase of the system. Other SFXTs (IGR J17544–2619, AX J1845.0–0433, IGR J08408–4503) do not show evidence for high local absorption (see table 6.1) since their N_H is compatible with the interstellar one along the line of sight.

The typical peak luminosities of all fast X-ray outbursts detected by INTEGRAL from the 8 SFXTs are in the range $(0.5–21)\times10^{36}$ erg s^{-1}. Whereas, the quiescent luminosities inferred by X-ray missions such as XMM, Chandra and Swift XRT have values or upper limits in the range $10^{32}– 10^{33}$ erg s^{-1}. SFXTs are therefore characterized by typical luminosity ratios $L_{Max} / L_{Min} \sim 10^4$. As for the 6 candidate SFXTs, their distance is still unknown. However, a rough estimation was obtained from their location in the direction of the galactic center and of the galactic spiral arms Norma and Scutum (see table 6.2). With these assumptions, their peak luminosities were found to be in the range $(0.66 – 81)\times10^{36}$ erg s^{-1}.

As for the physical explanation of the unusual fast X-ray behaviour of SFXTs, very little is known. The orbital parameters of the 8 firm SFXTs are still unknown. A knowledge of their system geometry is strongly needed to unveil the underlying physical processes behind their fast X-ray transient activity. However, some possible explanations have been proposed (Negueruela et al. 2006a, in't Zand 2005). First of all, the short duration is not compatible with viscous timescales in a typical accretion disc; therefore fast X-ray outbursts from SFXTs must be due to a completely different mechanism. It seems that they are not related to the nature of the compact object (in't Zand 2005) since they have been detected in slow X-ray pulsars (i.e. IGR J16465–4507) or faster X-ray pulsars (i.e. AX J1841.0–0536). They should be related to the early-type supergiant companion donor star, even if there is nothing in their optical/infrared characteristics which sets them apart from the supergiant stars hosted in classical persistent SGXBs (Negueruela et al. 2006b). The wind accretion mass transfer mode from the supergiant star to the compact object in SFXTs could be different to that in classical persistent SGXBs. It might be that in SFXTs the supergiant star ejects material in a non-continuous way. In fact, many early-type stars are suspected to have massive winds that are highly structured and variable (Prinja et al. 2005). They could have a fundamentally clumpy nature. The capture of these clumps by a nearby compact object could then produce fast X-ray flares thereby explaining the observed timescales. As for the low quiescent X-ray luminosities of SFXTs, it could be explained by very eccentric orbits, much wider than those of classical persistent SGXBs

which are typically less than ~ 15 days. Because of this, the compact object in SFXTs should accrete from a less dense environment and spend most of the time far away from the supergiant donor star. However, this should imply a periodicity of the outbursts as they should occur always relatively close to the periastron passage. To date, recurrent, but no periodic outbursts have been observed from the 8 known SFXTs. Only in one case (IGR J11215–5952) is there an indication of a possible periodicity since the detected outbursts are spaced by intervals of ~ 330 days (Sidoli et al. 2006). A complete and definitive explanation of the physical reasons responsible for the very unusual fast X-ray transient behaviour of SFXTs can only be possible through a knowledge of their orbital parameters and system geometry. To this aim, a major effort is required through multiwavelength observations (optical, infrared, soft and hard X-rays).

Before the launch of INTEGRAL in 2002, it was widely believed that the total galactic population of SGXBs could not be very large because of the evolutionary timescale involved. In fact, only a dozen bright persistent SGXBs were discovered in almost 40 years of X-ray astronomy and it was expected that they represented a substantial fraction of all SGXBs in our galaxy. Since its launch, INTEGRAL is dramatically changing this classical picture. In just a few years it discovered several hugely absorbed persistent SGXBs. In particular, this thesis showed that INTEGRAL is playing a key role in studying a new kind of SGXBs which have been named as Supergiant Fast X-ray Transient (SFXTs). In just a few years, 8 of them have been reported in the literature and ~ 8 optically unidentified X-ray sources have been proposed as candidate SFXTs, based on their fast X-ray transient behaviour. In the light of these new and exciting INTEGRAL results, the size of the population of SGXBs in our galaxy could have been severely underestimated. In particular, the class of SFXTs could be much larger than the 8 firm as well as 8 candidates reported in the literature. An entire population of still undetected SFXTs could be hidden in the Milky Way. Ongoing observations with INTEGRAL may yield many newly discovered SFXTs as well as provide breakthrough information to further insight into the system geometry, so allowing the study of the physical reasons behind their very unusual fast X-ray transient behaviour.

Table 6.1: Summary of characteristics of the 8 SFXTs , •=assuming a distance of 10 kpc, ⊙ = assuming a distance of 6 kpc

Source	Distance (kpc)	spin rate	N_H 10^{22} cm^{-2}	No burst	duration (hours)	flux peak (mCrab)	lum peak (10^{36} erg s^{-1})	kT_{BB} (keV)	kT_{BR} keV)	Γ	E_c
XTE J1739−302	~ 2.3		3–38	1	~ 2	~ 210 (20–60 keV)	~ 1.5		$21.5^{+2}_{-1.7}$	$1.25^{+0.1}_{-0.1}$	$19^{+2.8}_{-2.3}$
				2	~ 14	~120 (18–60 keV)			~ 22		
				3	~ 7	~60 (18–60 keV)					
				4		~280 (20–30 keV)	~ 0.8				
				5	~ 1.5	~250 (20–30 keV)	~ 0.7				
				6		~480 (20–60 keV)	~ 1.8				
				7	~ 6	~210 (20–60 keV)	~ 1.5		23.5^{+4}_{-3}	$2.1^{+0.1}_{-0.1}$	
IGR J17544−2619	~ 3		~3	1	~ 2	~400 (20–40 keV)	~ 3.2		$9^{+0.8}_{-0.8}$		
				2	~ 8	~80 (25–50 keV)					
				3	~ 10	~240 (20–60 keV)	~ 3	$4.4^{+0.25}_{-0.25}$	$9.5^{+0.9}_{-0.9}$		
				4	~ 0.5	~150 (20–30 keV)	~ 0.7	$2.9^{+0.4}_{-0.4}$			
				5		~150 (20–40 keV)	~ 1.2				
AX J1841.0−0536		4.7 s	~6	1	~ 7	~120 (20–80 keV)	~ 21 •	$8^{+0.9}_{-0.9}$			
				2	~ 1.1	~120 (20–80 keV)	~ 21 •	$9^{+0.9}_{-0.9}$			
				3	~ 2.8	~130 (20–60 keV)	~ 18.1 •	$7.7^{+0.7}_{-0.6}$	32^{+9}_{-6}		
				4	~ 55	~51 (20–40 keV)					
AX J1845.0−0433	~ 3.6		1.6–3.6	1		(0.7–10 keV)	~ 1.5			$1^{+0.07}_{-0.07}$	
				2		~60 (20–40 keV)	~ 0.7		19^{+15}_{-7}	$2.5^{+0.6}_{-0.5}$	
				3		~80 (20–40 keV)	~ 0.93			$2.9^{+0.9}_{-0.7}$	
SAX J1818.6−1703			~6	1	~ 14	~ 446 (20–100 keV)		$7.1^{+0.5}_{-0.5}$	25^{+5}_{-4}		
				2	~ 1	~120 (20–60 keV)		$6^{+0.8}_{-0.7}$	$17^{+6.5}_{-4.3}$	$3.2^{+0.5}_{-0.5}$	
				3	~ 3	~185 (20–30 keV)					
				4		~70 (20–40 keV)					
IGR J11215−5952	~6.2	187 s	~11	1		~40 (20–40 keV)	~ 1.4	$6.2^{+0.6}_{-0.6}$	$19^{+5}_{-3.5}$	$0.5^{+0.4}_{-0.6}$	15^{+5}_{-4}
				2	~ 72	~35 (20–40 keV)				$2.6^{+1.8}_{-0.6}$	
				3		~130 (20–60 keV)	~ 7		$18^{+3.5}_{-2.5}$	$3.2^{+0.25}_{-0.25}$	
IGR J16465−4507		227 s	~60	1		~50 (20–40 keV)					
				2		~94 (20–30 keV)	~ 3 ⊙	$6.6^{+0.7}_{-0.7}$	$21^{+6.5}_{-4.5}$		
IGR J08408−4503	~2.77		~ 0.1	1	~ 1	~70 (20–40 keV)	~ 0.47	6.5^{+1}_{-1}	23^{+13}_{-7}		
				2	~ 1	~250 (20–40 keV)	~ 1.7				

Table 6.2: Summary of characteristics of the 6 candidate SFXTs

Source	spin rate	N_H 10^{22} cm^{-2}	No burst	duration (hours)	flux peak (mCrab)	lum peak (10^{36} erg s^{-1})	kT_{BB} (keV)	kT_{BR} keV)	Γ	E_c
IGR J16479−4514		6–12	1	~ 3.5	~ 850 (20–30 keV)	16 ⊖	$6.8^{+0.6}_{-0.6}$			
			2	~ 1.5	~40† (20–30 keV)					
			3	~ 0.5	~160† (20–30 keV)					
			4	~ 3.5	~150 (20–30 keV)	2.9 ⊖				
			5		~44† (20–30 keV)					
			6	~ 11	~140 (20–80 keV)					
			7	~ 2	~80 (20–60 keV)	4 ⊖				
			8	~ 2.5	~120 (20–60 keV)	6 ⊖	$7.4^{+0.5}_{-0.5}$		$2.6^{+0.2}_{-0.2}$	
			9	~ 2.5	~60 (20–60 keV)	3 ⊖				
			10		~120 (20–60 keV)	6 ⊖				
			11	~ 0.5	~240 (20–60 keV)	12 ⊖	8^{+1}_{-1}		$2.4^{+0.4}_{-0.4}$	
IGR J17407−2808			1	~ 0.5	~140 (20–30 keV)	5.4 ⊙	$4.8^{+1.5}_{-1}$	$11.5^{+13.7}_{-4.5}$		
			2	~ 0.05	~805 (20–60 keV)	81 ⊙	$7^{+0.7}_{-0.7}$	$23^{+7}_{-4.5}$		
AX J1749.1−2733		~ 20	1	~ 31	~65 (20–60 keV)	6.6 ⊙	$7.7^{+0.3}_{-0.3}$	$28^{+3.5}_{-3}$	$1.5^{+0.3}_{-0.3}$	30^{+12}_{-7}
IGR J11321−5311			1	~ 3.5	~80 (20–300 keV)				$0.55^{+0.18}_{-0.18}$	
IGR J18483−0311	21 s	9	1	~ 43.2	~120 (20–100 keV)	7.8 •		$21.5^{+2.5}_{-2}$	$1.4^{+0.3}_{-0.3}$	$22^{+7.5}_{-4.5}$
			2	~ 11★	~95 (20–60 keV)	4.4 •	$6.5^{+0.45}_{-0.45}$	20.6^{+4}_{-3}	$2.9^{+0.25}_{-0.25}$	
			3	~ 84	~80 (20–60 keV)	3.6 •	$7.2^{+0.25}_{-0.25}$	$25.2^{+2.5}_{-2.2}$		
			4	~ 7.9★	~135 (20–40 keV)	4 •	$7.8^{+0.6}_{-0.6}$	$32.5^{+10.5}_{-6.7}$		
			5	~ 31.2★	~75 (20–60 keV)	3.2 •		$22^{+2}_{-2.5}$	$2.9^{+0.15}_{-0.15}$	
AXJ J161929−4945		7–12	1	~ 1.5	~45 (20–40 keV)	1 ⊕	$5.5^{+2}_{-1.5}$			
			2	~ 1	~50 (20–30 keV)	0.66 ⊕	$5.2^{+1.4}_{-1.8}$	$13^{+14}_{-5.5}$	$3.6^{+1.4}_{-1}$	
			3	~ 0.5	~17∗ (20–40 keV)					
			4	~ 0.5	~17∗ (20–40 keV)					

∗ = average flux (20–40 keV) during the outburst. † = average flux (20–30 keV) during the outburst.
★ = lower limit on the duration.
• = assuming a distance of ~ 5.7 kpc. ⊖ = assuming a distance of ~ 6 kpc.
⊙ = assuming a distance of ~ 8.5 kpc. ⊕ = assuming a distance of ~ 5 kpc.

Bibliography

[] Ambruster, C. W.; Wood, K. S., 1986, ApJ,311, 258

[] Bamba, A., Yokogawa J., Ueno M. et al., 2001, PASJ, 53, 1179

[] Barba, R., Gamen R., Morrell, M., 2006, ATEL 819

[] Belloni, T., Dieters S., Van Den Ancker, M. E., et al. 1999, ApJ, 527, 345

[] Bildsten, L.; Chakrabarty, D.; Chiu, J.; et al. 1997, ApJS, 113, 367

[] Bird, A. J., Malizia, A., Bazzano, A., et al. 2007, astro-ph/0611493, to be published on ApJ Suppl.

[] Bird, A. J., Barlow, E. J., Bassani, L., et al. 2006, ApJ, 636, 765

[] Boella, G.; Butler, R. C.; Perola, G. C., et al. 1997, A&AS, 122, 299

[] Bradt, H. V.; Rothschild, R. E.; Swank, J. H., 1993, A&A Supplement Series, 97, 355

[] Brinkmann, W.; Papadakis, I. E.; Raeth, C., et al. 2005, A&A, 443, 397

[] Cardelli, J.A., Clayton, G.C., & Mathis. J.S. 1989, ApJ, 345, 245

[] Castro-Tirado, A. J.; Brandt, S.; Lund, N.;, et al. 1999, A&A, 347, 927

[] Chaty & Rahoui 2006, astro-ph/0609474

[] Chernyakova, M, Lutovinov, A., Capitanio, F., 2003, ATEL 157

[] Chernyakova, M., Lutovinov, A., Rodríguez, J. & Revnivtsev, M. 2005, MNRAS, 364, 455

[] Coe, M. J.; Fabregat, J.; Negueruela, I., et al. 1996, MNRAS, 281, 333

[] Connors, A.; Serlemitsos, P. J.; Swank, J. H., 1986, ApJ, 303, 769

[] Cornelisse, R.; Heise, J.; Kuulkers, E.;, et al. 2000, A&A, 357, L21

[] Cornelisse, R.; Kuulkers, E.; in't Zand, J. J. M.;, 2002, A&A, 382, 174

[] Costa, E.; Frontera, F.; Heise, J.;, et al. 1997, Nature, 387, 783

[] Dean, A. J., Bazzano, A., Hill A. B., et al. 2005, A&A, 443, 485

[] Derdeyn S.M., et al. 1972, Nucl. Instr. and Methods, 98, 557

[] Fanaroff, B. L.; Riley, J. M., 1974, MNRAS, 167,31

[] Finger, M. H.; Wilson, R. B.; Harmon, B. A., 1996, ApJ, 459, 288

[] Fishman, G. J.; Meegan, C. A.; Wilson, R. B., et al. 1989, Bulletin of the American Astronomical Society, 21, 860

[] Foschini, L.; Pian, E.; Maraschi, L.;, 2006, A&A, 450, 77

[] Giacconi, R., Gursky, H., Paolini, F., et al. 1962, Phys. Rev. Letters, 9, 439

[] Gehrels, N., Chipman, E., Kniffen, D., 1994, APJ, 92, 351

[] Gehrels, N., Chincarini, G., Giommi, P., et al. 2004, APJ, 611, 1005

[] Golenetskii, S.; Aptekar, R.; Frederiks, D.;, et al. 2003, ApJ, 596, 1113

[] Gonzlez-Riestra, R.; Oosterbroek, T.; Kuulkers, E., et al. 2004, A&A, 420, 589

[] Grebenev, S. A.; Lutovinov, A. A.; Sunyaev, R. A., 2003, ATEL 192

[] Grebenev, S. A.; Rodriguez, J.; Westergaard, N. J., et al. 2004, ATEL 252

[] Grebenev, S. A.; Sunyaev, R. A., 2005, A&A, 31, 672L

[] Greiner, J.; Hartmann, D. H.; Voges, W., et al. 2000, A&A, 353, 998

[] Grimm, H.-J.; Gilfanov, M.; Sunyaev, R., 2002, A&A, 391,923

[] Gotz, D.; Mereghetti, S.; Mowlavi, N., et al. 2004, GCN Circular, 2793

[] Gotz, D.; Schanne, S.; Rodriguez, J.; et al. 2006, ATEL 813

[] Gotz, D.; Falanga, M.; Senziani, F., et al. 2007, ApJ, 655, 101L

[] Halpern, P. J., Gotthelf E. V., 2004a, ATEL 341

[] Halpern, J. P., Gotthelf, Helfand, et al. 2004b, ATEL 289

[] Halpern, J. P., Gotthelf, E. V., 2006, ATEL 692

[] Hartman, R. C.; Bertsch, D. L.; Bloom, S. D.;, et al. 1999, ApJS, 123, 79

[] Heise, J.; in't Zand, J., 2004, NuPhS, 132, 263

[] Hicks et al. 1965, IEEE Trans. Nucl. Sci., 1965, 12, 54

[] Hill, A. B., Walter, R., Knigge, C., et al. 2005, A&A, 439, 255

[] Hill, A. B., 2006, Ph.D. Thesis, School of Physics and Astronomy, University of Southampton, UK

[] Hoffman, J. A.; Lewin, W. H. G.; Doty, J., et al. 1978, ApJ, 221, 57L

[] Horne, J. H., Baliunas, S. L., 1986, ApJ, 302, 757

[] in't Zand J., 1992, Ph D Thesis 16I, University of Utrecht

[] in't Zand J.; Heise, J.; Smith, M.; et al. 1998, IAUC, 6840

[] in't Zand J., Kuulkers, E., Bazzano, A., et al 2000, A&A, 357, 520

[] in't Zand, J.; Heise, J.; Ubertini, P., et al. 2004, Proceedings of the 5th INTEGRAL Workshop on the INTEGRAL Universe, ESA SP-552, 427

[] in't Zand J., 2005, A&A,441, L1

[] in't Zand, J.; Jonker, P.; Mendez, M.; et al. 2006, ATEL 915

[] Jager, R.; Mels, W. A.; Brinkman, A. C.;, et al. 1997, A&AS, 125, 557

[] Kanbach, G., Bertsch, D. L., Fichtel, C. E., et al. 1988, Space Science Reviews, 49, 69

[] Kaper, L.; van der Meer, A., 2005, astro-ph/0502314

[] Kaspi, V. M.; Gavriil, F. P.; Woods, P. M., et al. 2003, ApJ, 588, 93L

[] Kaspi V. M., 2006, to appear in proceedings of the conference Isolated Neutron Stars: From the Interior to the Surface, Astrophysics & Space Science in press, astro-ph/0610304

[] Kennea, J. A.; Pagani, C.; Markwardt, C., et al. 2005, ATEL 599

[] Kennea, J. A. & Campana S., 2006, ATEL 818

[] Klebesadel, Ray W.; Strong, Ian B.; Olson, Roy A., 1973, ApJ, 182, 85

[] Kraushaar & Clark, 1962, Scientific American, 52

[] Kretschmar, P.; Staubert, R.; Kreykenbohm, I;, et al. 2004, Proceedings of the 5th INTEGRAL Workshop on the INTEGRAL Universe (ESA SP-552), p.267

[] Kretschmar, P.; Mereghetti, S.; Hermsen, W.;, et al. 2004b, ATEL 345

[] Krivonos, R.; Molkov, S.; Revnivtsev, M.;, et al. 2005, ATEL 545

[] Kuiper, L.; Hermsen, W.; den Hartog, P. R.;, et al. 2006, ApJ, 645, 556

[] Labanti, C.; Di Cocco, G.; Ferro, G., et al. 2003, A&A,411, 149L

[] Landi, R., Kennea J., Giommi, P., et al. 2007, ATEL 991

[] Laurent, P.; Paul, J.; Denis, M.; Ballet, J.;, et al. 1995, A&A, 300, 399

[] Lebrun, F.; Leray, J. P.; Lavocat, P.; et al. 2003, A&A, 411, 141L

[] Leitch, E.M., & Vasisht, G. 1998, New Astronomy, 3, 51

[] Lewin, W. H. G.; Joss, P. C., 1981, Space Science Reviews, 28, 3

[] Lewin, W. H. G.; Vacca, W. D.; Basinska, E. M., 1984, ApJ, 277, 57L

[] Lewin, W. H. G.; van Paradijs, J.; Taam, R. E., 1993, Space Science Reviews, 62, 223

[] Liu Q. Z., Van Paradijs, J., Van den Heuvel, E. P. J., 2000, A&A Suppl. Ser.,147, 25

[] Liu Q. Z., Van Paradijs, J., Van den Heuvel, E. P. J., 2001, A&A,368, 1021

[] Liu Q. Z., Van Paradijs, J., Van den Heuvel, E. P. J., 2006, A&A, 455, 1165

[] Lubinski, P.; Bel, M. C.; von Kienlin, A.; et al. 2005, ATEL 469

[] Lund, N.; Budtz-Jrgensen, C.; Westergaard, N. J., et al. 2003, A&A, 411, 231L

[] Lutovinov, A.; Rodrigues, J.; Budtz-Jorgensen, C.; et al. 2004, ATEL 329

[] Lutovinov, A., Revnivtsev, M., Gilfanov, M., et al. 2005, A&A, 444, 821L

[] Lutovinov, A.; Revnivtsev, M.; Molkov, S., et al. 2005b, A&A, 430, 997L

[] Mangano, V., Romano, P., Sidoli, L., 2007, ATEL 995, ATEL 996

[] Masetti, N., Palazzi, E., Pian, E. et al. 2003, A&A, 404, 465

[] Masetti, N., Pretorius, M. L.; Palazzi, E.;, et al. 2006a, A&A, 449, 1139

[] Masetti, N., Bassani L., Bazzano, A., et al. 2006b, ATEL 815

[] Masetti, N., Morelli, L., Palazzi, E., et al. 2006c, A&A, 459, 21

[] Mas-Hesse, J. M.; Gimnez, A.; Culhane, J. L., et al. 2003, A&A, 411, 261L

[] Mereghetti, S., Sidoli, L., Paizis A., et al. 2006, ATEL 814

[] Meszaros, 2001, Science, 291, 79

[] Miller, J. M.; Fabian, A. C.; Wijnands, R.;, et al. 2002, ApJ, 570, 69L

[] Miniutti, G.; Fabian, A. C.; Miller, J. M., 2004, MNRAS, 351, 466

[] Molkov, S.; Mowlavi, N.; Goldwurm, A.;, et al. 2003a, ATEL 176

[] Molkov, S., Lutovinov, A., Grebenev, S., 2003b, A&A, 411, L357

[] Molkov, S., Cherepashchuk, A. M., Lutovinov, A., et al., 2003c, astro/ph 0402416

[] Molkov, S. V.; Cherepashchuk, A. M.; Lutovinov, A. A.;, et al. 2004, A&A, 30, 534L

[] Negueruela, I., 1998, A&A, 338,505

[] Negueruela, I., 2004, astro-ph/0411335

[] Negueruela, I., 2004b, astro-ph/0411759

[] Negueruela, I., Smith, D. M., Chaty S., 2005, ATEL 429

[] Negueruela, I., Smith, D. M., Reig, P., et al. 2006a, ESA SP-604, 165, astroph/0511088

[] Negueruela, I., Smith, D. M., Harrison, T. E., et al. 2006b, ApJ, 638, 982

[] Negueruela, I., Smith, D. M., 2006c, ATEL 831

[] Negueruela & Schurch, 2007, A&A, 461, 631

[] Nespoli, E., Fabregat, J., Mennickent, R., 2007, ATEL 983

[] Orosz, J. A.; Kuulkers, E.; van der Klis, et al. 2001, ApJ, 555, 489

[] Paul, J.; Ballet, J.; Cantin, M.; et al. 1991, Advances in Space Research, 11, 289

[] Pellizza, L. J.; Chaty, S.; Negueruela, I., 2006, A&A, 455, 653

[] Perryman, M. A. C.; Lindegren, L.; Kovalevsky, J., et al. 1997, A&A, 323, 49L

[] Predehl, P., & Schmitt, J.H.M.M. 1995, A&A, 293, 889

[] Press, W. H. & Rybicki, G. B., 1989, ApJ, 338, 277

[] Prinja, R. K.; Massa, D.; Searle, S. C., 2005, A&A, 430L, 41

[] Pye, J. P.; McHardy, I. M., 1983, MNRAS, 205, 875

[] Reig P., Roche, 1999, MNRAS, 306, 100

[] Remillard, 2001, IAUC 7707

[] Revnivtsev, M.; Sunyaev, R.; Gilfanov, M.;, et al. 2002a, A&A, 385, 904

[] Revnivtsev, M.; Gilfanov, M.; Churazov, E.;, et al. 2002b, A&A, 391, 1013

[] Risaliti & Elvis, 2004, astro-ph/0403618

[] Rodriguez, J., Domingo Garau, S. Grebenev, et al. 2004, ATEL 340

[] Romano P., Sidoli L., Mangano V., 2007, ATEL 994

[] Sakano, Masaaki; Koyama, Katsuji; Murakami, Hiroshi;, et al. 2002, ApJS, 138, 19

[] Scargle, J. D., 1982, ApJ, 263, 835

[] Scarsi, L.; Bennett, K.; Bignami, G. F. et al. 1977, ESA Recent Advan. In Gamma-Ray Astronomy p 3-11 (N78-11899 02-88)

[] Schoenfelder, V.; Aarts, H.; Bennett, K.; et al. 1993, APJ, 86, 657

[] Sguera, V.; Bird, A. J.; Dean, A. J.;, et al. 2007, A&A,462, 695

[] Sguera, V.; Bazzano, A.; Bird, A. J.;, et al. 2006, ApJ, 646, 452

[] Sguera, V.; Barlow, E. J.; Bird, A. J., et al. 2005, A&A, 444, 221

[] Sidoli, L.:, Belloni, T., Mereghetti, S., et al. 2001, A&A, 368, 835

[] Sidoli, L.; Vercellone, S.; Mereghetti, S.;, et al. 2005, A&A, 429, 47L

[] Sidoli, L.; Paizis, A.; Mereghetti, S., 2006, A&A, 450, 9L

[] Sidoli, L., Mereghetti, S., Vercellone S., et al. 2007, ATEL 997

[] Skinner & Ponman, 1994, MNRAS, 267, 518S

[] Smith, D. M.; Main, D.; Marshall, F., et al. 1998, ApJ, 501, 181L

[] Smith D. M., Remillard, R.; Swank, J., et al., 1998b, IAUC 6855

[] Smith, D. M.;, 2005, ATEL 338

[] Smith, D. M.; Heindl, W. A.; Markwardt, C. B., et al. 2006a, ApJ, 638, 974

[] Smith, D. M.; Bezayiff N., Negueruela I., 2006b, ATEL 766, ATEL 768, ATEL 773

[] Staubert, R.; Kreykenbohm, I.; Kretschmar, P., et al. 2004, Proceedings of the 5th INTEGRAL Workshop (ESA SP-552) p.259

[] Steeghs, D., Torres M.A.P., Jonker P. G., 2006, ATEL 768

[] Stephen, J. B., Bassani, L., Malizia, A., et al. 2006, A&A, 445, 869

[] Sugizaki, M.; Mitsuda, K.; Kaneda, H., et al. 2001, ApJS, 134, 77

[] Sunyaev, A.Lutovinov, S.Molkov, et al. 2003a, ATEL 181

[] Sunyaev, R. A.; Grebenev, S. A.; Lutovinov, A. A.;, et al. 2003b, ATEL 190

[] Swanenburg, B. N.; Bennett, K.; Bignami, G. F., et al. 1981, ApJ, 243, 69L

[] Swank, J. H.; Becker, R. H.; Boldt, E. A., et al. 1977, ApJ, 212, 73L

[] Swank J.H., , Smith D. M., , Markwardt C. B., 2007, ATEL 999

[] Tanaka, Y., Lewin, W. H. G., 1995, in X-Ray Binaries, ed. W. H. G. Lewin, J. van Paradijs, & E. P. J. van den Heuvel (Cambridge Univ. Press), 126

[] Tawara, Y.; Kii, T.; Hayakawa, S.; Kunieda, H., et al. 1984, ApJ, 276, 41

[] Tomsick, J. A.; Kalemci, E.; Corbel, S., et al. 2003, American Astronomical Society, HEAD meeting; Bulletin of the American Astronomical Society, 35, 615

[] Tomsick, J. A.; Chaty, S.; Rodriguez, J.;, et al. 2006, ApJ, 647, 1309

[] Tovmassian, G.; Tomsick, J. A.; Mennickent, R., 2006, ATEL 804

[] Ubertini, P.; Lebrun, F.; Di Cocco, G.;, et al. 2003, A&A, 411, 131L

[] Urry, C.; Padovani, P., 1995, PASP, 107, 803

[] Van den Heuvel, Heise, 1972, Nat 239, 67

[] Van Paradijs, J., 1996, ApJ, 464, 139L

[] Vedrenne, G.; Roques, J.-P.; Schnfelder, V.;, et al. 2003, A&A, 411, 63L

[] Vijapurkar, J.; Drilling, J. S., 1993, ApJS, 89, 293

[] Wagner, S. J.; Witzel, A., 1995, ARA&A, 33, 163

[] Walter, R.; Bodaghee, A.; Barlow, E. J., et al. 2004, ATEL 229

[] Walter, R.; Zurita Heras, J.; Bassani, L.;, et al. 2006, A&A, 453, 133

[] Waters, L. B. F. M.; van Kerkwijk, M. H., 1989, A&A, 223, 196

[] Wegner, W. 1994, MNRAS, 270, 229

[] White N. E., Nagase, F., Parmar, A. N., 1995, in X-ray Binaries, ed. W. H. G. Lewin, J. van Paradijs, & E. P. J. van den Heuvel, Cambridge University Press

[] Winkler, C., 2001, Proceedings of the Fourth INTEGRAL Workshop, ESA SP-459, 471

[] Winkler C., Courvoisier, T. J.-L.; Di Cocco, G., et al. 2003, A&A, 411, L1

[] Woods, P. M., Thompson, C., Kaspi, V. M., et al. 2004, ApJ, 605, 378

[] Yamauchi, S.; Aoki, T.; Hayashida, K.; et al. 1995, PASJ, 47, 189

[] Zhang, 2006, astro-ph/0611774

[] Ziolkowski, 2002, Mem. Soc. Astron. Ital., 73, 1038

[] Zurita J. H., Walter R., 2004, ATEL 336